Terms and Conditions of Use of Digitised Theses from Trinity College Library Dublin

Copyright statement

All material supplied by Trinity College Library is protected by copyright (under the Copyright and Related Rights Act, 2000 as amended) and other relevant Intellectual Property Rights. By accessing and using a Digitised Thesis from Trinity College Library you acknowledge that all Intellectual Property Rights in any Works supplied are the sole and exclusive property of the copyright and/or other IPR holder. Specific copyright holders may not be explicitly identified. Use of materials from other sources within a thesis should not be construed as a claim over them.

A non-exclusive, non-transferable licence is hereby granted to those using or reproducing, in whole or in part, the material for valid purposes, providing the copyright owners are acknowledged using the normal conventions. Where specific permission to use material is required, this is identified and such permission must be sought from the copyright holder or agency cited.

Liability statement

By using a Digitised Thesis, I accept that Trinity College Dublin bears no legal responsibility for the accuracy, legality or comprehensiveness of materials contained within the thesis, and that Trinity College Dublin accepts no liability for indirect, consequential, or incidental, damages or losses arising from use of the thesis for whatever reason. Information located in a thesis may be subject to specific use constraints, details of which may not be explicitly described. It is the responsibility of potential and actual users to be aware of such constraints and to abide by them. By making use of material from a digitised thesis, you accept these copyright and disclaimer provisions. Where it is brought to the attention of Trinity College Library that there may be a breach of copyright or other restraint, it is the policy to withdraw or take down access to a thesis while the issue is being resolved.

Access Agreement

By using a Digitised Thesis from Trinity College Library you are bound by the following Terms & Conditions. Please read them carefully.

I have read and I understand the following statement: All material supplied via a Digitised Thesis from Trinity College Library is protected by copyright and other intellectual property rights, and duplication or sale of all or part of any of a thesis is not permitted, except that material may be duplicated by you for your research use or for educational purposes in electronic or print form providing the copyright owners are acknowledged using the normal conventions. You must obtain permission for any other use. Electronic or print copies may not be offered, whether for sale or otherwise to anyone. This copy has been supplied on the understanding that it is copyright material and that no quotation from the thesis may be published without proper acknowledgement.

DEVELOPMENT OF ACCURATE METHODS OF WEIGHING TRUCKS IN MOTION

Two Volumes

I

by

Arturo González

Thesis submitted to the University of Dublin, Trinity College,
for the Degree of Doctor of Philosophy

2001

DECLARATION

The author hereby declares that this thesis, in whole or in part, has not been submitted to any other university as an exercise for a degree. Except where reference has been given in the text, it is entirely the author's own work.

The author confirms that the library may lend or copy this thesis upon request, for academic purposes.

Arturo González

March, 2001

ACKNOWLEDGEMENTS

I have used great many sources in writing this thesis. They include lecture notes, unrecorded conversations, Internet pages, results of personal investigations, and many textbooks and research papers. I have recorded my debt to the authors of a number of books listed in the Bibliography by mentioning them in the text, and suggesting them as valuable references for further study. At a more personal level, it is a pleasure to thank:

First, my supervisor Professor Eugene O'Brien for his friendship, encouragement, inspiration, suggestions, comments and guidance all along this thesis, formerly lecturer at Trinity College Dublin, and currently Head of Civil Engineering in University College Dublin. I am deeply indebted to him.

To Professor Simon Perry, Head of Civil Engineering in Trinity College Dublin for his support during my postgraduate studies.

To the staff in the Department of Civil Engineering for their generous assistance provided throughout this project. Especially, Chris O'Donnovan, George Jones, Dave McAulay, Ken Byrne and Gerrard McGrananghan. I would also like to express my gratitude to those in the Swedish National Road Authority, CETÉ de l'Est (France) and Technische Universität München (Germany) for their help while working abroad.

To Mark Green and Xie Haiyin from Queen's University, Kingston (Canada) for their contribution with theoretical simulations.

To a couple of very special colleagues: Samuel Grave and Alan O'Connor for always being there.

To my fellow researchers: Tony Dempsey, Sarah Prichard, Seamus O'Brien, Damien Keogh, Sean Brady, Conleth O'Loughlin and Niall Kealy for their friendship and inestimable help.

To Maria José Franco for so many answers.

To Santiago Muñoz, Gonzalo Álvarez, Alfonso Arroyo, Ana García, AnneMette O'Connor, Peter McNulty, Erwin Penka, Katrin Kessler, Pauline Quinn, Eddie Cosgrove, Cathy Ryan, Fiona McGaughey, Ciaran McNally, Victoria Medrano, Javier Añó, Luis, Luisin and Martin Costas, Mercedes de La Peña, Carmen Puente, Aileen and Kara Fogarty, Vince, Francis and Antonella Carbone, and the members of the molleja club for their encouragement and support over the past years.

To my family: Arturo, Amparo and Kelly Ana González, Angela De La Peña and Eloisa Ruiz, without whom this thesis would have never been written. This thesis is dedicated to my daughter Kelly Ana.

This research has received financial support from the Department of Civil Engineering in Trinity College Dublin, Trinity College Award, Forbairt and Trinity Trust Travel Grant Scheme. There has also been funding from the Transient Directorate, DG VII, of the European commission under the 'WAVE' project. WAVE (Weigh-in-motion of Axles and Vehicles for Europe) is a transport research project in the 4th Framework program.

ABSTRACT

The need to weigh and classify vehicles is based on the damage that large trucks cause to road infrastructure. Weigh-in-Motion (WIM) data can be used to predict future traffic volumes and weights for the planning of new constructions, the management of maintenance activities, the identification/reduction of overloading problems and the evaluation of the performance of pavements and bridges.

Most WIM systems are based on weighing sensors that are embedded in the pavement or placed on top of the road surface and which measure wheel or axle pressure that is applied as the vehicle passes over them. As the effect of the applied force is recorded during a very short period of time, accuracy is limited by the dynamic nature of the vehicle motion. Additionally, these systems are subject to durability problems due to traffic and the environment. An alternative approach to WIM which increases the length of the load-sensitive element and the durability of the system is to use a bridge as a weighing scales (Bridge WIM); this approach is the subject of the research reported in this thesis.

The installation of a Bridge WIM system is described. Axle weights are obtained from the information supplied by strain gauges under the bridge deck and axle detectors on the road surface as a vehicle passes over the bridge. Despite many advantages, Bridge WIM algorithms have generally failed to predict axle weights accurately due to vehicle and bridge dynamics and differences between theoretical models and measured bridge responses. Considerable work is carried out on the dynamic modelling of trucks on bridges for the purpose of providing a more accurate algorithm. New contributions include calibration procedures, dynamic algorithms and the extension to multiple longitudinal sensor locations along the bridge (traditionally measurements are made at just one longitudinal section).

Experiments were carried out at four different sites. Bridge WIM data was collected continuously in a 16 m simply supported skew bridge in Delgany (Ireland). A program that

processes the traffic data from road and strain sensors into vehicle velocity, classification and weights is developed for this purpose. An innovative calibration procedure purely based on the experimental record (without any reference to the structural bridge behaviour) is introduced. A 110 m continuous box-girder bridge in Belleville (France) is used for checking the performance of a Bridge WIM system when the bridge response has a very significant dynamic component. An instrumented truck participated in the experiment. A Bridge WIM system is also tested in a 30 m two-span integral bridge in Luleå (Sweden) under harsh climatic conditions. Finally, a 32 m simply supported bridge in Slovenia is instrumented with strain sensors in different longitudinal locations allowing for the study of a multiple sensor algorithm.

The data input is particularly difficult to analyse from the dynamic response of bridges due to the wide range of trucks on bridges with different classifications and with different dynamic properties. Theoretical simulations are used for testing Bridge WIM accuracy in a variety of scenarios. A planar numerical approach and a three-dimensional finite element technique are employed for simulating the passage of a vehicle over a bridge. The finite element modelling of vehicles and bridges has been done with the general-purpose finite element analysis package MSC/NASTRAN for Windows. The dynamic interaction of the bridge-vehicle system incorporates the road surface profile and is implemented using a set of auxiliary functions to enforce the compatibility conditions at the bridge/vehicle interface. Apart from these dynamic models, other numerical data from truck models validated experimentally are provided by Green (Queen's University, Kingston, Canada) for further analysis. Accuracy results for different Bridge WIM algorithms are given according to the COST323 European Specification on WIM.

A dynamic Bridge WIM algorithm based on one longitudinal location has achieved better results than the static approach in a few particular cases. Other findings as a new experimental procedure and/or the sensor location have leaded to significant improvements in accuracy. A Bridge WIM algorithm based on multiple sensor locations has generally been found the most accurate. However, this algorithm might require an excessive number of sensors in relatively short span bridges and the convenience of this installation will depend on the required level of accuracy.

CONTENTS

VOLUME I

VOLUME II

1

INTRODUCTION

Heavy trucks cause a great deal of wear and damage to pavements and bridges. There is a need for weight control to reduce the likelihood of illegally overloaded vehicles and to preserve the road infrastructure. Traditional weigh stations with static scales can not accommodate high volumes of truck traffic and Weigh-In-Motion (WIM) technology offers a solution to weigh trucks travelling at highway speeds automatically. WIM systems can pre-sort those trucks that are suspected of being overloaded to direct them to static scales, minimising unnecessary stops and delays for drivers. At the beginning of the 1990's, some European countries expressed a great demand for this technology in order to (Jacob 1999):

- Improve knowledge of traffic for economic surveys, statistics, road management and traffic monitoring;
- Improve the technical basis for pavement and bridge design and maintenance;
- Ensure fair competition in transport and road safety, by enforcing harmonised legislation of vehicle weights across Europe;
- Provide to government authorities the information necessary for a harmonised tax system.

However, vehicles in motion have constantly varying axle weights as a result of road roughness and vehicle dynamic properties. The variation from the static weight can be up to 100% and is commonly of the order of 20%. Hence, conventional Weigh-in-Motion (WIM) systems had limited accuracy for estimating static weights, in particular for legal purposes. European road authorities required more accurate and reliable systems to weigh vehicles in motion, preferably at low cost and under a wide range of environmental conditions. Large European research projects such as WAVE (**W**eigh-in-Motion of **A**xles and **V**ehicles for **E**urope) (Jacob et al. 2000) have taken place to effect a significant step forward in the development of WIM technology, specially in the fields of fibre optic sensors, multiple-sensor WIM and Bridge based WIM systems.

Bridge WIM (B-WIM) systems were initially introduced in the United States in the late 1970's (Moses 1979). Instrumented bridges can be used to determine the weights of vehicles at full highway speed. Generally, axle weights are obtained from the information supplied by strain gauges placed under the bridge deck and axle detectors on the road surface. Some B-WIM systems can obtain axle weights solely from strain measurements without any need for an installation on the road surface. As in road WIM sensors, dynamics is identified as an impediment to improvements in accuracy. In addition to the dynamics of the truck, the bridge and the interaction between both has been reported as a major potential for inaccuracy in B-WIM systems (O'Brien et al 1999b). However B-WIM offers the possibility of measuring the effect due to the dynamic wheel forces over an extended period of time and for different points of the bridge structure. This amount of information can be fully exploited to improve the estimation of static weights and gain information on the truck and bridge dynamic behaviour.

The principal objective of this thesis is the development of more accurate B-WIM systems through new algorithms. The sub-objectives have been:

- Numerical modelling of the dynamic vehicle/bridge interaction problem for a better understanding of the parameters influencing the bridge response.
- The implementation of a finite element technique to simulate the passage of a vehicle over a bridge.
- The collection of data at different B-WIM sites for testing the accuracy of a B-WIM system on the field.
- The collection of data in a B-WIM site during a period of two weeks and the development of software to process this data into traffic characteristics on a continuous basis.
- The theoretical testing of a number of B-WIM algorithms for different types of trucks, road profiles and bridge models.

Chapter 2 is devoted to the applications of Weigh In Motion data, as well as an introduction to Weigh In Motion systems. The use of WIM data for bridge and pavement applications, road planning and management purposes, and for the enforcement of illegally

overloaded trucks is discussed. The basic types of WIM systems (bending plates, strip sensors and multiple sensor WIM) and their levels of accuracy are described.

Chapter 3 provides an explanation of existing Bridge Weigh In Motion algorithms. In recent years, Bridge weigh-in-motion systems have seen different approaches to the calculation of axle weights. Some efforts have concentrated on a better definition of the input variables to the static algorithm as defined by Moses (1979). Accordingly, influence lines have been corrected experimentally, signal filtering has been improved and the sensitivity of the algorithm to axle spacing and speed has been minimised through the application of optimisation techniques. Other research has focused on the development of a dynamic algorithm. The formulation and some accuracy results for these contributions are reviewed.

Chapter 4 describes the hardware and software involved in B-WIM systems. Various aspects of the installation are examined. Strain gauges/transducers or mechanical strain amplifiers can be used to measure the bridge flexure. From the point of view of axle detection, B-WIM systems can use sensors mounted in/on the road surface (pneumatic tubes, tape switches or low-grade piezo electric sensors) or in appropriate sites, strain readings can be used to identify axles (Free of Axle Detector systems). The Australian, Slovenian and Irish B-WIM systems are introduced.

Chapter 5 deals with the problem of dynamic modelling of a vehicle passing over a bridge. In B-WIM practice, vehicle loads can only be found through the measurement of the bridge response (i.e., strains). This chapter analyses the difficulties involved in determining applied forces by simulating the data available for a B-WIM calculation. The bridge is idealised as a prismatic beam, for which the differential equations of motion are solved by numerical methods. The truck has been modelled as a two-axle linear sprung body. The body is represented by a distributed mass subjected to rigid-body motions. Vertical displacements and pitching rotation are considered. Tyres are treated as linear elastic spring components. Linear spring and damping elements are used to simulate the suspension at each axle. The model takes account of the vehicle speed, dynamic behaviour of vehicle and bridge, and road roughness (generated from a power spectral density function). This four degree-of-freedom vehicle and continuous beam model offers an easy numerical implementation (In addition to reduced computer time and computer memory

storage) for preliminary studies on the influence of different bridge, truck and/or road parameters on the dynamic response.

A more sophisticated eleven degree-of-freedom model developed and validated experimentally by Green et al (1995) is also briefly introduced. The results of this four-axle vehicle model will be used in a later chapter for testing the B-WIM algorithm. In Chapter 5, Green's models are analysed for two types of suspension: steel-spring and air-spring, and different road conditions (suspensions are treated as non-linear devices that dissipate energy during each cycle of oscillation).

The finite element method is covered in Chapter 6. It is obvious that a simple beam model can not represent two- or three-dimensional behaviour, particularly in the case of a moving vehicle with paths that are not along the centreline of the bridge. For those reasons, Chapter 6 describes a finite element technique that enables bridges to be modelled with plate and beam elements and to interact with two- or three-dimensional vehicle models. This sophisticated modelling allows for a large number of different parameters to be considered such as:

- Number of vehicles, their number of axles, speed, wheel path on the bridge and characteristics of each vehicle (including mass distribution, elements to model suspension and tyre, etc.).
- Characteristics of the bridge structure, such as the bridge geometry, support conditions, and mass and stiffness distribution.
- Pavement roughness prior to and on the bridge, and other singular large irregularities such as a joint.

A number of bridge finite element models are designed for theoretical testing of B-WIM accuracy. These three-dimensional models are a simply supported isotropic slab, two-span isotropic slab, slab with edge cantilever, voided slab deck, beam and slab, skewed bridge and a cellular bridge type. Some models incorporate end diaphragms that provide lateral support and greatly affect the lateral bending and torsional characteristics of the bridge. MSC/NASTRAN for Windows software was used to model vehicles and bridges. This software provides the capability to determine transient dynamic response. A program was developed in C++ to perform simulations of truck models crossing a bridge. The code

generates the interaction conditions to be read by NASTRAN for any arbitrary one-dimensional or spatial bridge and vehicle finite element models. Simultaneous traffic events running in the same or opposite directions can also be specified. These simulations will be used to assess the accuracy of the BWIM algorithm in Chapter 9.

Chapter 7 is focused on the development of new algorithms for the calculation of weights in Bridge Weigh In Motion systems. Conventional static bridge WIM algorithms might not be very accurate due to vehicle dynamics, bridge vibration and dynamic interaction of the vehicle and the bridge. A least squares error minimisation approach is generally used to calculate the axle loads which give a best fit between theoretical and measured strains. This function has an averaging effect on the dynamic variation of the load and has been shown to be moderately accurate (O'Brien et al. 1999b). An approach to the dynamic problem could be the prior removal of the dynamic components of the signal. However, this is not always possible without also removing part of the static response. For example, low-pass filtering can remove frequency components of the static response at relatively high frequencies depending on the shape of the influence line and the truck axle configuration.

An alternative dynamic bridge WIM system based on a frequency spectrum approach is presented in this chapter. A bridge allows for the collection of a lot of readings and a good definition of the frequency components of the signal. This algorithm does not require any prior knowledge of the bridge influence line. Other algorithms have been developed in the time domain to solve the inverse problem of the bridge-truck interaction models described in Chapter 5. They seek to correct the deviation from the static weight that bridge and truck dynamics can introduce in the measured strain. The formulation described here uses theoretical bridge and truck dynamic models whose parameters can be estimated by minimising the difference between the predicted strain spectrum and the measurement spectrum. These algorithms are based on the mathematical solution for simple cases of moving loads on bridges (i.e. constant loads or sprung masses in an iterative process). Other algorithms are based on an approximate solution, i.e., modal decoupling as suggested by Dempsey (1997).

The dynamic approach is further extended in Chapter 7 with the use of multiple sensors. Bridge WIM systems had used sensors at one longitudinal location (normally at midspan)

until recently, when Kealy and O'Brien (1998) extended the algorithm to the use of several sensors along the length of the bridge. This approach provides the complete distribution of varying axle forces as the truck traverses the bridge but it has limitations in the number of axles that can be weighed simultaneously due to the dependency of the equations relating applied load to measured strain. These limitations are overcome with further considerations on the treatment, number and location of the strain readings. Furthermore, calibration of a B-WIM system tends to be highly dependent on the properties of the truck used for the process. The sensitivity of the results to the differences in the properties of the truck being weighed and those of the calibration vehicle are also investigated.

Chapter 8 assesses field measurements from B-WIM systems, using data from experiments carried out on bridges in Ireland, Sweden, France and Slovenia. Each of these sites has different environmental, traffic and structural characteristics: short span skew bridge in Ireland, two-span integral bridge in Sweden, long span continuous box-girder in France and simply supported medium span in Slovenia.

In Delgany (Ireland), one vehicle of known weight is passed over the bridge several times at different speeds and small variations in lateral position on the road to calibrate the system. For any Bridge WIM system, based on static or dynamic principles, there is a difficulty in obtaining an accurate system calibration. In static terms, the calibration consists of determining an accurate influence line for the bridge. This is often determined by scaling and/or adjusting a theoretical influence line to give a best fit of measured to theoretical results for the calibration vehicle. For a dynamic algorithm, an attempt can be made to characterize the bridge in a similar way. A new calibration method based on the representation of the experimental record in the frequency domain is presented. The method allows for an easy adjustment to allow for uncertainties in such items as the sensor sensitivity, the shape of the unit response or the bridge boundary conditions.

For the first time, Bridge WIM data was collected to calibrate the Eurocode for bridge loading for Irish conditions (O'Brien et al. 1998b). A specific program was developed by the author for the purpose of processing the traffic data from road and strain sensors into vehicle velocity, classification and weights on a continuous basis. The effect of accelerating/braking forces on B-WIM accuracy is also analysed.

In Belleville (France), the performance of a B-WIM system is tested in a two-span bridge, 110 m long. The problem in this bridge is threefold: significant dynamics, the allocation of the truck along the bridge, and difficulty in identifying the effect of individual axles in a long bridge. All these factors are aggravated by the likely presence of simultaneous traffic events. Piezo-electric sensors were used as permanent axle detectors, and the bending of the bridge was measured with strain gauges glued to the steel stiffeners. An instrumented truck participated in the experiment.

The bridge in Luleå (Sweden) has a two-span reinforced concrete section, with a total length of 30 m. The Irish B-WIM system was tested at this site in extreme climatic conditions (minus 30 degrees Celsius). The instrumentation was composed of mechanical strain amplifiers, rubber tubes for detecting axles and data acquisition equipment. For the purposes of calibrating, two vehicles were passed over the bridge several times at different speeds with small variations in lateral position on the road. Finally, the multiple-sensor B-WIM algorithm was tested in a 32 m Slovenian bridge, where sensors were spaced longitudinally every 4 m. The load history for two vehicle configurations is represented.

In Chapter 9, simulations from Chapters 5 and 6 are used to determine the best algorithm for calculating the static weights of moving trucks. Truck configurations with three different loading conditions and speeds are crossed over different bridge finite element scenarios for testing. Additionally, the bridge response for a one-dimensional bridge model when traversed by three combinations of speed and weight for two-axle and four-axle trucks is provided from an independent source (Green, Queen's University, Kingston, Canada). The influence of bridge structural behaviour, sensor location, vehicle suspension and road profile on the performance of each algorithm is analysed. Accuracy results for different algorithms are given according to the classification system of the COST323 European Specification on Weigh-In-Motion of road vehicles.

The last chapter is devoted to final conclusions. Several appendices are also included at the end of the text, which facilitate the comprehension and application of the various theories included in the main text. They include definitions, specifications, graphs, tables, and mathematical treatments, as well as basic principles of data acquisition, signal processing, structural analysis and computer programs.

2

WEIGH IN MOTION

2.1 INTRODUCTION

Transport plays a major role in the social welfare and economic growth of a community. Governments are responsible for this network and they must ensure that people can carry out their activities in safe and effective conditions. Most of this transport is provided by road infrastructure, which are severely damaged by heavy goods vehicles. If knowledge of the traffic composition was improved, the design, construction and maintenance costs of roads and bridges could be decreased. In addition, the reduction of trading barriers between European countries and the demand for ensuring fair competition have emphasised the need for more strict vehicle weight control. Traditionally, this task had been carried out by static weighing scales. However, this system only gets information on a reduced number of vehicles and the search for new more effective procedures has become a priority in the policy of many road authorities, particularly in Europe.

Weigh-in-Motion (WIM) is the technology that appeared to overcome the limitations of static weighing scales. A first division of WIM systems can be made by distinguishing On-Board WIM from Pavement or Bridge based WIM. The first group computes gross vehicle weight solely from measurements of force and acceleration taken through equipment in the vehicle. The second group consists of measuring wheel effects in sensors mounted in or on the road pavement or on an existing bridge structure, and estimating the corresponding static loads with appropriate algorithms. Depending on the speed of operation, pavement WIM systems can be classified in two basic categories: low-speed WIM (LS-WIM) and high-speed WIM (HS-WIM). A LS-WIM system is installed in a specific weighing area where vehicles are diverted from traffic flow and weighed at speeds lower than 15 km/h. These systems are accurate enough for legal enforcement and road pricing. A HS-WIM system is installed in the traffic lanes and continuously collects data on truck weights, speeds, time of travel, axle configurations and traffic patterns as they pass at normal speeds. The main advantage of HS-WIM systems is that all trucks are recorded with

minimal or no interruption to the traffic flow. The information provided by these systems is used in statistical calculations relating to pavement, bridge and road management applications.

2.2 THE DEVELOPMENT OF WEIGH IN MOTION TECHNOLOGY

Research on WIM systems for the estimation of vehicle weights as they travel at full speed has been going on since the 1950's in the United States. Early studies measured the mechanical strain induced in load cells and highway bridges to derive the corresponding weights. In the 1960's and 1970's, the digital computer made it possible to handle the large quantity of data supplied by these sensors. In the 1970's and 1980's sensors embedded in or placed on the road became commercially available. In the mid-1990's, On-Board WIM started to be an object of study under contract with the American Federal Highway Administration (FHWA)[1]. A large quantity of WIM data has been collected within the Long-Term Pavement Performance (LTPP) program in the US[2].

France and the UK initiated the development of WIM in Europe in the 1970's. Some European countries expressed a great demand for WIM, and in 1992, the Forum of European Highway Research Laboratories (FEHRL) underlined WIM as a priority topic for co-operative actions to be supported by the DG VII of the European Commission. As result, COST323 (WIM-LOAD) (1993-1998), part of the COST (**C**o-**O**peration in **S**cience and **T**echnology) Transport programme, was initiated as the first European co-operative action on Weigh-In-Motion of road vehicles. Its objective was to promote the development and implementation of WIM techniques and systems throughout Europe. Another objective was to provide a significant step forward in the understanding of WIM performance and applications with respect to road network manager's and decision maker's requirements. It was also necessary to harmonise and explain the best practice of WIM for the users and vendors, as well as to fix the vocabulary to facilitate communication between them. The main objectives of the COST323 action were (Jacob 1998a):

- Inventory of WIM requirements in Europe.
- Collection and evaluation of existing WIM information.
- Preliminary work on the development of a European technical specification on WIM.

- Agreement of mechanisms and protocols for a pan-European database of WIM sites and data.
- Collection and dissemination of scientific and technical information.
- Exchange of experiences and conclusions from other international projects.
- Recommendations on the application of WIM to enforcement and traffic management, bridge and pavement engineering.

A reduced glossary of WIM terms and European Specification on WIM, a result of the COST 323 action, are given in Appendices A and B respectively.

Another large European research project, WAVE (**W**eigh in motion of **A**xles and **V**ehicles for **E**urope) supported by the European Commission, started in 1996 with a duration of two years. The project was organised in four main packages (Jacob 1999):

- Accurate estimation of static weights using WIM systems: Multiple Sensor WIM and Bridge WIM.
- Quality, management and exchange of WIM data: WIM data quality assurance, and WIM data format and database structures.
- Consistency of accuracy and durability: durability of WIM systems in cold climates and calibration of WIM systems.
- Optical WIM sensors, technology for the future: sensor design, optoelectronic head, and data acquisition and processing unit.

Nowadays, there are about 1000 WIM stations working around the world of which approximately 45% are in the US, 30% in Europe and 15% in Australia. Figure 2.1 shows the countries participating in the COST323 action and WAVE projects and the approximate number of WIM sites in Europe. More information about the COST323 action or the WAVE projects can be found in their web sites[3,4,5].

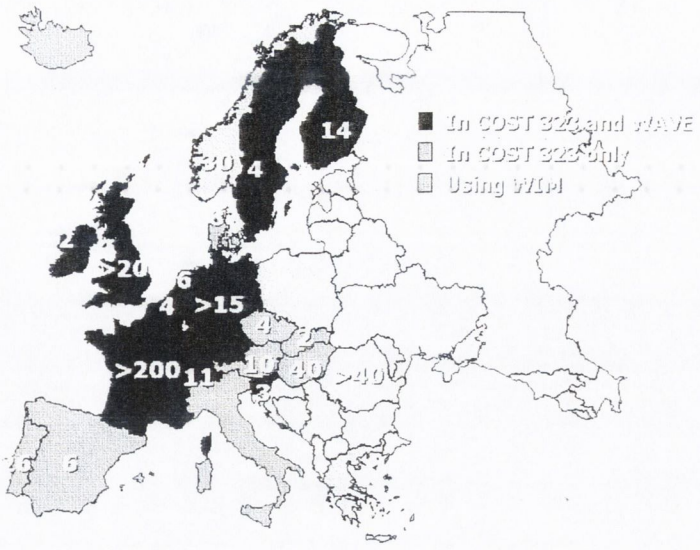

Figure 2.1 – Approximate number of WIM stations in Europe[6]

2.3 STATIC WEIGHING SCALES

Until the appearance of WIM systems, static weighing was the only way to detect overweighing. The dissuasive effect caused by static scales was small as only a reduced number of vehicles could be intercepted, stopped and diverted to static weighing areas. Compared to a WIM system, a static scale can store and retrieve additional information on customers, products, hauliers, driver Ids, vehicle registrations, trailer Ids, stored tares for tractors and trailers, suppliers and destinations. Some of these features can be obtained with WIM systems if used in combination with video (Henny 1999).

A truck scale consists of a scale frame that supports the weight of a truck without major bending, load cells, junction boxes and a weight indicator. There are two types: Stationary platform scales and portable wheel load scales. The accuracy of both systems makes them eligible for enforcement purposes.

2.3.1 Platform Scales

As the truck rolls on to a scale, the load cells register the pressure from the wheels. Each load cell converts this pressure into an electrical signal through strain gauges placed on its surface with special adhesives. As the surface to which the gauges are attached becomes strained, they stretch or compress changing their resistance proportionally to the applied load (Figure 2.2(a)). The precise positioning of the gauges, the mounting procedure, and

the materials used all have a measurable effect on overall performance of the load cell. The electronic signals from all of the load cells are sent out to junction boxes. Junction boxes sum all of the signals into one indicator that shows how much the truck weighs.

These traditional scales are available in a wide range of sizes and weighing capacities, in both pit-mounted and surface-mounted versions, with steel or concrete platforms (see Figure 2.2 (b)). A platform scale gives a typical maximum permissible error band of 0.5% for the gross vehicle weight. However, as vehicles must be stopped on the scale, the weighing system is time consuming and inconvenient for drivers. WIM systems overcome this problem, but their calibration and testing still depends on the information supplied by a reliable static weighing scale.

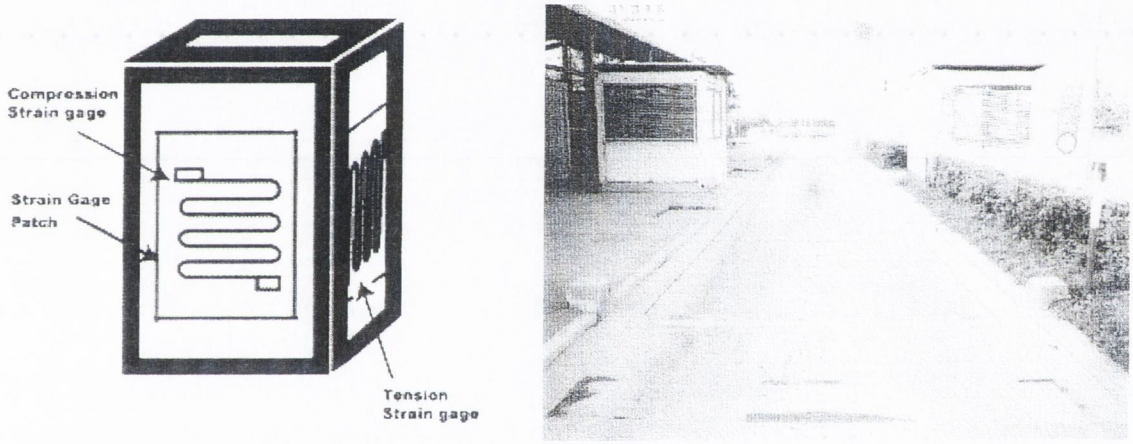

(a) Strain gauges (b) Static platform

Figure 2.2 – Static weighing

2.3.2 Portable wheel load scales

Portable wheel load scales have been developed to allow for measuring wheel and axle loads as well as gross vehicle weights. They are also used for spot checks. Each wheel is measured individually, but their precision is somewhat lower than platform scales. Depending on how many scales are used, additional errors may occur because of weight transfer between axles in vehicles with 3 or more axles. The sources of these errors are:

- Longitudinal tilting of the vehicle
- Wrong sensor levelling
- Site evenness

- Sensor tilting
- Mechanical friction in the suspension
- Residual friction forces induced by braking

The influence of these factors in the results in axle group or gross vehicle weight is reduced by using the same number of scales as number of wheels in an axle group or in the whole vehicle. A set of 6 wheel load scales can achieve a maximum error band of less than 1% in gross vehicle weight, but they are slow and require a lot of labour. A set of 2 wheel load scales can achieve a maximum error band between 1% (good site and vehicles in good condition) and 3% (average site and vehicles in poor condition) in gross vehicle weight (Scheuter 1998).

2.4 PAVEMENT BASED WEIGH-IN-MOTION SYSTEMS

Today there exist many pavement WIM systems all competing in a diverse and highly competitive market. As mentioned in section 2.1, these systems can be divided into LS-WIM and HS-WIM systems. The latter systems are not as accurate as the former, but they allow recording of all vehicles uninterruptedly.

HS-WIM systems can be pavement or bridge based. Bridge WIM (B-WIM) will be discussed in later chapters. Pavement systems are sensors on or embedded in the road surface which record axle weights as a truck travels across the sensor at normal highway speeds. Their accuracy levels are not as good as low-speed systems, and they depend on the quality of the sensor, site location and approach. These WIM sensors can be divided into two categories according to their width: Bending plate and strip sensors. Unlike bending plates, the width of a strip sensor only covers a portion of the whole tyre. Hence, the wheel load is estimated from integration of the signals corresponding to the parts of the wheel acting on the strip at each instant. These sensors are sensitive to factors such as truck dynamics, road unevenness and temperature, which must be taken into account during the calibration of a WIM system. Recent developments show that the estimate of the static axle weights can be improved by combining an array of individual sensors. This procedure, known as Multiple-Sensor WIM (MS-WIM), is reviewed in the last sub-section.

2.4.1 Low-speed WIM

LS-WIM systems are commonly weighing scales which utilise strain gauges or load cells. These systems provide the high level of accuracy needed for enforcement or road pricing. They are based on the same principle as static weighing. Vehicles must also be taken aside by the police towards an area beside the roadside. However, vehicles are weighed while driving at a speed about 10 km/h over the system, and this makes possible the weighing of about ten times as many vehicles as static weighing. They can be portable or fixed. The fixed systems are based on platforms mounted in an excavation. The weighing platform should be longer (□ 30 m) than for static weighing (□ 15 m). The full plate LS-WIM maximum permissible error band is between 1 and 5%. 1% relates to a perfect fixed installation with vehicles in good shape, and 5% to a good mobile system with access ramps on an average site and vehicles in poor condition (Scheuter 1998).

Portable system

Portable LS-WIM systems are installed on a flat area with a ramp approach as illustrated in Figure 2.3.

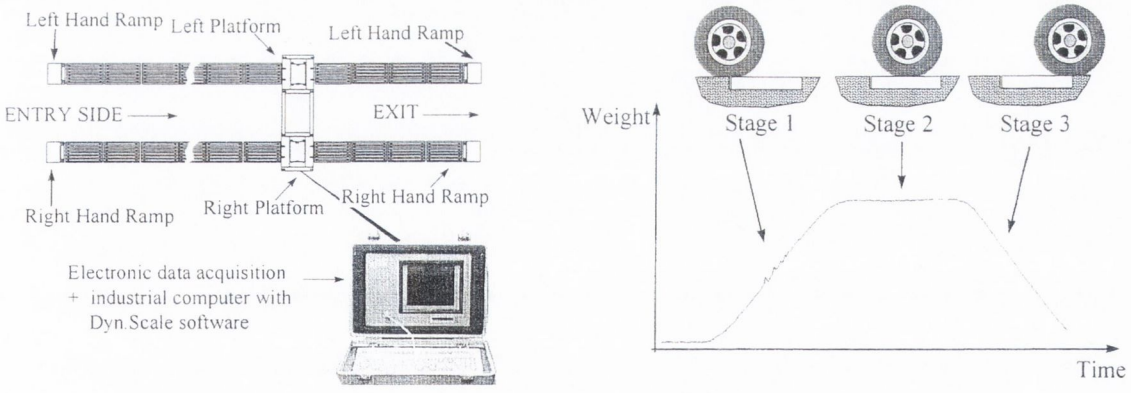

(a) Portable low-speed system by Captels

(b) Recorded signal during the passage of an axle across the scales

Figure 2.3 – Low-speed WIM systems (after Dolcemascolo et al. 1998)

Through different tests, the need has been proven for a long ramp prior to the scales to avoid dynamic effects induced when an axle mounts the system. The ramp length after the scales should be greater than the axle spacing between extreme axles, to avoid oscillations induced when the first axle passes off the ramp. A distance of 30 m before the approach ramps is also required. It follows that the total site should be at least 70 to 80 m long.

There is also an influence of speed on final results: loads may be overweighed at speeds lower than the ideal speed and underweighed at higher speeds. This problem can be overcome through a software modification. This portable version could meet the requirement for overload enforcement with a careful implementation and an increase in its reliability (Dolcemascolo et al. 1998).

The semi-fixed version is based on scales installed in excavations, but without a ramp approach. This system should satisfy the required accuracy without the inconvenience introduced by the ramp.

2.4.2 High-Speed Bending plate

High-speed WIM systems collect continuous data that can be used for statistical purposes, while minimising traffic disturbance. One of the most accurate systems is the Bending plate. These plates are made of steel or aluminium with strain gauges attached to the underside. The width of a plate is big enough to take a complete pair of wheels. Figure 2.4(a) shows the dimensions and components of a commercially available bending plate system, and Figure 2.4(b) illustrates a bending plate after installation.

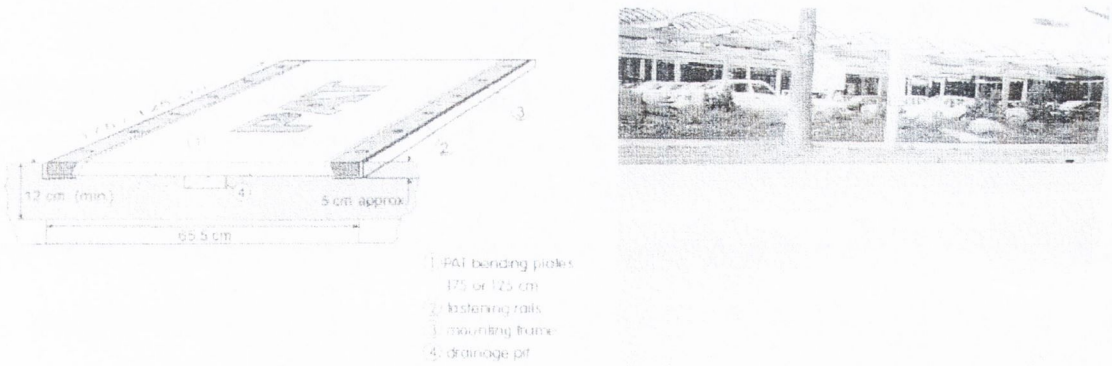

(a) Bending plate by PAT (after Hallström 1999)

(b) Bending plates at Zurich test site[6]

Figure 2.4 – Bending plate WIM

2.4.3 High-Speed Strip Sensors

Strip sensors are high-speed WIM systems. They provide a more economical solution than bending plates, though their results are not generally as accurate. Strip sensors available today are capacitive, piezoelectric, quartz and fibre optic. The physical properties of each

type will govern their performance under real traffic loading. Sophisticated algorithms are being developed to improve overall accuracy through the use of an array of strip sensors (MS-WIM).

Preparing the highway and placing the sensors is one of the most expensive elements of any WIM system and it also has a major impact on their final performance. Some sensors can be placed on the roads while others must be installed in a slot cut in the road surface and bonded in place using epoxy resin. These weighing sensors are usually used in combination with inductive loops or piezoelectric axle detectors that provide data on vehicle speed, chassis height and length.

Inductive loops

Loop detectors operate on the principle of electrical inductance, the property of a wire or circuit element to induce currents in isolated but adjacent conductive media. An electromagnetic field is generated around the loop when driving an alternating current through the wires. When a car passes through the field, it absorbs electromagnetic energy and simultaneously decreases the inductance and resonant frequency of the loop, which indicates the presence of a vehicle.

Capacitive systems

Capacitive systems consist of two or more parallel steel plates separated by a dielectric material encased in a rubber housing. As a wheel passes over the sensor, the upper plates deflect and the change in capacitance is proportional to the applied load. Figure 2.5(a) shows the installation of an array of capacitive sensors.

Piezoelectric systems

Piezoelectric sensors are made of a conductor surrounded by highly compressed pressure-sensitive piezoelectric material. An increase in pressure on the sensor provides a measurable voltage that can be used for vehicle detection, speed detection, vehicle classification and weighing. A charge is only generated when the forces are changing, so if a constant force is applied, the initial charge will decay.

Quartz crystal

The quartz sensor is based on a change of its electrical properties as a function of the applied stresses. The quartz elements are mounted in a specially designed aluminium extrusion. This section maximises the transfer of vertical load onto the sensing elements whilst preventing lateral pressures from influencing the measurements (Hoose & Kunz 1998). An example of this system on site is shown in Figure 2.5(b).

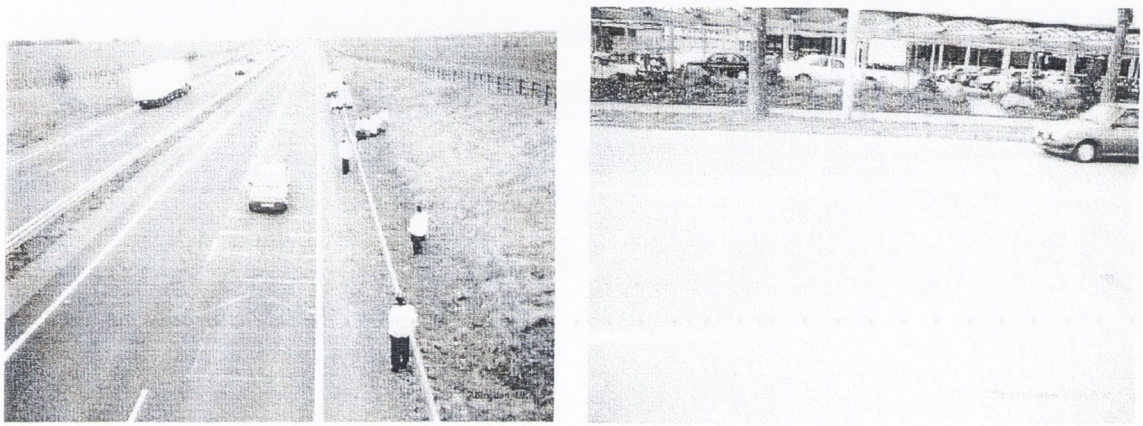

(a) Capacitive strip multi-sensor array at Abingdon, UK

(b) Quartz and Piezo-ceramic sensors at Zurich test site

Figure 2.5 – Installation of strip sensors[6]

Fibre Optic

A fibre optic sensor ribbon is made of two metal strips welded around an optical fibre as illustrated in Figure 2.6(a). The sensor principle uses induced photoelastic properties in glass fibre under a vertical compressive force. This induces the separation in two propagating modes: a vertical faster mode and a slower horizontal mode. The pressure transferred to the optical fibre creates a phase shift between both polarisation modes, which is directly related to the load on the fibre. Some of the advantages of fibre optic sensors include good operation from stationary vehicles to speeds over 40 m/s, low temperature dependence, electromagnetic immunity, easy installation, no requirement for electric supply and data processing in real time. Field tests indicate a good behaviour of sensors in a two year test with heavy traffic (Caussignac and Rougier 1999). This technology can evaluate parameters such as tyre pressure (Figure 2.6(b)), vehicle acceleration or suspension condition.

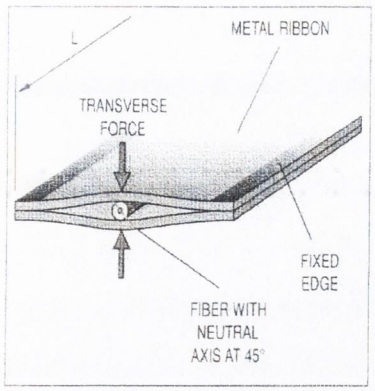

(a) Scheme of the sensor element

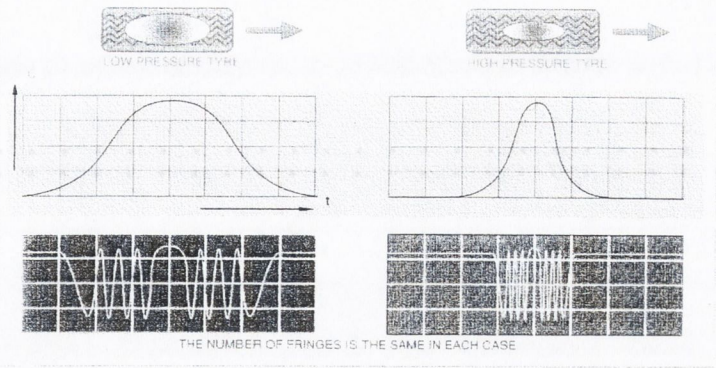

(b) Weight signature and pressure tyre influence for an identical weight at different pressures

Figure 2.6 – Fibre Optic Technology (after Caussignac et al. 1998)

2.4.4 Calibration of Pavement Systems

The European specification on WIM gives guidelines on how to calibrate Pavement WIM systems in relation to the calibration method, site, vehicles, loading conditions, speed and number of runs. The calibration of a WIM system with respect to the static load, is commonly based on the hypothesis of proportionality between the static gross vehicle weight of the calibration trucks and the sum of the dynamic axle loads measured in motion by the system. This constant of proportionality is the calibration factor (C), which can be obtained by minimising the mean square error between dynamic and static loads. Equation (2.1) shows how this factor is calculated (COST323 1997).

$$C = \frac{\sum_i n_i}{\sum_i \left[\frac{\sum_{j,k} Wd_{ijk}}{Ws_i} \right]} \qquad \begin{array}{l} i=1,\ldots number\ calibration\ trucks \\ j=1,\ldots number\ runs \\ k=1,2\ldots number\ of\ axles \end{array} \qquad (2.1)$$

where Ws_i is the static gross weight of the calibration truck i, n_i the number of runs of truck i, and Wd_{ijk} the measured dynamic load of axle k for run j in truck i.

If used for enforcement, calibration will have to be improved removing almost all the bias on axle and gross vehicle weights. However, there are difficulties with a calibration based on static axle weights due to the dynamic character of the applied wheel load. The deviations from the static value will depend on the truck dynamics, speed and the road

profile, and so, even very smooth roads and good suspensions induce a variation of at least ±10%. Therefore, some systems are sensitive to temperature variations or need a new calibration after a certain period of time. These aspects and some other interesting features are briefly reviewed in the following subsections.

Spatial Repeatability

Jacob and Dolcemascolo (1998) show how the maximum ratio of dynamic impact force to the static weight (maximum *IF*) may easily reach 1.25 to 1.5 on a rather smooth pavement, and up to 2.0 (air suspension) or 2.5 (steel suspension) on a rough pavement. This is the motivation of the site classification proposed in the European specification on WIM (COST323 1997). If the same vehicle passed the same road path several times at the same speed, the total applied axle force would present a similar pattern in a phenomenon known as spatial repeatability (Figure 2.7(a)). If one vehicle passed several times at different speeds the curves are more scattered as shown in Figure 2.7(b).

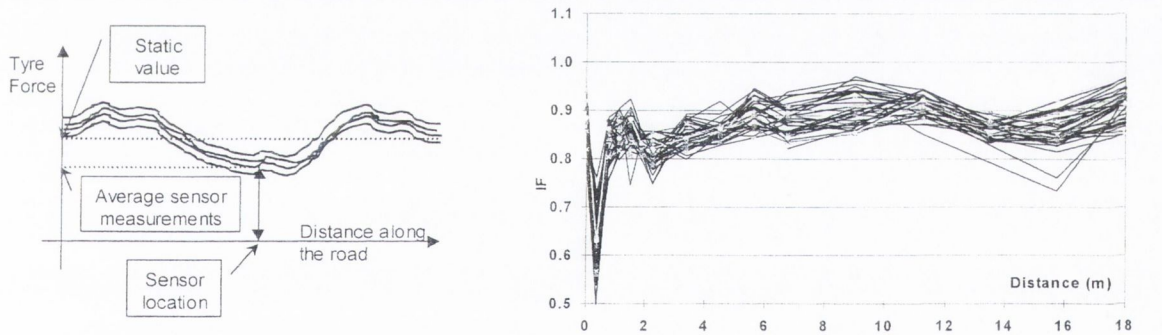

(a) Pattern of spatial repeatability

(b) Patterns of spatial repeatability for 40 passes at all speeds (after Jacob and Dolcemascolo 1998)

Figure 2.7 – Effect of spatial repeatability on the calibration of a single WIM sensor

The curves become more scattered if using more than one only vehicle. If different axles of different vehicles travelled along the same road profile at different speeds, the tendency to present a similar load pattern is known as statistical spatial repeatability (O'Connor 1996, O'Connor et al. 1999). This phenomenon is explained by the averaging of the individual vehicle characteristics while the pavement effect becomes dominant as the size of the sample increases. The effect of spatial repeatability can be minimised by MS-WIM systems that obtain results at different road sections.

Instrumented trucks

The instantaneous dynamic axle force measured by an instrumented truck and the value measured by a WIM system can be compared for a more accurate calibration. This possibility was studied by VTT (Technical Research Centre of Finland) as part of the WAVE project (Huhtala 1999). Dynamic wheel forces are matched to the WIM systems using an electric eye to detect reflective tapes glued across the road lane. Figure 2.8 shows the axle forces measured by a WIM system (bending plate) versus the instantaneous dynamic wheel measurements.

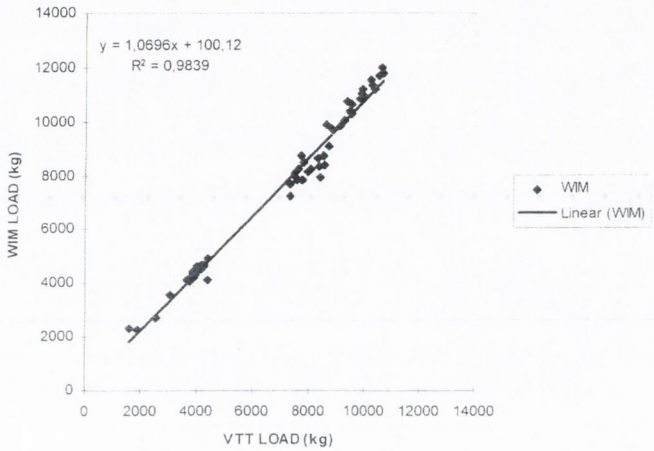

Figure 2.8 – Dynamic axle loads measured in the vehicle and by a WIM system (after Huhtala 1999)

The instrumented vehicle is a 3-axle rigid truck with a rear tandem, and axle static weights: 6000, 8800 and 7200 kg. The static values in all the runs of the figure are the same, but the dynamic loads are different due to changes in speed. The scatter is introduced by inaccuracy of the WIM system and/or the instantaneous wheel load measurement.

Environmental conditions

Many narrow strip sensors are sensitive to temperature. Further, they are affected by variations of the resin modulus and pavement support in which they are fixed. This is why they need periodic calibrations. An automatic self-calibration procedure was developed to avoid this inconvenience (Stanczyk & Jacob 1999). This procedure is based on the identification of characteristic vehicles from the traffic. Then, typical weights are adjusted to target values of these characteristic vehicles from a statistical knowledge of traffic.

Stanczyk (1999) points out mean bias in the determination of static axle load for several WIM sensors due to load transfers from axle to axle for different truck categories. This bias is related to the vehicle dynamics and driving conditions, the local road conditions and the WIM sensor and system response. For example, WIM systems generally under-weigh first axles which could be due to aerodynamic and torque effects. As result, some corrections by axle to reduce the mean bias show a promising improvement in calibration procedures (Tierney et al. 1996).

2.4.5 Multiple-sensor WIM

Up to this, individual pavement sensors have been discussed. One sensor records the instantaneous load applied by a tyre, and a significant error in the determination of the static weight could take place as a consequence of the dynamic load oscillations. Different procedures have been used to reduce these errors based on the use of multiple sensors at different road sections: A simple average of all the sensor readings, a signal reconstruction method, and a maximum likelihood method have been tested and a neural network approach is under development. These procedures are described below.

Simple Average

Dolcemascolo & Jacob (1998) estimate static axle loads as the spatial mean of the impact forces measured over a sufficiently long path. Sensors are placed at uniform spacing to avoid any bias due to spatial repeatability, and they should cover a length in excess of the longest wavelength of the impact force signal. Axle loads are estimated by the average of the individual measurements of the sensors considered. The following formula (Cebon 1999) is used for the calculation of the optimum spacing (d) between sensors:

$$d = \frac{2V(n-1)}{fn^2} \tag{2.2}$$

where V is the mean traffic speed (m/s), n the number of sensors and f the mean bounce motion frequency. This formula was obtained by minimising the average quadratic error between the real and the estimated static weights computed by the average method and

uniformly spaced sensors, with the assumption of random distribution of speed and frequency around their mean value.

An increase in the length of the sensor array has a very strong influence on the accuracy of gross vehicle weight, as the averaging procedure smoothes the bias resulting from spatial repeatability.

Signal Reconstruction and Kalman Filtering method

A method for the estimation of the static axle load based on the reconstruction of its dynamic variation is proposed by Sainte-Marie (1998). The continuous signal representing the dynamic axle weight is generated from the discrete measurements given by each sensor through the use of different functions: trigonometric polynomials, non-harmonic Fourier series and cardinal series. Figure 2.9 represents the re-constructions from two simulated instrumented vehicles.

Static axle weight is estimated as the average of the reconstructed signal along a certain length. This length depends on the rolling and bouncing frequencies of the vehicles which are obtained through extended Kalman filtering. Further developments involve the consideration of load transfer from one axle to another, the road profile and truck interaction and the use of functions based on the eigenmodes of simplified vehicle models.

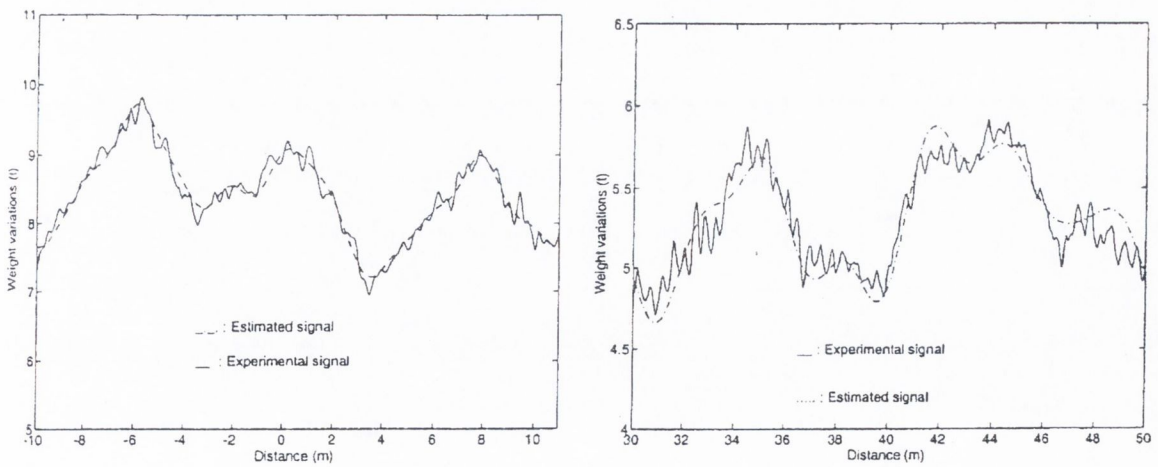

(a) Canadian truck with non-noisy measurements

(b) German trailer noise to signal ratio: 10%

Figure 2.9 – Reconstruction carried out with 13 samples (after Sainte-Marie et al. 1998)

Maximum likelihood technique

A probabilistic method based on the Maximum Likelihood estimator has been developed by a transporation research group in the University of Cambridge (Stergioulas et al. 1998, Cebon 1999). The Maximum Likelihood method adjusts the signal model parameters by maximising the probability that the estimated data is the correct one. Through the knowledge of the main oscillation modes of dynamic tyre forces, the method proposes two main generic vehicle models:

- A quarter car model representing about 80% of truck suspensions. These trucks have a main frequency corresponding to a body-bounce mode in the range 1.5-4.5 Hz. The vehicle model can be idealised by a constant (static weight) plus a single sine wave of low frequency. The model has 4 unknown parameters: static weight, and amplitude, frequency and phase of the sine wave. Hence, a minimum number of 4 sensors is necessary for the solution of the Maximum Likelihood calculation.
- A walking beam model representing about 20% of truck suspensions. These trucks have two significant frequencies. One corresponds to the body-bounce, while the other corresponds to an axle hop mode in the range 8-15 Hz. A constant plus two sinusoidal components of low and high frequency can approximate this model. A minimum number of 7 sensors is required in this case.

2.5 ACCURACY OF WEIGH-IN-MOTION SYSTEMS

The performance of a WIM system is best evaluated by testing. The quality of the results, performance and durability of the different systems can be best compared under the same environmental and testing conditions. Only long-term tests (over a full year) allow the WIM systems to be subjected to all seasonal conditions and their durability to be assessed. Test vehicles make repetitive runs over the test site, and the resulting WIM data is processed and compared with static weight measurements of the same vehicles. Alternatively, vehicles taken randomly from the traffic are weighed statistically and used to assess the WIM system accuracy.

The analysis of WIM results and accuracy classes defined here refers to the European specification for WIM of road vehicles (COST 323, 1997). The COST323 specification, like the ASTM standard, applies a statistical definition of accuracy using confidence

intervals. Other recommendations dealing with legal applications, such as the draft OIML (**O**rganisation **I**nternationale de **M**étrologie **L**égale) standard, define accuracy as maximum permissible error (Dunmill 1998).

The COST323 specification considers six classes of accuracy, A, B, B+, C, D and E with A being the most accurate. The accuracy class of a particular site is obtained from the confidence interval width (δ), mean (m), and standard deviation (s), of the errors in weighing a sample of n trucks. If the probability (π) of measuring results within a certain interval exceeds a specified minimum (π_o), this WIM system will comply with a given accuracy class. This minimum depends on the number of trucks, the duration of the test and type of test carried out. There are three kinds of environmental conditions: (I) repeatability, for a short test over a few consecutive days and the same climatic conditions, (II) limited reproducibility, for a test carried out over several days or weeks within the same season, and (III) full reproducibility, for a long term test over a year or more. There are four criteria for the type of test plan carried out during that time: (r1) full repeatability, if only one truck is used, with one load and speed, (r2) extended repeatability, if only one truck is used, but with several loads and/or speeds, (R1) limited reproducibility, if a small set of trucks are used, and (R2) full reproducibility, if a large set of trucks from the traffic flow are used, each of them passing only once on the WIM system. Appendix B gives a more detailed explanation of the statistical issues involved in this COST323 accuracy class classification.

The results presented herein show the great influence of the quality of the site on the accuracy of any WIM system. The best accuracy class met by a HS-WIM system on a trafficked road was B(10) on an excellent site. Best systems could not get an accuracy better than C(15) in average or good sites (Jehaes 1999a).

2.5.1 Long Term Test on Urban Road (Zurich, 1993-1995)

The first major European test took place on an urban road in Zurich (Blab et al. 1997, Jehaes 1999a). Various systems available on the commercial market were tested together. These systems included capacitive strips, piezo-ceramic strips, bending plates, piezoquartz strips and piezopolymer strips. The test had some limitations due to the reduced number of vehicle types, low traffic flow and speed in the particular urban conditions, the fact that

only gross vehicle weights were considered and the rather poor pavement conditions – class III site –. Best results were obtained by a bending plate system that achieved class C(15) as expected in a class III pavement. It revealed the strong need to improve the understanding of WIM system performance and influence of different environmental factors in further trials[7].

2.5.2 Alpine Tests (Switzerland, 1995-1998)

Two WIM systems were installed in different tunnels in main alpine transit routes in 1995: 4 capacitive strips in each direction in a class I site, and two bending plates in each direction in a class II site. Both systems were exposed to tunnel air conditions, use of salt and high concentrations of corrosive substances. The capacitive strips failed and were replaced by 2 piezoquartz strips, while the bending plate system survived over three years. The results in full reproducibility conditions (R2) were class C(15) for the capacitive and piezoquartz strips in one direction, and E(30) and D+(20) respectively in the other direction and environmental repeatability conditions (I). The strip sensor system in one of the directions was affected by the curvature of the road. Bending plates were in class B(10) and C(15) respectively for the north and south directions in limited reproducibility conditions (II) during three years (Jehaes 1999b).

2.5.3 Weigh In Motion Experience in Belgium (1994-1998)

Henau (1998) reports about the testing of four WIM systems installed on a motorway interchange (E42 and E411) at Namur, Belgium in July 1994. The systems were composed of inductive loops and a glass-fibre reinforced bar-type piezoceramic weight detector. E42 has a rigid structure comprising a continuous reinforced concrete pavement, and E-411 has a semi-rigid structure with a bituminous concrete pavement on top of a concrete base. These sites conform to classes II and III respectively. Accuracy class D(25) was obtained by the best system in limited reproducibility conditions (R1) and environmental repeatability conditions (I). This accuracy class is in accordance with a site class from II to III. However, all systems in the fast lane were in class E for full repeatability conditions (r1). The WIM system was affected by the presence of a local underpass some tens of metres upstream that induced some high vehicle dynamics.

2.5.4 Portable and Multiple-Sensor WIM systems trial (Trappes, 1996)

A short trial took place near Trappes, France in June 1996. A prelimirary draft of the COST323 European Specification on WIM was applied to the results. A MS-WIM system composed of piezo-ceramic strip sensors was installed in this class II site.

Sainte-Marie et al (1998) report on results on isolated axles by using the signal reconstruction technique referred to above (Axles of an axle group were not considered as their more complex dynamic behaviour is under study). In full reproducibility conditions (R2) and a sample of 34 five-axle vehicles (2 axles in the tractor and 3 in the trailer) from the traffic flow, the reconstruction technique based on 6 or 12 sensors achieved class B(+7) for the first two axles. For the same sample, a simple mean average leads to class B(10) with 5 sensors and B(+7) with 13 sensors. In the same scenario, Dolcemascolo and Jacob (1998) reported a study on MS-BWIM based on an averaging technique and uniform sensor spacing. Conclusions reveal that a number of sensors above 7-10 should increase the robustness of the results, rather than achieve a higher accuracy. Better accuracy can be achieved through improvements of the individual sensor performances.

Dolcemascolo (1999) evaluates the performance of the three different MS-BWIM approaches presented in 2.4.5 with the following conclusions:

- The Likelihood method based on two sine waves (LK2) is less reliable than the others.
- The Simple Average (SA) and Likelihood method based on one sine wave (LK1) have a good robustness and are less sensitive to noisy sensors.
- The accuracy of SA and LK1 methods are very similar.
- The signal reconstruction (SR) and LK2 method need more parameters and they are more sensitive to the number of sensors.
- Class A(5) was only obtained for single axles of two axle rigid trucks and a sub-array of 13 sensors.
- Accuracy of SR, LK1 and LK2 methods should improve with less noisy sensors.

During this trial, four portable WIM systems (3 capacitive mats and 1 capacitive strip) were also tested. All these systems felt into classes from E(30) to E(60). Their inaccuracy

was mainly due to the dynamic impacts induced in the axles of a group by the thickness of the sensors laid on the road.

2.5.5 The European Test Programme (1996-1998)

The COST323 action conducted a large-scale series of trials, the European Test Programme (ETP) (1997-1998), to evaluate the accuracy and durability of WIM systems. The main general objectives of the ETP were (Henau and Jacob 1998):

- Evaluation of WIM systems in various environments and over long term periods.
- Comparison of the WIM system performances with the requirements of the draft European specification and the users' needs and requirements.
- Acquisition of data for research and statistical studies.

These tests were carried out in two different environments: the Cold Environment Test (CET) in a main road in Northern Sweden (Luleå) and the Continental Motorway Test (CMT) in a heavily trafficked motorway in Eastern France. The first test site is related to the performance and durability of WIM systems in cold climates under harsh conditions (frost heave of pavement, mechanical impact of snowploughs, etc.), while the second site is more concerned with aggressive traffic conditions, representative of main European routes. The CET was the most significant large-scale trial ever organised in Europe and the results are summarised below.

The Cold Environmental Test

The Swedish National Roads Administration (SNRA) managed the tests in Sweden, and the Belgium Road Research Centre (BRRC) and Institute of Road Construction and Maintenance in Austria (ISTU) analysed the accuracy of the results. The traffic density at the site is 350 heavy lorries per day in each direction, and their speed limit is 80 km/h. The road has two lanes and a class II profile according to the European WIM Specification. The WIM systems being tested were: one Bridge system and four high-speed systems embedded in the pavement: a piezoceramic nude cable, one prototype combination of two piezoquartz strip sensors, a bending plate based on strain gauges, and a 'bending beam' prototype.

Jehaes and Hallström (1998) show the accuracy of results and their evolution over a complete climatic year. During each test, two types of population were examined: at least one calibration vehicle with several loads and speeds, and some post-weighed vehicles selected from the general traffic flow at random. Some of the systems did not work properly and all became somewhat less accurate during the winter period with temperatures below –30°C or spring due to the large variations of temperature in 24 hour periods. All of them recovered their initial accuracy during the following summer. Only the system based on quartz crystal piezoelectric bars was able to achieve an accuracy class C(15) for any period and vehicle test. The post-weighed vehicles are analysed in full reproducability conditions (R2), and the test vehicles in limited reproducability conditions (R1). The results of this system in full environmental reproducability conditions (III) are shown in Tables 2.1 and 2.2. In these accuracy tables, the first columns represent the statistics of the relative error *(Wd-Ws)/Ws*, where *Wd* is the predicted weight and *Ws* is the static weight, *n* is the number of data, *ide is* the percentage of correctly identified vehicles, *m* the mean and *s* the standard deviation. In the remaining columns, *class* represents the accuracy class for each criterion class, δ the tolerance of the retained accuracy class, δ_{min} the minimum width of the confidence interval for π_o, π_o the required level of confidence, and π the level of confidence of the interval $[-\delta,\delta]$.

Table 2.1 – Accuracy classification for general traffic during one complete year

(**n**: Total number of vehicles; **Ide**: Percentage of vehicles correctly identified by the system; **m**: mean; **s**: Standard deviation; π_0: level of confidence; δ: tolerance of the retained accuracy class; δ_{min}: minimum width of the confidence interval for π_0; π: Level of confidence of the interval $[-\delta,\delta]$)

	Relative error statistics					**Accuracy calculation**				
Quartz piezo – general traffic	**n**	**Ide**	**m**	**s**	π_0	**Class**	δ	δ_{min}	π	**Class retained**
Criterion		(%)	(%)	(%)	(%)		(%)	(%)	(%)	
Single axle	750	90	0.29	10.25	92.0	**C(15)**	20.0	18.7	93.9	**C(15)**
Axle of group	1721	91	1.41	10.02	92.4	**B(10)**	20.0	18.5	94.6	
Group of axles	838	91	1.41	7.33	92.0	**C(15)**	18.0	13.6	98.1	
Gross Weight	460	90	0.92	7.53	91.6	**C(15)**	15.0	13.9	94.0	

Table 2.2 – Accuracy classification for test vehicles during one complete year

(**n**: Total number of vehicles; **Ide**: Percentage of vehicles correctly identified by the system; **m**: mean; **s**: Standard deviation; π_0: level of confidence; δ: tolerance of the retained accuracy class; δ_{min}: minimum width of the confidence interval for π_0; π: Level of confidence of the interval $[-\delta,\delta]$)

	Relative error statistics					Accuracy calculation				
Quartz piezo - test vehicles	**n**	**Ide**	**m**	**s**	π_0	**Class**	δ	δ_{min}	π	**Class retained**
Criterion		(%)	(%)	(%)	(%)		(%)	(%)	(%)	
Single axle	361	83	2.58	5.48	93.7	**B(10)**	15.0	11.9	98.3	**C(15)**
Axle of group	845	95	5.19	10.29	94.2	**C(15)**	25.0	22.5	96.6	
Group of axles	368	95	5.40	6.42	93.7	**C(15)**	18.0	16.0	96.8	
Gross Weight	310	87	3.93	5.21	93.6	**C(15)**	15.0	12.5	97.7	

The bending plate obtained a final accuracy of D(25) (conditions R2, III) due to a lack of temperature compensation in the winter period. The system used temperature compensation in the summer achieving D+(20). The other two WIM systems being tested were in class E.

The Continental Motorway Test

The objectives of this test were to evaluate WIM systems commercially available in Europe over a period of 12 to 18 months, and to compare their performance on a smooth pavement against the proposed requirements of the current European Specification on WIM. In addition, the reliability of sensors, electronic equipment and software were being monitored. The test was carried out by CETE de l'Est and the Laboratoire Central des Ponts et Chaussées (LCPC) in France. The site is situated on the slow lane of the A31 motorway between Metz and Nancy with international traffic of 40000 vehicles/day of which 20% are heavy vehicles. The pavement is classified as class I according to the European specification for WIM. The different typologies of weighing sensors being tested were four piezo-ceramic bars, a piezo-ceramic nude cable and a capacitive mat. Magnetic sensors and inductive-loops were used for axle detection. Results are reported by Stanczyk and Jacob (1999).

The capacitive mat and one of the piezo-ceramic systems achieved class B(10), another two systems class C(15), and the other two class D+(20) and class E(30) in conditions of full reproducibility (R2) and environmental reproducibility (III). The results of the piezo-ceramic system are shown in Table 2.3.

Table 2.3 – Accuracy of the best system for all the pre-weighed traffic trucks

(**n**: Total number of vehicles; **Ide**: Percentage of vehicles correctly identified by the system; **m**: mean; **s**: Standard deviation; π_0: level of confidence; δ: tolerance of the retained accuracy class; δ_{min}: minimum width of the confidence interval for π_0; π: Level of confidence of the interval $[-\delta,\delta]$)

	Relative error statistics				Accuracy calculation				
Piezo-ceramic	n	m	s	π_0	Class	δ	δ_{min}	π	Class
Criterion		(%)	(%)	(%)		(%)	(%)	(%)	Retained
Single axle	1485	-1.77	8.02	92.3	B(10)	15.0	14.91	92.4	B(10)
Axle of group	1328	2.67	8.49	92.2	B(10)	20.0	16.18	97.2	
Group of axles	588	2.63	5.97	91.8	B(10)	13.0	11.85	94.5	
Gross Weight	686	0.61	4.60	91.9	B(10)	10.0	8.46	96.2	

The capacitive mat achieved B+(7) under the criterion of axle of a group. However, this system failed due to the presence of humidity in the link cables and in the mat and it had to be replaced twice along the test. Temperature changed during the tests in the different seasons between 2 and 31°C. The capacitive mat is insensitive to this variation while the piezo-ceramic bars corrected well through automatic self-calibration.

2.6 APPLICATIONS OF WEIGH IN MOTION DATA

National Road Administrations are the main users of WIM. There are different fields where governments can apply WIM data. I.e. development of design codes for pavements and bridges, assessment of traffic aggressivity for a pavement, road and traffic management, enforcement and road pricing.

And the requirements in accuracy of WIM systems will vary depending on their final application:

- Legal purposes: Better accuracy than 5% with respect to the static weights is required (Jacob and Stanczyk 1999). Low-speed WIM can provide accuracy results of A(5) and even better taking precautions during installation and operation of the system.
- Traffic statistics, traffic and road monitoring, and road infrastructure and design: High-speed WIM can achieve accuracy in the range of 10 to 25% which is fully accepted in these applications.

2.6.1 Pavements

The road network is one of the largest investments of any country. Design procedures require the prediction of the total traffic that the roads will carry over their design lives. The service lifetime and periodic maintenance will depend on the deterioration of the road structure, progressively damaged by heavily loaded vehicles. Thus, WIM data can lead to improvements in maintenance methods and more reliable pavement design.

Design

There is often assumed to be a linear relationship between damaging effect on the road structure and the number of repetitions, but the relationship between magnitude and damaging effect is a power law with a high exponent. The linear relationship depends on the type of axle (single, tandem or tridem axle) or vehicle and the pavement material and structure. The exponent depends on the pavement type. This exponent is often assumed to be 4, so a small increase in axle weight involves a high increase in road wear. WIM data can save material by providing a better knowledge of the load histogram.

Serviceability or driving comfort by the user, is a subjective concept which is difficult to evaluate. However, pavement design methods such as AASHTO give guides based on a specific total traffic volume and a minimum level of serviceability along a certain period. When the level of serviceability decreases below a certain value, overlaying or re-paving is deemed necessary.

It can be seen that the evolution of serviceability is difficult to predict, and the use of WIM systems for preventing overloaded axles can prolong the pavement life cycle.

Influence of WIM errors

Data from WIM measurements can be used to estimate the magnitude of axle loads and the number of repetitions. Collop et al (1998) have studied the effects of different types of WIM errors when estimating cumulative traffic for a design life:

- Calibration error, due to adjustments made every six months of any drifts in the WIM measurements.

- Random sensor error, due to the inaccuracy of the WIM sensors that might introduce random errors into the measurement.
- Errors due to differences between instantaneous dynamic and static loads

WIM systems must be re-calibrated with vehicle(s) of known axle loads. The impact factor (*IF*) is measured at each run and the mean of all *IF*'s is used to adjust the sensor calibration factors. The relative difference in mean *IF* between consecutive calibrations is known as the calibration error. The difference in mean *IF* indicates a drift in the WIM system, but it is often not possible to determine if this drift took place gradually or suddenly over a short period of time.

Calibration data from 13 WIM sites resulted in an average mean calibration error between 1 and 6% depending on the manufacturer, standard deviation of the calibration error of about 11% and random sensor plus dynamic load effect approximately 11%. If using a 4^{th} power law, these errors result in an over-prediction of 40% in the design traffic, and an increase in the pavement thickness of between 10 and 20 mm.

Future requirements

An extension on the information supplied by traditional WIM technology is recommended to predict rutting in upper layers, ravelling and cracking (Caprez 1998, George 1999). For example:

- Lateral position of the passing wheels, contact pressure and frequency of loading which are important for the use of visco-elastic pavement models.
- Vertical contact pressure and horizontal contact stresses to prevent deterioration mechanisms in upper layers.
- Type of tyre wheel: Rut is deeper under a single tyre wheel than under twin wheels.
- Road safety authorities have a great interest in data on tyre pressure to detect under-inflated tyres that could be the cause of accidents.
- Width of the tyre, contact area, pavement temperature.

2.6.2 Bridges

WIM data can be applied to different fields of bridge engineering such as load models, dynamic impact, assessment, fatigue and monitoring.

Load Models

A sub-committee of COST323 has made a significant contribution to the articulation of the Bridge applications of WIM (O'Brien et al. 1998a). One of the objectives of this sub-committee was to review the traffic load model specified in the Eurocode, EC1, Part 3. This model is based on traffic statistics collected at various WIM facilities. As traffic loads were found to vary significantly between different sites, the site with the highest loading was initially chosen as a basic reference to design a conservative main load model. This WIM data is used to simulate traffic flow over a wide range of bridge forms and spans in order to determine characteristic load effects corresponding to a return period of 1000 years.

Extrapolations of the extreme load effects were performed under the assumption that the load effect behaves as a stationary Gaussian Process. Rice's probability distribution function assumes a Normal tail which governs the extrapolation. Under this hypothesis, the tails histograms of level crossings of the load effect obtained from WIM records are fitted to the Rice function. This function has a Normal tail that governs the extrapolation for minimal or maximal effects for a given return period. The final basic load model should reproduce these load effects as closely as possible. Newer WIM data shows less variance due to recent improvements in the accuracy of WIM systems. This has leaded to a re-assessment of Eurocode 1, Part 3 (O'Connor et al. 1998).

The Eurocode allows correction factors on the main model specified above depending on the local traffic conditions of a country and road class. This correction requires the collection of axle weights and spacings (plus vehicle speed and inter-vehicle spacing in dual carriageways) from a number of representative sites over a sufficient period of time. Seasonal variations should also be taken into account.

A design traffic model for bridges with spans in excess of 200 m is needed in most design codes, including Eurocode 1, Part 3. The traffic load combinations to be considered include:

- An equivalent uniformly distributed load for each individual lane (EUDL). This EUDL can be modelled for each lane from the application of WIM data.
- A group of concentrated loads simulating a vehicle model to evaluate local effects. These concentrated loads can also be obtained from information on axle loads provided by WIM data.
- Exceptional vehicles in excess of 100 tonnes, which depends on policy issues.

Dynamic impact

A dynamic impact factor represents the difference between the total traffic effect to which a bridge may be subjected and the purely static effect. This total effect differs from the static one due to the dynamic interaction between bridges and vehicles.

Dynamic impact factors used in the design of short span bridges are usually very conservative as proven in different simulation studies. A certain static load can have a total effect after dynamic amplification in excess of a greater static load with a lesser dynamic amplification factor. The worst loading case in these bridges is generally associated with a two-truck event, but its dynamic impact factor can be less than the one corresponding to a smaller load. Thus, WIM systems provide a tool for collecting information on the relationship between static and dynamic loads.

O'Brien et al (1998) underline the need for simulations and/or Bridge WIM measurements of the dynamic traffic load effects with a focus on the load cases which govern the limit states on a range of bridges.

Assessment

The use of site-specific traffic load models rather than design load models obviate the need for bridge strengthening or traffic restrictions. Bridges can be assessed using WIM records in a similar way to the derivation of the Eurocode traffic model. Crémona and Carracilli (1998) assess the added tensions induced by traffic effects on the cables of a cable stayed bridge and a suspension bridge through WIM systems installed on the bridges to derive the

corresponding histograms. Regarding the safety of both bridges, ultimate design loads are larger than the extrapolated ones.

Fatigue

Fatigue damage is a function of the magnitude and frequency of the load effect cycles as well as the fatigue strength of the structure. The fatigue is studied through three different procedures: First, a simplified procedure will allow for the determination of whether maximum stresses are higher than a safe threshold value. If this is the case, more detailed approaches are necessary. These approaches are:

- Miner's law to quantify fatigue damage. WIM data is useful to implement the traffic loads with probabilistic methods.
- Fracture Mechanics to predict crack size based on the stress range history.

Fatigue lifetime is extremely sensitive to traffic loads, and WIM data is extremely valuable for the design and assessment of steel and composite bridges. It is also necessary to keep a WIM database to perform fatigue calculation taking into account the past loading history (Jacob 1998b).

Monitoring

WIM systems can be used to monitor traffic loading of bridges in real time. Data collected can provide information on the existing loads and if a maximum safe bridge load is reached, warnings, traffic lights or barriers could be activated to limit the traffic loading and protect the bridge. It could also lead to criteria for the need of bridge strengthening.

2.6.3 Road and Traffic Management

The efficiency of highway infrastructure can be increased with accurate data on vehicle types, speed, weight, traffic density or environmental conditions. Traffic management in real time allows the distribution of traffic flows in time and space, or warning to drivers of conditions on the road ahead when an incident has been detected. Other applications include:

- Detection of violation of reserved lanes.
- Effect of the percentage of slow vehicles on lane capacity.

- Management of rest areas.
- Tolling.
- Statistical information for studies on economy, traffic patterns, or relationship between traffic and air pollution or accidents.

2.6.4 Enforcement and Road Pricing

Overloading must be penalised to increase the safety of road transport, to ensure fair competition and to preserve the infrastructure. Therefore, the road contractor, who must guarantee the road conditions over a specified period, has the right to check that no overloaded axles are damaging the structure. Static weighing scales were unable to detect a significant proportion of these overloaded axles, but the use of WIM systems allows for an instantaneous check of all traffic without any disturbance to the road users. A dissuasive way to discourage overweight vehicles is by increasing enforcement activity. According to the Legal Metrology Division of the French Ministry of Industry (Marchadour 1998), the accuracy level required in a weighing system should fulfil the tolerances of class A(5) according to the European Specification on WIM (COST323 1997) or at least B+(7) for all criteria, and improvements should be proposed by the manufacturer to reach A(5) within a year. The system should alternatively be in class 5 of the OIML draft recommendation on WIM (Dunmill 1998), or at least in class 10, to be improved up to class 5 within a short time period.

WIM systems can also be used in road pricing if vehicle weights are taken into account in the tax system. This tolling can take place in two different ways (Doscemascolo and Jacob 1999, Jacob and Stanczyk 1999):

- Taxation according to the individual weight. Class A(5) or higher is required.
- 'Shadow Toll' procedure: Annual fee paid by the infrastructure's owner to the road operator and those responsible of maintenance. This fee is adjusted as a function of real traffic measurements. Class B+(7) is required.

LS-WIM can be used for enforcement. At low and constant speed, vehicle bounce and load transfers due to drag or changes in acceleration are small. However, load transfers due to

differences in height between the bogie axles on the weighing platform and the surrounding area are likely, and they should be minimised.

Newton (1998) suggests the use of transponders (electronic license plates) fitted to the vehicles that could transmit the information on the maximum permitted weights to the WIM system. These transponders could also incorporate a system whereby the driver could get messages sent to a weighing site for enforcement.

HS-WIM systems can be used for selecting vehicles for enforcement weighing, monitoring the level of overloading or automatic weight. Video can be used in combination with WIM systems for pre-selection of overloaded vehicles (WIM-VID). Dienst Weg-En Waterbouwkende (DWW) carried out a pilot project to investigate this possibility. Two types of WIM systems were tested: Bending plates that almost achieved class B(10), and piezoceramic sensors in class C(15), acceptable for pre-selection (Henny 1998). Weight information and a video picture of the vehicle are captured in a PC screen as illustrated in Figure 2.10. Overloaded axles and gross vehicle weights are shown in red if exceeding the limit. As a result, a wider range of vehicle types were selected and the efficiency of selected vehicles that were overloaded was raised from 46% without WIM to 96% with WIM (Van Dijk 1999).

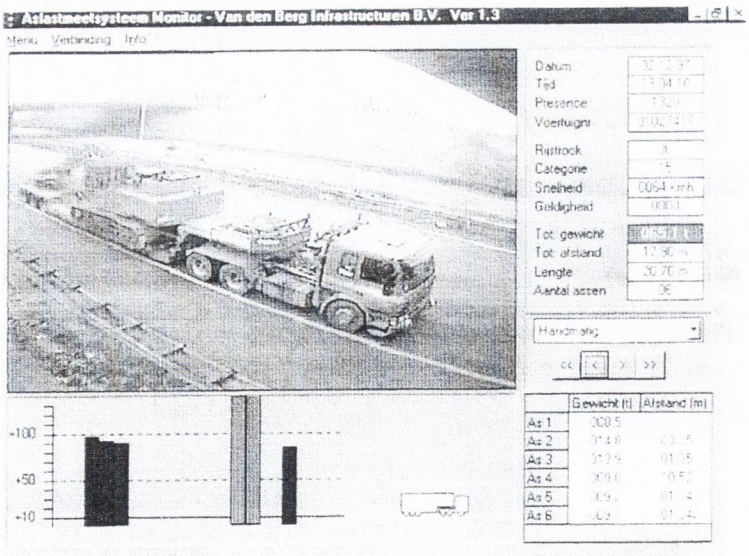

Figure 2.10 – Example of PC screen for pre-selection (after Henny 1999)

Figure 2.11 summarises the implementation of the ideas expressed above by a commercial system.

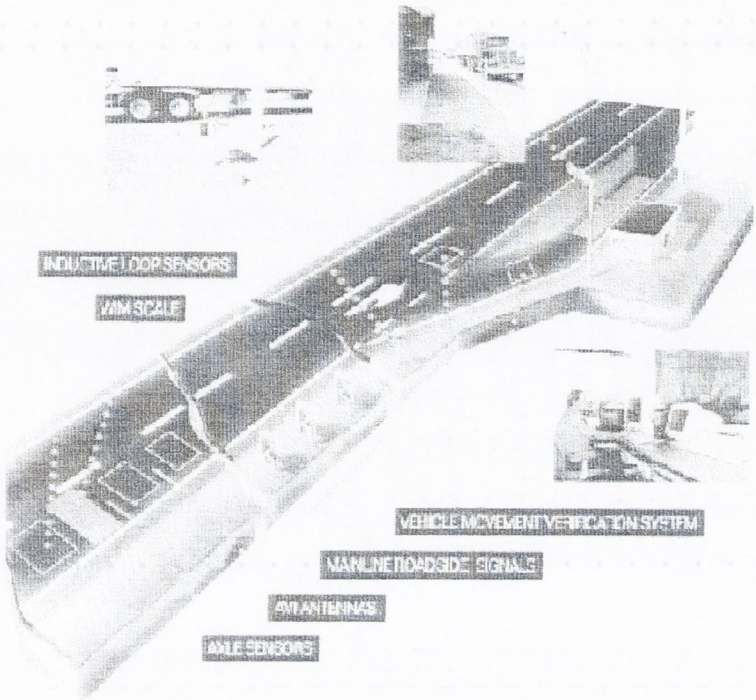

Figure 2.11 – IRD mainline WIM weigh station system[9]

Chou and Tsai (1999) have studied the possibility of using HS-WIM for direct enforcement. The required WIM accuracy for legal enforcement can be derived from the maximum allowable reduction in pavement service life and the maximum allowable rate of misjudged overloading. However, the accuracy of HS-WIM systems must still be improved before being applied with this purpose, except in countries where gross overloading is commonplace.

Further progress with regard to legislation on the maximum weight of vehicles for national transport is expected in the EU, particularly relating to harmonisation of maximum weight limits for both vehicles and axles. In the opinion of Missen (1998), the political attitude of the Member States in this field in the next millennium will come about as a result of two independent factors. Firstly, an increase in vehicles that operate to their national weight limits performing cabotage in another country. Secondly, the development of weigh-in-motion equipment to control the degree of vehicle overloading that occurs. This is an area where WIM is of major importance, as static scales are expensive, scarce and easily avoided by lorry drivers.

3

BRIDGE WEIGH IN MOTION SYSTEMS

3.1 INTRODUCTION

A Bridge Weigh In Motion (B-WIM) system is based on the measurement of the deformation of a bridge and the use of the measurements to estimate the attributes of passing traffic loads. This technology generally consists of devices for measuring the strain caused in the bridge by the vehicles, axle detectors for collecting information on vehicle velocity and axle spacing, and data acquisition equipment. Details of a typical installation will be given in Chapter 4. The information provided by strain sensors and axle detectors is converted into axle weights through the application of an algorithm. This algorithm obtains truck weights by comparing theoretical models to a measured response. This chapter introduces existing ways to carry out this calculation while new algorithms will be developed in Chapter 7.

In the 1970's in the USA, the Federal Highway Administration (FHWA) started studying the use of Bridge WIM systems to acquire WIM data. Moses (1979) introduced an algorithm based on the assumption that a moving load will cause a bridge to bend in proportion to the product of the load magnitude and a reference curve representative of the bridge behaviour, the influence line. In the 1980's, Peters (1984) developed AXWAY in Australia. This B-WIM system is based on the same concept of influence line. A few years later, he derived a more effective system for weighing trucks using culverts, known as CULWAY (Peters 1986). Both the American and Australian systems have been used for commercial applications on bridges and culverts. Bridge Weighing Systems Inc. developed one of the first commercial B-WIM systems in 1989 on the basis of Moses' algorithm (Snyder 1992). In the 1990's, three new independent B-WIM systems were developed in Ireland, Slovenia and Japan (O'Connor 1994, Žnidaric & Baumgärtner 1998, Ojio et al. 2000).

B-WIM systems have not been widely used in Europe to date due to some limitations such as: a) durability problems due to wear and tear of axle detectors, b) restrictions on bridge type, c) Inaccuracy due to bridge and truck dynamics and d) extreme sensitivity to errors in axle spacing, influence line and/or speed. Recent progress through the European COST323 action and the WAVE project (O'Brien et al. 1999a) and other researchers have led to significant improvements in the performance of B-WIM systems in many situations that were problematic in the past. Developments include new dynamic algorithms (O'Connor & Chan 1988a, 1988b, Dempsey et al. 1998b), use of optimisation techniques (Dempsey et al. 1998a, 1999a), algorithms based on the use of multiple sensor locations (Kealy 1997), extension to other bridge types (Žnidaric et al. 1998, 1999b, Dempsey et al. 1998a, 1999a), and Free of Axle Detector (FAD) systems that allow velocity and axle spacings to be found purely from strain measurements, removing the need for axle detectors (Gagarin et al. 1994, Žnidaric et al. 1999a). This chapter reviews these developments while new approaches are in the subject of later chapters.

3.2 GENERAL CHARACTERISTICS OF BRIDGE WEIGH IN MOTION SYSTEMS

Figure 3.1 illustrates the components of a B-WIM installation: Instrumented beams giving information on the bridge response to the passing of a vehicle, axle detectors locating the vehicle in time and giving information on its dimensions, and finally hardware and software to process all this information.

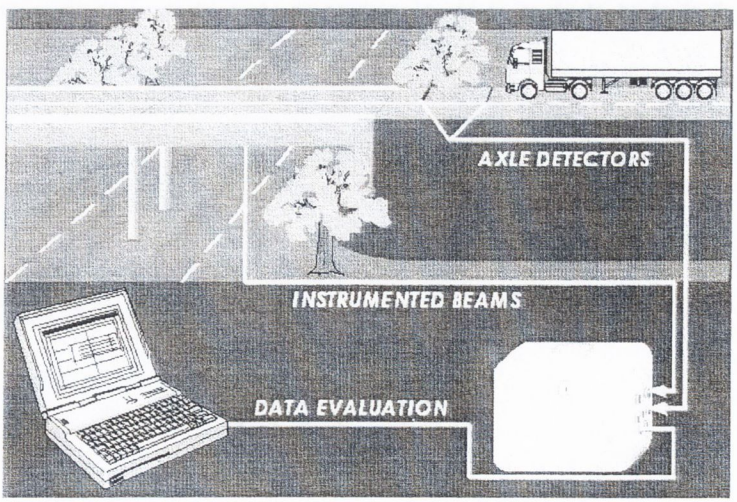

Figure 3.1 – General overview of a B-WIM system (after O'Brien et al. 1997)

3.2.1 Advantages

Both Pavement and Bridge WIM systems use the information on voltage supplied by measuring devices to work out applied load through algorithms. However, there are some noticeable differences:

- From the point of view of the installation: Most WIM systems are based on weighing detectors embedded into the pavement. A B-WIM system only requires minor traffic disruption when using portable axle detectors on the road surface. In the case of free-of-axle-detector (FAD) B-WIM systems, the interruption of traffic is not necessary at all. First applications of FAD systems on orthotropic decks and short concrete slab bridges are very promising (Jacob et al. 2000). Another feature of B-WIM is the relatively low cost of the installation: They use an existing bridge and strain transducers can be bolted to the bridge and reused. The portability of the monitoring instrumentation allows for the surveying of many sites for heavy vehicles.
- From the point of view of maintenance: As for all WIM systems, B-WIM is more accurate when the road surface is very smooth. The maintenance of the road in a good condition is much easier in B-WIM systems, as the weighing sensor is not mounted in or on the road surface. Measurement devices in B-WIM systems are not as sensitive to weather conditions (with appropriate strain sensors compensating for temperature changes), aging or deterioration due to traffic as other WIM systems. If the characteristics of the site allow for a FAD system, durability will be further improved.
- From the point of view of vehicle dynamics: B-WIM systems are not as sensitive to truck dynamic oscillations. Pavement WIM systems measure an instantaneous force for the time the tyre is supported on the WIM sensor. This time depends on the sensor width and vehicle speed and only a small portion of the tyre oscillation is recorded (a few milliseconds). The deviations above or below the static value could be in excess of 15% on a pavement in 'good' condition (Huhtala 1999). If a WIM system was able to measure the load for a full period of the lowest frequency, the problem of dynamic oscillation would be overcome. The only existing WIM system able of achieving this uninterrupted record is a B-WIM system. B-WIM systems measure truck forces continuously as the truck travels on the bridge. As the bridge length increases, the period of measurement increases and lower frequency components of the force can be successfully detected. This is simply not possible in pavement strip sensors due to the very short period of measurement. Pavement WIM systems try to reduce the effect of

truck dynamics through the choice of a very good road site, a frequent re-surfacing and the use of new techniques involving multiple sensors (Section 2.4.5).

B-WIM systems are often more difficult to detect by a driver than other WIM systems, as there is hardly any visible indication of instrumentation (primarily located under the bridge). These unbiased B-WIM measurements supply information that can be used for purposes other than WIM. For instance, raw data used for bridge monitoring (as carried out in the Tagus suspension bridge in Lisbon) or storage for further processing (such as fatigue calculation).

In addition to the factors given in the preceding paragraph, if truck mass is negligible compared to bridge mass, truck dynamic effects on measurements are reduced by the bridge inertia. A truck can be easily located on a lot of existing bridges in the same way a typical static weighing scale would do. The difference is the existence of the bridge and truck dynamic behaviour. If bridge dynamics are removed efficiently, the result in gross vehicle weight should be clearly very accurate. In the case of culverts and bridges with very short spans, bridge dynamics are negligible.

3.2.2 Disadvantages

In order for B-WIM to be implemented, there is a need for the presence of a suitable bridge in the route of interest. A previous test using trucks with loading close to the expected mean gross weight should be run to analyse the suitability of a bridge for a given WIM purpose. Results with unloaded, full and half-loaded vehicles at different speeds should not exhibit any inconsistency or non-linearity depending on their speed or weight (Jacob et al. 2000). If there is non-linearity, input parameters must be checked or correction functions applied. A 2-axle or 3-axle rigid truck is useful to identify the existence of dynamic problems (i.e. a poor pavement or a bump). Results should indicate what accuracy class could be expected for that site. Some bridges might not even qualify for a B-WIM installation. For instance:

- If the bridge is too stiff, the existing instrumentation might not be able to measure any significant strain induced by the load.
- If the bridge is too long, accuracy will decrease, as there could be a lot of vehicles crossing the bridge simultaneously. Therefore, the bridge is less likely to qualify for

FAD, as it will be very difficult to distinguish the effect of individual axles. Further, no known B-WIM system has yet been developed to cater for multiple vehicle presence. Spans shorter than 20 m are generally preferred for most B-WIM systems and bi-directional traffic, though spans up to 40 m can be used if axles from a group are not an important issue (Žnidaric & Baumgärtner 1998).

- If the weight of the moving load is low, there can also be difficulties recording a significant strain.
- If the bridge is too skew, there is a possible influence of lateral positioning of the vehicle, that must be taken into account. Žnidaric and Baumgärtner (1998) suggest even angles up to 45° can be acceptable, except in the case of bridges with measured span shorter than its width (i.e., culverts, where skewness is not recommended at all).
- If the bridge has a lot of lanes, the effect of a single axle will be very difficult to distinguish from axles present in other lanes simultaneously.
- If the bridge section is too thick, strain peaks are smoothed out, and the site might not qualify for FAD.
- Many B-WIM algorithms assume a constant speed along the bridge, so sites where this does not occur should be avoided (i.e. where traffic jams are likely or in very long bridges).

The system is usually more accurate for GVW than axle weights. Further, it is difficult to distinguish individual axle weights inside closely spaced axle combinations (tandems or tridems). While results for Gross Vehicle Weight are expected to be very accurate, the determination of axle weights is more difficult. The effect of all the vehicle axles on a bridge is measured simultaneously and it is necessary to differentiate the contribution of each axle based on knowledge on the bridge-truck structural system. If there is a single vehicle travelling on a bridge, only the effect of the first and last axle can be measured individually for a very short period of time, i.e., when entering and leaving the bridge respectively. This difference in accuracy for GVW and axle weights does not apply to culverts or very short span bridges, where it is possible to weigh axles or axle groups individually.

Depending on the algorithm adopted, a BWIM system requires a prior knowledge of the bridge structural behaviour, i.e., the influence line for the bending moment at the sensor

location. A larger difference between assumed and real bridge behaviour will result in higher errors in results. Better results can be obtained when the bridge model is adapted using measured strains at the site during calibration. The necessity for this model makes B-WIM systems require more computation time per vehicle than a pavement WIM system, though modern computers can generally allow for calculation in real time.

It has also been found that accuracy decreases in the cases where the first natural period of the bridge is greater than the time taken for the truck to cross the bridge. Low-pass filtering could reduce the influence of dynamics, but this technique is not recommended except for very high frequencies, as important static components can be removed in the case of very closely spaced axles and/or high vehicle speeds.

Existing known B-WIM Systems can only weigh a single vehicle on the bridge. Interference from other vehicles decreases accuracy. For this reason, the AXWAY system limits its use to traffic densities below 500 trucks per hour. The problem with high traffic densities is the possibility of simultaneous traffic events: vehicle whose weight is being measured might be overweighed due to the presence of vehicles in adjacent lanes.

3.3 MOSES' ALGORITHM

First approaches in the USA in the early 1970's used highway bridges as weighing scales. They measured and related the maximum peak strain recorded during the truck crossing to its GVW. Acceptable results were obtained, but this correlation was only valid when applied to the same vehicle type. It was quickly noticed that axle detectors mounted on the road surface were necessary for:

- Distinguishing the vehicle type by number of axles and spacings
- Introducing new algorithms that require number of axles, spacings and speed in their formulation. The objective of these algorithms is to achieve: (a) an improved accuracy in GVW, taking into account the small differences of weight distribution between axles that affected the magnitude of the maximum strain peak; (b) results for individual axle weights.

As result, Moses (1979) developed a system that used instrumented bridge girders combined with timings from axle detectors to predict the axle and gross weights of trucks in motion. This prediction is based on the fact that a moving load along a structure will set up stresses in proportion to the product of the value of the influence line and the axle load magnitude. An influence line is defined as the bending moment at the point of measurement due to a unit axle load moving along the bridge. At this time, Moses proved that weight predictions were feasible and results were repeatable when using a calibration truck. The bridge WIM system described by Moses was the first of its kind and nowadays it is widespread in the USA and elsewhere. FASTWEIGH is an American B-WIM system that uses Moses' algorithm, giving on site readings through a matrix solution technique.

3.3.1 Ideal Site

First bridges used for weighing purposes were composed of multiple beams and a slab. The reason for the choice of this type of bridge was its length and relative stiffness in the longitudinal direction compared to the transverse one. These longitudinal beams primarily carry the traffic loads. Therefore, all girders are usually identical, though some differences in section modulus can appear in edge members. The simplest bridge to apply Moses' algorithm would be a single span beam-and-slab bridge with no skew. Studies prior to Moses (1979) indicated a sequence of single spans less than 18 m as an ideal bridge length to predict axle weights. A larger span, over 24 m, would be preferable for determining GVW. Moses tested his algorithm in a 3-span continuous bridge, and his optimisation process showed no statistically significant advantage to either span for weight prediction. In fact, best results were achieved by averaging predictions obtained from each set of gauges at different longitudinal locations. Other bridges could be used for WIM, once an influence line of the bending moment can be obtained and the relation between measurements and this influence line is reliable. Thus, concrete slab bridges, trusses, skew girders or orthotropic decks can also be instrumented for weighing purposes.

3.3.2 Principle

If a vehicle is considered at a certain static position on the bridge, there will be a relation between the strain ($\square_i$) generated at strain transducer i, and the bending moment (M_i) given by:

$$M_i = ES_i\varepsilon_i \tag{3.1}$$

where E is modulus of elasticity and S_i section modulus of the i^{th} girder.

The total bending moment (M) will be given by the sum of all strain transducers at each girder i transversely for a given longitudinal location as:

$$\begin{aligned} M &= \sum_{i=1}^{no\_girders} M_i \\ &= \sum_{i=1}^{no\_girders} ES_i\varepsilon_i \end{aligned} \tag{3.2}$$

As Moses' algorithm is based on a one-dimensional approach, the signal from all sensors in different transverse locations and the same longitudinal location are added. The difference in section modulus induces an error in this sum. However, this effect is not significant due to the smaller load carried by the outer members and the fact that the truck will always run in the same transverse location within the lane. So, if E and S_i are assumed to be constant for each girder, then

$$M = ES \sum_{i=1}^{no\_girders} \varepsilon_i \tag{3.3}$$

Thus, total bending moment and measured strain are directly related by the product of two constants (ES), which is independent of vehicle position. In theory, this constant can be calculated from bridge dimensions and material properties, but in practise, it is derived from measuring the effect of the crossing of a truck of known weight over the bridge.

This total bending moment (M) can be related to the individual axle weights for each vehicle position. Then, the total number of unknowns (N), number of axles, can be calculated from a knowledge of N strain records corresponding to N different positions of the truck along the bridge. This system of equations requires the use of the influence line of the bending moment for that bridge location. The ordinate of the influence line indicates the bending moment for a unit axle load located at a certain point along the bridge. An advantage of using beam-and-slab bridges is that generally their real behaviour

corresponds well with simple influence lines based on simple beam theory. The influence line can also be found by crossing a calibration vehicle of known weights slowly across the bridge while recording the strain. Figure 3.2 illustrates the unknowns and the input data that is necessary for the calculation of axle weights in a B-WIM algorithm.

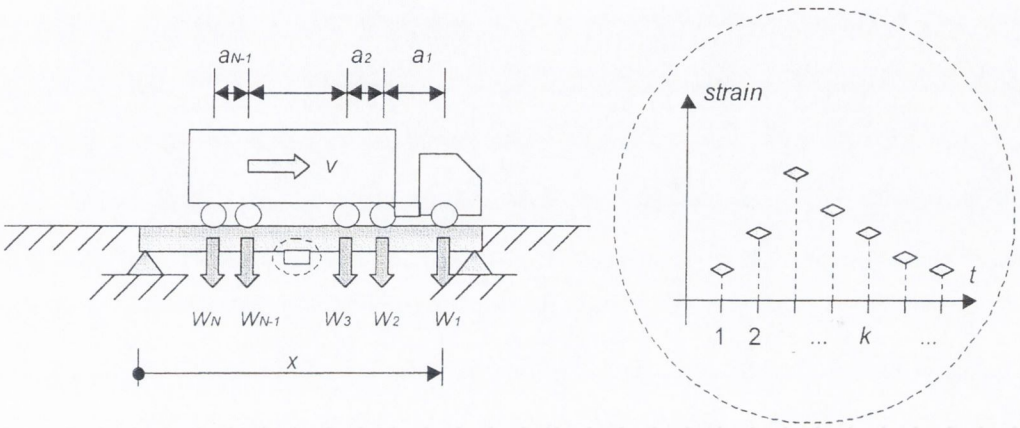

Figure 3.2 – Parameters involved in a B-WIM algorithm

If the first axle is located at a distance x from the support, the bending moment is:

$$M(x) = W_1 I(x) + W_2 I(x - a_1) + W_3 I(x - a_1 - a_2) + \ldots \tag{3.4}$$

i.e.,

$$M(x) = \sum_{i=1}^{N} W_i I(x - \sum_{j=1}^{i-1} a_j) \tag{3.5}$$

where $I(\,)$ is the influence ordinate.

As real strain is being sampled at discrete time intervals, for a further comparison in the same terms, the theoretical moment (M) can be expressed as a function of time t_k, where k is the reading number. The total number of readings is related to the frequency at which measurements take place.

$$M(t_k) = \sum_{i=1}^{N} W_i I(t_k - \frac{\sum_{j=1}^{i-1} a_j}{v}) \tag{3.6}$$

where v is velocity. The value of the influence line as a function of time ($I_i(t_k)$) can be calculated for each axle i from axle spacings and speed. This speed is obtained from the axle detectors and assumed to be constant along the bridge.

3.3.3 Removal of Dynamics

Up to this point, the theoretical static response of the bridge ($M(t)$) has been presented. In reality, bridge response is not static, but oscillates around a static position of equilibrium as shown in Figure 3.3.

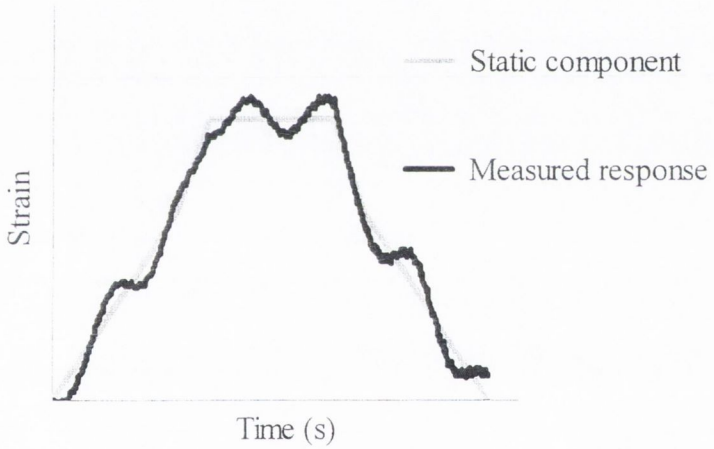

Figure 3.3 – Theoretical static strain ($M(t_k)$) versus typical measured strain ($\widetilde{M}(t_k)$) at midspan

Moses uses the fact that a lot of measurements are available during the truck crossing to smooth out the dynamic component. This is achieved by minimising an error function φ, defined as follows:

$$\varphi = \sum_{k=1}^{T} [M(t_k) - \widetilde{M}(t_k)]^2 \tag{3.7}$$

i.e.:

$$\varphi = \sum_{k=1}^{T}[\sum_{i=1}^{N} W_i I(t_k - \frac{\sum_{j=1}^{i-1} a_j}{v}) - \widetilde{M}(t_k)]^2 \tag{3.8}$$

where $\widetilde{M}(t_k)$ is the measured strain and T is the number of scans while the truck is on the bridge. A minimum condition is imposed by:

$$\frac{\partial \varphi}{\partial W_i} = 0 \quad ; \quad i = 1,2,...N \tag{3.9}$$

This gives:

$$\sum_{k=1}^{T}[2(\sum_{j=1}^{N} W_j I(t_k - \frac{\sum_{r=1}^{j-1} a_r}{v}) - \widetilde{M}(t_k))I(t_k - \frac{\sum_{r=1}^{i-1} a_r}{v})] = 0 \quad ; \quad i = 1,2,...,N \tag{3.10}$$

And re-ordering:

$$\sum_{k=1}^{T}\left[\sum_{j=1}^{N} W_j I(t_k - \frac{\sum_{r=1}^{j-1} a_r}{v})\right] I(t_k - \frac{\sum_{r=1}^{i-1} a_r}{v}) = \sum_{k=1}^{T} \widetilde{M}(t_k) I(t_k - \frac{\sum_{r=1}^{i-1} a_r}{v}) \quad ; \quad i = 1,...,N \tag{3.11}$$

which is equivalent to using a least-squares fitting method of measurement to theory to find axle weights. Equation 3.8 can be expressed in matrix form as:

$$[F]_{NxN}\{W\}_{Nx1} = \{B\}_{Nx1} \tag{3.12}$$

where:

$$[F_{ji}] = \sum_{k=1}^{T} I(t_k - \frac{\sum_{r=1}^{j-1} a_r}{v}) I(t_k - \frac{\sum_{r=1}^{i-1} a_r}{v}) \tag{3.13}$$

$$\{B_i\} = \sum_{k=1}^{T} \tilde{M}(t_k) I(t_k - \frac{\sum_{r=1}^{i-1} a_r}{v}) \tag{3.14}$$

and $\{W\}$ is the vector of unknown axle weights.

$[F]$ only depends on the influence line, axle spacing and speed, while $\{B\}$ depends on the same factors and measured strain as well. Finally, axle weights $\{W\}$ can be found by:

$$\{W\} = [F]^{-1}\{B\} \tag{3.15}$$

Gross vehicle weight is found by summing individual axle weights:

$$GVW = \sum_{i=1}^{N} W_i \tag{3.16}$$

Therefore, Moses recommends combining axle weights when there is a tandem group. He also emphasised that the accuracy of calculated weights is highly sensitive to an accurate estimation of axle spacings and in particular, speed.

3.4 ALLIED STATIC ALGORITHMS FOR CALCULATION OF WEIGHTS

AXWAY is a system developed by Peters (1984) in Australia in the early 1980's. As with Moses' algorithm, AXWAY relies on an influence line as a good reference of the strain caused in a bridge by the vehicle weight. When culverts were tested, results indicated that a simpler and better system could be developed for these structures (Peters 1986). This system, called CULWAY, uses existing concrete culverts and obtains truck masses from measured strain through a unit influence line algorithm. Nowadays, CULWAY dominates the Australian highway speed WIM market with around 150 installations and systems in China, Malaysia and New Zealand. This section also introduces a novel method developed by Dempsey (1997) for calculating gross vehicle weights.

3.4.1 AXWAY

Peters (1984) assumes that total strain is proportional to the applied load due to the linear elastic nature of bridge material. This system was tested in a single span slab bridge first. Strain measurements from conventional strain gauges were not high and consistent enough for weighing purposes. The need arose for the development of mechanical strain amplifiers that amplified the actual strain about ten times. Considerable progress was also made in the durability and reliability of axle detection systems. Though AXWAY uses the same concept of unit influence line as Moses, there are some differences in the final calculation of weights that will be reviewed in this section.

Ideal site

Peters suggests:

- Single span quite short to ensure a high probability of having only one vehicle on the bridge at a time.
- A linear strain response. The measured strain should also be sufficiently large (0.5 με/ton of vehicle weight).
- One or two lanes preferably.
- Bridge dynamic characteristics should allow for at least four vibration periods per vehicle pass.
- A relatively smooth roadway surface is required both prior to and on the bridge to reduce vibration amplitudes.

Determination of the influence line

Strains are measured at midspan and all strains across the bridge at this point are added together. The sum of all such strains should give the same total regardless of the transverse position of the truck in a lane. Most bridges are quite wide and tend to act as plates rather than beams, and so, the influence line for locations in different lanes will be quite different. Accordingly, this influence line is calculated by applying the theory of bending plate for that particular bridge. The magnitude of this unit influence line can be obtained by measuring the strain caused by a truck of known axle weights.

Technique to remove dynamics

Every bridge has a main mode of vibration corresponding to its first natural frequency. The amplitude of this vibration depends on the dynamic characteristics of the bridge. The removal of this component prior to the weight calculation should improve the accuracy of the final results.

Peters proposed a moving average technique based on the assumption that the total strain response is a combination of the vehicle response and the bridge vibration at its natural frequency. If the vibrations on certain bridges do not oscillate around a static position, then this filtering technique might not be suitable. If this vibration is a sinusoidal wave of constant natural period, even if there is a gradual change in wave amplitude, the integral of the bridge vibration over any integral number of periods should be zero. Peters recommends about a minimum of four periods of the bridge natural frequency for a good smoothing of the original strain signal by this technique.

As bridge vibration takes place in combination with bridge static response, the filtered signal will be the result of integrating the measured strain over the natural period at each step. As plate theory is assumed, bending at midspan is likely to take place in two directions. Hence, sharp peaks, typical in longitudinal bending of a narrow beam, do not tend to occur and the corruption of the static response by this filtering is not as significant. For instance, the spectral representation of a response with sharp peaks contains higher and more spread frequency components than a smooth response. However, part of the static component can still be removed dangerously when having very closely spaced axles and/or high speeds.

Iterative technique in the calculation of weights

Iterative techniques increase computer time, so processing of weights in real time can be difficult to achieve. Once a strain record has been obtained as a function of time and dynamics have been filtered out, the procedure to obtain the vehicle weights suggested by Peters was the following one:

- Strain is expressed as a function of the vehicle position coordinates through vehicle speed.

- GVW is assumed to be proportional to the area under the strain-position curve. The exact value for GVW is obtained from the product of this area and a weight correction factor.
- Then, axle weights are calculated. Some initial axle values are obtained by distributing GVW equally between all axles. Then, the following iterative process takes place:

[1] Generate expected response curve from axle values using unit influence line.

[2] Compare theoretical and real strain record and find greatest difference between both curves.

[3] Locate axle most likely to be causing this difference, i.e. nearest axle. Then, increase or decrease that axle weight in proportion to the magnitude of the misfit.

[4] Readjust axle weights to maintain the correct GVW.

[5] Check actual axle group weights with previous estimates.

[6] If change for all axle weights < 0.05 tonnes, solution is assumed to have been reached. Otherwise, re-start process at [1].

The correct longitudinal location of the truck on the bridge at each instant is very important for accurate weighing. An axle detector prior to the bridge acts as a trigger to start the strain record. This starting point is the same for every vehicle. A deviation between the estimated truck location and its corresponding strain record could have a very significant influence on the individual axle weights. The effect on GVW would be smaller as some axles would be overloaded and others underloaded, resulting into a compensated total weight. The correct adjustment between the axle detector, the strain record and the vehicle is carried out during calibration. A test vehicle is passed several times on each lane. Then, the likely mismatch is adjusted in intervals of 0.1 m, which is the division interval used in the algorithm. This adjustment is particularly relevant in skew bridges.

Like Moses, Peters treats loads within an axle group as if the total weight of the tandem or tridem was equally distributed between all axles in the group. Thus, though all axle weights are calculated individually, when these axles belong to an axle group, the weight obtained for each axle in a group is added together and divided between the number of axles to get the final axle weight. This is due to the difficulty of distinguishing between closely spaced loads. Axles are considered to be in the same axle group when the spacing is less than 1.5 m for tandems or tridems, or less than 2 m for twin steers.

3.4.2 CULWAY

CULWAY (Peters 1986) uses two axle sensors to collect information on the speed and axle spacings of the vehicle (Figures 3.4(a) and (b)). These sensors also work like triggers. When the first axle of the vehicle hits the first axle sensor, the system measures the initial strain at the culvert midspan. Then, each time the second axle sensor is hit by an axle, the system measures the strain change, which is related to the axle weight.

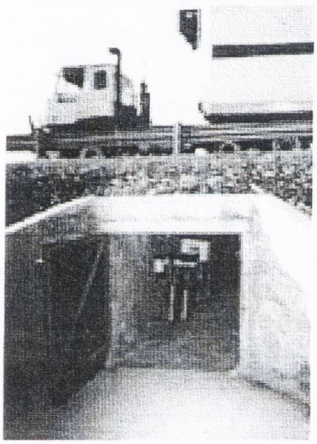

(a) Site[9]

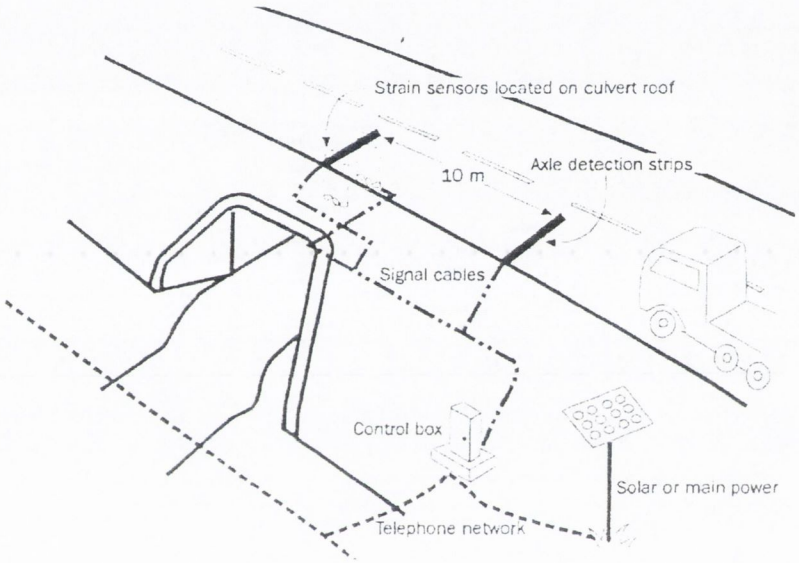

(b) Installation (after Peters 1998)

Figure 3.4 – CULWAY system

Ideal site

Peters (1986) suggests the ideal culvert would include the following features:

- Single span box culverts or reinforced concrete pipes, less than 2.7 m span. This limitation avoids more than one axle group on the culvert at a time. When there are more than one axle present at a time, the measured strain will be the sum of the contributions of the different axles.
- Good road surface. Culvert and road preferably built at the same time to avoid settlement.
- No or virtually no skew.
- Soil cover over 600 mm, but less than 1500 mm. These limits are due to the need to avoid dynamics while receiving a strain signal that is strong enough.

- Clear access to underside is required. The sensors are placed right underneath the wheel tracks on the road. If the culvert was made from precast segments with lengths of less than 1.2 m, one strain gauge per box or pipe, placed centrally, is recommended. This placement is chosen to reduce the influence of the likely different transverse position of the vehicle being weighed.
- Box culverts with continuous lid bridging two cells should be avoided to facilitate calculations.

Calculation of weights

Calibration takes place with trucks of known weights travelling at the expected speeds. Tests have indicated that the influence of speed on results is negligible. CULWAY minimises the errors due to variations in the lateral position of the vehicle by simply adding the strain response of each individual sensor.

There is a systematic error which results in underweighing of steer axles. There are several theories to explain this phenomenon: Smaller contact area of tyre, strain non-linearity of concrete or dynamic weight of steer axles inferior to the static weight due to aerodynamic and torque effect. CULWAY manages the issue with a site-specific correction function to allow for this effect. A plot is made of known single axle weights against their respective strain responses. If a non-linear effect is observed, a function is derived to correct for the misfit between the measured and static weight W_i of axle i. The function can be defined as in Equation 3.17:

$$W_i = C\varepsilon_i^{\gamma} \tag{3.17}$$

where C is a calibration factor and γ a non-linearity correction factor. C represents ratio between strain values ε_i and weights W_i, and γ will normally be 1 unless the plot suggests otherwise. It is necessary to adjust a third factor which is the length of the unit influence line. This is not necessary for measuring single axles but it is very important when there are overlapping influence of axles in groups such as tandems and tridems. The effective influence line length should be taken as the clear span of the culvert plus twice the depth of fill unless evidence suggests otherwise.

Advantages

Some of the advantages of CULWAY systems are:

- Vibration of the culvert is virtually non-existent. Strain response is clear of the dynamic problems found in bridges. The measured strain in a culvert is mainly static, this is, purely induced by the axle mass, and to a minor extent the dynamic load of the vehicle. This is due to the total restraint by the surrounding embankment and pavement on culverts. This soil cover damps high frequency vibrations out, while being adequately stiff to transmit the wheel loads to the concrete culvert. Hence, the strain signal does not require filtering to remove any dynamics.
- WIM systems (or B-WIM) generally often have a bump or discontinuity in pavement profile as a result of the joint between the road and the road sensor (or bridge). This bump excites the truck dynamically and generates high amplitudes in the axle weight variation. There is no joint or discontinuity between the road and culvert, though some settlement might have taken place. There is no excitation of the vehicle dynamics as a result of the weighing system installation and so, the only dynamic effects are those inherent to the vehicle and the road surface profile.
- Strain sensors are located well away from the road surface. This circumstance preserves them from traffic or weather aggressiveness, and little or no site maintenance is required.

Long Term Performance

The effects of seasonal moisture, temperature and stiffness variation of the pavement materials over the culvert have been investigated by Peters (1998). Some seasonal variations in measured vehicle mass have been noticeable at some culvert sites. The concrete bends more in winter than in summer, which could be due to a change in the properties of the pavement, less stiff in winter than in summer, probably originating from a higher moisture content, temperature conditions or a combination of both. The analysis has shown the variation to be consistent from year to year. Culverts with larger cover exhibit less variation. An algorithm was designed to correct seasonal variations due to climatic factors. This algorithm applies a monthly percentage correction to all measured values. Peters has also shown that calibration of a WIM site can be carried out with long term data at a far lower cost than regular site re-calibration. This adjustment has to be checked

carefully as the seasonal differences in vehicle weights could be due to a change in loading patterns instead of climatic factors.

3.4.3 Left Slope Alignment

An alternative method to calculate gross vehicle weights of trucks was developed by Dempsey (1997). This weight is obtained by comparing the measured bridge strain due to a truck of unknown weight to that of a calibration truck by a best fit procedure. The approach minimises the squared difference between measured ($\tilde{\varepsilon}$) and calibration truck (ε) strain values as given in Equation 3.18,

$$\text{Minimise} \quad \varphi = \sum_{i=1}^{n} \left[\varepsilon_i - \gamma \tilde{\varepsilon}_i\right]^2 \tag{3.18}$$

where n is the number of discrete points along the bridge at which strain is being recorded and γ is a scaling factor. If the solution is totally accurate, then γ is the ratio of the weight of the calibration truck to that of the truck whose weight is sought.

Theoretical static bridge responses were generated for five different truck configurations. All errors were below 6% regardless of the truck chosen for calibration. It also became evident that accuracy could be improved by aligning the left hand slope of the strain responses of both trucks before minimising Equation 3.18. This aligning policy reduces the influence of gross weight distribution within the truck. It was also found that transverse offsets of trucks from that of the lane centre line of up to 1 m do not affect accuracy in a significant manner. Experimental tests proved that a dynamic calibration performs better than a static calibration. A static calibration involved a truck of known weight being positioned at different points along the span of the bridge, while the dynamic calibration was obtained from passing a truck of known weight across the bridge at various speeds.

3.5 FURTHER DEVELOPMENTS

The application of new techniques to improve the performance of a static algorithm is discussed in the following sections. These recent contributions include artificial neural

networks, optimisation techniques, multiple sensors or a combined B-WIM and Pavement WIM system.

3.5.1 Sources of Inaccuracy

After analysing the results of many tests, it became evident that the parameters with the highest influence on final accuracy were (Žnidaric and Baumgärtner 1998):

- Selection of influence line
- Accurate assessment of vehicle velocity
- Dynamics of vehicles and bridge, depending on the structure
- Calibration methods

The first three aspects are reviewed next, while the influence of calibration is discussed in Section 3.7.2.

Influence Line

Most B-WIM algorithms are based on the concept of an influence line. Figure 3.5 shows influence lines for a simply supported single-span beam (determinate structure), a fixed-ended single-span and a two-span continuous beam (indeterminate structures). The length of the influence line can extend beyond the centre-lines of the supports as shown by the discontinuous lines in Figure 3.5. The real influence line of a bridge will correspond to partially constrained rotation at the supports (between the theoretical simply supported and fixed situations represented in the figure).

The prediction of axle weights can be very inaccurate if a wrong influence line is chosen, especially in bridges with longer span. An idea of the magnitude of these errors for two different spans is given in Figure 3.6. The values of this figure are obtained by simulating a signal from an influence line between the simply supported and fixed cases, and then calculating weights when using other influence lines. While the error is below 10% for the 2 m span bridge and it is similar for GVW and axle weights, errors of several hundred percent were observed for 32-m long bridges. The greater the difference between the integrals of measured and theoretical strains, the higher the errors in the results (Žnidaric and Baumgärtner 1998).

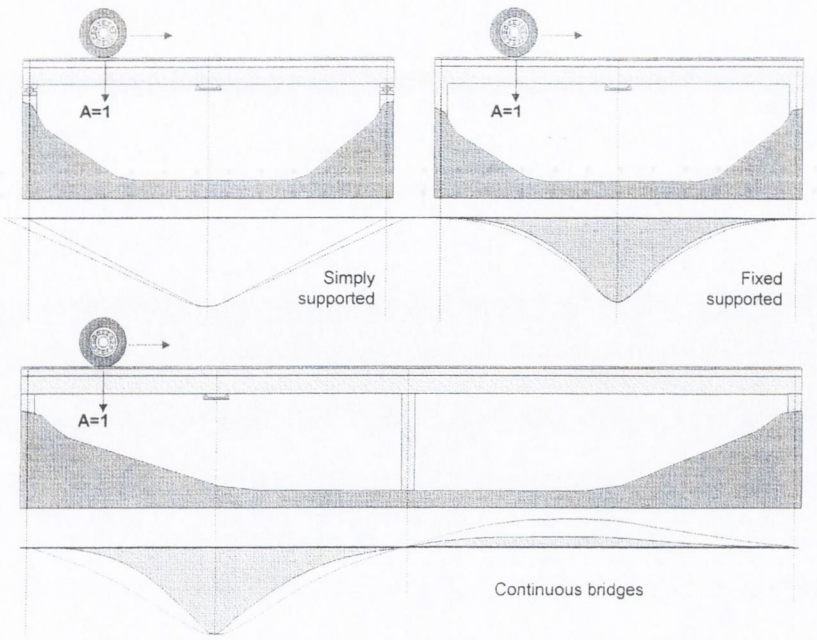

Figure 3.5 – Influence lines of bending moment at midspan for simply and fixed supported (integral) single-span bridge and for a 2-span bridge (after Jacob et al. 2000)

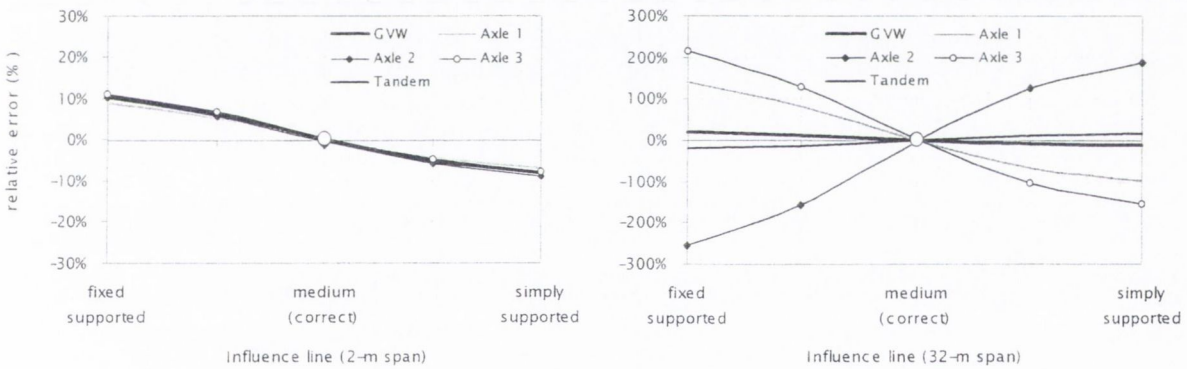

(a) 2 m span (b) 32 m span

Figure 3.6 – Errors in weights due to wrong selection of the influence line (after Žnidaric & Baumgärtner 1998)

The influence line should be corrected based on measured strains at site. Žnidaric et al (1998) and McNulty (1999) propose different methods to carry out this experimental adjustment in the Slovenian (SiWIM) and Irish (DuWIM) systems respectively. The degree of accuracy of both systems is similar as will be shown in Section 3.7.4.

Speed

Vehicle velocity is one of the most important parameters affecting the accuracy of final results. A small error in velocity can result in significant errors in weights, even in short span bridges. Several solutions have been adopted to overcome this problem (Žnidaric & Baumgärtner 1998):

- Placement of the second axle detector above the strain transducers, i.e., further apart from the first than usual.
- Measurement of velocity at more than one location on the bridge.
- Allowance for acceleration and deceleration.
- Optimisation of the results by finding velocity, axle spacings and axle loads which minimise the difference between the theoretical and measured responses of the bridge. The results of applying this technique for a 2 m and 32 m span are shown in Figure 3.7.

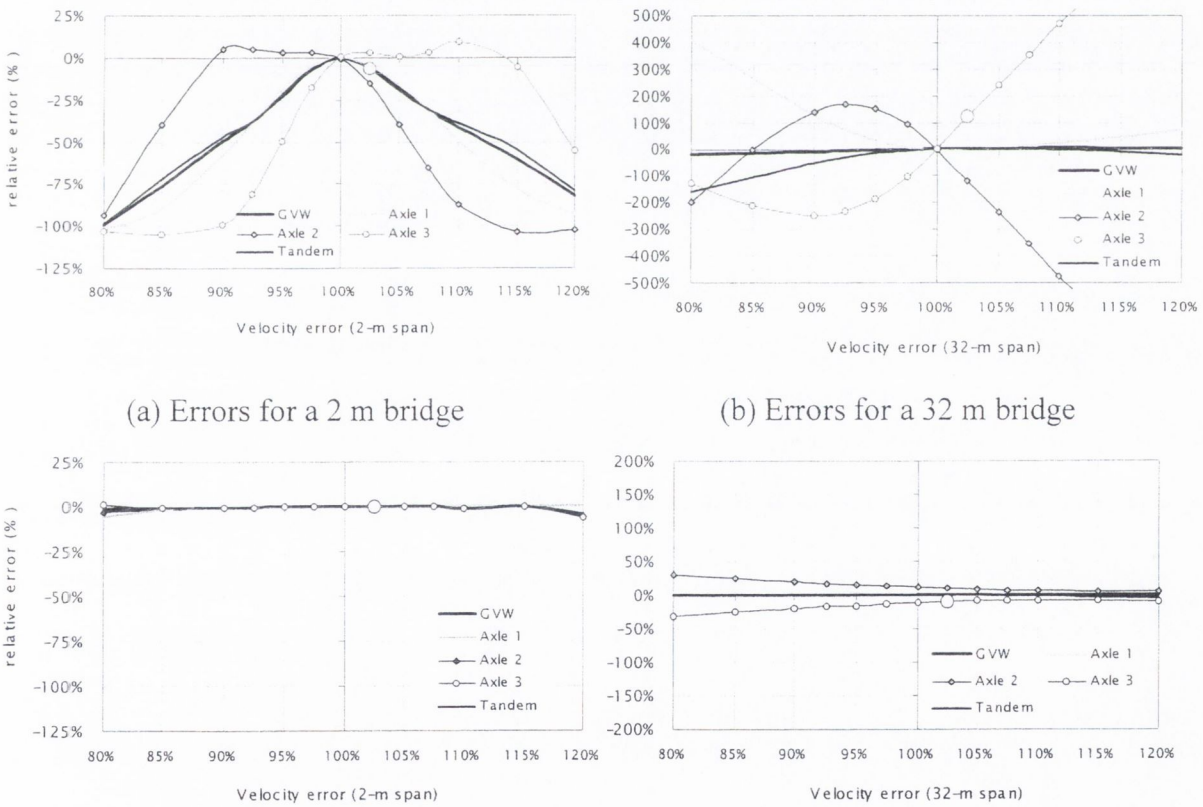

(a) Errors for a 2 m bridge

(b) Errors for a 32 m bridge

(c) Errors for a 2 m bridge after applying optimisation

(d) Errors for a 32 m bridge after applying optimisation

Figure 3.7 – Errors of weights due to an error in velocity for 2 m and 32 m long bridge (after Žnidaric & Baumgärtner 1998)

Dynamics

Jacob et al (2000) recommend choosing bridges:

- With a smooth approach and no bump just before or on the bridge. Dynamic wheel forces up to 100% have been measured in an instrumented truck due to a bump just before the bridge (Lutzenberger & Baumgärtner 1999).
- With high eigen-frequencies. This high frequency of the bridge avoids dynamic interaction with the truck frequencies of body bouncing and pitching. If the eigen-frequency is low, a significant static component of the applied load can be removed by low-pass filtering. Figure 3.8 shows unfiltered and filtered longitudinal strain recorded in a bridge with low first natural longitudinal frequencies: 1.35 and 2 Hz.

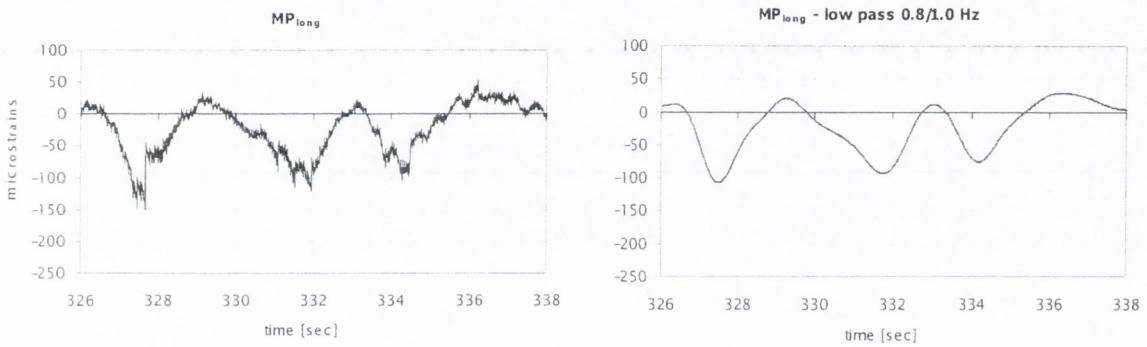

(a) Unfiltered data (b) Filtered data

Figure 3.8 – Low-pass filtering of signal (after Žnidaric & Baumgärtner 1998)

Theoretical dynamic simulations can be used to detect likely problems or to determine the location of the sensors which minimises errors.

3.5.2 Artificial Neural Networks

Artificial Neural Networks (ANNs) are computational models based on the neural structure of the brain. The brain basically learns from experience. Gagarin et al (1994) introduce a B-WIM algorithm that uses neural networks to determine axle weights, vehicle classification and velocity purely from the strain readings taken from the bridge as the truck travels along. This procedure removes the need for axle detectors on the road surface to obtain axle spacings and velocity. This is a very relevant advantage as axle detectors mounted on the road surface are rapidly worn by heavy traffic, apart from warning drivers about the presence of instrumentation on the bridge.

The ANN architecture recommended by Gagarin is the Radial-Gaussian Incremental-Learning Network (RGIN). This architecture is based on a layered feed-forward that provides a mapping function from a vector of input values x_i (i.e., vector of measured strains at different times during the passage of the truck) to a corresponding vector of output values y_i (i.e., vector of quantities representing velocity, axle loads and axle spacings) in neighboring layers. ANN is applied to B-WIM in two network levels. A single network should be possible, but pilot experiments showed it impracticable due to the unacceptable length of the training period. Accordingly the first level, made of one network module, classifies the trucks and the second level, made of different network modules (one for each type of truck), estimates velocity, axle spacings and weights. Figures 3.9 and 3.10 represent these two layered modular structures.

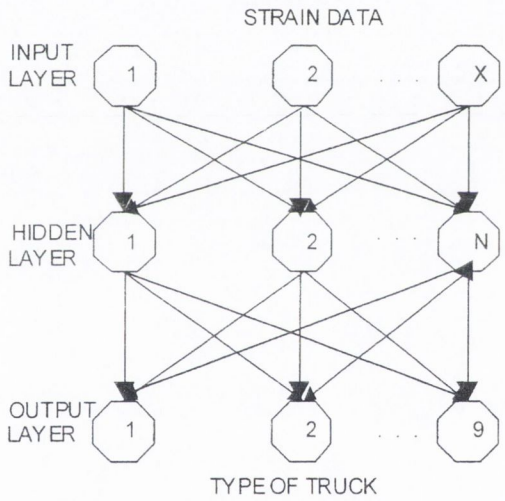

Figure 3.9 – First Level Network

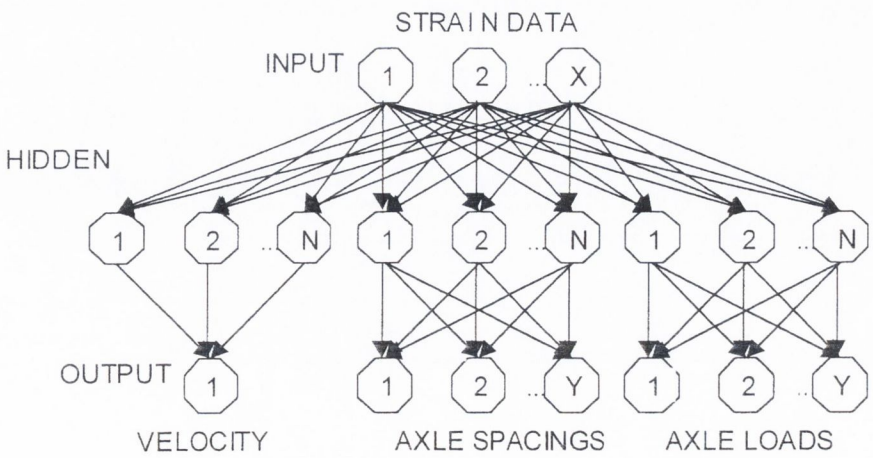

Figure 3.10 – Second Level Network

The network is trained to provide real-time assessments of truck attributes based on a variety of truck configurations and corresponding strain data. During this training, the network must develop a surface that approximates each value y_i in the output vector against its values in the input vector $\{x\}$. The output value y_q of a hidden neuron q is given by the Gaussian-shaped function:

$$y_q = \sum_{j=1}^{M} e^{\left[-s_j \sum_{k=1}^{N} (x_k - c_{km})^2\right]} w_{jq} \tag{3.19}$$

where s_j is a parameter that determines the width of the Gaussian-shaped function, c_{km} constants (known as offsets) from values passed along a link, w_{jq} weights associated with the output values, N the number of input vectors into the neuron, and M the number of output vectors.

This system is built by training one neuron at a time (represented by octagons in Figures 3.9 and 3.10). Initially, a network is set up with the required number of input and output neurons but without hidden neurons, that will be added and trained in a posterior stage until reaching a predefined level of accuracy. New neurons are added in such a way that the centroid of the generated Gaussian-shaped function will focus in regions with the highest errors. This is achieved with the correct c_{km} values. Then, w_{jq} is adjusted so that the amplitude of the Gaussian-shaped bump matches that of the error. Finally, the parameter s_j is adjusted to minimise the remaining errors. In other words, network training is essentially a surface-fitting exercise.

The truck attributes are calculated as follows: The strain is given to the first network level and values y_q are generated at each output neuron (Figure 3.9). The output with the greatest value denotes the type of truck under the assessment of the first level network. Once the type of truck is known, the appropriate module (there is a different module for each type of truck) of the second level network is selected. The same strain input data used in the first level is input into this module, divided into three networks that determine the output neurons corresponding to velocity, axle spacings and axle loads (Figure 3.10). The system is designed for a truck crossing the bridge on its own, but it could be extended to multiple

truck events by including a neural network at the front of the existing two levels. This additional network would uncouple the strain components of the different trucks.

Ideally, training patterns should be taken from strains measured as trucks pass over the bridge. A Fourier transform filter can remove dynamic effects from raw strain data, though the successful design of a filter in the time domain can reduce the overall time calculation. However, patterns based on experimental trials are inconvenient and time-consuming, and thus, only a few patterns can be obtained in this way. A theoretical bridge-truck model validated with real data collected from the bridge can provide a comprehensive set of training patterns that cover most regions of the problem domain. Though this theoretical bridge response involves errors, this approach is necessary if the system is to give accurate solution to any variation of the problem.

3.5.3 Extension to Orthotropic Bridges

Free of axle detector (FAD) algorithms have been developed for orthotropic bridges (OB-WIM) by Dempsey et al (1998a, 1999a). Velocity, number of axles and axle spacings are all calculated from the strain readings underneath the bridge at two different longitudinal locations. The values obtained for these parameters are not as accurate as axle detectors mounted on the road surface, but FAD systems are a solution to sites where installation of road sensors or road closure is not feasible. The prediction of axle and gross vehicle weights must allow for inaccurate estimates of axle spacings and velocity to some extent. This initial error is overcome using optimisation techniques.

Once a truck occurrence has been identified, the objective function to be minimised is the sum of squares of differences between the measured bending moments and the expected bending moments. The expected bending moment is generated from a theoretical model and it will depend on the truck parameters: Number of axles, velocity, axle spacing, axle weights and a parameter that aligns the measured response with the modelled response (offset).

This objective function must be examined with respect to certain truck parameters to determine an accurate optimisation procedure. The Hessian matrix was used to characterise the convexity of this function for a 2-axle rigid truck with axle spacings and weights as

parameters. It was found that while a simply supported beam is perfectly convex (only one minimum), there are multiple minima for a continuous beam (hence initial values in the optimisation procedure have a strong influence on final results). Figure 3.11(a) visualises the objective function of a 2-axle truck in a continuous beam where all parameters are maintained constant, except for the weight of the first axle and axle spacing. Figure 3.11(b) shows the objective function for a 5-axle truck on a continuous beam where the varying truck parameters are the axle spacings between the first three axles.

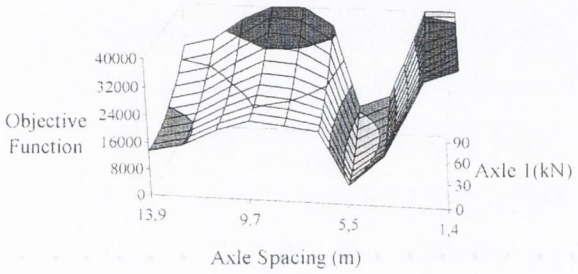

(a) Variation of Weight of First Axle and Axle Spacing (2-Axle Truck Objective Function)

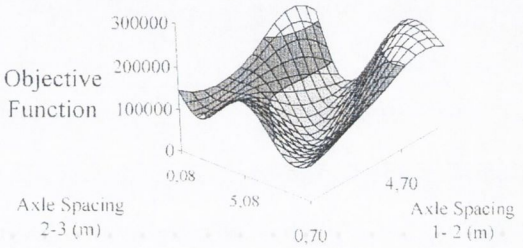

(b) Variation of Axle Spacing 1-2 and 2-3 (5-Axle Truck Objective Function)

Figure 3.11 – Evaluation of objective functions with respect to variation of truck parameters (after Dempsey et al. 1998a)

The correct minimum is more likely to be achieved if there is a good initial estimate of the truck parameters such as offset between measured and theoretical. It was found that the alignment of the first peak of the measured data with the first peak of the modelled data determines a sufficiently accurate value for the offset parameter. Errors in this parameter would generally result in small errors in axle weights and spacings. Hence, it was decided not to allow this parameter to vary in the optimisation to speed up calculations.

The optimisation problem was also extended to incorporate a 2-dimensional (2-D) bridge model, where each strain sensor at a different transverse location has a different influence line. In this case, the objective function to be minimised can be defined as (Dempsey et al. 2000):

$$O(p) = \sum_{j=1}^{S} \sum_{x=1}^{K} [M_j(x) - M_j{}^{M}(x)]^2 + k|p - p_0|^2 \tag{3.20}$$

where $M_j(x)$ and $M_j{}^{M}(x)$ are the theoretical and measured strains respectively at sensor j when the truck is at position x, S is the number of sensors transversely, K is the number of strain readings for a truck crossing, k a constant, and p_0 the initial values of the optimisation parameters p. The parameters p to be varied in the process are: velocity, axle spacings, axle weights and transverse location of the truck.

The OB-WIM algorithm first identifies a truck occurrence and calculates initial values of certain truck parameters. These first calculations are based on the distinct peaks left on the strain readings by the pass of each axle. If there is a correlation between the number of peaks and the time between different peaks at two instrumented sections, the number of axles are positively identified. If there is not a good correlation (i.e. problems in identifying closely spaced lightly loaded axles), a slightly modified algorithm is adopted that considers the possibility of a higher number of axles. A correct initial estimate of the velocity parameter is critical in finding the correct minimum. The time delay chosen for calculating speed is that which minimises the sum of squares of differences when superposing the measured responses at both sections. Initial values for axle spacings can be derived from this initial speed and the time between peaks in the measured record. Initial values for axle weights are taken as 30 kN (these parameters are not critical). Theoretical and measured responses are aligned prior to optimisation based on the first peak of the response, as stated earlier. Powell's method is recommended to carry out the optimisation constraining the speed parameter to a variation ± 5% with respect to the initial estimate. The solution is obtained when, for one iteration of the optimisation process, the change in the parameters is below a specified tolerance.

3.5.4 Multiple-longitudinal sensors

Kealy (1997) developed a weigh in motion system which is capable of giving a history of axle and gross vehicle weights at each point in time as a truck crosses a bridge at normal highway speed. This new bridge weigh in motion system is based on the use of multiple strain gauge sensor locations along the length of the bridge (MS-BWIM).

Principle

For the purpose of developing the required equations, the bridge will be assumed to act as a series of parallel longitudinal beams. This MS-BWIM system is based on a system of equations generated by assuming a static response of a bridge subjected to a vehicle loading. Bridge vibration is neglected in this instantaneous calculation (but truck vibration could be allowed for). The gross bending moment M at any longitudinal location along the span can be found by summing the individual bending moments as in Equation 3.3.

The bending moment at any point along the bridge for an N-axle vehicle can be expressed for any distance x of the first axle from the support, as a function of the influence line ($I(x)$) and applied loads (W_i) (Equation 3.4). In order to set up the necessary static equations, the bending moment influence line ($I_p(x)$) is required for each longitudinal sensor location p. For any truck crossing the bridge, a set of simultaneous equations as given in Equation 3.4 or 3.5 (as many as gauges) can be established for each point in position or time. Thus, a position or time based history of calculated axle weights can be determined.

The majority of trucks with four or more axles involve tandems, tridems or a combination of both. If we assume that all the axles within an axle group, whether a tandem or tridem, are of equal weight, we can reduce the number of unknowns when using Equation 3.5. This principle can be extended and applied to any vehicle where the number of individual axles exceeds the number of gauge locations. For most typical trucks, three gauge locations are adequate for the determination of axle weights. However, the equations must be independent and the number of axle groupings must be less than or equal to the number of independent equations.

Ideal Site

Single span bridges are not optimal for use with the MS-BWIM system as unique solutions to the generated simultaneous equations only occur for two axle vehicles when they are between the two strain gauge locations. As only two independent equations can be obtained, weights of a three-axle vehicle can not be obtained. Figure 3.12 shows influence lines and regions of dependence for three different strain gauges in a single span bridge (at ¼, ½ and ¾ span). All three gauges are dependent in Region I, while it is possible to find two independent gauges in Region II (between gauges 1 and 3).

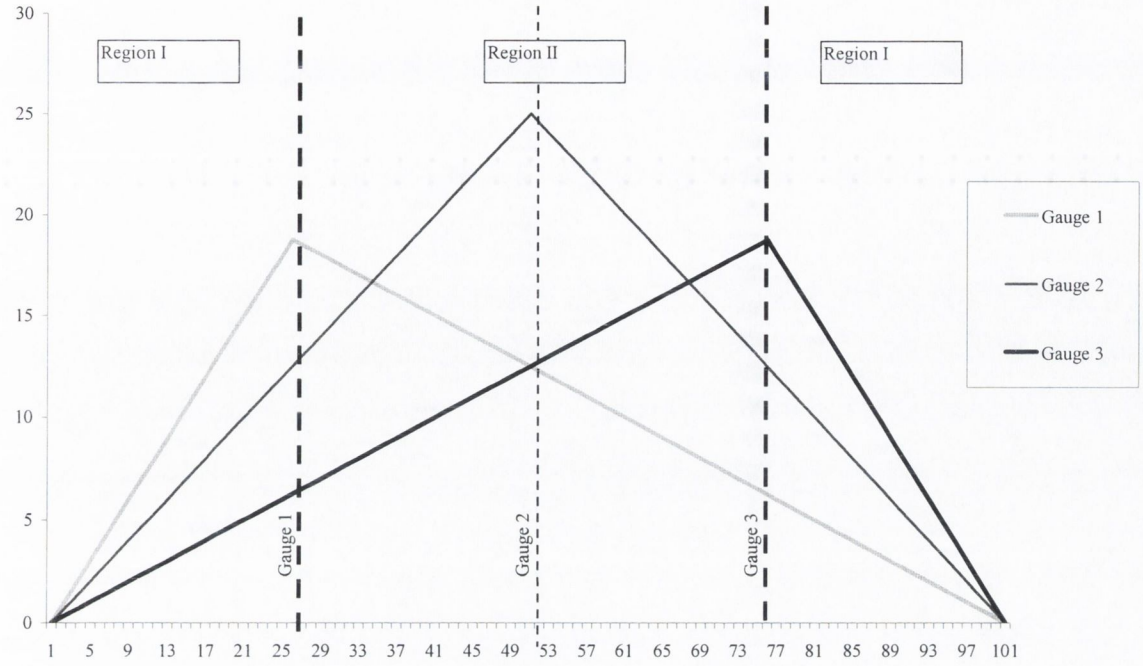

Figure 3.12 – Influence lines and regions of dependency in a single span

If a two span bridge is used, it is possible to determine weights for a 3-axle truck, but there are regions of the bridge where the determinant of the matrix of the equations equals or is approximately equal to zero, and axle weights can not be accurately calculated. Figure 3.13 shows influence lines and regions of dependency for strain at five gauge locations in a two-span bridge (at central support and ¼ and ¾ span from the central support). Only in region III (limited by gauges 2 and 4, located at ¼ span from the central support) there are three independent equations and instantaneous calculation of a three-axle truck becomes possible.

Kealy (1997) tested this algorithm on the two span continuous Belleville bridge on the A31 Motorway between Metz and Nancy in Eastern France. The calculated axle weights were very poor. This poor accuracy can, in part, be attributed to the manner in which velocity and the position of the vehicle on the bridge were monitored (a radar speed gun and a video camera) and the poor magnitudes of recorded strain.

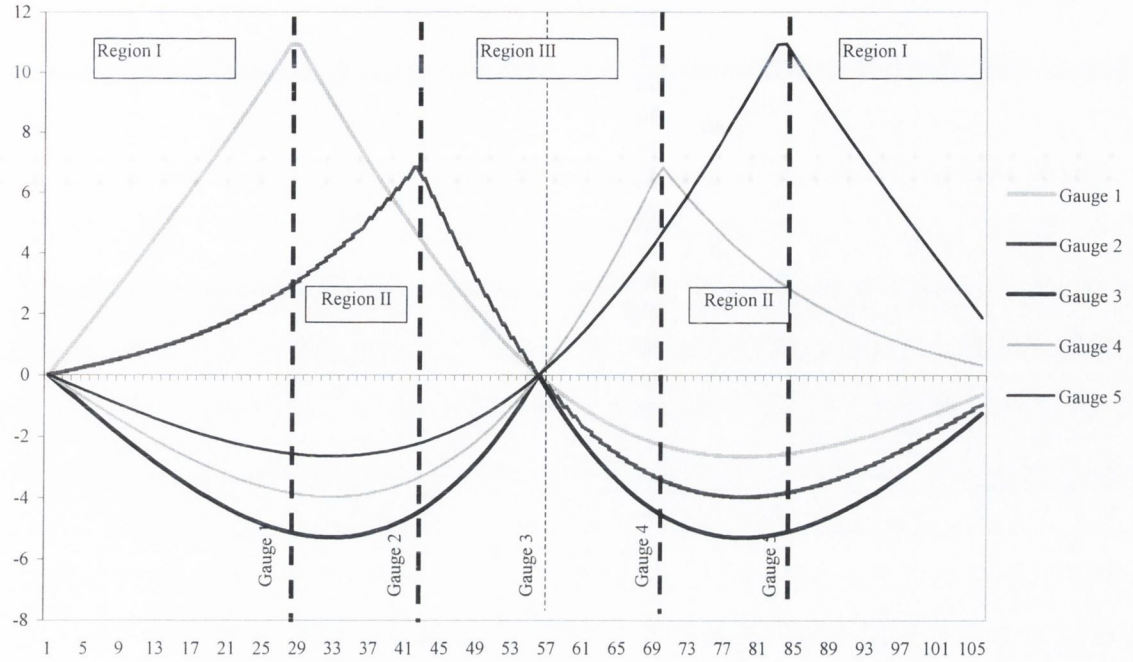

Figure 3.13 – Influence lines and regions of dependency in a two-span bridge

3.5.5 Combined System

Jacob et al (2000) introduces first theoretical studies on an algorithm that combines data from a pavement WIM system with continuous strain data taken from a B-WIM system. The algorithm minimises an error function given by the difference between theoretical and measured strain records in the B-WIM system (ε and $\tilde{\varepsilon}$ respectively), plus the difference between the real static axle weights and the calculated instantaneous axle weight by the WIM system (W_i and R_i respectively). This function is shown in Equation 3.21.

$$\varphi = \frac{\lambda}{T}\sum_{k=1}^{T}\left[\varepsilon(t_k) - \tilde{\varepsilon}(t_k)\right]^2 + \frac{(1-\lambda)}{N}\sum_{i=1}^{N}\left[W_i - R_i(t_i)\right]^2 \tag{3.21}$$

where T is the number of time increments for which strain is recorded on the bridge, N is the number of axles, and λ represents the relative weighting given to calculations of B-WIM compared to pavement WIM data. Thus, λ=0 represents a pure pavement WIM system, while λ=1 is a B-WIM system.

By minimising φ with respect to W_i (setting all partial derivatives to zero), the axle weights can be predicted from the matrix formulation:

$$[H]\begin{Bmatrix} W_1 \\ W_2 \\ \dots \\ W_N \end{Bmatrix} = \begin{Bmatrix} \frac{\lambda}{T}\sum_{k=1}^{T}\tilde{\varepsilon}(t_k)I_1(t_k)+\frac{(1-\lambda)}{N}R_1(t_1) \\ \frac{\lambda}{T}\sum_{k=1}^{T}\tilde{\varepsilon}(t_k)I_2(t_k)+\frac{(1-\lambda)}{N}R_2(t_2) \\ \dots \\ \frac{\lambda}{T}\sum_{k=1}^{T}\tilde{\varepsilon}(t_k)I_N(t_k)+\frac{(1-\lambda)}{N}R_N(t_N) \end{Bmatrix} \tag{3.22}$$

where the square matrix *[H]* is given by :

$$[H] = \begin{bmatrix} \frac{\lambda}{T}\sum_{k=1}^{T}I_1(t_k)I_1(t_k)+\frac{(1-\lambda)}{N} & \frac{\lambda}{T}\sum_{k=1}^{T}I_2(t_k)I_1(t_k) & \dots & \frac{\lambda}{T}\sum_{k=1}^{T}I_N(t_k)I_1(t_k) \\ \frac{\lambda}{T}\sum_{k=1}^{T}I_2(t_k)I_1(t_k) & \frac{\lambda}{T}\sum_{k=1}^{T}I_2(t_k)I_2(t_k)+\frac{(1-\lambda)}{N} & \dots & \frac{\lambda}{T}\sum_{k=1}^{T}I_2(t_k)I_N(t_k) \\ \dots & & & \\ \frac{\lambda}{T}\sum_{k=1}^{T}I_N(t_k)I_1(t_k) & \frac{\lambda}{T}\sum_{k=1}^{T}I_N(t_k)I_2(t_k) & \dots & \frac{\lambda}{T}\sum_{k=1}^{T}I_N(t_k)I_N(t_k)+\frac{(1-\lambda)}{N} \end{bmatrix} \tag{3.23}$$

From theoretical studies based on the generation of randomly varying dynamic forces on a bridge, results showed that the bandwidth of the confidence interval of the error in axle weights decreases for a certain range of λ. Accuracy class in axle weights and Gross Vehicle Weights improved from B(10) for λ equal to 0 or 1 (this is, both WIM or B-WIM systems considered individually) to B(+7) for a combination corresponding to λ between 0.4 and 0.6.

3.6 DYNAMIC ALGORITHMS

Most operating algorithms are static, this is, based on linearity and static equations of equilibrium. As the data being recorded is the sum of static and dynamic components, the dynamic component is generally ignored. Bridge and truck dynamics have been proven to be one of the sources of inaccuracy of static algorithms. Traditional averaging or filtering techniques are not suitable for the removal of dynamics in every case. A need was identified by the author to include dynamics in some way inside the formulation of the algorithm. Some modern algorithms use equations of dynamic equilibrium that require as input the unfiltered measured data. Three different approaches are known: O'Connor & Chan (1988a, 1988b) develop a dynamic algorithm for the calculation of wheel loads based

on the use of multiple longitudinal locations. Ghosn & Xu present an algorithm to describe the varying dynamic axle load. Dempsey (1997, Dempsey et al. 1998b) calculates axle loads from a consideration of the first modal component of the applied force when measuring strains in one only longitudinal location. These three dynamic algorithms are described in the following sections.

3.6.1 O'Connor & Chan

O'Connor & Chan (1988a, 1988b) develop a dynamic B-WIM algorithm with the purpose of identifying high-impact vehicles on short span bridges. This algorithm is based on the measurement of strain at different longitudinal locations. Then, dynamic truck wheel loads are predicted from the bridge measurements. Two different types of bridge measurement are tested: displacements and strains. Through theoretical and laboratory tests, it is seen that the use of strains gives better estimates of dynamic load than displacements. The accuracy strongly depends on a good knowledge of the equivalent bending stiffness and strain-bending moment relationships.

First, the bridge is modelled as an assembly of n lumped masses interconnected by massless elastic beam elements. The measured displacement Y_i at node i can be expressed as in Equation 3.24.

$$Y_i = Y^A{}_i - Y^I{}_i - Y^D{}_i \tag{3.24}$$

where $Y^A{}_i$ is the static displacement caused at node i by the applied loads, $Y^I{}_i$ that due to the inertial forces and $Y^D{}_i$ that due to the damping forces.

The displacement due to the applied load ($Y^A{}_i$) at node i is a function of the m applied wheel loads ($\{W\}_{mx1}$ = vector made of m rows and 1 column) that are on the bridge. This relationship is shown in Equation 3.25.

$$\{Y^A\}_{nx1} = [Y^u]_{nxm}\{W\}_{mx1} \tag{3.25}$$

where $Y^u{}_{ij}$ represents the deflection at node i caused by a unit load acting at the position of the j^{th} load, not necessarily at node i.

The displacement Y^I_i due to the inertial forces can be expressed as equation 3.26.

$$\{Y^I\}_{nx1} = [Y^f]_{nxn}[m]_{nxn}\{\ddot{Y}\}_{nx1} \tag{3.26}$$

where $[Y^f]$ is the flexibility matrix relating nodal displacements and nodal loads, $[m]$ the mass matrix, and $\{\ddot{Y}\}$ the nodal accelerations.

In the assumption of Rayleigh viscous damping, the displacement Y^D_i can be formulated as:

$$\{Y^D\}_{nx1} = [Y^f]_{nxn}[C]_{nxn}\{\dot{Y}\}_{nx1} \tag{3.27}$$

where $[C]$ is the damping matrix and $\{\dot{Y}\}$ is the vector of velocity of nodal displacements.

The problem can also be expressed as a function of total bending moment M_i as given in Equation 3.28:

$$M_i = M^A_i - M^I_i - M^D_i \tag{3.28}$$

where:

$$\{M^A\} = [M^u]\{W\} \tag{3.29}$$

$$\{M^I\} = [M^f][m]\{\ddot{Y}\} \tag{3.30}$$

$$\{M^D\} = [M^f][C]\{\dot{Y}\} \tag{3.31}$$

The result is the equation that governs the dynamic problem. In terms of bending moment, this equation is given by:

$$\{M\} = [M^u]\{W\} - [M^f][m]\{\ddot{Y}\} - [M^f][C]\{\dot{Y}\} \tag{3.32}$$

Then, applied forces can be found from measured strain, displacements, velocities or accelerations. If displacements Y_i are to be measured, nodal velocities or accelerations can

be found by central numerical differentiation. This differentiation can lead to poor results due to discontinuities in Y_i as wheel loads traverse a node. In any event, there are significant practical difficulties in measuring deflections.

If accelerations $\ddot{Y}_i$ are to be measured, velocity or displacements can be found by integration. Results using nodal accelerations were badly affected by errors in the integration of accelerations (O'Connor & Chan 1988a). There is a possibility of occurrence of high frequency noise in the records, leading to errors in computed deflections and larger errors in the estimates of applied forces.

Velocity $\dot{Y}_i$ can be measured using velocimeters. The errors derived from obtaining displacements through integration of the velocity curve should not be as important as in the case of accelerations.

O'Connor & Chan state that predicted loads are much more sensitive to an error in the measurement of displacements than an error in the measurement of strains. Hence, strains are the preferred input data of O'Connor & Chan in the dynamic algorithm. However, the use of strains demands the establishment of a relationship between nodal displacements and nodal bending moments. This relationship that gives displacement as a function of strain, requires the unknown loads W. These loads are approximated by the values in the preceding time step. Then, velocities and accelerations are derived from these nodal displacements.

If accelerations, displacements or bending moment are known for all interior nodes at all times, then the number of knowns n will exceed the number of unknown applied forces, which generally requires a solution through a least-squares technique.

The choice of the sections to be instrumented has been proved to be important in final accuracy, i.e., avoiding undefined solutions due to zero nodal displacements or bending moments in some non-zero load cases. Based on common axle spacings of vehicles, O'Connor and Chan avoid zero nodal bending moment by an end element of less than 1 m, a second element less than 1.4 m, and an intermediate element less than 1.7 m. For a span length $L \geq 4.8$ m, the required number of elements N is given by:

$$N = INT\left(\frac{L-4.8}{1.7}\right)+5 \tag{3.33}$$

where L is span length.

Laboratory tests were carried out to confirm conclusions from theoretical analysis. This identified calibration as one of the most important factors in final accuracy. In particular:

- Determination of flexural stiffness of the beam (EI)
- Determination of calibration factors (C_F) relating bending moment and measured strains

The flexural stiffness (EI) and calibration factors (C_F) were obtained by comparing an increasing load at a fixed location to the measured displacement and the corresponding bending moment to the measured strain respectively. Static and dynamic calibrations based on the application of incremental load steps and sinusoidal loads at different frequencies respectively, were analysed. Agreement was found to be poor when the frequency of the sinusoidal load was close to the natural frequency of the beam. Best results in predictions were obtained when both calibration parameters were determined dynamically (O'Connor & Chan 1988b). This was due to the great sensitivity of EI to minor changes for this case.

3.6.2 Ghosn & Xu

Ghosn & Xu present a modified B-WIM algorithm that allows the calculation of the dynamic amplitude of the bridge vibration in addition to the axle weights of a truck as it crosses over a bridge. The unknown axle weights (W_i) are calculated by minimising an error function (φ) given by the squared difference between a theoretical ($\varepsilon(t)$) and a measured ($\tilde{\varepsilon}(t)$) strain record as in Equation 3.34.

$$\varphi = \left[\varepsilon(t) - \tilde{\varepsilon}(t)\right]^2 \tag{3.34}$$

The algorithm starts by finding dominant frequencies (f_i) using a Fourier analysis of the strain record of an end girder. These end girders usually carry little static but considerable

dynamic effect. This makes it easier to distinguish between the static components and the purely dynamic components of the Fourier Transform.

The theoretical strain record ($\varepsilon(t)$) is made up of two components: A static component related to the influence line ($I(t)$) and a dynamic component given by "dynamic influence lines" of different frequencies f_i. Equation 3.35 shows this approach:

$$\varepsilon(t) = \sum_{i=1}^{N} W_i I_i(t) + \sum_{i=1}^{N_f} (D^s{}_i \sin(\omega_i t) + D^c{}_i \cos(\omega_i t)) \tag{3.35}$$

where N is number of axles, N_f is number of frequencies, $\omega_i = 2\pi f_i$ is circular frequency, and $D^s{}_i$ and $D^c{}_i$ are the amplitudes of the sine and cosine waves for the ith frequency, respectively. These amplitudes and the axle weights are unknown and they are calculated by minimising φ (Equation 3.34) with respect to W_i, $D^s{}_i$ and $D^c{}_i$ as shown in Equations 3.36 to 3.39.

$$\frac{\partial \varphi}{\partial W_i} = 0 \qquad i = 1, \ldots, N \tag{3.36}$$

$$\frac{\partial \varphi}{\partial D^s{}_i} = 0 \qquad i = 1, \ldots, N_f \tag{3.37}$$

$$\frac{\partial \varphi}{\partial D^c{}_i} = 0 \qquad i = 1, \ldots, N_f \tag{3.38}$$

This results in a matrix formulation given by:

$$\begin{bmatrix}
I_1 I_1 & I_1 I_2 & \ldots & I_1 \sin(\omega_1 t_j) & I_1 \sin(\omega_2 t_j) & \ldots & I_1 \cos(\omega_1 t_j) & I_1 \cos(\omega_2 t_j) & \ldots \\
I_2 I_1 & I_2 I_2 & \ldots & I_2 \sin(\omega_1 t_j) & I_2 \sin(\omega_2 t_j) & \ldots & I_2 \cos(\omega_1 t_j) & I_2 \cos(\omega_2 t_j) & \ldots \\
\ldots & & & & & & & & \\
\sin(\omega_1 t_j) I_1 & \sin(\omega_1 t_j) I_2 & \ldots & \sin(\omega_1 t_j)\sin(\omega_1 t_j) & \sin(\omega_1 t_j)\sin(\omega_2 t_j) & \ldots & \sin(\omega_1 t_j)\cos(\omega_1 t_j) & \sin(\omega_1 t_j)\cos(\omega_2 t_j) & \ldots \\
\sin(\omega_2 t_j) I_1 & \sin(\omega_2 t_j) I_2 & \ldots & \sin(\omega_2 t_j)\sin(\omega_1 t_j) & \sin(\varpi_2 t_j)\sin(\omega_2 t_j) & \ldots & \sin(\omega_2 t_j)\cos(\omega_1 t_j) & \sin(\omega_2 t_j)\cos(\omega_2 t_j) & \ldots \\
\ldots & & & & & & & & \\
\cos(\omega_1 t_j) I_1 & \cos(\omega_1 t_j) I_2 & \ldots & \cos(\omega_1 t_j)\sin(\omega_1 t_j) & \cos(\omega_1 t_j)\sin(\omega_2 t_j) & & \cos(\omega_1 t_j)\cos(\omega_1 t_j) & \cos(\omega_1 t_j)\cos(\omega_2 t_j) & \ldots \\
\cos(\omega_2 t_j) I_1 & \cos(\omega_2 t_j) I_2 & \ldots & \cos(\omega_2 t_j)\sin(\omega_1 t_j) & \cos(\varpi_2 t_j)\sin(\omega_2 t_j) & & \cos(\omega_2 t_j)\cos(\omega_1 t_j) & \cos(\varpi_2 t_j)\cos(\omega_2 t_j) & \ldots \\
\ldots & & & & & & & &
\end{bmatrix}
\begin{Bmatrix} W_1 \\ W_2 \\ \ldots \\ D^s{}_1 \\ D^s{}_2 \\ \ldots \\ D^c{}_1 \\ D^c{}_2 \\ \ldots \end{Bmatrix}
=
\begin{Bmatrix} \widetilde{\varepsilon} I_1 \\ \widetilde{\varepsilon} I_2 \\ \ldots \\ \widetilde{\varepsilon} \sin(\omega_1 t_j) \\ \widetilde{\varepsilon} \sin(\omega_2 t_j) \\ \ldots \\ \widetilde{\varepsilon} \cos(\omega_1 t_j) \\ \widetilde{\varepsilon} \cos(\omega_2 t_j) \\ \ldots \end{Bmatrix} \tag{3.39}$$

Initial results show that this method is capable of estimating the dynamic response of highway bridges under random truck crossings by extending the B-WIM algorithm as

proposed by Moses. However, the method is limited when a significant dynamic component and the static component of the Fourier Transform have similar frequencies. In this case, some of the static component might be included in the estimate of the dynamic amplitude or vice versa and the algorithm will be inaccurate.

3.6.3 Dempsey

Dempsey (1997, 1998b) introduced a new dynamic algorithm based on a single longitudinal sensor location. His algorithm determines axle weights by minimising an error function given by the squared difference between experimental and theoretical approximations of the first modal component of the applied force ($\widetilde{F}_1$ and F_1 respectively) as follows:

$$\varphi = \sum_{k=1}^{T} [F_1(t_k) - \widetilde{F}_1(t_k)]^2 \tag{3.40}$$

The first modal component of the applied force $\widetilde{F}_1$ can be estimated from measurements that are normalised (divided by bridge modal mass m_1) as given in Equation 3.41:

$$\frac{\widetilde{F}_1(t_k)}{m_1} = \ddot{y}_1(t_k) + 2\zeta_1\omega_1\dot{y}_1(t_k) + \omega_1^2 y_1(t_k) \tag{3.41}$$

where ω_1 is the modal circular frequency and ζ_1 the modal damping ratio. This equation, derived from the fundamental equation of dynamics and modal decoupling, requires generalised displacements y_1. Velocities ($\dot{y}_1$) and accelerations ($\ddot{y}_1$) can be obtained by differentiation. However, strains are generally measured instead of displacements. In this case, displacements can be approximated by integrating the bending moment diagram suggested by the measured strain. This calculation requires an iterative process until the difference between the results in applied loads from two successive calculations is small enough.

The theoretical modal component of the applied force is obtained through multiplication of the applied load by the value of the bridge mode shape at that load location (Equation 3.42).

$$F_1(t_k) = \{\Phi\}^T \{F(t_k)\} \tag{3.42}$$

where $\{\Phi_{ij}\}$ is a vector containing the values of the mode shape ordinate at the strain gauge location for the position of axle i at instant t_k.

By minimising error function defined in Equation 3.40:

$$\frac{\partial \varphi}{\partial F_{1_j}} = 0 \quad ; \quad j = 1,2,...N \tag{3.43}$$

where N is number of axles.

This gives:

$$\sum_{k=1}^{T}[2(\sum_{i=1}^{N} F_{1_i}\Phi_1(t_k - \frac{\sum_{r=1}^{i-1} a_r}{v}) - \widetilde{F}_1(t_k))\Phi_1(t_k - \frac{\sum_{r=1}^{j-1} a_r}{v})] = 0 \quad ; \quad j = 1,2,...,N \tag{3.44}$$

where v is velocity and a_j is axle spacing between axle j and $j+1$ (Figure 3.2).

And re-ordering:

$$\sum_{k=1}^{T}\left[\sum_{i=1}^{N} F_{1_i}\Phi_1(t_k - \frac{\sum_{r=1}^{i-1} a_r}{v})\right]\Phi_1(t_k - \frac{\sum_{r=1}^{j-1} a_r}{v}) = \sum_{k=1}^{T}\widetilde{F}_1(t_k)\Phi_1(t_k - \frac{\sum_{r=1}^{j-1} a_r}{v}) \quad ; \quad j = 1,...,,N \tag{3.45}$$

This least squares fitting method between F_1 and $\widetilde{F}_1$ let derive a matrix formulation as:

$$[H]_{NxN} * \{F_1\}_{Nx1} = \{P\}_{Nx1} \tag{3.46}$$

where $\{F_1\}$ are the first modal component of the applied force and n number of axles. $\{F_1\}$ is assumed to be related to the axle weights through a calibration factor. The matrix $[H]$ and vector $\{P\}$ are defined as :

$$[H_{ij}] = \sum_{k=1}^{t} \Phi_1(t_k - \frac{\sum_{r=1}^{i-1} a_r}{v}) \Phi_1(t_k - \frac{\sum_{r=1}^{j-1} a_r}{v}) \tag{3.47}$$

$$\{P_j\} = \sum_{k=1}^{t} \frac{\widetilde{F}_1(t_k) \Phi_1(t_k - \frac{\sum_{r=1}^{j-1} a_r}{v})}{m_1} \quad ; \quad j = 1,..,N \tag{3.48}$$

Dempsey et al (1998b) reveal the potential of a dynamic B-WIM algorithm for bridges with short spans and high dynamics in the measured record. However, the author addresses some shortcomings in this algorithm:

- The first modal component of the force is estimated by applying the decoupled equation of dynamics for the first bridge mode shape (Equation 3.41). This equation requires displacements, velocity and accelerations. Additionally, bridge modal mass, modal damping and frequency for that mode shape are necessary. As strains are generally measured instead of deflections, some errors will result from integration of the bending moment diagram.
- As the algorithm is based on one longitudinal sensor location, the shape of the bending moment diagram is assumed and the diagram reconstructed from the strain measurements at one single longitudinal location. Additionally, the bending effect of damping and inertial forces is ignored in the bending moment diagram. Though convergence might arise after a few iterations, the final result could be quite far from the static value due to the inaccuracy of the bending moment diagram.
- Another error is introduced by the use of total displacements in a modal equation (Equation 3.41) that requires generalised displacements corresponding to a specific mode shape.
- The algorithm assumes that the first modal component of the applied forces and the static weights are directly related, which can clearly differ from reality. If a series of

concentrated loads are represented by the modal components of the bridge vibration (this is, the sum of the products of the load magnitude and the value of the mode shape at the load location for each load), the most significant contribution is not going to be made by the first modal component at every instant. The highest modal component will depend on the axle spacing, applied load, bridge length and vehicle location. In other words, only one modal component (not always the most representative) is used to represent a force, and hence, an incorrect assumption of proportionality between this single representation and the force is made.

3.7 ACCURACY OF BRIDGE WEIGH IN MOTION SYSTEMS

Traditionally, B-WIM systems were recommended for culverts or bridges with spans between 8 and 25 m. Work was necessary to establish which bridge types could effectively serve for weigh-in-motion purposes. The COST323 action and the WAVE project have tested B-WIM systems in cold climates and for a wide range of bridges, i.e. short slab bridges, integral bridges and orthotropic deck bridges. Results of different test trials prior to WAVE and as part of WAVE (Jacob et al. 2000) are presented in this section. It has also been proven that different types of bridge can be used without axle detectors mounted on the road surface (Žnidaric et al. 1999a).

3.7.1 American, Australian and European Bridge WIM prior to WAVE

In Australia, CULWAY has been found to typically estimate static gross vehicle weight within ±10%, and the individual axle weights within ±15% at 95% confidence limits[10]. Tierney et al (1996) found similar accuracy of two pavement WIM (Australian plate in ground on load cells and German strain gauged plate in ground) and three B-WIM systems (CULWAY, AXWAY and FASTWEIGH), with poorer results from a pavement WIM based on a surface mounted capacitive weigh pad, which is not flushed with the road surface.

All accuracy classification until the end of the chapter is given according to the COST323 Specification (1997). In 1995, a European (first DuWIM) and a commercially available American B-WIM system were first tested together on a bridge in Slovenia (O'Brien et al. 1999b). Both systems were giving an accuracy class of D+(20) for gross vehicle weights,

but when considering single axle and axle group results, only an accuracy class E was achieved.

3.7.2 Slovenia

B-WIM tests have been carried out in Slovenia as part of the WAVE project. The study centred on concrete slab bridges. Final accuracy was found to be strongly related to a number of parameters (Section 3.5.1) such as: influence line, calibration methods, velocity, road unevenness and bridge skew. Žnidaric et al (1999b) report on the influence of these parameters on final accuracy, which results are summarised in this section. The B-WIM system being used for analysis is referred to as SiWIM (Žnidaric et al. 1998), which is briefly described in Chapter 4. The SiWIM software uses Moses' algorithm as the basis for the calculation of axle weights.

Influence of Influence line

A 10 m span, 9° skew integral slab bridge was investigated. A common calibration factor was obtained from a test vehicle and applied to all vehicles. If the theoretical influence line for a single fixed (encastré) supported span is taken, the accuracy class retained is D(25) due mainly to inaccuracy in single axles. B(10) and C(15) accuracy are obtained respectively for the individual criteria of group of axles and gross weight. These results can be improved by using an experimental influence line based on the measured strains, which has become common practice (McNulty 1999). Thanks to a better accuracy in single axles, the overall accuracy is raised to D+(20). The results are presented in Table 3.1.

Table 3.1 – Accuracy classification for experimental influence line

(**n**: Total number of vehicles; **m**: mean; **s**: Standard deviation; π_0: level of confidence; δ: tolerance of the retained accuracy class; δ_{min}: minimum width of the confidence interval for π_0; π: Level of confidence of the interval $[-\delta,\delta]$)

	Relative error statistics				Accuracy calculation				
Criterion	**n**	**m (%)**	**s (%)**	**π_0 (%)**	**Class**	**δ (%)**	**δ_{min} (%)**	**π (%)**	**Class Retained**
Single axle	60	2.71	9.81	91.8	D+(20)	25	20.52	91.6	
Group of axles	18	-1.05	4.26	86.5	B+(7)	10	8.99	89.1	**D+(20)**
Gross Weight	31	1.59	5.48	89.8	C(15)	15	11.62	89.3	

Influence of Calibration Methods

Accuracy can be improved by using different calibration factors for different vehicle types. If two calibrations factors are adopted, the overall accuracy improves from the previous D+(20) to C(15).

Influence of Velocity

The effect of a bad first estimation of speed can be overcome with the use of optimisation techniques (Sections 3.5.1 and 3.5.3). The accuracy classification when applying two calibration factors, experimental influence lines and optimisation, is given in Table 3.2. Compared to the last results, optimisation brings gross weight from C(15) up to B(10). This improvement will be more important if estimation of speed is not good in first instance.

Table 3.2 – Accuracy classification with 2 calibration factors and optimisation

(**n**: Total number of vehicles; **m**: mean; **s**: Standard deviation; π_0: level of confidence; δ: tolerance of the retained accuracy class; δ_{min}: minimum width of the confidence interval for π_0; π: Level of confidence of the interval $[-\delta,\delta]$)

	Relative error statistics				Accuracy calculation				
Criterion	**n**	**m** (%)	**s** (%)	π_0 (%)	**Class**	δ (%)	δ_{min} (%)	π (%)	**Class Retained**
Single axle	60	1.41	7.59	91.8	C(15)	20	15.61	97.73	**C(15)**
Group of axles	18	-2.40	4.16	86.5	B+(7)	10	9.53	88.75	
Gross Weight	31	-0.09	4.63	89.8	B(10)	10	9.50	91.72	

Finally, overall accuracy can be brought up to B(10) with a 4% fixed redistribution of load from the first axle to the others in vehicles with more than 2 axles. This approach is similar to the calibration by axle rank discussed in Section 2.4.4.

Influence of Road Evenness

A similar bridge to the one above, but with a bump on the bridge, has been tested experimentally by Žnidaric et al (1999b). This bump induced considerable excitation of truck wheel loads and, even though accuracy in gross weight remains as B(10), the overall accuracy is E(40) as shown in Table 3.3. However, if all axles below 20 kN are ignored, the overall accuracy is improved to C(15). These axles and group of axles show a high bias

in results for single axles and group of axles. This indicates that better results could be obtained if using an additional calibration by axle rank.

Table 3.3 – Accuracy classification for bridge with bump

(**n**: Total number of vehicles; **m**: mean; **s**: Standard deviation; π_0: level of confidence; δ: tolerance of the retained accuracy class; δ_{min}: minimum width of the confidence interval for π_0; π: Level of confidence of the interval $[-\delta,\delta]$)

	Relative error statistics				Accuracy calculation				
Criterion	**No**	**Mean (%)**	**St.D. (%)**	π_0 (%)	**Class**	δ (%)	δ_{min} (%)	π (%)	**Class Retained**
Single axle	52	-6.22	7.86	96.2	D(25)	30	28.4	97.32	**E(40)**
Group of axles	32	6.94	11.85	95.4	E(40)	43	40.28	96.84	
Gross Weight	34	0.00	3.23	95.5	B(10)	10	9.82	95.92	

Influence of Bridge Skewness

Two integral slab bridges, each with two spans of about 10 m, were used to check how skew could affect accuracy. They are very similar except for their skewness, which was 7° and 26°. Results are presented in Table 3.4.

Table 3.4 – Effect of bridge skew on accuracy classification

(**n**: Total number of vehicles; **m**: mean; **s**: Standard deviation; π_0: level of confidence; δ: tolerance of the retained accuracy class; δ_{min}: minimum width of the confidence interval for π_0; π: Level of confidence of the interval $[-\delta,\delta]$)

	Relative error statistics				Accuracy calculation				
7° Skew Criterion	**n**	**m (%)**	**s (%)**	π_0 (%)	**Class**	δ (%)	δ_{min} (%)	π (%)	**Class retained**
Single axle	31	5.24	8.32	89.8	C(15)	20	19.46	90.89	**C(15)**
Group of axles	33	-0.84	4.77	90.0	B+(7)	10	9.89	90.43	
Gross Weight	32	0.43	3.17	89.9	B+(7)	7	6.55	92.31	
	Relative error statistics				**Accuracy calculation**				
26° Skew Criterion	**n**	**m (%)**	**s (%)**	π_0 (%)	**Class**	δ (%)	δ_{min} (%)	π (%)	**Class retained**
Single axle	27	7.29	9.26	89.3	D+(20)	25	22.96	92.69	**D+(20)**
Group of axles	37	2.20	4.24	90.3	B+(7)	10	9.5	92.17	
Gross Weight	32	2.84	3.53	89.9	B(10)	10	8.78	94.62	

The inaccuracy for the criterion of single axles is related to the fact that most of them corresponded to very lightly loaded steering axles. Once again, this could be improved if using calibration by axle rank due to the significant bias in single axles. In conclusion, slab bridges were found suitable for B-WIM measurements with accuracy comparable to beam bridges (Žnidaric et al 1999b).

3.7.3 Autreville

Tests on orthotropic steel bridges took place in Autreville, Eastern France, as part of the WAVE project (Section 2.2), during August 1997 and July 1998. Two longitudinal sections were instrumented with strain sensors at seven different transverse locations (on each of the seven stiffeners under the slow lane). Dempsey et al (1999a) carried out the analysis by implementing the OB-WIM algorithm described in Section 3.5.3. When using an optimisation algorithm based on a 1-dimensional bridge model, accuracy class D+(20) was achieved for all criteria. This accuracy was raised to C(15) when considering both longitudinal and transverse directions were represented (2-D model). This accuracy class was achieved without any axle detectors on the road surface. The results for this second approach are shown in Table 3.5.

Table 3.5 – Accuracy classification for orthotropic bridge

(**n**: Total number of vehicles; **m**: mean; **s**: Standard deviation; π_0: level of confidence; δ: tolerance of the retained accuracy class; δ_{min}: minimum width of the confidence interval for π_0; π: Level of confidence of the interval $[-\delta,\delta]$)

	Relative error statistics				Accuracy calculation				
Criterion	**n**	**m (%)**	**s (%)**	**π_0 (%)**	**Class**	**δ (%)**	**δ_{min} (%)**	**π (%)**	**Class Retained**
Single axle	55	0.79	8.95	91.6	C(15)	20	18.3	91.6	**C(15)**
Group of axles	27	0.17	8.22	89.1	C(15)	18	16.9	89.1	
Gross Weight	28	0.55	5.55	89.3	C(15)	15	11.5	89.3	

3.7.4 Luleå Tests in Cold Environment

B-WIM measurements performed by TCD (Trinity College Dublin) took place in June 1997, March and June 1998 as part of the Cold Environmental Test in Luleå (Section 2.5.5). The B-WIM system was re-installed and re-calibrated each time. Data was filtered at 4 Hz in the first two tests, while data remained unfiltered in the third test. The bridge is

an integral structure composed of two spans, 14.6 m each. UCD (University College Dublin) and ZAG (Slovenian National Building and Civil Engineering Institute) carried out analysis of the measured data independently. Though both Dublin (DuWIM) and Slovenian (SiWIM) approaches use a static algorithm similar to the one proposed by Moses, one of their differences lies in the adjustment of the influence line taken as the reference.

Different bridge behaviour (influence line) was detected in the Summer and Winter seasons, perhaps due to the extreme weather conditions (river frozen around the columns of the bridge). Final accuracy has been achieved by detecting and removing those vehicles with anomalies (i.e. wrong identification of the vehicle being weighed in the static scale and recordings interfered with, either electronically or by a multiple vehicle presence). From analysis of the Winter results, the daily temperature fluctuation was found to have a significant effect as shown in Figure 3.14. This was due to a difference in temperature between the active gauge (on the bridge) and the dummy gauge (in the data acquisition equipment in a car). When allowing for a temperature correction, results for random traffic improved from an overall accuracy of D+(20) to C(15). Best results were achieved in June 1998 due to the use of unfiltered data, a new gauge configuration all located on the bridge and a better data acquisition card (16 bits instead of 12 bits) which improved strain amplification by nearly 10.

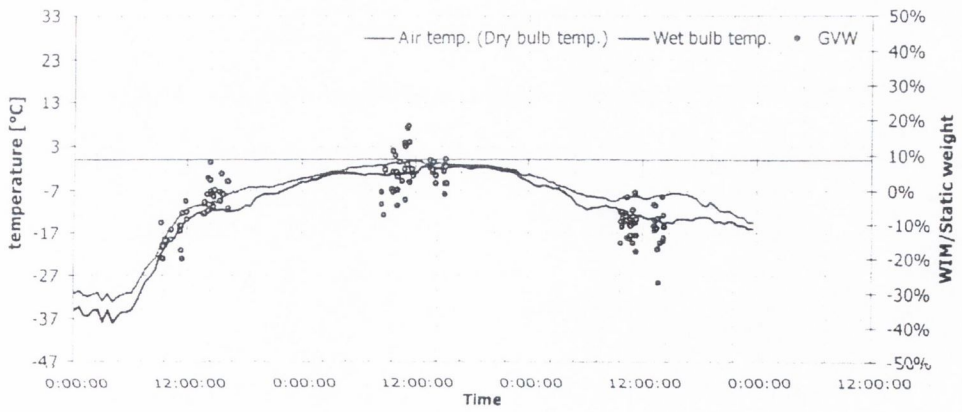

Figure 3.14 – Temperature dependence of Luleå B-WIM measurements (after Žnidaric et al 1999b)

ZAG

Results from test vehicles and random traffic for the first two tests were found by ZAG to be C(15). The results corresponding to the calibration of the second summer season are shown in Table 3.6.

Table 3.6 – Accuracy classification for test vehicles in June 1998

(**n**: Total number of vehicles; **m**: mean; **s**: Standard deviation; π_0: level of confidence; δ: tolerance of the retained accuracy class; δ_{min}: minimum width of the confidence interval for π_0; π: Level of confidence of the interval $[-\delta,\delta]$)

	Relative error statistics				Accuracy calculation				
Criterion	**n**	**m (%)**	**s (%)**	π_0 (%)	**Class**	δ (%)	δ_{min} (%)	π (%)	**Class Retained**
Single axle	34	0.32	4.27	95.5	B(10)	15	13.00	98.05	**B(10)**
Group of axles	54	0.01	2.57	96.2	B+(7)	10	7.72	99.36	
Gross Weight	34	0.00	2.30	95.5	B+(7)	7	7.00	95.50	

When the population from random traffic was analysed first, results were class D(25), surprisingly. Further analysis showed that there was a mismatch between the vehicles weighed by the B-WIM system and the static scale. Removing the outliers, B+(7) was obtained over a total sample of 104 vehicles. However, the system remained in B(10) because of the criterion of group of axles and single axles (Table 3.7).

Table 3.7 – Accuracy classification for random traffic in June 1998

(**n**: Total number of vehicles; **m**: mean; **s**: Standard deviation; π_0: level of confidence; δ: tolerance of the retained accuracy class; δ_{min}: minimum width of the confidence interval for π_0; π: Level of confidence of the interval $[-\delta,\delta]$)

	Relative error statistics				Accuracy calculation				
Criterion	**n**	**m (%)**	**s (%)**	π_0 (%)	**Class**	δ (%)	δ_{min} (%)	π (%)	**Class Retained**
Single axle	187	0.75	6.42	93.7	B(10)	15	13.00	96.9	**B(10)**
Group of axles	191	-0.86	5.75	93.7	B(10)	13	11.7	96.2	
Gross Weight	104	-0.03	2.83	92.9	B+(7)	7	5.7	97.5	

UCD

McNulty (1999) obtains accuracy classes of C(15), C(15) and B(10) for the three respective tests. The reduced accuracy in the first two trials is due to the effects of low pass filtering (already discussed in Section 3.5.1). Detailed results of the three tests for random traffic are shown in Tables 3.8 to 3.10.

Table 3.8 – Accuracy classification for random traffic in June 1997

(n: Total number of vehicles; **m**: mean; **s**: Standard deviation; π_0: level of confidence; δ: tolerance of the upper accuracy class; δ_n: tolerance of the lower accuracy class; π: Level of confidence of the interval of the retained accuracy class)

	Relative error statistics				Accuracy calculation				
Criterion	**n**	**m** (%)	**s** (%)	π_0 (%)	**Class**	δ B(10)	δ_n C(15)	π (%)	**Class Retained**
Single axle	156	1.318	8.562	93.5	C(15)	15	20	96.8	**C(15)**
Group of axles	162	3.7	6.02	93.6	C(15)	13	18	98.6	
Gross Weight	95	3.09	4.08	92.8	B(10)	10	10	93.1	

Table 3.9 – Accuracy classification for random traffic in March 1998

(**n**: Total number of vehicles; **m**: mean; **s**: Standard deviation; π_0: level of confidence; δ: tolerance of the upper accuracy class; δ_n: tolerance of the lower accuracy class; π: Level of confidence of the interval of the retained accuracy class)

	Relative error statistics				Accuracy calculation				
Criterion	**n**	**m** (%)	**s** (%)	π_0 (%)	**Class**	δ C(15)	δ_n D(20)	π (%)	**Class Retained**
Single axle	188	-0.757	8.562	94.5	C(15)	20	25	97.09	**C(15)**
Group of axles	227	-1.904	8.325	94.9	C(15)	18	23	95.23	
Gross Weight	125	-1.008	6.373	94.4	C(15)	15	20	96.84	

Table 3.10 – Accuracy classification for random traffic in June 1998

(n: Total number of vehicles; **m**: mean; s: Standard deviation; π_0: level of confidence; δ: tolerance of the upper accuracy class; δ_n: tolerance of the lower accuracy class; π: Level of confidence of the interval of the reained accuracy class)

	Relative error statistics				Accuracy calculation				
Criterion	**n**	**m (%)**	**s (%)**	π_0 **(%)**	**Class**	δ **B(7)**	δ_n **B(10)**	π **(%)**	**Class Retained**
Single axle	188	-1.312	7.267	93.7	B(10)	11	25	94.12	**B(10)**
Group of axles	239	-0.885	3.72	95.4	B(10)	10	13	98.08	
Gross Weight	122	-0.182	5.259	93.2	B(10)	7	10	98.54	

3.8 CONCLUSIONS

B-WIM was developed by Moses (Section 3.3) in the 1970's as an alternative to pavement WIM systems. These systems convert the information provided by bridge measurements into traffic data through the application of an algorithm. First algorithms were based on static equations of equilibrium and the concept of influence line. These systems were recommended in beam & slab bridges initially, and they were successfully implemented in culverts in the 1980's (Section 3.4.2). However, the use of B-WIM in other bridge forms was not always feasible due to durability problems of axle detectors embedded in or mounted on the road surface, bridge and truck dynamics and errors derived from the estimation of axle spacing, speed and/or influence line (Section 3.5.1).

In recent years, the use of optimisation techniques (Section 3.5.3) and experimental influence lines have overcome some of these limitations. So, B-WIM has been extended to slab (Section 3.7.2) and orthotropic bridges (Section 3.7.3), and a B-WIM system installed in a two-span integral bridge has achieved excellent levels of accuracy in a major trial test under extreme climate conditions (Section 3.7.4). The use of more sensors (Section 3.5.4), neural networks (Section 3.5.2) and dynamic equations of equilibrium (Section 3.6) are expected to further improve the accuracy, durability and range of applicability of B-WIM.

4

DATA COLLECTION AND PROCESSING

4.1 INTRODUCTION

This chapter describes the hardware necessary for detecting and measuring traffic loads on bridges and the software developed by the author to process these measurements. Further details on the PC-based instrumentation used by the Irish team can be found in Appendix C. A B-WIM system is generally composed of devices to measure bridge strain, sensors to detect vehicle axles, a personal computer, software, signal conditioning and data acquisition (DAQ) hardware (Figure 3.1).

The bridge bending is measured either by strain gauges or reusable strain transducers. These devices produce an electrical signal proportional to the strain they are monitoring. If a B-WIM algorithm based on one sensor location is to be applied, this single longitudinal position is normally located in a main structural member at a point where strains get highest values (i.e. midspan in a simply supported beam). Multiple-sensor B-WIM algorithms use several longitudinal locations for more accurate weighing and their ideal number and location will be considered in Chapter 7.

Most existing B-WIM systems obtain the vehicle silhouette and velocity from axle detectors installed on the road surface. These detectors can be removable (tape switches, pneumatic tubes) or permanent (low-grade piezo-electric sensors or other built-in pavement sensors). Information on times is generated when an axle passes over them. If a pair of sensors is placed in each lane, it is possible to derive velocity and axle spacings for all vehicles. These axle detectors become unnecessary when a FAD (**F**ree **A**xle **D**etector) system is able to achieve the required accuracy. FAD identifies axles purely by measuring strain in appropriate locations of the bridge structure.

Software is composed of two main parts: Data acquisition and calculation of axle weights. Data acquisition is common to all B-WIM systems. This part of the program acquires

information on voltages from strain gauges/transducers and road sensors, while the latter part implements the B-WIM algorithm that converts voltages into weights. Three different approaches are described: CULWAY, SiWIM and the Irish DuWIM.

42 STRAIN MEASUREMENT

Strain (ε) is defined as the fractional change in length shown in Figure 4.1.

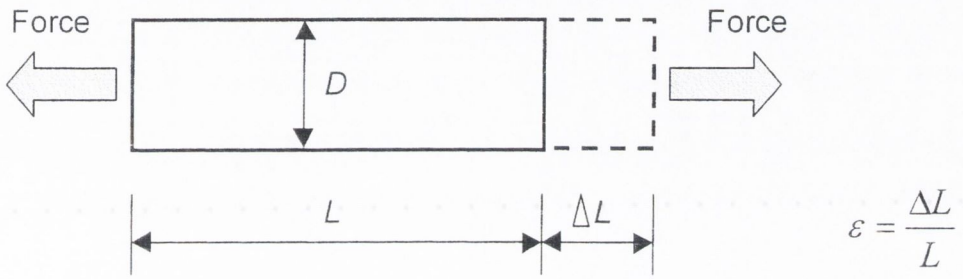

Figure 4.1 – Definition of strain (ε)

Strain can be positive (tensile) or negative (compressive). The magnitude of measured strain is often expressed as microstrain ($1\ \mu\varepsilon = 10^{-6}\ \varepsilon$).

Figure 4.2(a) shows a strain transducer and Figure 4.2(b) strain gauges glued directly onto the bridge deck. Several methods of measuring strain in bridges are presented next.

4.2.1 Strain gauges

The strain gauge is bonded to the bridge surface (Figure 4.2(b)). Then, the strain experienced by the bridge is transferred directly to the gauge, which responds with a linear change in electrical resistance.

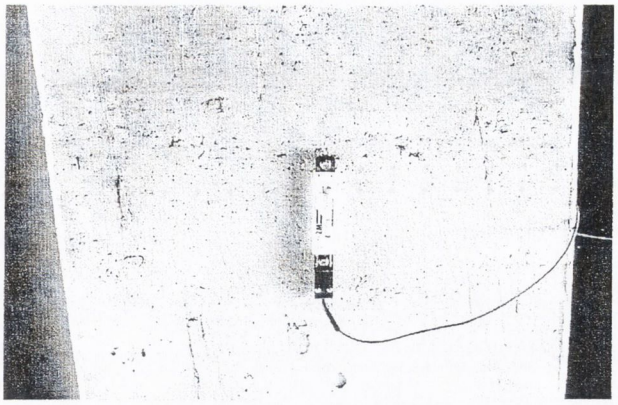

(a) Strain transducer (after Jacob et al. 2000)

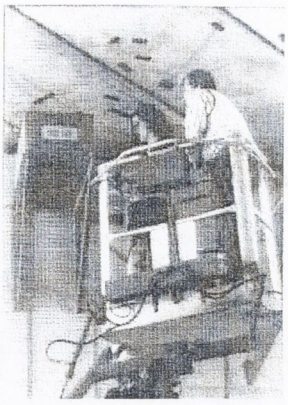

(b) Installation of strain gauges

Figure 4.2 – Instrumentation to measure strain in a bridge deck

The bonded metallic strain gauge is the most widely used, which consists of a very fine wire or, more commonly, metallic foil arranged in a grid pattern (Figure 4.3(a)). The cross sectional area of the grid is minimised to reduce the effect of shear strain. Strain is detected by the change in electrical resistance of the gauge grid. Because these changes in resistance are very small, strain gauges are usually measured in a Wheatstone Bridge configuration as shown in Figure 4.3(b).

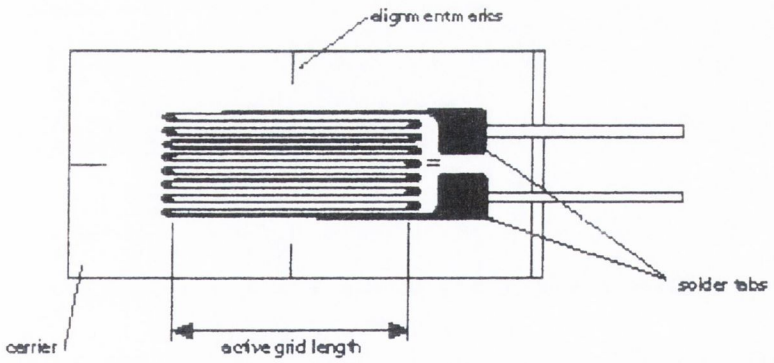

(a) Layout

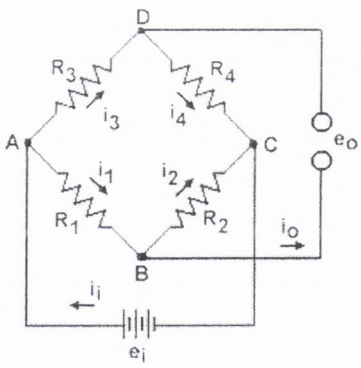

(b) Typical configuration

Figure 4.3 – Description of strain gauges

In this figure, R_1, R_2, R_3, and R_4, represent resistors, and e_o and e_i the excitation voltage powering the Wheatstone bridge and the voltage measured by the DAQ system, respectively. The measured voltage, e_i, can be obtained by applying Ohm's laws, resulting in Equation 4.1. As strain is applied to the gauge, its resistance value changes, causing a change in the voltage at e_i.

$$e_i = \left(\frac{R_2}{R_2 + R_4} - \frac{R_1}{R_1 + R_3} \right) e_o \tag{4.1}$$

The Irish team has commonly been using strain gauges type PL-90[11]. This type is composed of polyester wire (Cu-Ni), with a normal operational temperature range from –20°C to 80°C and 120 Ω resistance. Strain is related to the fractional change in electrical resistance through the gauge factor (*GF*), a parameter that measures the sensitivity of the gauge. The gauge factor for metallic strain gauges is typically around 2.

Strain gauges can occupy one, two or four arms of the Wheatstone bridge, with any remaining positions filled with fixed resistors. One arm was used in the experiments in Belleville, France (Chapter 8), where the gauge was directly glued onto the steel bridge deck. In this case, R_4 was replaced with an active gauge subjected to the applied force, $R_1 = R_3$ are fixed resistors, and R_2 a dummy gauge with the same nominal value as R_4. By using an active and a dummy gauge, the effect of temperature is avoided. The temperature effects, identical for both gauges, do not change the ratio of their resistance or the measured voltage in Equation 4.1. Strain in this quarter bridge is given by Equation 4.2.

$$\varepsilon = \frac{-4\left(\frac{e_i(unstrained) - e_i(strained)}{e_o} \right)}{GF\left[1 + 2\left(\frac{e_i(unstrained) - e_i(strained)}{e_o} \right) \right]} \left(1 + \frac{R_L}{R_2} \right) \tag{4.2}$$

where R_L is the resistance in the lead wires of the strain gauges.

Alternatively, using two active gauges can double the sensitivity of the Wheatstone bridge. To achieve this, R_2 is mounted in compression and R_4 in tension, or vice versa. Using all four arms of the Bridge can further increase sensitivity. To achieve this, R_2 and R_3 are mounted in compression, and R_1 and R_4 are mounted in tension. Equation 4.2 changes when using such half or full Bridges. These two configurations are applied to the mechanical strain amplifier described in the following section.

4.2.2 Strain Amplifiers

Strain amplifiers are necessary when a better strain definition than the one occurring in the structure is required. The principle of a mechanical strain amplifier is concentrating the elongation or shortening of a given length on the bridge into a highly strained section of the amplifier. The mechanical strain amplifiers are connected to the deck of the bridge via either steel anchor plates that are glued or bolted to the bridge deck or by directly bolting the gauge to the structure.

Different models of strain amplifier are shown in Figure 4.4. There are two different approaches: a) Amplification by direct measurement of axial deformation into a smaller and more flexible inner section (Peters 1984, González 1996) and b) Amplification of strain by conversion of axial deformation into localised bending (Peters 1984, Dempsey 1997). The latter approach has been proven to be more robust and stable according to the Australian and Irish experience. The Irish model is reviewed next.

(a) Commercial strain transducers (outside) and Irish mechanical strain amplifiers (inside) attached to a bridge soffit (after Jacob et al. 2000)

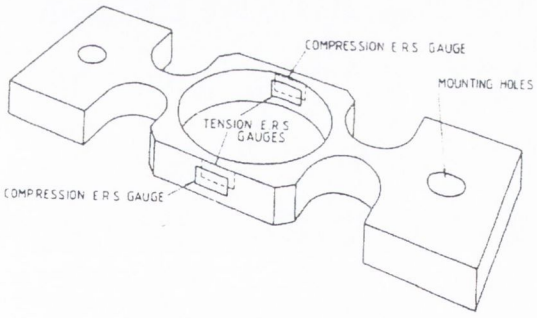

(b) Australian mechanical strain amplifier (after Peters 1984)

Figure 4.4 – Strain Transducers

Irish Model

This Irish amplifier was designed by Dempsey (1997) to overcome the limitations of strain gauges in stiff bridges. His purpose was converting axial strain in a portion of the bridge into a greater bending strain in the amplifier. As shown in Figure 4.5, the amplifier is

composed of two separate parts: an instrumented aluminium beam and a bar inducing an imposed displacement at midspan of the beam.

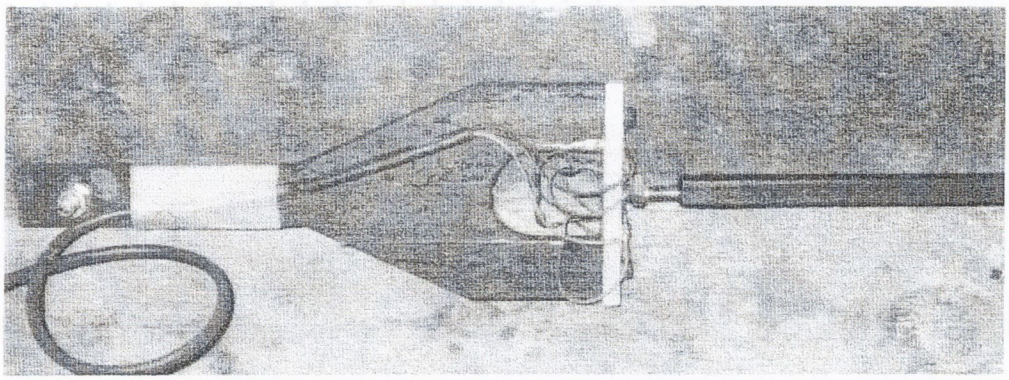

Figure 4.5 – Irish mechanical strain amplifier

Assuming the beam is fixed at the ends, the approximate degree of amplification can be derived from the following formula (González 1996):

$$Amplification = \frac{L_m^{\ 2}}{12 h_m d_m} \tag{4.3}$$

where L_m, h_m and d_m are defined in Figure 4.6.

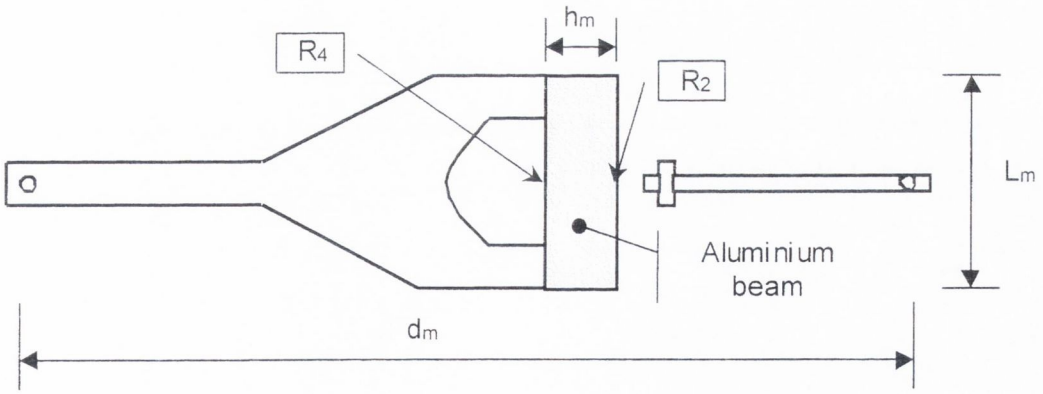

Figure 4.6 – Parameters of Irish mechanical strain amplifier

The original amplifier has dimensions L_m = 60 mm, h_m = 6 mm and d_m = 400 mm, which is equivalent to a strain about eight times bigger than gluing a gauge directly onto the bridge. Strain gauges in compression and tension in Figure 4.6 have the same nomenclature, R_2

and R_4, as in Figure 4.3(b). R_1 and R_3 in this scheme would be fixed resistors in the module block (Appendix C) to complete a half Wheatstone bridge. This is the configuration originally used in the first experiments carried out by the Irish team. Strain in such a configuration is given by:

$$\varepsilon = \frac{-2\left(\frac{e_i(unstrained) - e_i(strained)}{e_o}\right)}{GF}\left(1 + \frac{R_L}{R_2}\right) \tag{4.4}$$

where symbols have the same meaning as in Equation 4.2.

As mentioned in the preceding section, amplification can be improved by the use of four active gauges. In this case, the sections at both supports of the aluminium beam would be instrumented. To achieve this, R_2 and R_4 would be located on compression and tension sides respectively in the section at one support of the aluminium beam, and R_1 and R_3 would be located in a symmetric manner at the other support. The amplifier in Figure 4.5 has this type of installation. This full bridge was used in the experiments that took place place in Luleå, Sweden, and Delgany, Ireland, which results are analysed in Chapter 8. In the case of a full Wheatstone bridge, strain (ε) is given by:

$$\varepsilon = \frac{e_i(unstrained) - e_i(strained)}{GFe_o} \tag{4.5}$$

where e_i, e_o and GF are measured voltage, excitation voltage and gauge factor respectively.

4.3 AXLE DETECTION HARDWARE

Axle detectors, which are mounted on or embedded in the pavement, provide information on speed, axle spacing and vehicle classification. This information is used to locate the truck on the bridge when applying a B-WIM algorithm; the detectors are most conveniently placed at a close distance prior to or on the bridge. Section 3.5.1 describes how sensitive the inferred axle weights are to the axle detector measurements. Fortunately this problem is not as important now since the recent use of optimisation techniques for some bridges to improve initial estimates of vehicle location and speed. Nonetheless, even

for suitable bridges, a good approximation in the initial value of speed is still required to find the true solution (Section 3.5.3).

From the point of view of durability, axle detectors represent the most vulnerable part of any B-WIM system, especially in harsh climates. New developments propose their replacement by appropriate strain readings from underneath the structure in some specific bridges (FAD). The initial estimates of axle location and speed from FAD are not as accurate as from direct measurement, but they benefit from optimisation to improve their results after a few iterations. These systems offer a solution in sites where road surface installations are not feasible (e.g., due to a very thin pavement, a necessity to guarantee waterproofing of the bridge deck, etc.).

4.3.1 Road Sensors

A single sensor can be used for axle counting. Two road sensors, placed at a known distance apart (between 2 and 5 m typically), can accurately measure speed and axle spacings by time and distance (Figure 4.7(a)). By setting two sensors at right angles to the traffic flow, and one other at a known angle between the two (e.g., 45°), it is possible to estimate the lateral position of each vehicle across the road and the width of vehicle.

Removable Sensors

Removable sensors can be pneumatic tubes or tape switches. Both types are placed on the road surface and they are more economical than a permanent solution. Their installation requires less time and traffic delays than other sensors embedded in the pavement, and in certain circumstances, they could be placed without the need for a road closure. However, they are more exposed to traffic aggressiveness and they are not recommended in sites with high traffic densities.

Tape switches are composed of a pair of steel strips, one above the other and held apart by rubber spacers, laid across the road surface. Each time a vehicle's wheel crosses the detector, the two strips are pressed together thus completing an electric circuit which is detected at the roadside. Compared to pneumatic tubes, they have a shorter life and an extra cost that is justified by the possibility of placing them in a single lane transferring the signal across other lanes through a wire. They are often used for limited duration surveys

and on low volume roads. The road surface is heated before placing the tape switch, and once it is on the ground, it is overlain by an adhesive tape that protects it and keeps it in position.

Pneumatic tubes are thick-walled rubber tubes mounted on the road surface. One end has an air-plug while the other end finishes in a converter that translates the pulse of air caused when the tube is squashed by a wheel into an electrical signal. The tube must be firmly fixed to the road to avoid being whipped up by passing vehicles and thus triggering multiple signals each time an axle crosses. Clamps at the roadside fix these tubes and asphalt-based tape can be used to reassure their location and protect them (Figure 4.7(b)). The air switch should be calibrated so that it is sensitive enough to detect all vehicles irrespective of speed but not so sensitive as to pick up reflected air pulses in the tube.

(a) Layout of axle detectors (b) Detail of a pneumatic axle detector

Figure 4.7 – Axle detectors mounted on the road surface (after Jacob et al. 2000)

An excitation voltage of 5 V or less is required by the pneumatic converter from Golden River[12] used by the Irish team. The voltage measured for the crossing of a 4-axle truck at a scanning frequency of 250 Hz is given in Figure 4.8. Section 4.5.3 gives details how specific software is used to obtain axles from this signal.

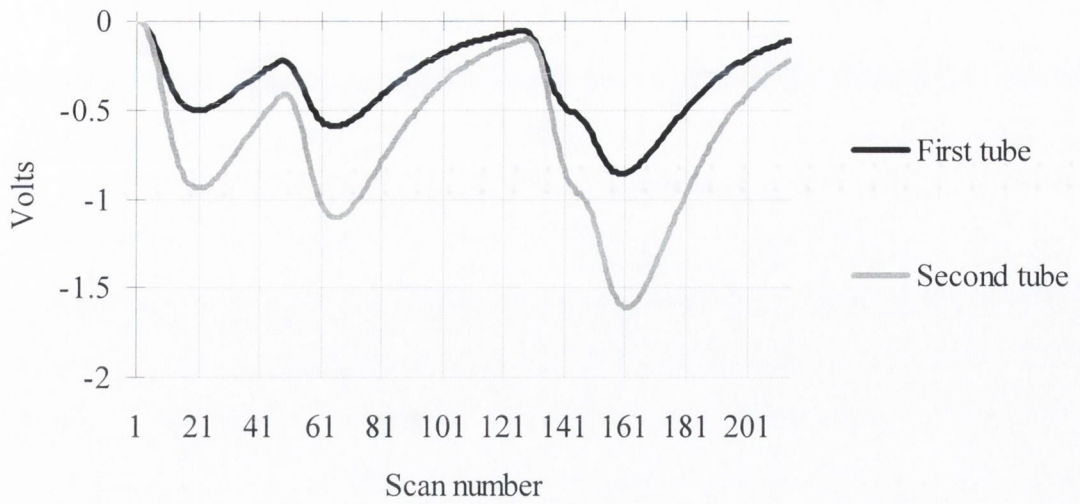

Figure 4.8 – Voltage Signal from rubber tubes at the start and at the end of the bridge

Both types of portable axle detector have been problematic due to the recording of multiple pulses from single axle events and also the missing of some axle events. This is the reason why the Irish team recorded all information in voltages and developed a post-processing algorithm to analyse subsequently those cases considered suspect, i.e., cases for which there was different numbers of axle in each road sensor.

Permanent Sensors

Various types of multicore cable have been developed as an alternative to pneumatic tubes and contact strips laid across the road surface. The most commonly used, known as a tribo-electric cable, contains cores which induce a charge when they rub together and the cable is temporarily distorted by the passage of a vehicle. An increasingly popular variant on this is the piezo-electric cable which contains piezo-electric material such as polarised ceramic powder. A coaxial-conductor attached to the piezo-electric cable (Figure 4.9(a)) is subject to an electrical charge when the piezo is squashed. The housing should be impervious to attack from acids, alkalis, salts and ultraviolet light. All connections are fully sealed within the housing as shown in Figure 4.9(b).

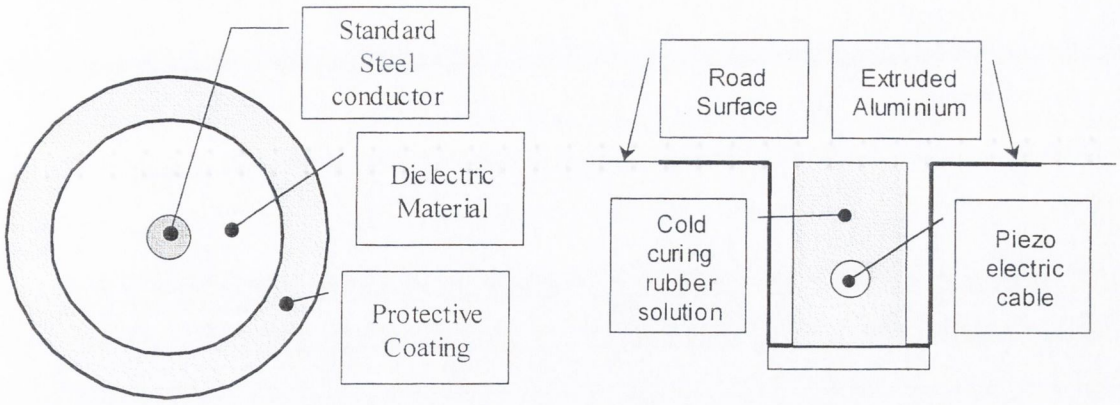

(a) Piezo-electric cable (cross section)

(b) Permanent installation of piezo electric cable in a slot (cross section)

Figure 4.9 - Piezo-electric axle detector

These axle detectors lie across the carriageway. They are all triggered by the passage of vehicle wheels and thus produce a count of axles rather than vehicles. They must be installed at right angles to the flow (otherwise they might detect two wheels on one axle as if they were separate axles) and this effectively prevents their use for counting axles of vehicles undertaking turning movements. Top grade piezo-electric cable is relatively expensive and needs careful installation and calibration but, since the change in signal is proportional to the load applied, it can be used for classifying vehicles according to their weight.

A BNC (**B**ayonet **N**ut **C**onnector) connector is fitted to the end of the coaxial cable with adequate stripping and cramping tools. This BNC connector is plugged into an interface that converts a very noisy input signal into a clean output pulse identifying the axle presence that will be recorded by the data acquisition system. The interface used by the Irish team is the T2000.44, a dual channel piezo-signal conditioning circuit, mounted on a printed circuit board developed by Traffic 2000. The interface gives a pulse width of 20 mS (adjustable) for every axle passage. Figure 4.10 shows the signal provided by the piezo-electric sensor interface at a scanning frequency of 1000 Hz. Each rectangular pulse represents an axle.

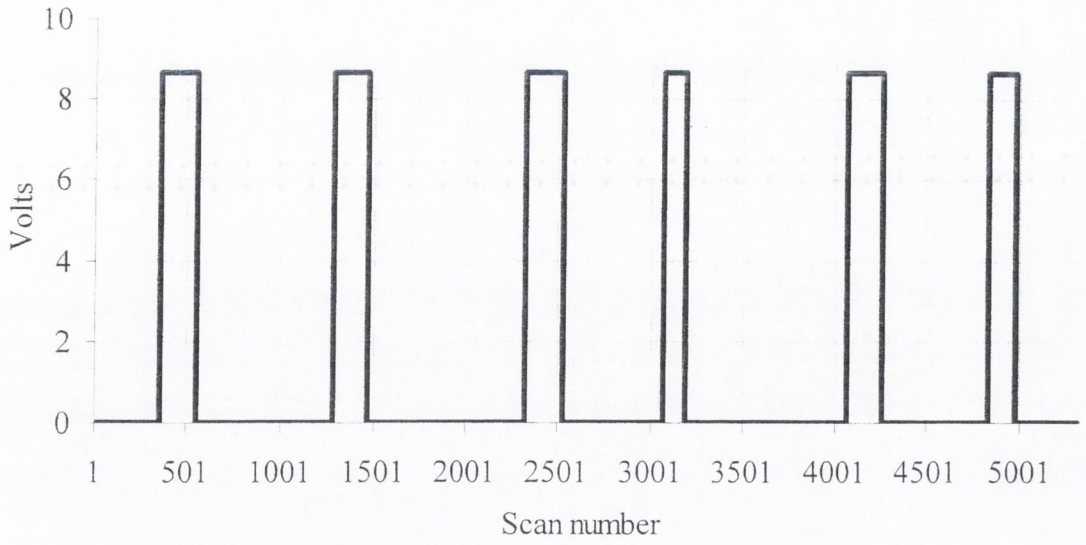

Figure 4.10 – Signal provided by piezos installation

Though piezoelectric axle detectors embedded in a groove in the road generally provide a longer life than those mounted on the road surface, they can fail in various ways:

- Total break in piezo cable or signal cable → No output.
- Joint failure → No output.
- Water in joint → Gradual increase in noise until it exceeds threshold leading to eventual failure through noise.
- Failure of piezo cable in body of sensor but core held together by elasticity of rubber → Very unusual indeed. Intermittent output.
- Poor BNC connection resulting in corrosion and build up of oxidation → Reduced output and intermittent.
- Poor BNC connection central core pin not driven home → Possible intermittent.

4.3.2 FAD Systems

One of the main problems with B-WIM installations is the longevity of axle detectors mounted on the road surface. These detectors are rapidly destroyed by heavy traffic. They also warn drivers about the presence of instrumentation on the bridge.

LCPC (**L**aboratoire **C**entral des **P**onts et **C**haussées) first considered the idea of using a B-WIM system without axle detectors as a requirement to ensure the waterproofing of the deck in the Pont de Normandie. Dempsey et al (1998a) and Žnidaric et al (1999a) studied

the performance of FAD systems for orthotropic and short slab bridges respectively. Two different longitudinal measurement locations are required to calculate velocity and axle spacings. Figure 4.11(a) shows FAD instrumentation at one section for an orthotropic bridge; the complete system consists of sensors at two such sections between transverse beams. Figure 4.11(b) shows the corresponding installation for a short slab bridge, where sensors are normally located around ¼ and ¾ of the span.

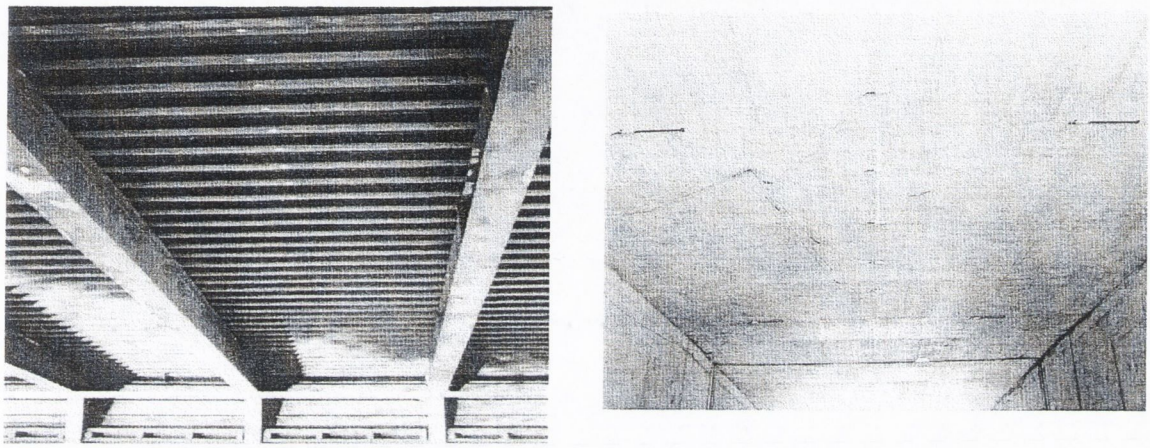

(a) Orthotropic Bridge Deck (b) Short Span Slab Bridge

Figure 4.11 – Installation for a Free Axle Detection System (after Jacob et al. 2000)

Principle

Bridges that qualify for FAD allow easy identification of axles from strain peaks. The exact location of these peaks can be obtained from the first derivative of strain with respect to time. If sensors are placed at two different longitudinal locations, it is possible to obtain velocity and axle spacings solely from strain records.

Velocity is readily calculated from geometric distance between sensors and time, Δt, taken by the vehicle to cross the sensors. In orthotropic bridges, Δt (Figure 4.12) is obtained from minimising an error function given by the squared difference between the strain in the first longitudinal location at time t and the strain in the second longitudinal location at time $t + \Delta t$ (Dempsey et al 1999b).

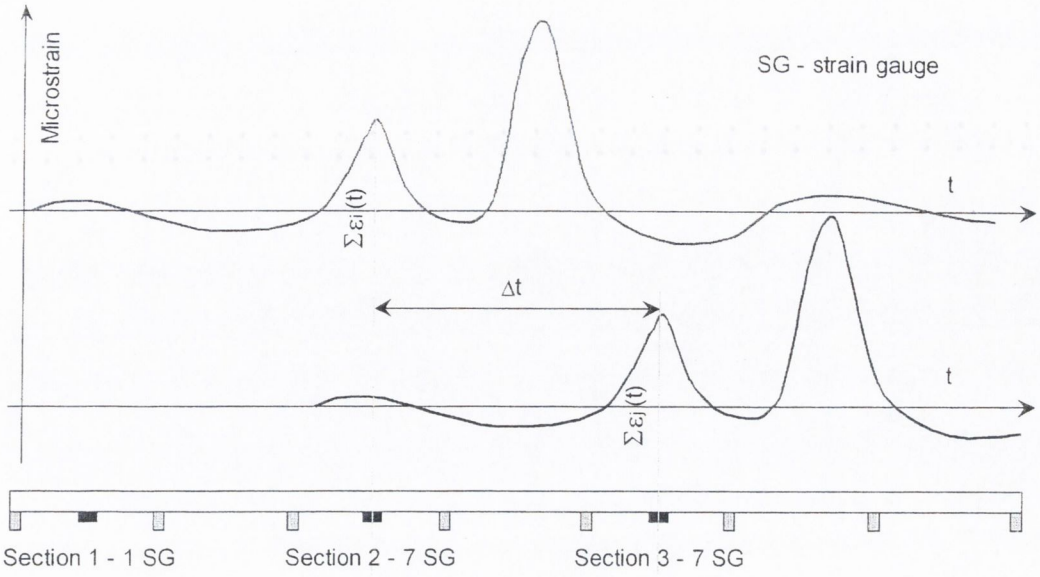

Figure 4.12 –Response to the passage of a 2-axle truck over an orthotropic deck (after Dempsey et al. 1999b)

Ideal Site

Axles are easier to identify in the strain record when they produce sharp peaks. The shape of the strain response depends on several factors:

- The shape of the influence line (Figure 3.5).
- The span length and axle spacings. Longer instrumented spans make it more difficult to distinguish individual axles. Figure 4.13 shows the response of an 8 m long integral bridge and a 32 m bridge to the passing of 5-axle semi-trailer. When looking at Figure 4.13(a), there are clear sharp peaks for individual axles, even the rear closely spaced axles of the tridem. In contrast to this response, the first mode of vibration of the long bridge prevents the identification of axles in Figure 4.13(b) and it does not qualify for FAD.
- The thickness of the instrumented superstructure. Thin superstructures provide sharper peaks, while greater depths smooth peaks out.

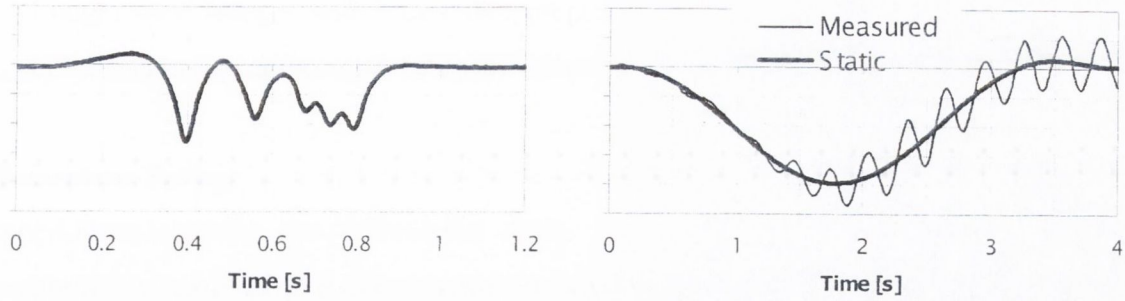

(a) Response of an 8 m long integral slab bridge

(b) Response of a 32 m long simply supported beam bridge

Figure 4.13 – Strain response for different bridge lengths (after Žnidaric et al. 1999a)

Jacob et al (2000) propose a coefficient to determine if a site qualifies for FAD. This is given in Equation 4.6:

$$C_{FAD} = \frac{Lh}{d_{\min} f_i} \tag{4.6}$$

where L is the span length, h the superstructure thickness, d_{min} the minimal axle spacing and f_i a factor depending on the influence line as defined in Figure 4.14.

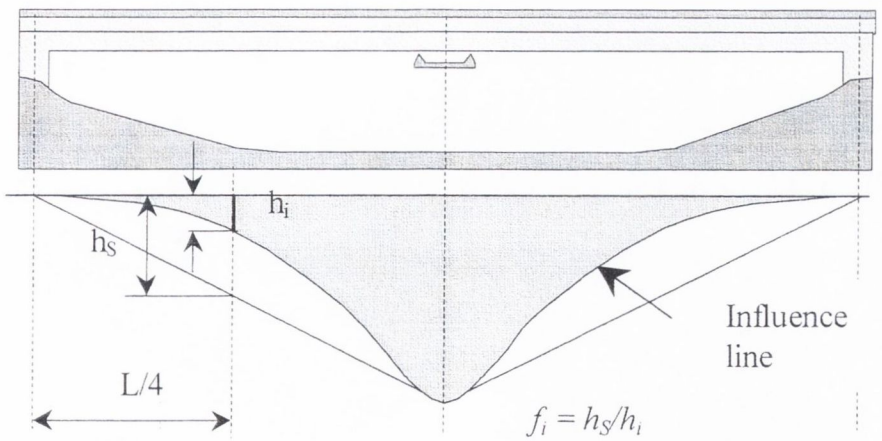

Figure 4.14 – Definition of f_i (after Jacob et al. 2000)

First studies by Jacob et al (2000) indicate that the following bridges qualify for FAD:

- Short span, frame-type slab bridges with $f_i \cong 3$ and $1 < C_{FAD} < 2$.

- Longer span bridges with a thin slab supported in the lateral direction by cross beams or stiffeners (i.e. orthotropic bridges) with $C_{FAD} < 0.5$.

Theoretical Testing

Experimental results for orthotropic decks have been given in Section 3.7.3. The possibility of extending FAD systems to other bridge types can be investigated with theoretical dynamic models. Dempsey et al (1999b) use two different theoretical models to test the FAD algorithm: A finite element model and a one-dimensional numerical model as proposed by Frýba (1972). This numerical approach will be discussed in Chapter 5. It was found good agreement between Frýba and finite element models. Strain results are analysed for three bridge span x width dimensions (5x8.5, 10x8.5 and 20x8.5 m), two boundary conditions (fixed-fixed and simply supported), and one vehicle (12 tonnes gross weight), whose characteristics are described below.

In this analysis, the author developed the finite element model using the MSC/NASTRAN software[18]. The bridge and vehicle models are represented in Figure 4.15.

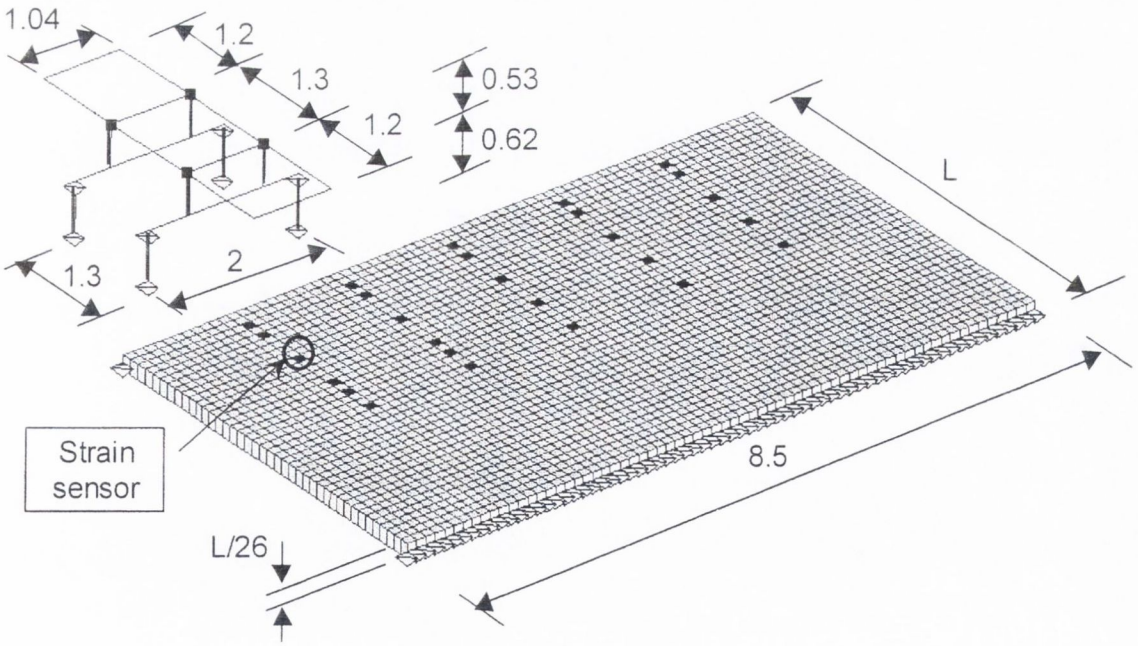

Figure 4.15 – Bridge-vehicle finite element model

The dynamic interaction of the bridge and the vehicle incorporates the road surface profile and it is implemented using a set of auxiliary functions to enforce the compatibility

conditions at the bridge/vehicle interface (Cifuentes 1989). Accordingly, software was developed to generate an entry into the assembled stiffness matrix of the vehicle-bridge system. This entry allows for the definition of the forces acting on the bridge due to the moving wheels and the equation of motion of the vehicle. A compatibility condition between the vertical displacement of the wheel and the bridge at the contact point is also established. This formulation is explained in detail in Chapter 6. In order to determine the most suitable locations for the position of the sensors, strain was obtained at seven longitudinal (1/16, 1/8, 1/4, 5/16, 3/8, 7/16 and ½ of the span length) and five transverse locations (sensors represented in black in Figure 4.15).

The bridge structure was fixed at both ends to simulate the conditions in an integral bridge. The section was made of an isotropic material of 36×10^9 N/m^2 Young's modulus, 2.45 t/m^3 unit weight, and uniform thickness taken as 1/26 of the bridge length. The first longitudinal and torsional natural frequencies were 30.9 and 33.07 Hz in the 5 m span (Figures 4.16), 15.4 Hz and 19.37 Hz in the 10 m span, and 7.66 and 13.78 Hz in the 20 m span bridge. Damping was taken as 1% in all cases.

(a) First mode shape (30.9 Hz) (b) Second mode shape (33.07 Hz)

Figure 4.16 – Bridge mode shapes (5 m span)

The vehicle was modelled as a rigid frame tandem with 1.3 m between axles (distinguishing between axles of a group is one of the greatest challenges in FAD systems). The tandem speed was 20 m/s and it was excited by the road roughness in the approach prior to the bridge. Road irregularities were idealised as a stochastic process and generated from power spectral density functions for 'good' conditions (Wong 1993). The inner and outer wheels followed a path 1 m and 3 m offset from the bridge centre line (Figure 4.15). The mass of each axle was 10^3 kg and the mass moment of inertia 600 kgm^2. A frame weighing 10^4 kg connected both axles. The suspension was modelled with spring and

damper elements at each wheel of values $1.8*10^6$ N/m and $5*10^3$ Ns/m respectively, while each tyre had a stiffness $2*10^6$ N/m and damping $3*10^3$ Ns/m (Kirkegaard et al. 1997). The main truck frequencies were 1.65 Hz body pitch (Figure 4.17(a)), 2.03 Hz frame twist (Figure 4.17(b)), 2.92 Hz body roll, 3.02 Hz body bounce, 13.96 Hz axle hop (out of phase), 14.19 Hz axle hop (in phase) and 16.84 Hz axle roll (out of phase).

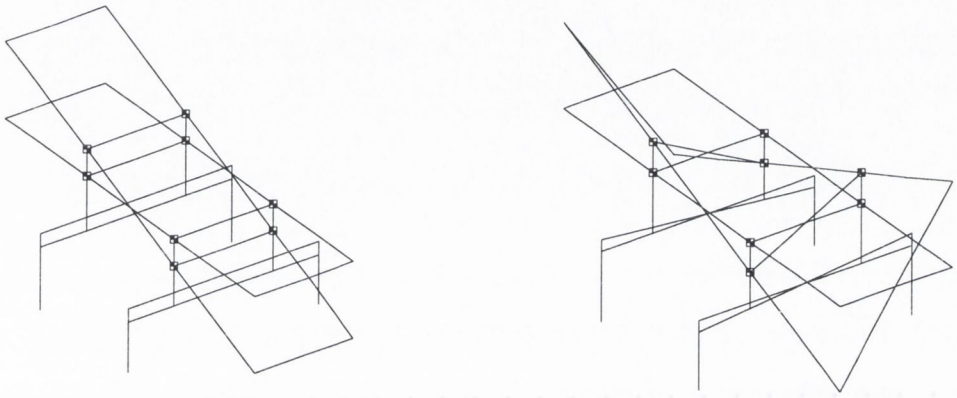

(a) Body pitch (1.65 Hz) (b) Frame twist (2.03 Hz)

Figure 4.17 – Truck modes of vibration

Figure 4.18 illustrates the response of the bridge to the passage of the tandem at different longitudinal locations (strains at different transverse locations are added up). From this figure, the ideal location of the FAD sensors for axle detection is between L/4 and 3L/8.

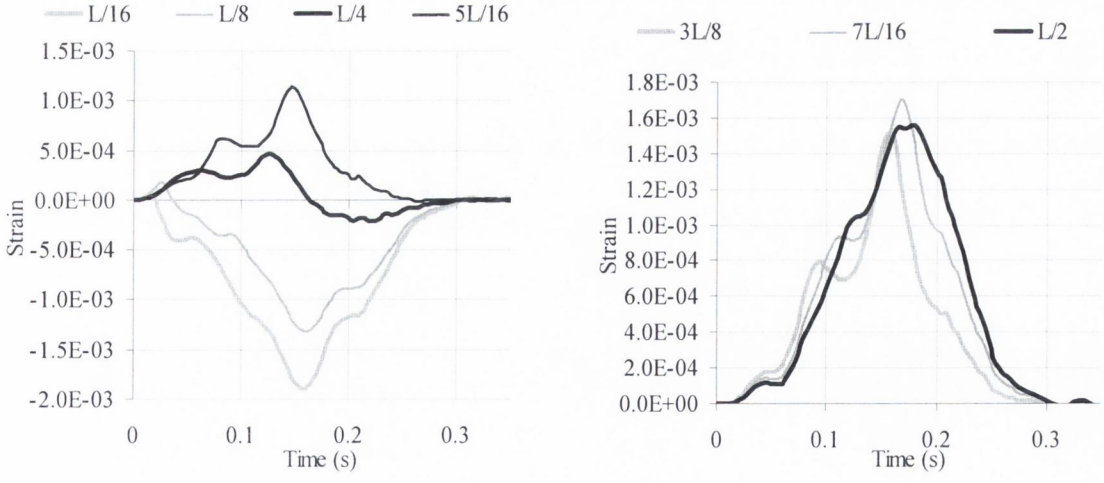

(a) Response at L/16, L/8, L/4 and 5L/16 (b) Response at 3L/8, 7L/16 and L/2

Figure 4.18 – Response at different longitudinal sections in the case of 5 m span length (L) to passage of tandem

Figure 4.19 shows the individual responses of strain gauges at different transverse positions for a longitudinal position at ¼ of the span length for the 5 m bridge. It can be seen that the axles of the tandem are far more distinct than in Figure 4.18 and that some transverse positions are clearly better than others (strain from sensors in Figure 4.18(b) is worse than Figure 4.18(a) for axle identification).

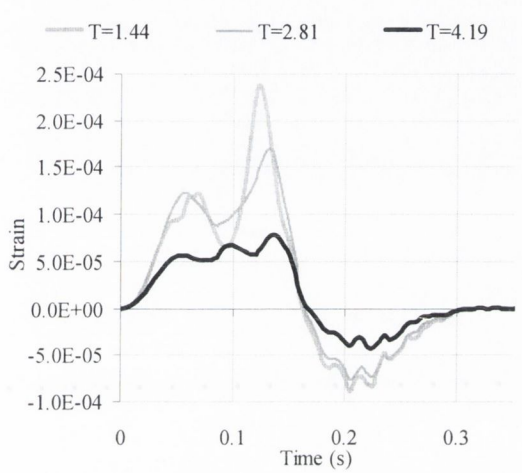

(a) Response at T=1.44, 2.81 and 4.19 m

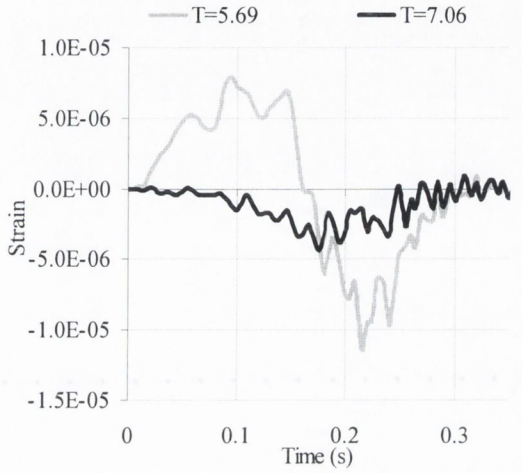

(b) Response at T=5.69 and T=7.06 m

Figure 4.19 – Response at ¼ of span length at different transverse locations in the case of 5 m span length (T is distance in m from the edge of the bridge driving lane)

Figures 4.20 shows the response of the 10 m bridge. From the seven longitudinal positions, axle peaks are easier to identify at L/4.

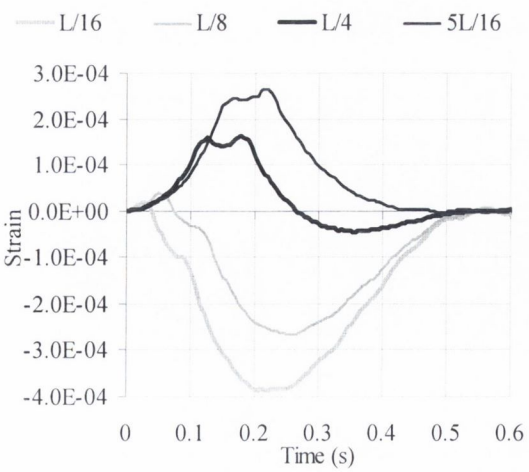

(a) Response at L/16, L/8. L/4 and 5L/16

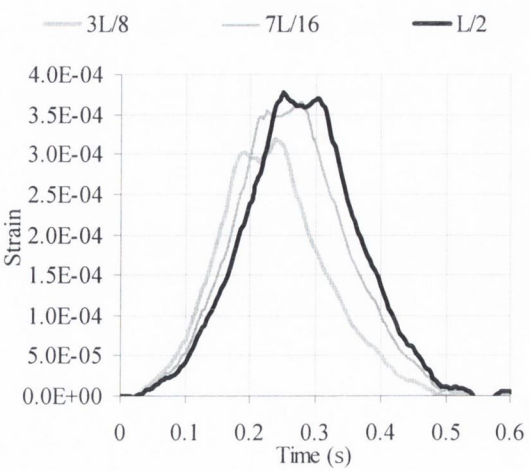

(b) Response at 3L/8, 7L/16 and L/2

Figure 4.20 – Response of 10 m span (L) bridge to passage of tandem

Figures 4.21 shows the response of the 20 m bridge. In the 20 m bridge studied in this paper, the in-phase and out of phase axle hop frequencies dynamically excite the first torsional mode of the bridge, interfering with the static response and making it impossible to use for FAD purposes.

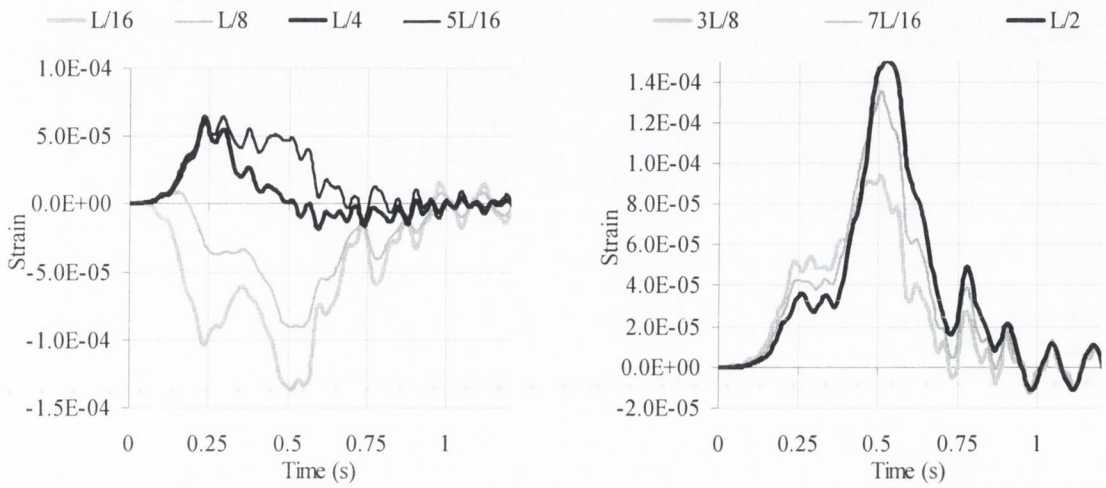

(a) Response at L/16, L/8. L/4 and 5L/16 (b) Response at 3L/8, 7L/16 and L/2

Figure 4.21 – Response of 20 m span (L) bridge to passage of tandem

As result of this study, the author in collaboration with others (Dempsey et al.1999b) makes the following recommendations:

- In the case of a simply supported bridge, the FAD algorithm is only suitable for spans shorter than 5 metres and both longitudinal sensor locations must be close to the supports, e.g., L/16 and L/8.
- In fixed-fixed bridges, a maximum span of 10 m or even greater is possible if it is proven that the total bridge response is not modified significantly by its dynamic interaction with the vehicle. Both axles of the tandem were identified in the 5 (Figure 4.18) and 10 m bridge (Figure 4.20). Velocity is better determined for an average longitudinal location of L/3 as illustrated in Figure 4.22(a).
- Velocity is more accurately defined for increased distances between sensors (Figure 4.22(b)) and increased scanning frequency. A minimum longitudinal distance between sensors of 1 m and a minimum scanning frequency of 200 Hz should be considered.

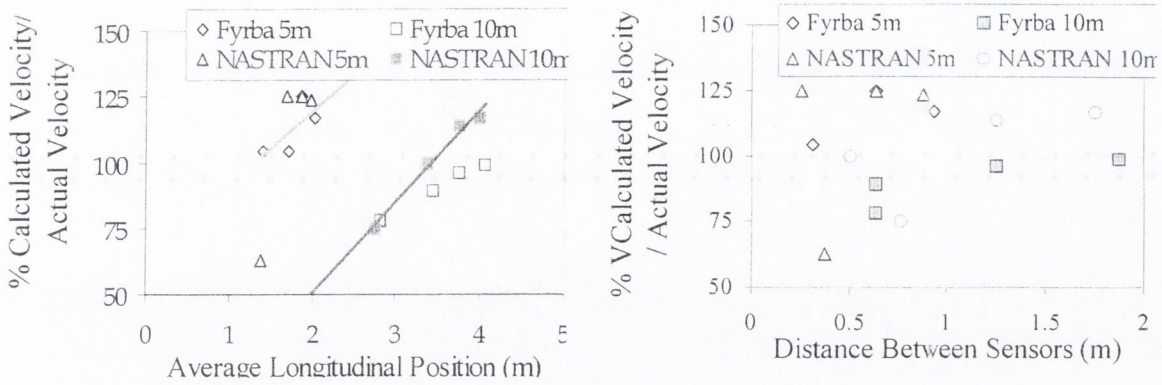

(a) Longitudinal Position of Sensors (b) Inter-sensor Distance

Figure 4.22 – Accuracy of calculated velocity from FAD algorithm for 5 m & 10 m bridges (after Dempsey et al. 1999b)

4.4 SOFTWARE

The software of a B-WIM system can be divided into two main parts: DAQ software and software for determination of axle weights. DAQ software integrates the strain signal, signal conditioning and DAQ hardware to provide a reliable input to the software that calculates the characteristics of traffic.

4.4.1 CULWAY

CULWAY is a high speed weigh-in-motion system that uses existing box culverts to automatically and unobtrusively monitor traffic. It can calculate accurate data for all vehicles travelling up to 150 km/h in up to 4 traffic lanes simultaneously, 24 hours a day with no operator required. It was developed by Peters (1986) of Main Roads, Western Australia and subsequently developed as a commercial product by ARRB Transport Research with substantial and ongoing input from all Australia State Road Authorities[10].

The CULWAY procedure to calculate weights has been described in Section 3.4.2. This system reports automatically via fax about: Data on weight - no. of axle groups, speed - axle group weight, length - axle spacings, width - tyres per axle, no. of axles - vehicle lane position. The first CULWAY system (Figure 3.4(b)) was programmed to work unattended by following the flow chart shown in Figure 4.23 (Peters 1986).

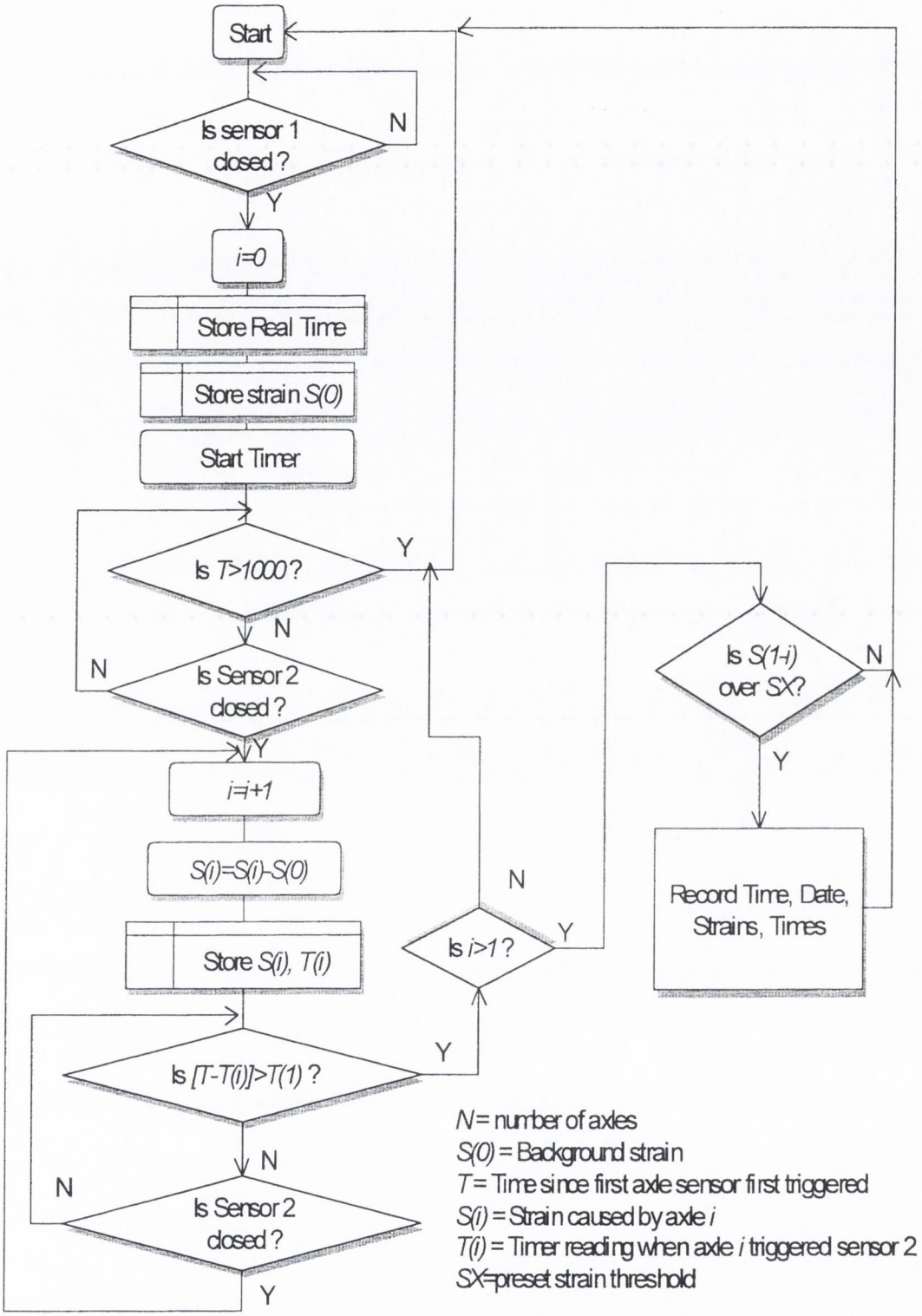

Figure 4.23 – CULWAY Flowchart

4.4.2 SiWIM

SiWIM is a Weigh-in-Motion program developed at ZAG, a research institute in Slovenia, within the framework of WAVE. The program runs in any 32-bit Microsoft Windows

environment. SiWIM uses National Instruments data acquisition products. Currently it supports two PCMCIA cards. When acquisition starts, depending on the choice, either the data acquisition device is initialised or an existing file is opened for input. The format in both cases is the same. Then, the data from the PCMCIA or the file is put into an internal queue. After saving this queue in a new file, data can be filtered in several ways. The filtered data is transferred to another queue from where it will be read for vehicle detection. There are two different options for vehicle detection: (a) based on signals from axle detectors mounted on the road surface or (b) based on signals from strain sensors (FAD). Data is stored in an internal queue until the last axle of the vehicle leaves the bridge. All this information can be fed to a preprocessed data queue or saved for later processing. The calculation of weights can be done with either an internal or an external algorithm. In the latter case, the pre-processed data is written into a file and a predefined executable file is called to calculate axle spacings and weights. The internal algorithm uses a development of Moses' approach for this calculation (Moses 1979). Finally, the initial results are refined through the application of an optimisation algorithm. Once results are obtained, they are displayed on the screen and, optionally, written to a file. Figure 4.24 shows how this system can also incorporate FAD technology.

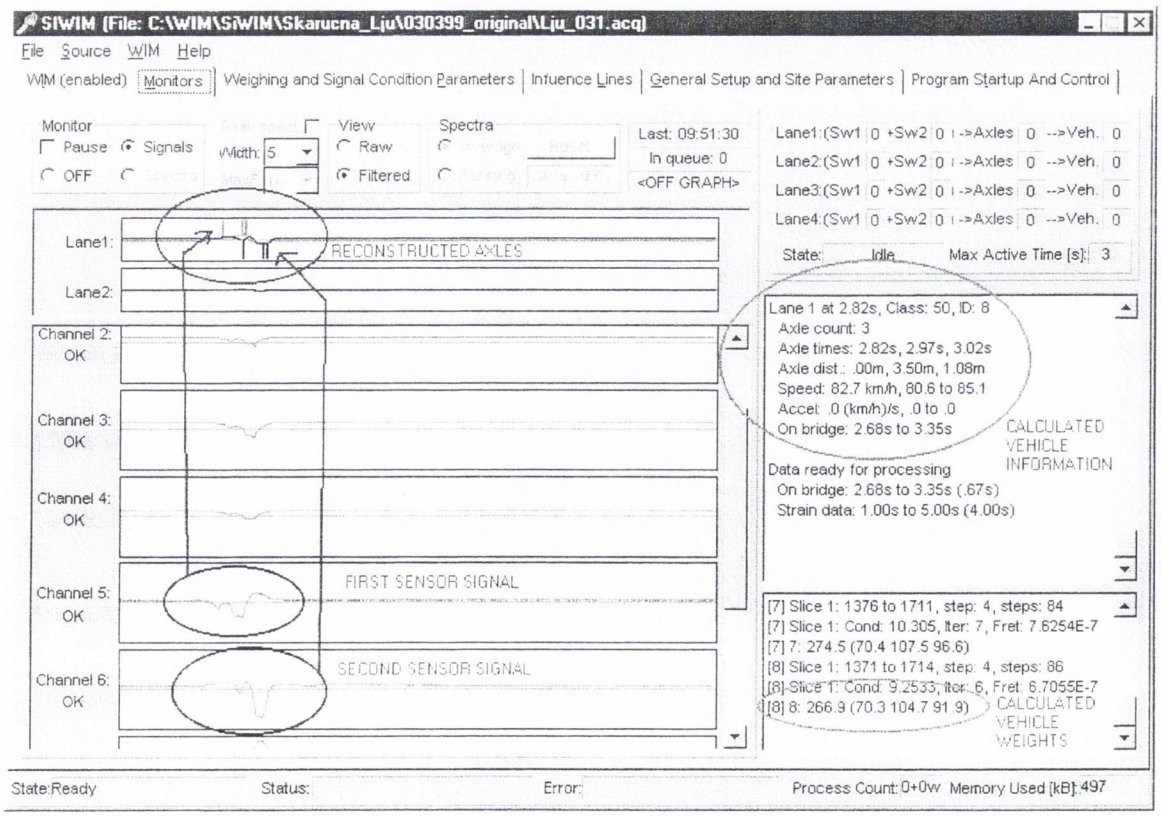

Figure 4.24 – SiWIM software (after Jacob et al. 2000)

WIMDAP© (Žnidaric et al. 1998) is another software developed at ZAG to correct the theoretical influence line by adjusting the boundary conditions of the span according to the guidelines given in Section 3.5.1, and smoothing the peaks to account for the smeared footprint of the tyre. Figure 4.25 shows the interface of this program.

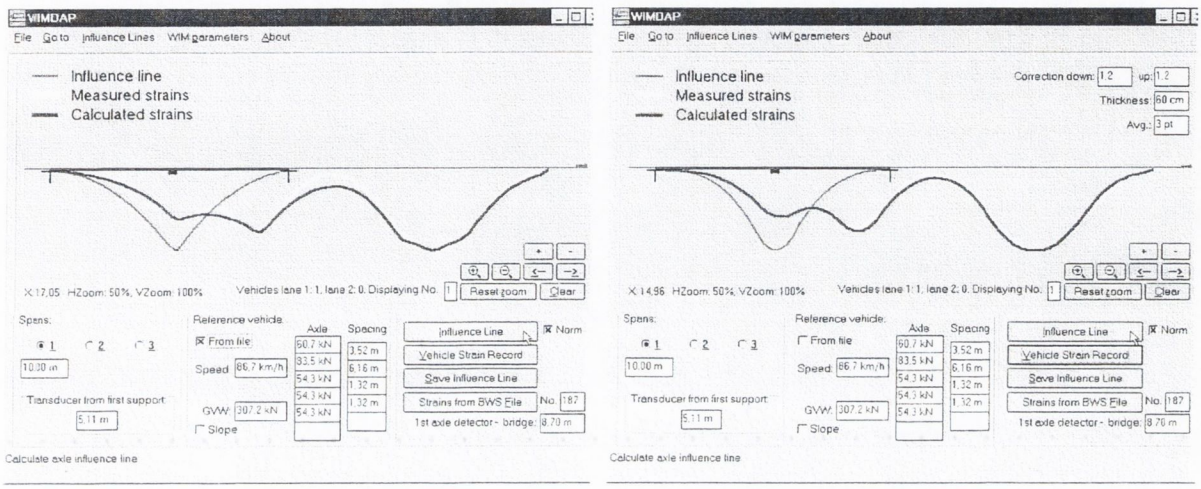

(a) Theoretical influence line (b) Optimised influence line

Figure 4.25 – Adjustment of the influence line in WIMDAP© software (2S3 semi-trailer) (after Žnidaric et al. 1998)

4.4.3 Irish B-WIM

Labview software[14] was used during data acquisition while post-processing was programmed in the C language[15]. The Labview programs to record voltage from axle detectors and strain sensors were written by Kealy (1997). The author developed C code to convert that information on voltages into vehicle classification and weights. First, the original voltage information is converted into times and strains for every vehicle. There is a time stored for each axle at each tube and strain is recorded while there is traffic on the bridge. After obtaining vehicle classification and speed, weights are calculated by applying Moses' static algorithm (Section 3.3).

Data Acquisition

Information on voltages can be acquired in two different ways: one writes data to a binary file (Figure 4.26(a)) and another to an ASCII file (Figure 4.26(b)). The latter allows graphical output and checking of the system in real time, but it requires more storage space.

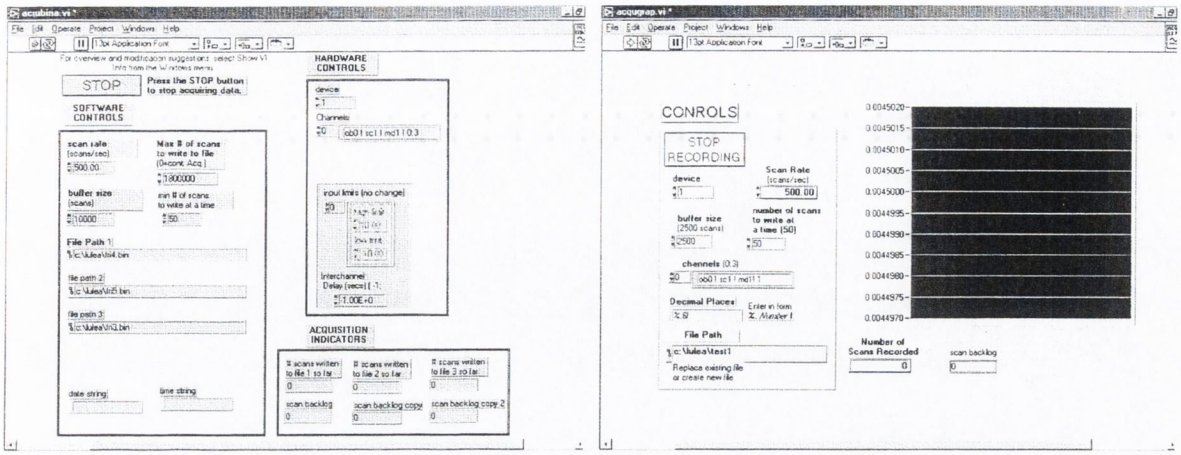

(a) Collection of Data in Binary Format (b) Graphical Collection of Data

Figure 4.26 – Data Acquisition Programs

The binary format is generally used when collecting data for long uninterrupted periods. If binary format is recorded, another Labview program allows a posterior conversion into text format. The two DAQ Labview programs use a circular buffer technique that continuously acquires data at the same time as retrieving and writing previously acquired data to a file. The input of these DAQ programs specify:

- DAQ card (see Appendix C).
- Number of scans per channel per second for all listed channels.
- Channels on the SCXI (**S**ignal **C**onditioning e**X**tensions for **I**nstruments) hardware that are to be scanned and to which channels on the DAQ card they are to be written (see Appendix C).
- File into which the acquired data is to be written.
- Minimum number of scans to be read from the buffer on each iteration. It is recommended as half the scan rate.
- Maximum number of scans which can be held in the circular buffer. It should be set to at least 0.75 times the scan rate.
- Maximum number of scans to write to each file, so a new file is created when the previous file reaches this limit.
- Time delay between scanning of two successive channels.
- Range of input voltages. If left empty values default to hardware settings.

Axle detection algorithm

Accurate speed and axle spacing are essential for a B-WIM algorithm. Small errors in axle spacing, and especially in speed, result in large errors in axle weights (Dempsey 1997). Initially the system was controlled through software written in C++ (O'Connor 1994) using rubber tubes fixed to the road with asphalt tape. This program controlled the whole data acquisition, as strains were only recorded when there were axles on the bridge. The disadvantage of such an approach is that an error in the axle detection device leads to loss of strain data. Problems with the tubes attached to the road in the Delgany site (Section 8.2) resulted in the purchase of new axle detectors: tape switches. However, tape switches gave multiple signals for just one axle hit and sometimes collapsed under the weight of the vehicles. Five different tape switches with different time delays were used, but none of them gave good results after the second day of use (González 1996). Finally, it was decided to record all data continuously and to process it afterwards in the laboratory. Pneumatic tubes taped to the road were again used but, this time, the voltage signal from the pneumatic convertor was monitored and stored during the data acquisition exercise (Kealy 1997). These changes provided access to both raw and processed signals facilitating the resolution of likely conflicts after processing. The voltage signal was converted into axle hits using purpose-written software run afterwards in the laboratory. This corrected most of the problems related to axle detection. Rubber tubes attached to the road with clamps were also used as axle detectors. As they tended to get loose, they were firmly fixed every two days to ensure an uninterrupted record. Several video records with a variety of different truck configurations and the corresponding tube signals were collected on site to check the reliability of the new system and it was found to operate quite effectively.

Considerable effort was expended by the author on the development of software to convert the voltage signal from the pneumatic convertors into times of axle hits. It was first determined that the slope of the voltage curve was clearer than the voltage curve itself, particularly for the detection of tandems. Figure 4.27 illustrates the slopes (first derivatives with time) from two tubes as a four-axle vehicle with a rear tandem passes over. The original voltage signals are shown in Figure 4.8. Further, the absolute magnitudes of voltage (i.e., using high and low values as triggers) were found to be unsuitable as they were dependent on axle weights, vehicle speed, synchronisation of both wheels on the tube, tyre characteristics, etc..

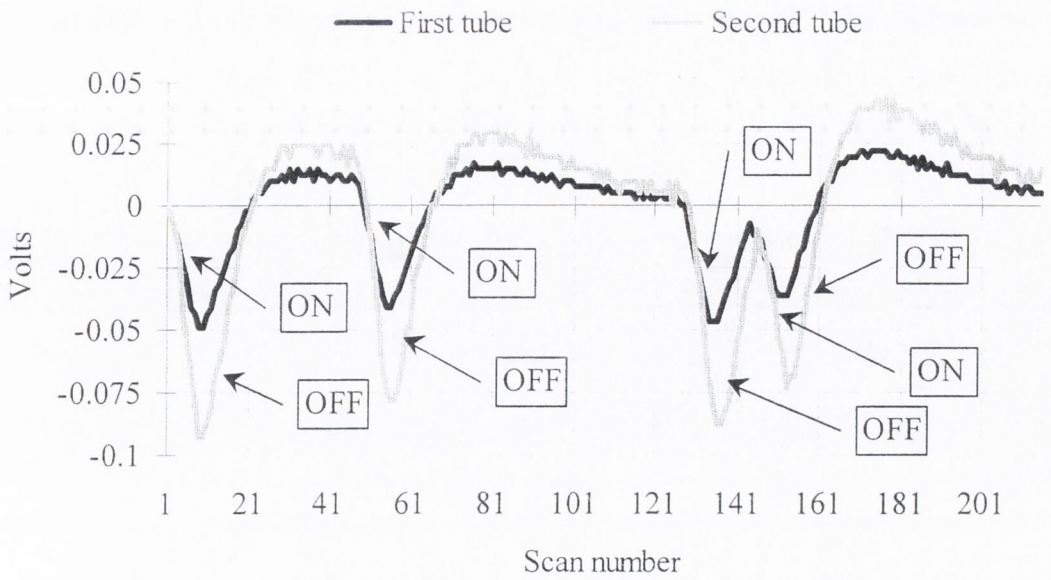

Figure 4.27 – Slope of Voltage signal in Figure 4.8

The following criteria to identify axles were adopted:

- There is a flag for each rubber tube signal corresponding to an axle hit. When the flag goes from OFF to ON, it indicates that there is an axle on the tube.
- The flag changes from OFF to ON if the slope decreases for consecutive p scans to ensure it is a truck (Figure 4.27). This number p has been adjusted with the sample and it depends on the quality of the voltage signal, the scanning frequency and the length of the tube and wiring. It is a time condition that minimises the influence of axle weight or vehicle characteristics. The assumption is that slope starts to decrease the moment an axle hits it. The inaccuracy is around 1 scan, given by the starting point. The total decrease in slope must be in excess of a certain value which is determined from the sample, and is different for each tube.
- The flag goes from ON to OFF when the slope increases for p scans. The same number of scans as before is used as, if there is an axle present after p scans, it is reasonable to also say that the influence of that axle hit disappears after another p scans. Conditions on the absolute values of the slope are not imposed, as such a condition cannot distinguish between the presence of an axle on the bridge and white noise. The flag also goes from ON to OFF when the slope decreases, but the second derivative increases for r scans (Figure 4.28).

The critical number of scans, p is needed to avoid the registration of more than 1 axle when only one is present, while r ensures axles are not missed in closely spaced configurations. Both temporal parameters are controlled through software. Tests in Delgany, Ireland, took place at a scanning frequency of 250 Hz, and $p = 5$ scans and $r = 6$ scans were adopted, though these values can be adjusted depending on the quality of the voltage signal. In Figure 4.26, which gives first derivative of voltage with respect to time, 5 to 8 scans can be clearly counted when the slope curve decreases in response to an axle.

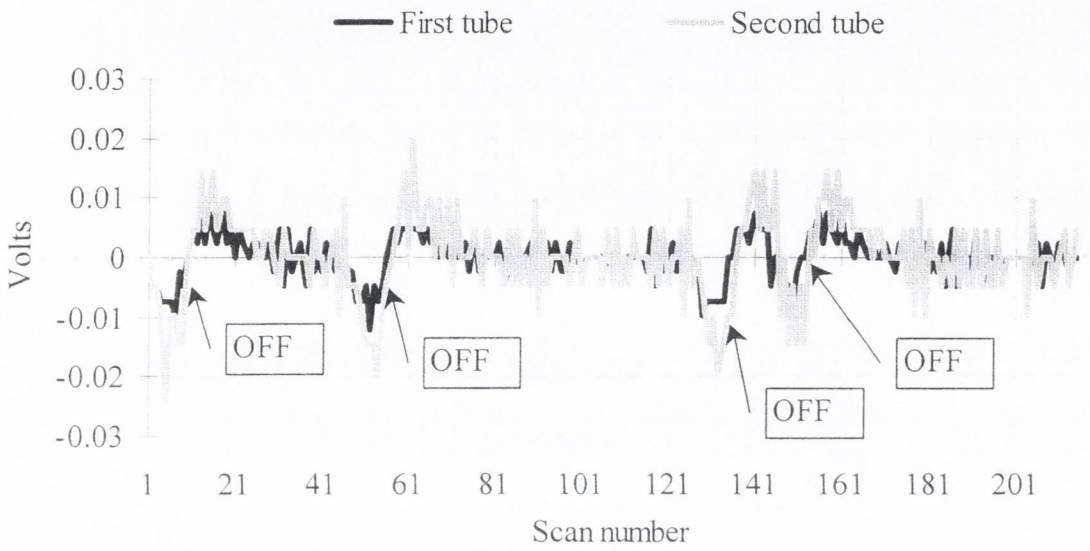

Figure 4.28 – Second derivative with time

Error detection

Sometimes there are anomalies in recordings: i.e., axles read in one axle detector but missed in others. These records are probably due to vehicle lane changes and are removed in weight calculations. The program detects these events by evaluating the number of axles on the bridge from both tubes. The program also compares the axle spacing in scans obtained from the first and second tube. If the difference between these is significant, the event will be marked as doubtful for weight calculation purposes.

Though unlikely, some closely spaced axles could be missed due to an incorrect layout of the tubes. This can occur if the portion of the rubber tube that lies off the road is not straight enough or is too long before being connected to the pneumatic converter. Either of these cases can result in the voltage signal being too weak. Alternatively, an air pulse could reach the detector before the tube recovering normal pressure, making it difficult to

distinguish pulses in the converter signal. For these cases, if one of the tubes failed to identify one axle but the other tube gets it, the axle will be counted as good, as experience confirms that the algorithm works well when a good voltage signal is provided. Given the characteristics of the algorithm, there have never been extra axles reported in a vehicle. The problem in the old system with multiple phantom axles has been solved.

The axle detection algorithm also checks for the maximum number of axles physically possible between rubber tubes. Each time an error is detected, that traffic event is recorded with a character indicating the source of error, and all variables are initialised for counting a new traffic event.

Speed and Distance between Axles

The author studied the best procedure for determining initial estimates of speed and axle spacing. Once the times for each axle at each tube have been obtained, speed and distance between axles can be readily calculated. Speed is considered to be approximately constant in the distance between rubber tubes (assumption also adopted in the calculation of weights), and is obtained by averaging all time references for an axle hit as given in Equation 4.7:

$$v = \frac{NL_t f}{\sum_{i=1}^{N} (q_{i2} - q_{i1})} \tag{4.7}$$

where v is velocity (m/s), q_{i2} , scan number for axle i to touch second tube, q_{i1}, scan number for axle i to touch first tube, f, scanning frequency (Hz), N, number of axles and L_t, distance between rubber tubes.

A degree of uncertainty is involving in the identification of the starting scan of an axle hit. This error is inversely proportional to the scanning frequency. During tests carried out in Delgany, Ireland, with a scanning frequency of 250 Hz and distance between tubes of 22 m, the maximum error in timing was calculated as the time for 1 scan = 1/250 = 0.004 seconds in ideal conditions. At 90 km/h (25 m/s), an axle would take a time of 0.88 seconds to cross between both tubes. If the measured time was 0.004 seconds higher due to the scanning frequency, the measured speed would be 0.44 % smaller. The final error

should be less than 0.44% as the definitive speed of the vehicle is calculated from averaging each axle speed.

Before obtaining axle spacing, the total distance between first and last axle (total wheelbase) is calculated by Equation 4.8:

$$S_{1N} = v\left(\frac{q_{N1} + q_{N2} - q_{11} - q_{12}}{2f}\right) \tag{4.8}$$

where S_{1N} is spacing (m) between 1st and last axle; q_{N1}, scan number at which the last axle hits the first tube, q_{N2}, scan number at which the last axle hits the second tube, q_{11}, scan at which the first axle hits the first tube, q_{12}, scan at which the first axle hits the second tube, and v, velocity, is defined in Equation 4.7.

Axle spacing is assigned based on the relative time interval. For example, the distance between second and third axle is calculated as:

$$S_{23} = \left(\frac{q_{31} + q_{32} - q_{21} - q_{22}}{q_{N1} + q_{N2} - q_{11} - q_{12}}\right) S_{1N} \tag{4.9}$$

where the subscripts have equivalent meaning to those in Equation 4.8.

When calculating axle spacings, errors are reduced by averaging times between axles given by each tube. An error of one scan represents 10 cms for a scanning frequency of 250 Hz and a speed of 25 m/s. A 3-axle truck with axle spacings 4.02 m and 1.2 m, was used to test the approach. Figures 4.29 and 4.30 show the results obtained for axle spacings when applying the axle detection algorithm. It can be seen that the influence of speed on accuracy is negligible between the first and second axle, but significant in the case of the rear tandem illustrated in Figure 4.30.

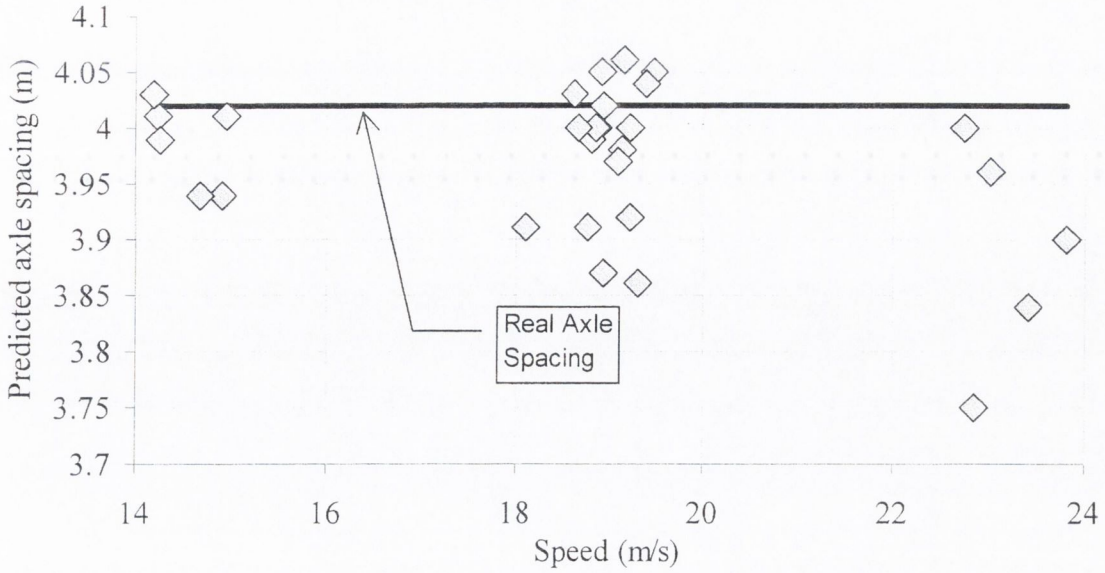

Figure 4.29 – Predicted axle spacing at different speeds for a real axle spacing of 4.02 m

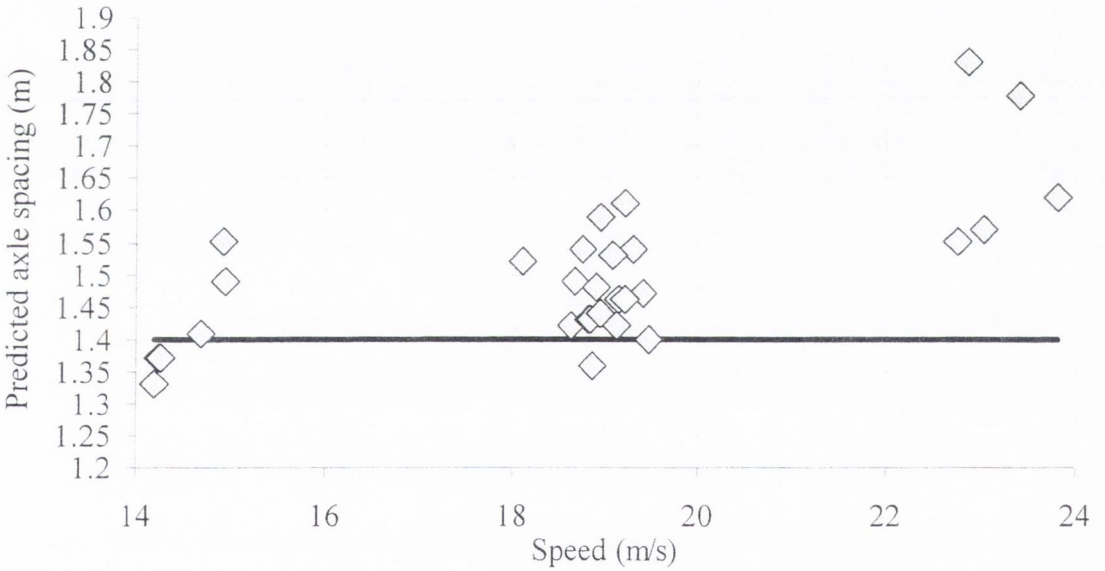

Figure 4.30 – Predicted axle spacing at different speeds for a real axle spacing of 1.40 m

In practise, there are sources of inaccuracy other than scanning frequency. For example, transverse location of the truck may cause errors and there are cases where directions of traffic flow are not perpendicular to the tube. As experienced in Delgany site, very closely spaced axles can induce two pulses of air, one immediately behind the other, distorting a clear record. An excessive length or twisting of the tube can also cause problems. Hence, the average measured errors from the figures above have been – 6 cms for the spacing between 1st and 2nd axle (spaced at 4.02 m), 9 cms for the 2nd and 3rd axle (spaced at 1.40 m), and 3 cms for the 1st and 3rd axle (spaced at 5.42 m). Best results are achieved for the

whole vehicle length. The accuracy of the latter improves the synchronisation between strains and truck location along the bridge.

Objectives of the Program

Initially, there was a Turbo-C program developed by Dempsey (1997) based on Moses' algorithm and a theoretical longitudinal beam model that analysed the signal corresponding to an isolated traffic event. The program also indexed the strain record by giving the starting and ending points for each truck crossing event to a binary file with the whole strain record. This binary file was acquired with DAQ software based in C and developed by O'Connor (1994). These pointer numbers depended on the signal given by the axle detectors, and so, when axle detectors failed to identify the vehicle, part of the strain record could have been missing and its recovery could be a tedious (if not, impossible) task. Therefore, the author re-wrote the code in C++ to allow:

- Reading an experimental influence line as a function of distance from a text file.
- Reading any input (binary or text) strain record.
- Introducing an interface to modify parameters readily, such as calibration factors, bridge length and truck characteristics (initially, the code had to change some values and be re-compiled every time one of these factors was varied).

The author, McNulty (1999) and Kessler (1997) used this new version for analysing the impact of an improved influence line on B-WIM accuracy (Section 3.7.4).

The Irish B-WIM program was originally designed to deal with one single vehicle at a time where strain record, number of axles, axle spacings and velocity had to be input manually. It was necessary to automate the processing of vast amounts of voltage data and a lot of traffic information continuously. It was the author's task to process the recorded voltage data from axle detectors and strain sensors into number of axles, speeds, axle spacings and axle weights. This task was accomplished by implementing the post-processing axle detection algorithm and Moses' algorithm described previously. As a result, traffic data corresponding to thousands of vehicles for two uninterrupted weeks was obtained to calibrate the Eurocode Bridge model for Irish conditions (O'Brien et al. 1998b). The findings of this test will be discussed in Chapter 8. This software was developed in a DOS platform and it is included in the CD-ROM attached in this thesis.

General Structure of the Irish B-WIM Program

The program was originally written in Turbo C++ v.3.0, while last modifications have been made in Borland C++ 4.5. Given the large quantity of data being recorded, the first stage of the process was the removal of redundant data to minimise storage. Every 280 minutes and 12 channels take 184.8 MB of hard disk space (950.4 MB/day). Accordingly, from the total information on voltage, great savings can be made if only times and strains when there is traffic on the bridge are stored. First of all, binary Labview is converted into text. This text file is between four and five times greater than the original Labview file. Then, the text file is reconverted into binary C (data format: floating point 16 bits) to save space in hard disk and facilitate further post-processing. Then, data is converted into axle hits first, velocity and axle spacings in a second stage and finally into weights. The flow and intermediate processes of the program are summarised in Figure 4.31.

The main menu of the B-WIM program displays the following options:

A. Data acquisition
B. Voltage signal
C. Strain & time storage
D. Calibration
E. Calculation of Weights
F. Files
Q. Quit

The access to the different options is organised through **.bat* files. Option A links the B-WIM interface with DAQ software and applications. Option B is related to signal analysis and a consideration of the most convenient choice of parameters for axle detection or the strain definition at different locations. Option C saves the parts of the voltage file corresponding to when there is traffic on the bridge. Option D provides a facility to look for a test vehicle in a file and determines the calibration factor as defined in Equation 2.1. Option E calculates weight data for a given voltage file. Option F displays the available files (i.e. voltage, strains, times, WIM data, information/model, header and source files). Further details on the contents of the program are given in Appendix D.

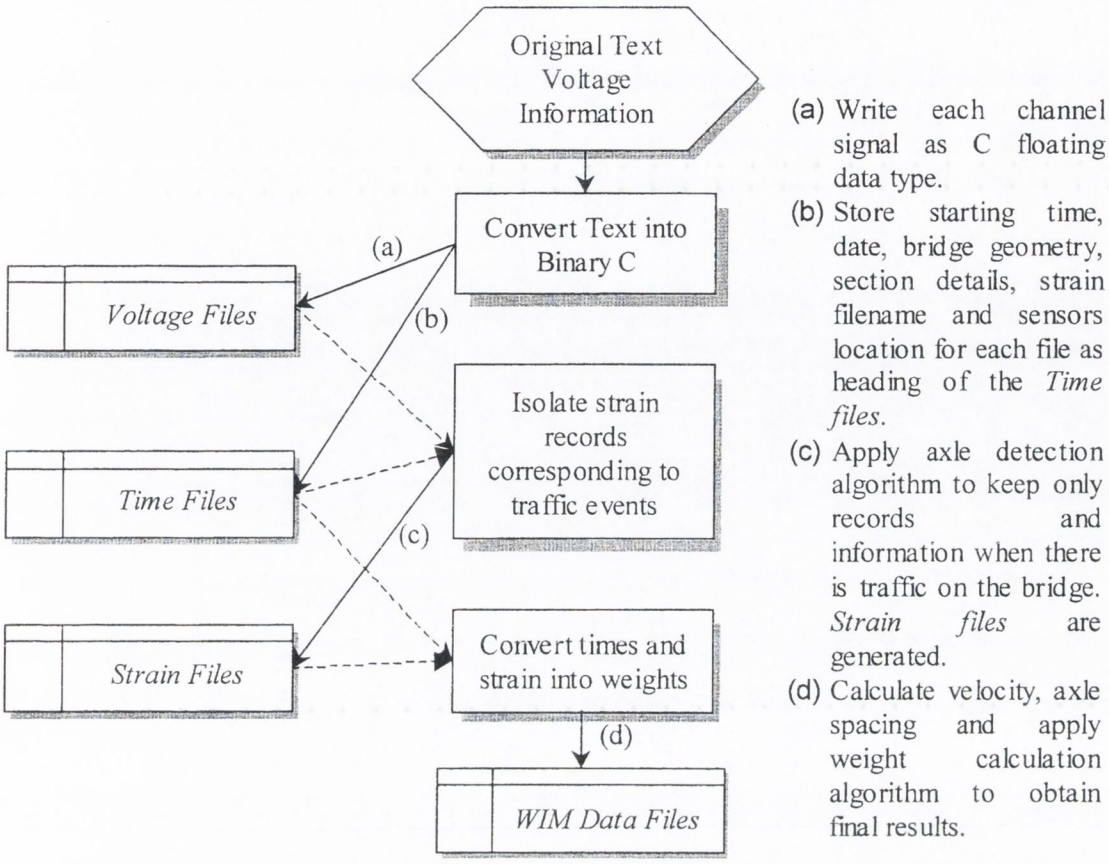

Figure 4.31 – General structure of the program

4.5 Summary

B-WIM systems estimate traffic loads from the bending that vehicles cause as they cross a bridge. This chapter has described the two types of device used by the Irish team to measure bending: (a) strain gauges, generally used in flexible bridges (i.e., steel bridges such as Belleville -Section 8.4.1-), and (b) mechanical strain amplifiers, used in stiff bridges, where a better strain definition is necessary. These amplifiers are bolted to the bridge and they are made of strain gauges connected in a quarter or full Wheatstone configuration. There is also a need to detect axles, which can be done in two different ways:

- From sensors mounted in/on the road surface, e.g., tape switches, rubber tubes, piezo electric sensors. Piezo electric sensors are expensive and extreme care must be taken during installation to ensure good results. Tape switches are very sensitive to traffic aggressiveness. The Irish team has obtained best results with rubber tubes, though they

can only be used in conditions of low traffic intensity and their attachment to the road must be checked periodically.

- From strain sensors attached to the soffit of the bridge (FAD). FAD systems are a very promising technology currently under development. One of their main limitations has been the reduced number of sites where they can be implemented successfully (i.e., orthotropic decks and short span slab bridges). First theoretical studies indicate that integral bridges with spans shorter than 10 m might qualify for FAD purposes.

Concerning the data acquisition hardware, the Irish B-WIM system has used National Instruments equipment that allows for scanning at rates of up to 333 kS/s. The increase in scanning frequency and number of channels that can be recorded simultaneously has made possible the development of FAD systems and multiple-sensor algorithms. Hardware low pass filters make the original data unrecoverable and they should not be applied unless there is certainty that no significant component of the signal is removed. The use of a 16-bit DAQ card instead of a 12-bit card improved resolution significantly.

All the information provided by strain sensors and axle detectors was recorded in a computer through data acquisition software. Originally, the information is recorded in binary format to save storage space and time. This system can be managed manually or left unattended on site for long periods of time. During post-processing, raw data from the different channels is converted into vehicle classification, weights, speeds, headways and gaps. A program to automate this process for two lanes of traffic has been developed by the author. The code implements two algorithms:

- An axle detection algorithm to convert signal from road sensors into number of axles, axle spacings and speed. There are also several routines that detect and deal with outliers and/or doubtful values (i.e., undetected axles by axle detectors or changes of lane).
- An algorithm for weight calculation based on static equations. This algorithm has been described in Section 3.3.

The program has been used to process data uninterruptedly from an Irish site and obtain traffic statistics necessary for the calibration of the bridge load model for Irish conditions (Section 8.2.3).

5

DYNAMIC MODELLING OF TRUCK CROSSING BRIDGE

5.1 INTRODUCTION

Bridge and truck dynamics are a significant source of inaccuracy in B-WIM systems (Section 3.5.1). This chapter presents the parameters that affect the bridge response and the passage of a truck over a bridge is modelled numerically. Some of this formulation will be taken as reference for the development of a dynamic B-WIM algorithm in Chapter 7. These are one-dimensional bridge and truck models while more sophisticated three-dimensional finite element models will be introduced in Chapter 6.

A key source of error for WIM systems is vehicle dynamics. There are two main movements:

- a body oscillation with a frequency between 1.5 Hz and 4.5 Hz, related to the stiffness of suspensions and sprung mass (vehicle body),
- an axle oscillation with a higher frequency (8 to 15 Hz), mainly related to the unsprung mass (wheels and axles) and tyre stiffness.

If a WIM system was able to measure the applied force for a full period of the lowest frequency, the problem would be overcome. The only existing system able to achieve a continuous record of the applied truck wheel forces for a sufficient length of time is a B-WIM system. However, the interaction between bridge and vehicle is a very complex system. Accordingly, the development of an accurate Bridge Weigh In Motion system requires an understanding of how roads and bridges are affected by the passing of vehicles. A lot of authors have studied the modelling of the dynamic response of bridges induced by moving vehicles. Recent progress has been made through research projects such as the OECD DIVINE (**D**ynamic **I**nteraction of **V**ehicle **In**frastructures **E**xperiment) programme and the Vehicle Infrastructure Interaction series of conferences, the fifth of which was held in Poland in September 1999.

The author has implemented the simulation of a four-degree of freedom two-axle vehicle running on a simply supported beam with road irregularities. Equations of motion can be set for the vehicle and the bridge. These equations are coupled due to the interaction forces existing at the contact points. This simple model makes possible the study of the influence of different bridge, truck and/or road profile parameters, a lot of which are not controllable or measurable in experimental trials. In addition, an eleven degree of freedom four-axle vehicle developed by Green et al (1995) is used to investigate the influence of the suspension type and road roughness. These numerical simulations will be used in Chapters 7 and 9 to assess the influence of dynamics on B-WIM accuracy.

5.2 PLANAR DYNAMIC MODELS

The dynamic characteristics of a beam and planar vehicle models are described. In these simplified models, torsional bridge vibration and vehicle roll motion are neglected.

5.2.1 Bridge

The bridge structure is modelled here as a simply supported beam. Its behaviour is governed by the following properties: Young's modulus (E), mass per unit length (μ), damping (ξ), second moment of area (I) and bridge length (L). The natural frequencies in Hz of the bridge are defined by Equation 5.1:

$$f_n = \left(\frac{n}{L}\right)^2 \frac{\pi}{2}\sqrt{\frac{EI}{\mu}} \quad ; \quad n = 1,2... \tag{5.1}$$

If damping was neglected, final results would be somewhat exaggerated. The exact magnitude of damping can be determined only from experimental tests on the real structure. As long as the amplitude of free vibration decays exponentially, it may be assumed that viscous type damping can be used in the mathematical model of the system. The damping factor, ξ, is obtained by measuring the number of oscillations N between two non-consecutive strain peaks (u_N and u_1) and applying Equation 5.2:

$$\frac{\xi}{\sqrt{1-\xi^2}} = \frac{Ln(u_N - u_1)}{2\pi N} \tag{5.2}$$

In Figure 5.1, a damping factor $\xi = 0.05$ results from $u_N = 0.1504$, $u_1 = 0.7279$ and $N = 5$. The values of the logarithmic decrement of damping ($\frac{Ln(u_N - u_1)}{N}$) for concrete bridges vary in the range [0.02,0.20] (Cantieni 1983, Narayanan & Roberts 1991).

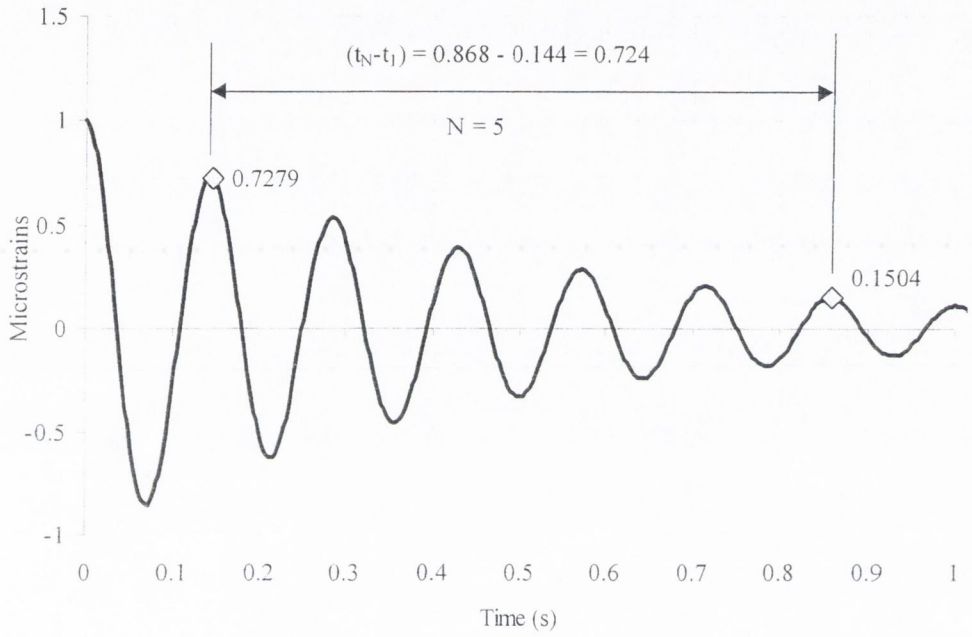

Figure 5.1 – Decay Record of Damped System

First damped frequency (f_d) is obtained by dividing the number of oscillations between two peaks (N) between their difference in time ($t_N - t_1$) (A peak in the spectrum of the record should confirm this value):

$$f_d = \frac{N}{t_N - t_1} \tag{5.3}$$

For the example in Figure 5.1, a damped frequency $f_d = 7$ Hz results from $N = 5$ and $(t_N - t_1) = 0.724$. The natural frequency of the bridge (f_n) is given by:

$$f_n = \frac{f_d}{\sqrt{1-\xi^2}} \tag{5.4}$$

where ξ is damping factor. For low values of damping, $f_n \cong f_d$. Bridges vary in natural frequency from 1 Hz to as high as 15 Hz (Cantieni 1983, Green et al. 1995). A further explanation of the relationships given in this section can be found in widely available structural dynamics books (Craig 1981, Clough & Penzien 1975, Nashif et al. 1985).

5.2.2 Truck

A truck is composed of body, suspension system and tyres. Mathematical models for these elements are defined below.

Static Model

The objective of a high-speed WIM system such as B-WIM is to achieve a degree of accuracy as close as possible to that given by a static scale. However, even for a vehicle stopped in a perfectly levelled site, static weights are influenced by vehicle mechanical parameters. When a load is applied normally to a tyre, the tyre deflects progressively as the load increases. The relationship between the load and deflection depends on the inflation pressure, and it is linear for a given inflation pressure, except at relatively low values of load, out of the range of practical interest (Wong 1993). Hence, the measured static weights depend on the compression of the springs of the suspension/tyre system.

If the springs are compressed differently and there are more than two axles (indeterminate structure), the real static weights can not be measured. In order to analyse this problem, a vehicle can be modelled as a sprung beam allowed to move vertically only at the axle locations. A simply supported beam would derive in the exact static axle weights due to equilibrium. Only in the case of an indeterminate structure –more than two axles–, there will be differences due to suspension springs if the supports are free to rotate. The gravity forces acting on the beam are due to a uniformly distributed mass per unit length, μ, and a concentrated mass, M (Figure 5.2).

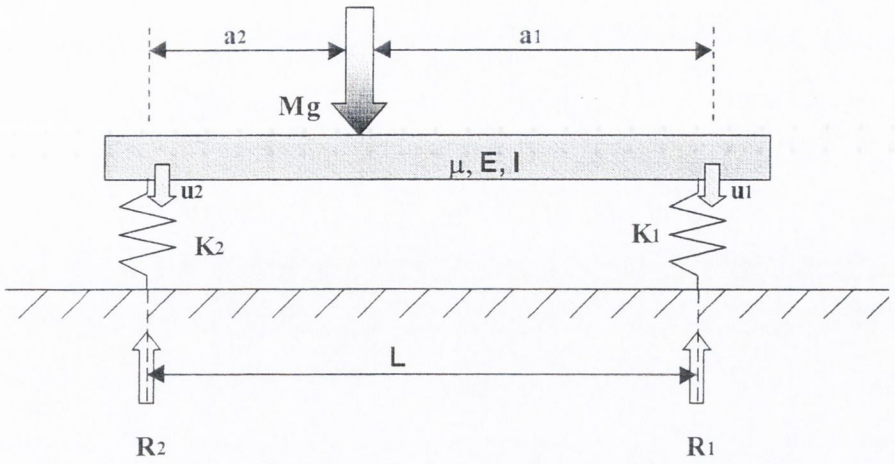

Figure 5.2 – Two-axle rigid vehicle idealised as a sprung beam

The problem is defined by the following parameters:

R_i : Static reaction at axle i (N),

K_i : Sprung stiffness corresponding to axle i (N/m),

a_i : Distance (m) from axle i to location of mass M,

μ : Mass per unit length (kg/m),

g : Acceleration of gravity (9.806 m/s^2),

E : Modulus of elasticity of the beam (N/m^2),

I : Second moment of area of the beam section (m^4),

M : Concentrated mass (kg),

L : Axle spacing (m),

u_i : Vertical displacement of axle i (m).

If the spring elements are ignored, the 'real' static axle weights W_1 and W_2 can be obtained from static equilibrium through Equations 5.5 and 5.6:

$$R_1 = \left(\frac{a_2}{L} M + \frac{\mu L}{2} \right) g \tag{5.5}$$

$$R_2 = \left(\frac{a_1}{L} M + \frac{\mu L}{2} \right) g \tag{5.6}$$

The stiffness matrix for the two degrees of freedom shown in Figure 5.2 is given by:

$$[K] = \begin{bmatrix} k_1 & 0 \\ 0 & k_2 \end{bmatrix} \tag{5.7}$$

The displacements of the springs at the front and rear axles are:

$$\begin{Bmatrix} u_1 \\ u_2 \end{Bmatrix} = \frac{1}{k_1 k_2} \begin{bmatrix} k_2 & 0 \\ 0 & k_1 \end{bmatrix} \begin{Bmatrix} \left(\frac{a_2}{L} M + \frac{\mu L}{2}\right) g \\ \left(\frac{a_1}{L} M + \frac{\mu L}{2}\right) g \end{Bmatrix} \tag{5.8}$$

These static displacements define the position of equilibrium of the vehicle. Measured vertical reactions (R_1 and R_2) depend on the displacements of the springs supporting the vehicle. The reactions at the front and rear axles are given by Equations 5.9 and 5.10:

$$R_1 = k_1 u_1 \tag{5.9}$$

$$R_2 = k_2 u_2 \tag{5.10}$$

Real (Equations 5.5 and 5.6) and measured static weights (Equations 5.9 and 5.10) give the same values as calculations correspond to a determinate structure. Minor differences will appear when there are more than two axles on the bridge. In this case, errors derived from measurements will depend on the load distribution, axle stiffness and beam stiffness. The results for the weight of an axle group or the whole vehicle can be improved by measuring all axles in one operation, as the differences in the compression of each spring compensate for each other (Equation 5.11).

$$\sum_{i=1}^{n} R_i = \sum_{i=1}^{n} W_i \tag{5.11}$$

where n is number of axles.

Tyres

In vehicle dynamics, the cushioning characteristics of a pneumatic tyre can be represented by a mass element and a linear spring (K_t) in parallel with a viscous damping element (C_t) representing the fundamental mode of vibration of the tyre (Figure 5.3).

The interaction force, R, between a tyre and the bridge is given by:

$$R = -(K_t z_t + C_t \frac{dz_t}{dt}) \tag{5.12}$$

where z_t is the displacement of the axle relative to the level of the road profile.

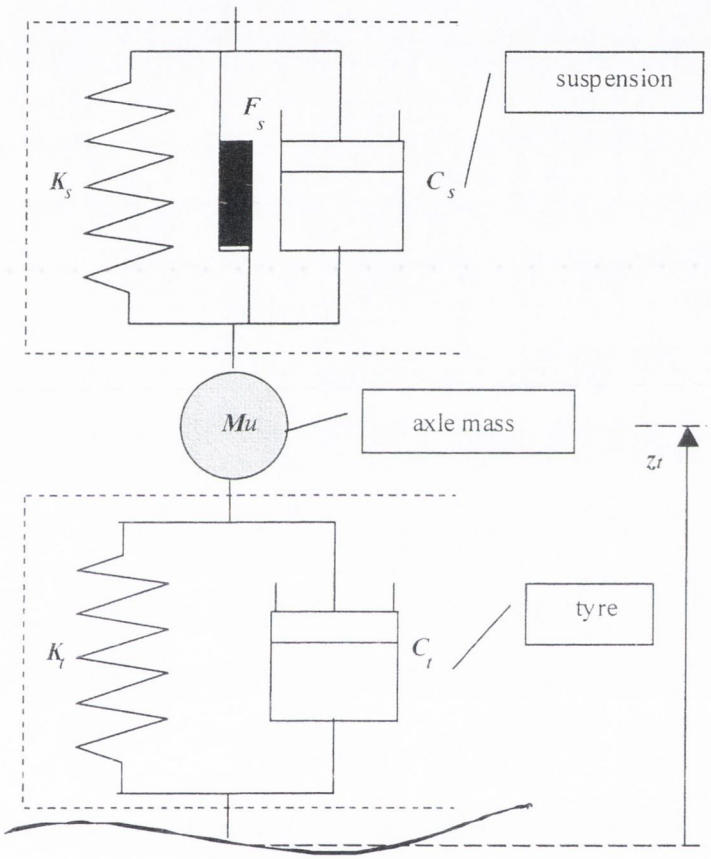

Figure 5.3 – Tyre and suspension idealisation

For a sample of truck tyres travelling at relatively low speed, Wong (1993) found that values of 'dynamic' vertical stiffness, K_t, vary between 764 and 1024 kN/m and stiffness of radial-ply tyres was generally lower than that of bias-ply tyres of similar size. This 'dynamic' vertical stiffness (i.e., that found by measuring the response of a rolling tyre to a known harmonic excitation) is preferred to the static vertical stiffness (from load-deflection curves) for simulation of vehicle dynamics. For heavy truck tyres, the dynamic

stiffness is generally approximately 5% less than the static stiffness, but values 26% lower than the static value have been reported for tractor tyres.

Wong shows that K_t decreases sharply as soon as the tyre begins rolling and the influence of speed becomes less important beyond a speed of approximately 20 km/h. The damping of a pneumatic tyre appears to be a combination of Coulomb-type and viscous-type damping, but an equivalent viscous damping factor, C_t, can be usually derived. Damping coefficient C_t drops rapidly as speed increases from 1 km/h to 5 km/h, after which an asymptote is reached. Further, dynamic stiffness K_t increases and damping coefficient C_t decreases with the inflation pressure.

Suspension

Figure 5.3 represents a simple model of a vehicle suspension system: A linear spring (K_s) is present in parallel with a linear viscous element of damping constant C_s and a Coulomb friction force F_s. The axial force S acting on the suspension system will be given by:

$$S = -\left(K_s z_s + C_s \frac{dz_s}{dt} + F_s \frac{dz_s/dt}{\left| dz_s/dt \right|} \right) \tag{5.13}$$

where z_s is the relative displacement between the axle and vehicle module.

However, the accuracy of this model is often unsatisfactory due to an overestimation of the response force (Kirkegaard et al. 1997). In practice, frequency and damping of the suspension are not independent parameters and it is difficult to design a suspension with effective damping above 2 Hz (OECD 1997). Section 5.6 introduces a more sophisticated suspension model based on data available from an instrumented truck.

Figure 5.4 illustrates types of mechanical behaviour that can be found as part of a suspension/tyre system. Figure 5.4(a) represents a linear spring with viscous damping where the damping force is proportional to the velocity of motion. Figure 5.4(b) represents Coulomb-damping friction, which is the result of sliding vibration bodies on a dry surface. A maximum force F_s equal to the applied force normal to the surface multiplied by the

coefficient of kinetic friction of the surface material is developed. Figure 5.4(c) represents other frictional forces with non-linear behaviour.

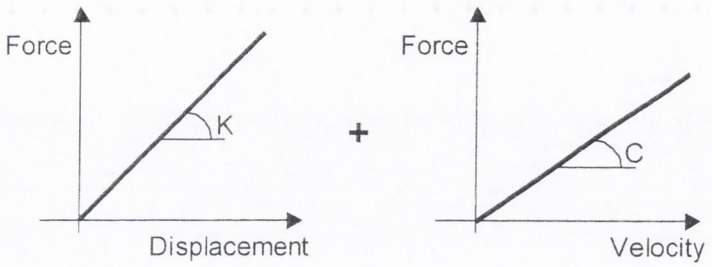

(a) Linear spring with viscous damping

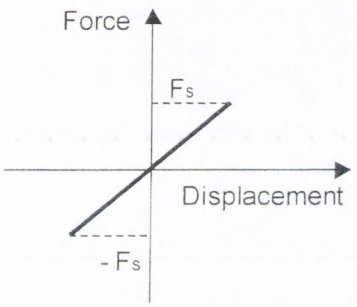

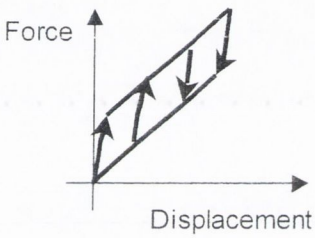

(b) Spring with Coulomb damping (c) Spring with non-linear behaviour

Figure 5.4 – Mathematical models for suspension/tyre elements

Body

The vehicle body is represented by a concentrated mass subjected to rigid-body motions. Two degrees of freedom are considered: vertical motion (z) and pitching rotation (φ). The dynamic characteristics of the body are mass moment of inertia of rotation (J) and body mass (M). Mass moment of inertia can be calculated from the weight distribution and dimensions of the body. In the case of a tractor-trailer configuration (Figure 5.5), the two modules are assumed to be linked together at a hinge.

Apart from the dynamic equations of equilibrium (Equations 5.13 to 5.16), it is necessary to set compatibility conditions between the relative displacements of each component (z_{t1}, $z_{t2},..,z_{ti},..,z_{tn}$ as relative displacements of the i^{th} axle relative to the mean level of the surface irregularities, $z_{s1},z_{s2},..,z_{si},..,z_{sn}$ as relative displacements between the i^{th} axle and the module, z_1, z_2, φ_1 and φ_2). These additional equations are based on the location of each degree of

freedom, rigid body translations in the x and z directions and rotations at the centres of gravity of the tractor and trailer.

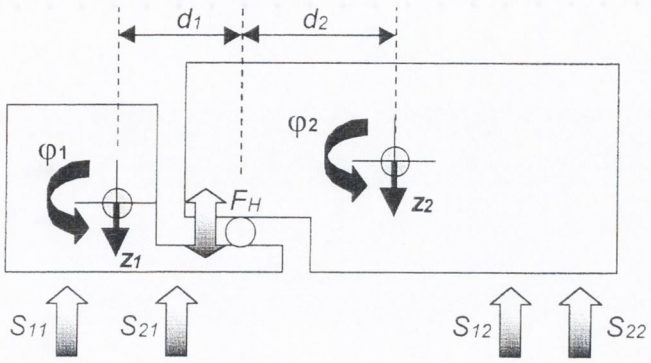

Figure 5.5 – Simplified Tractor + trailer body mass model

This hinge only allows a vertical force, F_H, to be transmitted between the modules. The equations of dynamic equilibrium for each module are:

$$M_j \frac{d^2 z_j}{dt^2} = \sum_{i=1}^{n_j} S_{ij} + F_H \quad ; j = 1,2 \tag{5.14}$$

$$J_j \frac{d^2 \varphi_j}{dt^2} = -(\sum_{i=1}^{n_j} S_{ij} l_{ij} + F_H d_j) \quad ; j = 1,2 \tag{5.15}$$

where

z_j : Vertical displacement of module j,

φ_j : Rotation of module j,

S_{ij} : Forces acting on the axle suspensions supporting the module j,

l_{ij} : Distance from axle i in module j to the mass centre of gravity of module j,

d_j : Distance from the hinge to the mass centre of gravity of module j,

M_j : Mass of module j,

n_j : Number of axles supporting module j,

J_j : Mass moment of inertia of rotation of module j.

5.3 BRIDGE SUBJECTED TO A MOVING CONSTANT LOAD

This section introduces the case of a moving load that exerts a constant force on a beam. The distributed mass of the beam will be taken into account, but the mass of the load itself is omitted.

5.3.1 Single load

A moving load R, acting downwards on a beam and moving from left to right at a constant velocity v is considered (Figure 5.6). The beam is simply supported at both ends. The cross-section is constant (Young modulus, E, Second moment of area, I, and damping coefficient, c) with uniform mass distribution (mass per unit length, μ). The formulation developed in this section will be taken as the basis for some of the dynamic Bridge WIM algorithms presented in the following chapter.

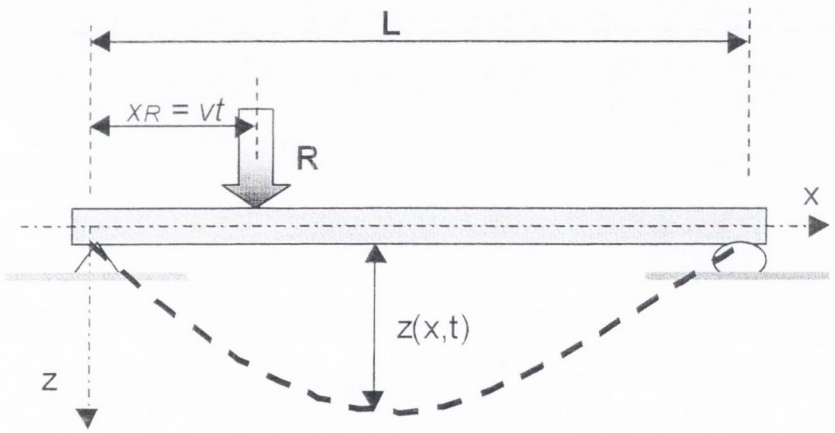

Figure 5.6 – Simply supported beam subjected to a constant moving force

The bridge deflection, $z(x,t)$, can be expressed in terms of the modal coordinates, Z_i, and natural modes, Φ_i, as given in Equation 5.16:

$$z(x,t) = \sum_{i=1}^{\infty} \Phi_i Z_i(t) \tag{5.16}$$

The equations of motion are derived directly from Lagrange's equations for each modal coordinate i:

$$\frac{d}{dt}\left(\frac{\partial K}{\partial \dot{\Phi}_i}\right)-\frac{\partial K}{\partial \Phi_i}+\frac{\partial V}{\partial \Phi_i}-\frac{\partial W_D}{\partial \Phi_i}-\frac{\partial W}{\partial \Phi_i}=0 \tag{5.17}$$

where K is total kinetic energy of the system calculated using the masses and velocities of the system components (Equation 5.18), V is the total potential energy of the system computed from the relative displacements (Equation 5.19), W_D is the dissipation energy of the system obtained from the damping forces (Equation 5.20) and W is the total virtual work (Equation 5.21):

$$K=\frac{1}{2}\int_0^L \mu\left(\frac{\partial z}{\partial t}\right)^2 dx \tag{5.18}$$

$$V=\frac{1}{2}\int_0^L EI\left(\frac{\partial^2 z}{\partial x^2}\right)^2 dx \tag{5.19}$$

$$W_D=\frac{1}{2}\int_0^L c\left(\frac{\partial z}{\partial t}\right)dx \tag{5.20}$$

$$\delta W=-R\delta z \tag{5.21}$$

As a result of substituting Equations 5.18 to 5.21 into Lagrange's equation (5.17), the bending vibration of the beam, $z(x,t)$, is defined:

$$EI\frac{\partial^4 z(x,t)}{\partial x^4}+\mu\frac{\partial^2 z(x,t)}{\partial t^2}+2\mu\omega_b\frac{\partial^2 z(x,t)}{\partial t^2}=\delta(x-x_R)R \tag{5.22}$$

where

$z(x,t)$: displacement of the bridge at position x and time t,

E, μ and I : Young's modulus, mass per unit length, and second moment of area of the bridge respectively,

δ : Dirac function,

$\omega_b = \frac{\xi\omega_1}{\sqrt{1-\xi^2}}$, where ξ is viscous damping factor ($\xi=\frac{c}{2\mu\omega_1}$) and ω_1 is circular natural frequency of the bridge ($\omega_1=2\pi f_1$),

R : applied force,

x_R = vt, is the distance of the force from the left support, where v is velocity.

The solution to Equation 5.22 is given by Frýba (1972):

$$z(x,t)=\frac{2RL^3}{\pi^4 EI}\sum_{i=1}^{\infty}\frac{\sin\left(\frac{i\pi x}{L}\right)}{i^2\left[i^2\left(i^2-\alpha^2\right)^2+4\alpha^2\beta^2\right]}\begin{Bmatrix} i^2\left(i^2-\alpha^2\right)\sin(i\omega t) \\ -i\alpha\left[i^2\left(i^2-\alpha^2\right)-2\beta^2\right]e^{-\omega_b t}\sin(\omega_i' t) \\ -2i\alpha\beta[\cos(i\omega t)-e^{-\omega_b t}\cos(\omega_i' t)\end{Bmatrix} \tag{5.23}$$

where

$$\omega=\pi v/L \tag{5.24}$$

$$\alpha=\frac{\pi v/L}{\omega_1} \tag{5.25}$$

$$\beta=\frac{\zeta}{\sqrt{1-\zeta^2}} \tag{5.26}$$

$$\omega_i'=\sqrt{\omega_i^2-\omega_b^2} \tag{5.27}$$

For this case of moving constant force, the only vehicle parameter affecting the bridge dynamic response is speed. As bridges have relatively low damping, the critical speed (speed at which the maximum deflection in forced vibration occurs) takes place when the travel time of the moving load to cross the beam span is from 0.7 to 1.0 times the fundamental period of the bridge (Michaltsos et al. 1996, Frýba 1972). Bridge deflection will decrease as vehicles increase their speed over the critical level, and bridge response will get closer to the static response as vehicles decrease their speed below the critical speed.

Strains are given by $\varepsilon=-h_g\frac{\partial^2 z}{\partial x^2}$, where h_g is the distance from the strain location to the neutral axis of the section. By differentiating Equation 5.23 twice with respect to x, strains can be expressed as in Equation 5.28:

$$\varepsilon = \frac{h_g RL}{4EI}\sum_{i=1}^{\infty}\frac{\frac{8i^2}{\pi^2}\sin\left(\frac{i\pi x}{L}\right)}{i^2[i^2(i^2-\alpha^2)^2+4\alpha^2\beta^2]}\begin{Bmatrix} i^2(i^2-\alpha^2)\sin(i\omega t)-\dfrac{i\alpha[i^2(i^2-\alpha^2)-2\beta^2}{\sqrt{i^4-\beta^2}}e^{-\omega_b t}\sin(\omega_i' t) \\ -2i\alpha\beta[\cos(i\omega t)-e^{-\omega_b t}\cos(\omega_i' t) \end{Bmatrix} \tag{5.28}$$

If velocity of the moving forces, v, is very small, $\alpha \approx 0$ in the equation above. Then the static strain of the beam for a force at position $x_R = vt$ is given by Equation 5.29:

$$\varepsilon_s = \frac{h_g RL}{4EI}\sum_{i=1}^{\infty}\frac{\frac{8}{\pi^2}\sin\left(\frac{i\pi x}{L}\right)\sin(i\omega t)}{i^2} \tag{5.29}$$

The dynamic component, ε_d, can be obtained by subtracting the static strain, ε_s, (as defined in Equation 5.29) from the total strain, ε (Equation 5.28). This dynamic strain is illustrated in Equation 5.30:

$$\varepsilon_d = \frac{h_g RL}{4EI}\sum_{i=1}^{\infty}\frac{\frac{8i^2}{\pi^2}\sin\left(\frac{i\pi x}{L}\right)}{i^2[i^2(i^2-\alpha^2)^2+4\alpha^2\beta^2]}\begin{Bmatrix} -i^2\alpha^2\sin(i\omega t) \\ -\dfrac{i\alpha[i^2(i^2-\alpha^2)-2\beta^2}{\sqrt{i^4-\beta^2}}e^{-\omega_b t}\sin(\omega_i' t) \\ -2i\alpha\beta[\cos(i\omega t)-e^{-\omega_b t}\cos(\omega_i' t) \end{Bmatrix} \tag{5.30}$$

Total strain at a certain point in space and time can be expressed as the sum of a static and a dynamic component ($\varepsilon = \varepsilon_s + \varepsilon_d$). Hence, substituting from Equation 5.28 gives:

$$\varepsilon = \varepsilon_s + \frac{h_g RL}{4EI}\sum_{i=1}^{\infty}\frac{\frac{8i^2}{\pi^2}\sin\left(\frac{i\pi x}{L}\right)}{i^2[i^2(i^2-\alpha^2)^2+4\alpha^2\beta^2]}\begin{Bmatrix} -i^2\alpha^2\sin(i\omega t)-\dfrac{i\alpha[i^2(i^2-\alpha^2)-2\beta^2}{\sqrt{i^4-\beta^2}}e^{-\omega_b t}\sin(\omega_i' t) \\ -2i\alpha\beta[\cos(i\omega t)-e^{-\omega_b t}\cos(\omega_i' t) \end{Bmatrix} \tag{5.31}$$

From beam theory, the static strain for a section at location x due to a load R located at x_R can be obtained from Equations 5.32 and 5.33:

$$\varepsilon_{0-x_R} = \frac{h_g}{EI}\frac{R(L-x_R)}{L}x \quad ; \; 0 \le x \le x_R \tag{5.32}$$

$$\varepsilon_{x_R-L} = \frac{h_g}{EI}\frac{Rx_R}{L}(L-x) \quad ; \; x_R \le x \le L \tag{5.33}$$

By substituting Equations 5.32 and 5.33 into Equation 5.31, the theoretical solution can be determined accurately with a smaller number m of mode shapes than the infinite number of Equaion 5.28:

$$\varepsilon_{0-x_R} = \frac{h_g}{EI}\frac{R(L-x_R)}{L}x + \frac{h_g RL}{4EI}\sum_{i=1}^{m}\frac{\frac{8i^2}{\pi^2}\sin\left(\frac{i\pi x}{L}\right)}{i^2[i^2(i^2-\alpha^2)^2+4\alpha^2\beta^2]}\left\{\begin{matrix}-i^2\alpha^2\sin(i\omega t)-\dfrac{i\alpha[i^2(i^2-\alpha^2)-2\beta^2}{\sqrt{i^4-\beta^2}}e^{-\omega_b t}\sin(\omega_i' t)\\ -2i\alpha\beta[\cos(i\omega t)-e^{-\omega_b t}\cos(\omega_i' t)\end{matrix}\right\}$$

$$0 \le x \le x_R \tag{5.34}$$

$$\varepsilon_{x_R-L} = \frac{h_g}{EI}\frac{Rx_R}{L}(L-x) + \frac{h_g RL}{4EI}\sum_{i=1}^{m}\frac{\frac{8i^2}{\pi^2}\sin\left(\frac{i\pi x}{L}\right)}{i^2[i^2(i^2-\alpha^2)^2+4\alpha^2\beta^2]}\left\{\begin{matrix}-i^2\alpha^2\sin(i\omega t)-\dfrac{i\alpha[i^2(i^2-\alpha^2)-2\beta^2}{\sqrt{i^4-\beta^2}}e^{-\omega_b t}\sin(\omega_i' t)\\ -2i\alpha\beta[\cos(i\omega t)-e^{-\omega_b t}\cos(\omega_i' t)\end{matrix}\right\}$$

$$X_R \le x \le L \tag{5.35}$$

5.3.2 Multiple loads

In the case of a system of concentrated moving forces, $R_1, R_2, ..., R_n$, spaced at $a_1, a_2, ..a_{n-1}$, from the position of the first force and all travelling at speed v, the total virtual work due to the applied forces is given by:

$$\delta W = -\sum_{i=1}^{n}\varepsilon_i\delta(x-x_i)R_i\delta z_i \tag{5.36}$$

where

δ : Dirac function,

n : total number of forces,

ε_i = 1 when force i is on the bridge (otherwise zero),

R_i : value of constant force i,

x_i = $vt - a_i$, is the position of force i (the position of first force on the bridge is $x_1 = vt$), where a_i is spacing between first force and i^{th} force.

By substituting in Lagrange's Equation (5.17), the bending vibration ($z(x,t)$) of the beam at position x and time t will be given by:

$$EI\frac{\partial^4 z(x,t)}{\partial x^4} + \mu\frac{\partial^2 z(x,t)}{\partial t^2} + 2\mu\omega_d\frac{\partial^2 z(x,t)}{\partial t^2} = \sum_{i=1}^{n}\varepsilon_i\delta(x - x_i)R_i \tag{5.37}$$

The solution to Equation 5.37 is:

$$\varepsilon = \sum_{j=1}^{j=n}\frac{h_j\varepsilon_j\delta(x - x_j)R_jL}{4EI}\left[\sum_{i=1}^{\infty}\frac{\frac{8i^2}{\pi^2}\sin\left(\frac{i\pi x}{L}\right)}{i^2[i^2(i^2-\alpha^2)^2 + 4\alpha^2\beta^2]}\left\{\begin{array}{l} i^2(i^2-\alpha^2)\sin\left(i\omega(t-\frac{a_j}{v})\right) \\ -\frac{i\alpha[i^2(i^2-\alpha^2)-2\beta^2}{\sqrt{i^4-\beta^2}}e^{-\omega_b t}\sin(\omega_i' t) \\ -2i\alpha\beta[\cos(i\omega t) - e^{-\omega_b t}\cos(\omega_i' t) \end{array}\right\}\right] \tag{5.38}$$

Hence, the principle of superposition applies when a system of constant forces moving on a bridge at uniform speed is considered.

5.4 RANDOM ROAD PROFILE MODEL

The unevenness of the road surface is an important factor that affects the dynamic response of bridge structures. Road irregularities and their input in a vehicle model are discussed in this section.

5.4.1 Definition of Road Roughness

To analyse the vehicle response, the road profile can be assumed to be a random process described by a power spectral density (PSD) function. The height of road irregularities (r) is generated from the formula (Yang & Lin 1995):

$$r(t) = \sum_{i=1}^{N} \sqrt{4S(\omega_i)}\Delta\omega \cos(\omega_i t - \theta_i) \tag{5.39}$$

where

$S(\omega_i)$: Power spectral density function ,

ω_i : Circular frequency (rad/s),

θ_i : Independent random variable uniformly distributed in the range from 0 to 2π.

N : Number of discrete frequencies.

Road profiles are different depending on the random numbers θ_i used in Equation 5.39. Attending to the classification of road roughness given by ISO (**I**nternational **S**tandards **O**rganisation) specifications, the PSD function for highway surface roughness is (Wong 1993):

$$\text{For} \quad \begin{cases} \omega \le \dfrac{1}{2\pi} cycle/m \Rightarrow S(\omega) = \dfrac{a}{(2\pi\omega)^2} \\ \omega > \dfrac{1}{2\pi} cycle/m \Rightarrow S(\omega) = \dfrac{a}{(2\pi\omega)^{1.5}} \end{cases} \tag{5.40}$$

Depending on the road conditions:

$$\begin{cases} a < 8x10^{-6} (very\_good) \\ 8x10^{-6} \le a < 32x10^{-6} (good) \\ 32x10^{-6} \le a < 128x10^{-6} (average) \\ 128x10^{-6} \le a < 512x10^{-6} (poor) \\ 512x10^{-6} \le a < 2048x10^{-6} (very\_poor) \end{cases}$$

where a (m^3/cycle) is the roughness coefficient (value of the spectral density at the discontinuity frequency $\frac{1}{2\pi}$). Appendix B gives an indication of what accuracy might be achievable from a WIM site with a measured IRI[17] (**I**nternational **R**oughness **I**ndex). Figure 5.7 relates the roughness coefficient, a, of the PSD function for $\omega \le \frac{1}{2\pi}$ and the IRI. An IRI of 6.0 is regarded as the minimum value for highways, which is equivalent to a

roughness coefficient of $a = 0.64(2\pi)^2 x10^{-6} = 25.3x10^{-6}$ m/cycle in Figure 5.7. Appendix B reconmends a WIM site with an IRI lower than 2.6 mm/m for accuracy class B, that is, lowe than $a = 0.1(2\pi)^2 x10^{-6} = 4x10^{-6}$ m/cycle (a 'very good' road profile according to Equation 5.40).

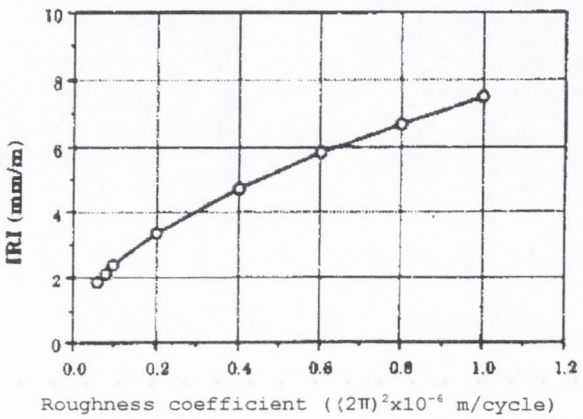

Figure 5.7 – Roughness coefficient of PSD versus IRI (after Hwang & Nowak 1991)

A porion of the theoretical vertical profile corresponding to a road in 'good' conditions ($a = 16x10^{-6}$ m/cycle, IRI ≅ 4.6 mm/m) is shown in Figure 5.8.

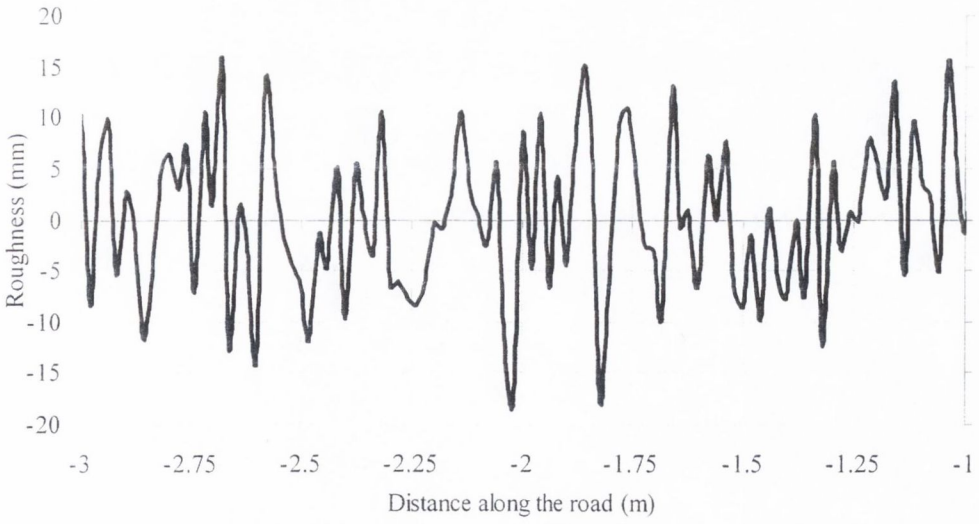

Figure 5.8 – Random road profile in 'good' conditions

The magnitude of the bridge response depends strongly not only on the unevenness of the road profile, but also on the velocity of the vehicles and the condition of the road leading to the bridge. The effects of occasional large irregularities such as potholes, misalignments at

the abutments or expansion joints have been removed in the previous analysis, but they can not be ignored and will be treated separately (Section 6.2.2). Though a B-WIM site with a smooth road profile improves accuracy, IRI does not properly account for the unevenness near the expansion joint (O'Brien et al. 1999b). Tests carried out on full-scale bridges have revealed that vehicles can cause excess stresses on bridges of 5 to 10% over smooth roads, 40 to 50% over poor bumpy roads, and 47 to 85% if there is an obstacle (impact effect) in the path of the wheel (Major 1980). Chompooming & Yener (1995) show how certain combinations of bump characteristic (i.e., height and length) and vehicle speed can result in very high dynamic effects.

5.4.2 Vehicle-Road profile interaction

An example of how to implement the road irregularities is presented next. Figure 5.9 represents a vehicle model composed of mass M, spring constant K, and damping coefficient C, moving at constant speed v along a road profile (vertical position $r(x)$).

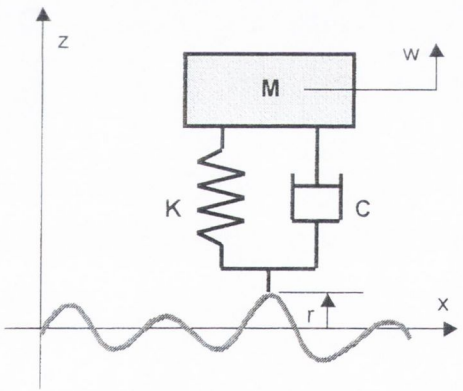

Figure 5.9 – Vehicle model moving on a road surface

The equation of motion for the vehicle model is given by Equation 5.41:

$$M\frac{d^2w}{dt^2}+C(\frac{dw}{dt}-\frac{dr}{dt})+K(w-r)=0 \qquad (5.41)$$

If $y = w - r$ then:

$$M\frac{d^2y}{dt^2}+C\frac{dy}{dt}+Ky=-M\frac{d^2r}{dt^2} \tag{5.42}$$

Since $r(x)$ is known, the vibration of the vehicle $w = r + y$ can be easily determined once the response y is solved for the given forcing function $\frac{d^2r(t)}{dt^2}$. This function represents the road profile $r(x)$ with $x = vt$. The road profile can be the result of measurements or a stochastic process as generated by Equation 5.39.

5.5 BRIDGE SUBJECTED TO A MOVING TWO-AXLE RIGID BODY

A planar two-axle body is implemented with the numerical methods proposed by Frýba (1972). Figure 5.10 shows the four degrees of freedom of the model, allowing for pitch and bounce of the truck body. A three dimensional model would be necessary to take roll motion into account, but the influence of roll on bridge dynamics has been proven to be small compared to that of pitch and vertical motions (Chompooming & Yener 1995). The vehicle parameters are: speed (v), axle spacing (D), body inertia (J), sprung mass ($m_s=m_{s1}+m_{s2}$), unsprung masses (m_{u1} and m_{u2}), tyre stiffness (K_{ti}), and damping (C_i) and (K_{si}) suspension stiffness at each axle. Compared to Equations 5.12 and 5.13, this simplified model assumes $C_t = 0$ and $F_s = 0$.

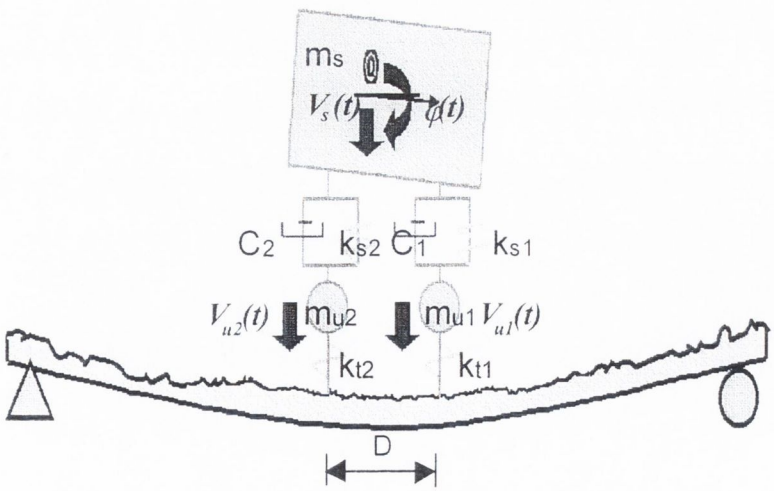

Figure 5.10 – Numerical simulation (Frýba model)

As introduced in Section 5.2.2, equations of motions are expressed by dynamic equilibrium of the different components of the structural system. Hence, Equation 5.43 defines the rotation (φ) of the sprung mass:

$$-J\frac{d^2\varphi(t)}{dt^2}+\sum_{i=1}^{2}(-1)^i\frac{m_s-m_{si}}{m_s}\left\{K_{si}\left[v_{ui}(t)-v_{si}(t)\right]+C_i\left[\dot{v}_{ui}(t)-\dot{v}_{si}(t)\right]\right\}=0 \tag{5.43}$$

where:

$$v_{si}(t)=v_s(t)-(-1)^i\frac{m_s-m_{si}}{m_s}\varphi(t) \tag{5.44}$$

and

v_s : Vertical displacement of sprung mass measured from the equilibrium position in which suspension springs are compressed by vehicle static mass,

v_{ui} : Vertical displacement of unsprung mass i measured from the position in which tyre springs are undeformed,

φ : Rotation of sprung mass measured in the clockwise direction from the horizontal.

Equation 5.45 represents the vertical motion (v_s) of the sprung mass:

$$-m_s\frac{d^2v_s(t)}{dt^2}-\sum_{i=1}^{2}\left\{K_{si}\left[v_{ui}(t)-v_{si}(t)\right]+C_i\left[\dot{v}_{ui}(t)-\dot{v}_{si}(t)\right]\right\}=0 \tag{5.45}$$

Equations 5.46 represent the vertical motions (v_{u1} and v_{u2}) of both unsprung masses:

$$m_{ui}g+m_{si}g-\frac{m_{ui}d^2v_{ui}(t)}{dt^2}+K_{si}\left[v_{ui}(t)-v_{si}(t)\right]+C_i\left[\dot{v}_{ui}(t)-\dot{v}_{si}(t)\right]-R_i(t)=0\ ;\ i=1,2 \tag{5.46}$$

Equation 5.47 provides an expression for the bending vibration ($z(x,t)$) of the beam,

$$EI\frac{\partial^4 z(x,t)}{\partial x^4}+\mu\frac{\partial^2 z(x,t)}{\partial t^2}+2\mu\omega_b\frac{\partial z(x,t)}{\partial t}=\sum_{i=1}^{2}\varepsilon_i\delta(x-x_i)R_i(t) \qquad (5.47)$$

where

$z(x,t)$: Displacement of the bridge at position x and time t,

E, μ and I : Young's modulus, mass per unit length, and second moment of area of the bridge respectively,

δ : Dirac function,

ε_i = 1 when axle i is on the bridge (otherwise zero),

ω_b = $\frac{\xi\omega_1}{\sqrt{1-\xi^2}}$, where ξ is viscous damping factor ($\xi=\frac{c}{2\mu\omega_1}$) and ω_1 is circular natural frequency of the bridge ($\omega_1=2\pi f_1$),

$R_i(t)$: Interaction force between the bridge and the applied axle force i,

x_i = $vt-a_i$, is the position of axle i (the position of first axle is $x_1 = vt$), where a_i is spacing between first axle and i^{th} axle, and v is velocity,

x_1 = vt and $x_2 = vt - D$ are the axle positions.

$R_i(t)$ is the applied axle i force at the point of contact on the beam and it is related to the rest of the vehicle by Equation 5.46. These forces, $R_i(t)$, are time-dependent, as the position of the axles change with time and the suspension of the vehicle oscillates due to irregularities of the bridge deck and bridge vertical displacement under tyres. Equation 5.48 takes into account the effect of bridge displacement and road profile on the interaction forces:

$$R_i(t)=K_{ti}\left[v_{ui}(t)-z(x_i,t)-r(x_i)\right] \quad ; \quad i=1,2 \qquad (5.48)$$

Frýba (1972) reduces this set of five differential equations (5.43 to 5.48) to a dimensionless form that can be readily solved by the method of finite Fourier integral transformation. Computer code has been developed by the author to solve the final differential equations of second order using the Runge-Kutta method (Appendix E). The program allows the user to specify bridge parameters (stiffness, length, mass), truck parameters (masses, suspension and tyre properties, speed, axle spacings) and a stochastic (Section 5.4) or a measured road profile (code included in CD-ROM accompanying thesis).

The interaction between the vehicle and the bridge can be included through the iterative procedure shown in Figure 5.11.

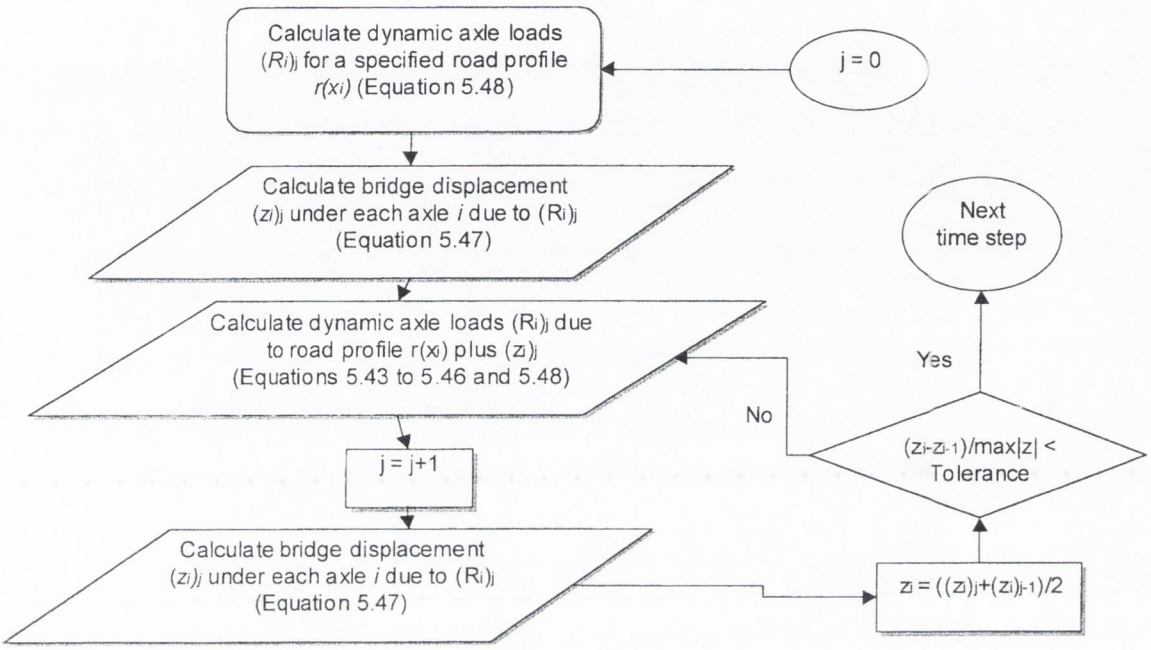

Figure 5.11 – Iteration technique for solving interaction at each time step

Preliminary studies on the bridge response have been carried out with only one iteration from the algorithm shown in Figure 5.11. In order to study the impact of a change in the truck dynamic parameters, some values are adopted as reference: speed 20 m/s, static load 58836 N on each axle, pitching inertia 50×10^3 kgm^2, axle spacing 4 m, tyre stiffness 700×10^3 N/m, suspension stiffness 80×10^3 N/m, and suspension damping 7×10^3 Ns/m at each axle. The characteristics of the bridge model are: span 20 m, mass (μ) 25.5×10^3 kg/m, flexural rigidity (EI) 3×10^{10} Nm^2, first natural frequency 4.26 Hz, critical damping 1%, and 'good' road conditions ($a = 16\text{x}10^{-6}$), unless otherwise specified.

5.5.1 Effect of Bridge Characteristics

From a B-WIM point of view, individual axle weights are easier to identify for shorter bridge lengths (i.e. culverts). However, the average applied axle force might be far from the static value if the bridge length and/or vehicle speed does not allow for a few dynamic oscillations. Therefore, a high excitation of truck dynamics by a road irregularity prior to the bridge might not have time to be damped out by the vehicle damping mechanisms. A

longer bridge allows for the recording and averaging of more readings, but the separation of the effect of a single axle from others might be more difficult (i.e., due to low vehicle/bridge mass ratio). Additionally, simultaneous traffic events are more likely to take place as the bridge length increases.

In medium to long span bridges, bridge-truck interaction can be estimated by a quarter car model with two mass elements being the bridge and gross vehicle mass (these two degrees of freedom represent the body bounce frequency and bridge natural frequency). OECD (1997) reports significant coupling for a modal bridge mass 20 times greater than the vehicle mass. This is not the case for short span bridges where the length of the truck might be greater than the bridge span, in which case bridge vibration is due to axle hop modes on the vehicle, rather than body bounce modes. Strong damping (>2%) can limit the dynamic response of short span bridges significantly (Chompooming & Yener 1995). Damping of longer bridges is less important.

Figure 5.12 shows the strain response at midspan due to the passing of the two-axle truck taken as reference for three different bridge lengths: 10, 20 and 40 m with natural frequencies of 17.04, 4.26 and 1.06 Hz respectively.

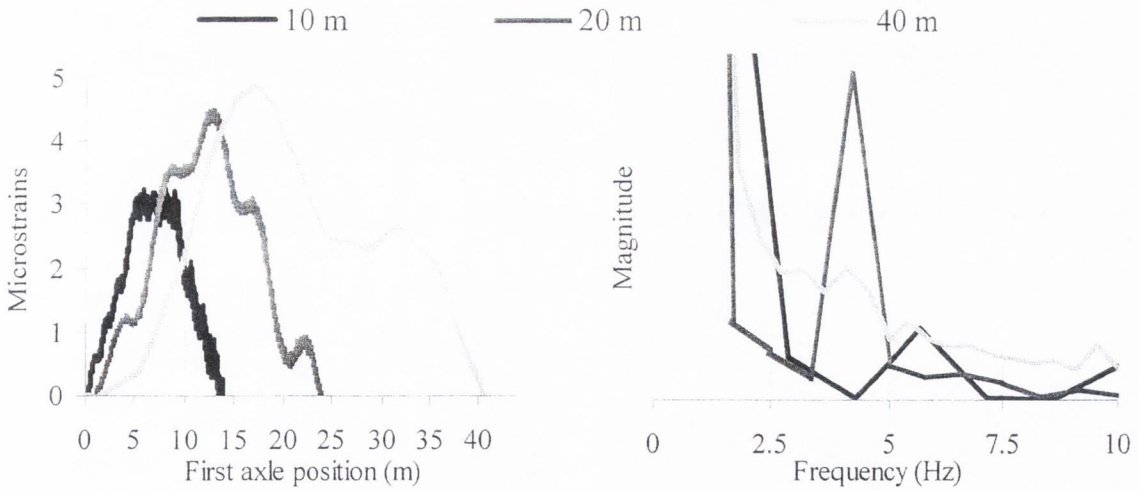

(a) Strain for different bridge lengths (b) Spectrum of the strain signal

Figure 5.12 - Influence of bridge length on strain measurements at midspan

It can be seen how the influence of bridge dynamics is very small on the 10 m bridge and static axle weights could be obtained accurately. In the 20 m bridge, there is significant dynamics, but its safe removal might be possible. In the 40 m bridge, the vehicle mass acts

on the bridge response as a whole, statics and dynamics are mixed at very low frequencies and their separation might involve the loss of some static component.

5.5.2 Effect of Truck Parameters

Applied dynamic axle forces tend to get higher with increasing speed. When the vehicle is on the bridge, the behaviour of the truck changes due to the bridge deflection. Figures 5.13(a) and (b) represent the force-position history for the front axle prior to and on the bridge respectively. It does not appear to be a dominant frequency due to the road roughness, but the amplitude of the oscillations is slightly bigger on the bridge.

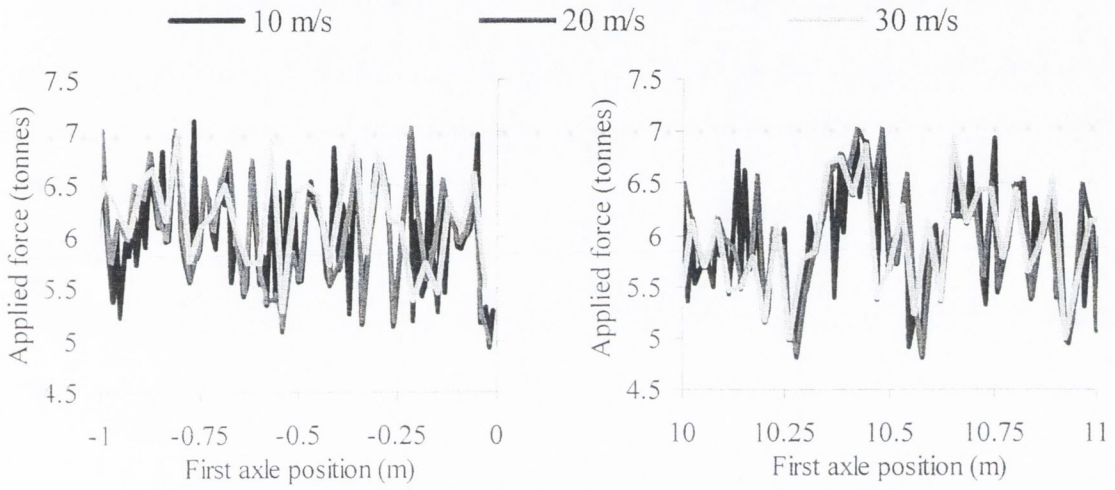

(a) Dynamic load prior to the bridge (b) Dynamic load on the bridge

Figure 5.13 - Influence of speed on applied axle forces

Bridge dynamic response increases with speed up to 20 m/s as shown in Figure 5.14(a). The spectrum of the total strain response reveals the influence of the first natural frequency of the bridge, 4.2 Hz, at 20 m/s (Figure 5.14(b)).

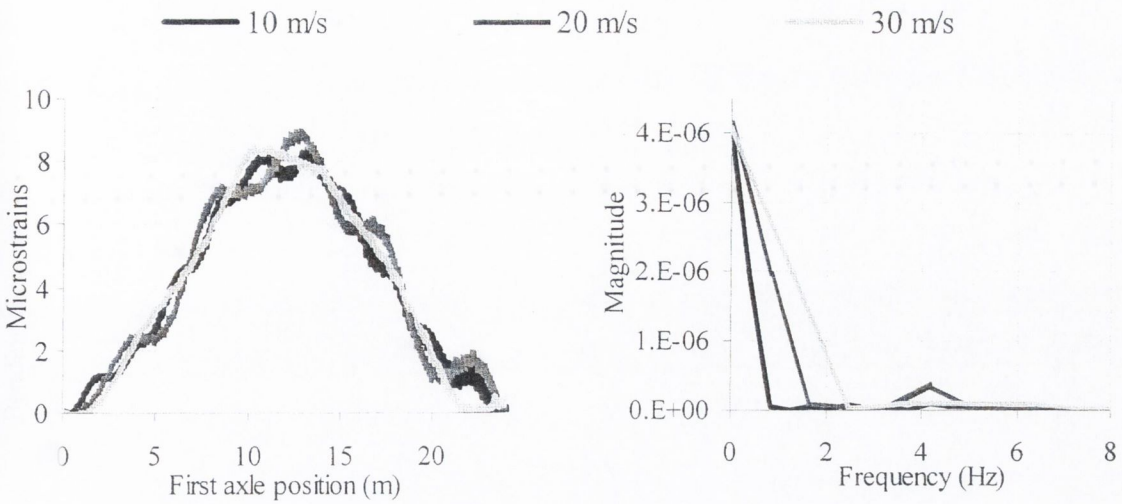

(a) Strain measurements (b) Spectrum of the strain signal

Figure 5.14 - Influence of speed on bridge response

There are a wide variety of truck mechanical characteristics that can cause different bridge responses. A 10 m short span bridge, mass 12×10^3 kg/m, flexural rigidity 2.7×10^9 Nm^2, first natural frequency of the bridge in flexure 7.45 Hz and critical damping 5% is used for testing. The road conditions are considered 'very good' ($a = 4\text{x}10^{-6}$). An increase/decrease in pitching inertia by 20% around the reference values did not induce significant changes in the bridge response. When suspension damping is increased by 20%, bridge response is slightly smaller. Truck frequencies change when masses on the vehicle change. Hence, higher dynamic amplification might result from lighter trucks depending on the frequency matching with the bridge.

In the case of Figure 5.15(a), the bridge response is approximately proportional to the change in mass and there is no coupling. Figure 5.15(b) represents the bending response due to an increase/decrease of 20% around the reference value for tyre stiffness. An increase in tyre stiffness causes a higher response: This can be due to a very low frequency that does not have enough time to go through a full cycle along the bridge or to the interaction of axle hop and bridge frequencies.

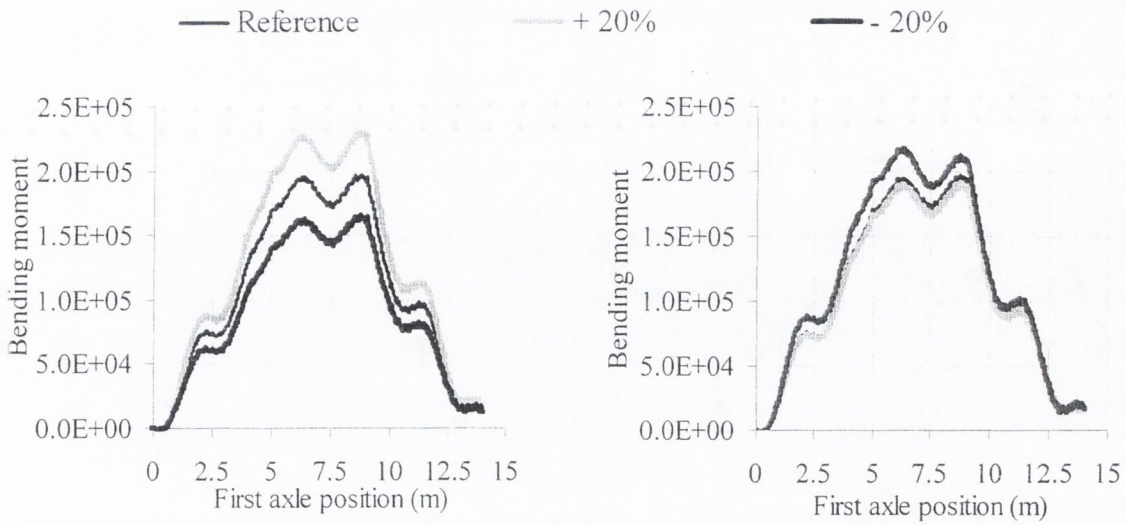

(a) Body mass (b) Tyre stiffness

Figure 5.15 – Effect of a change in body mass / tyre stiffness

In conclusion, if a truck is passed over a structure with the same masses, but different mechanical characteristics, bridge response can differ for each run. If these differences exhibit a significant deviation from the expected static response, the site might not be suitable for a high-accuracy B-WIM system.

5.6 EFFECT OF SUSPENSION TYPE AND ROAD ROUGHNESS

Through a collaboration with Green (Queen's University, Kingston, Canada), the author secured the dynamic bridge responses for heavy vehicles with steel-spring and air-spring suspensions and found the influence of suspension type on Bridge WIM accuracy. The bridge and truck are modelled separately and combined in an iterative procedure. The method involves convolution of the vehicle loads with modal responses of the bridge and the convolution integral is solved by transformation to the frequency domain using the fast Fourier transform. The method is then extended by an iterative procedure to include dynamic interaction between the bridge and an arbitrary mathematical model of a vehicle. Green & Cebon (1994) illustrate the effectiveness of this calculation method, the convergence of the iterative procedure and the good agreement with experimental data.

The vehicle models developed by Green et al (1995) are a steel sprung four-axle articulated vehicle validated experimentally, and a similar vehicle fitted with air suspensions and

of each of these two vehicles. The four-axle articulated vehicle has 11 degrees of freedom as shown in Figure 5.16. In this Figure, elements A (non-linear behaviour), B (Coulomb friction) and C (linear spring/damper) represent springs in Figures 5.4(c), (b) and (a) respectively.

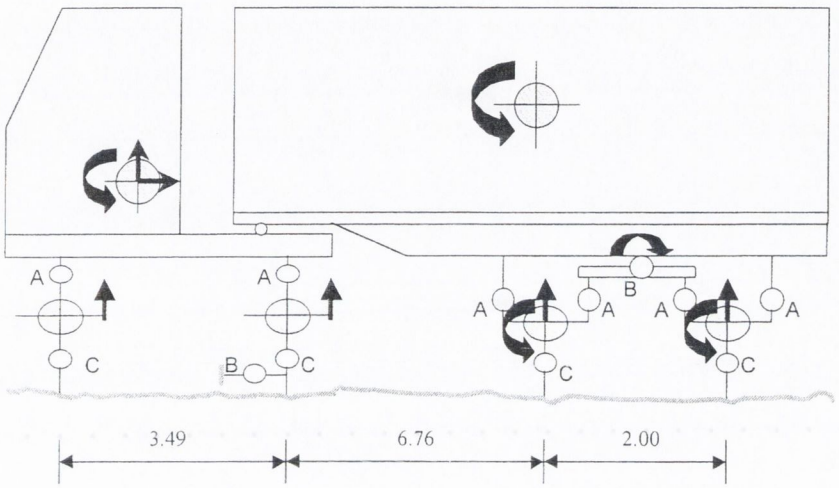

Figure 5.16 – Two dimensional tractor and trailer vehicle model with steel-spring suspensions (11 degrees of freedom)

For the vehicle with air suspension, models of air springs with parallel viscous dampers replace the steel-spring elements on the drive axle and the two trailer axles. The suspension on the steer axle is the same for both vehicle models. Two surface profiles, three different speeds (55, 70 and 85 km/h) and three different loading conditions are chosen for the simulations.

Figures 5.17 and 5.18 represent the applied dynamic forces over same length of smooth and rough road profile respectively.

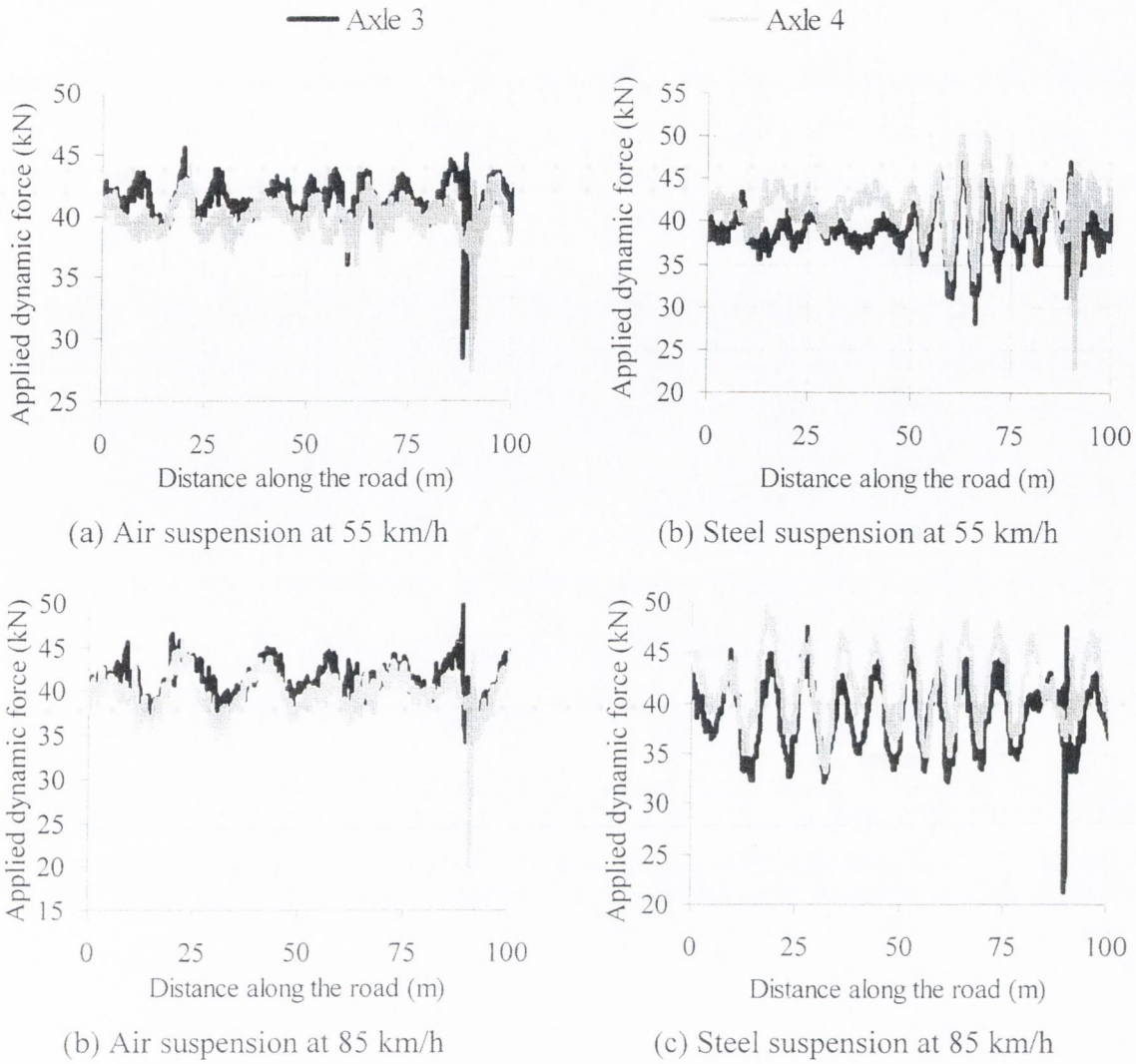

Figure 5.17 – Applied forces by air- and steel-sprung fully laden tandem (smooth profile)

It can be seen how these forces increase with speed and road roughness. Steel suspensions are clearly more sensitive to these changes, except for a singularity localised at about 90 m at the speed of 85 km/h. Generally, the dynamic response is lower for the air suspension than for the steel suspension vehicle as the air suspensions are better damped and the vehicle dampers absorb energy from the bridge vibrations. The load sharing between axles within the tandem of the air-sprung vehicle is also less than in the steel-sprung vehicle.

The amplitude of the applied dynamic wheels is higher for worse road conditions as shown in Figure 5.18. Thus, bridge response will increase with road roughness. Therefore, body bounce modes of vehicle vibration are excited by longer wavelength variations in road profile whereas axle hop are excited by short wavelength defects such as pot-holes, road

debris, a rough repair or a mis-aligned joint in a bridge, more likely to occur in a road in poor conditions.

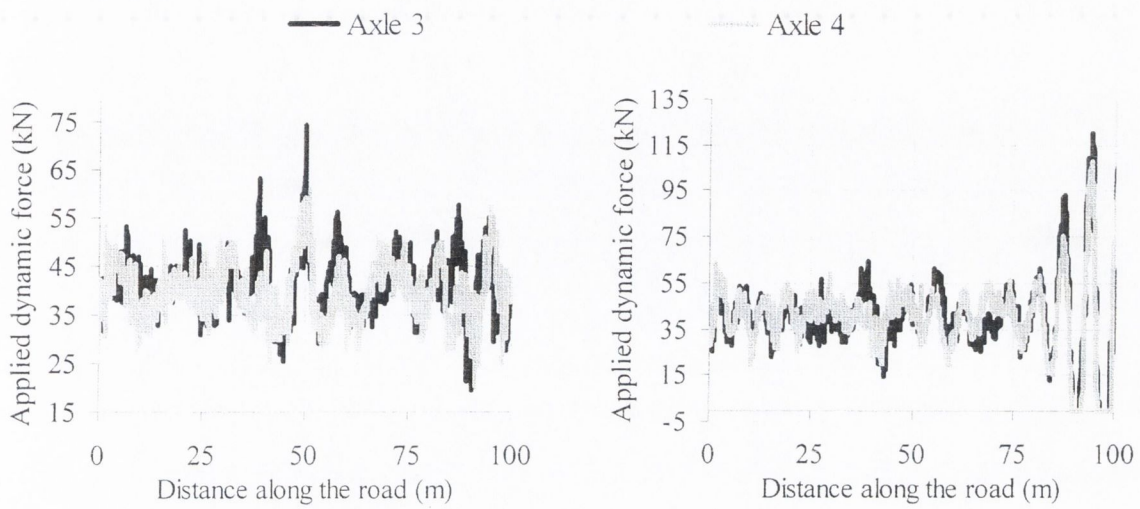

(a) Air suspension at 55 km/h

(b) Steel suspension at 55 km/h

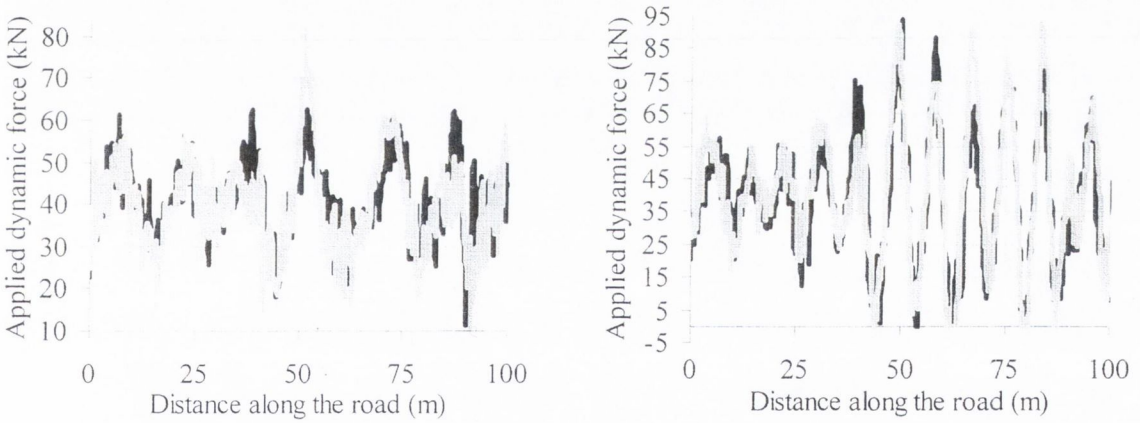

(b) Air suspension at 85 km/h

(c) Steel suspension at 85 km/h

Figure 5.18 – Applied forces by air- and steel-sprung fully laden tandem (rough profile)

The air-sprung vehicle has lower natural frequencies than the steel-sprung vehicle. Figures 5.19 and 5.20 shows the Discrete Fourier Transform for the second axle travelling at 70 km/h in unloaded and fully laden conditions respectively. There is not a dominant frequency for the air suspension vehicle in Figure 5.19(a) due to the heavy damping. This damping will minimise dynamic response even in the case of a bridge with low natural frequency and likely frequency matching. From Figure 5.19(b), the dynamic component of the truck at 3.38 Hz is very significant for the steel suspension.

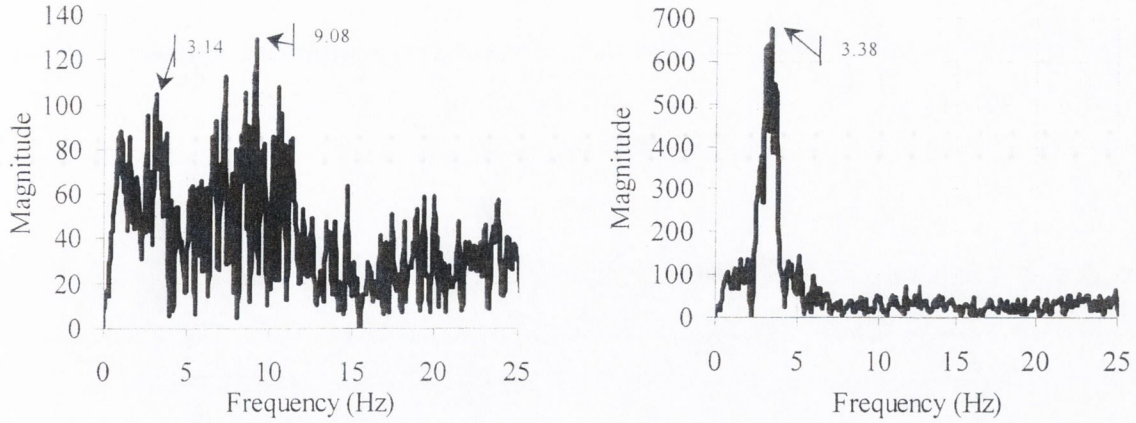

(a) Air suspension (b) Steel suspension

Figure 5.19 – Spectra analysis of 2rd axle in unloaded vehicle (70 km/h)

The increase of mass for the laden vehicle of Figure 5.20 decreases the value of the main natural frequencies. Therefore, the influence of air suspension damping is less important in heavier vehicles. Even so, the applied dynamic load by an air-suspension vehicle is still small.

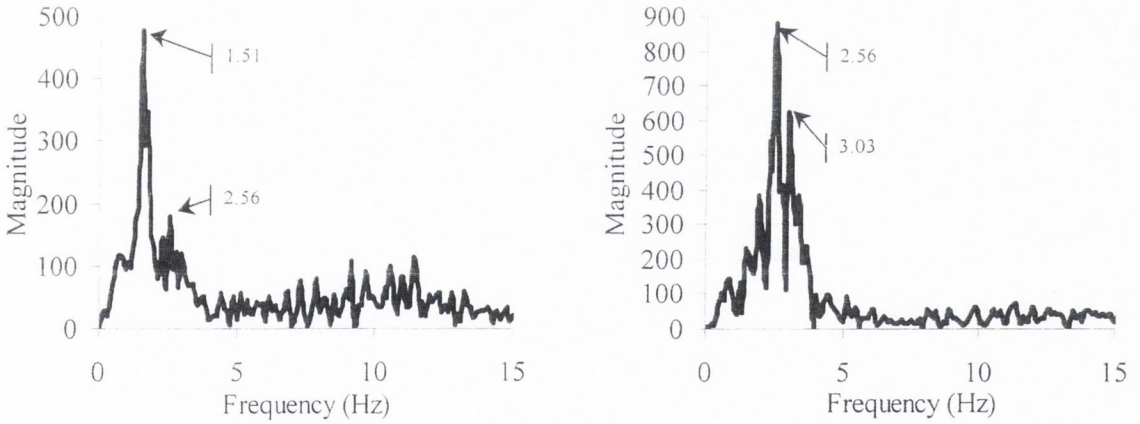

(a) Air suspension (b) Steel suspension

Figure 5.20 – Spectra analysis of 2rd axle in fully laden vehicle (70 km/h)

The Discrete Fourier Transforms of the force applied by all axles in the tractor and trailer for the fully laden vehicle are presented in Figure 5.21. Tractor and trailer bounce takes place at 1.51 Hz in the air suspension vehicle and 2.56 Hz in the steel suspension vehicle.

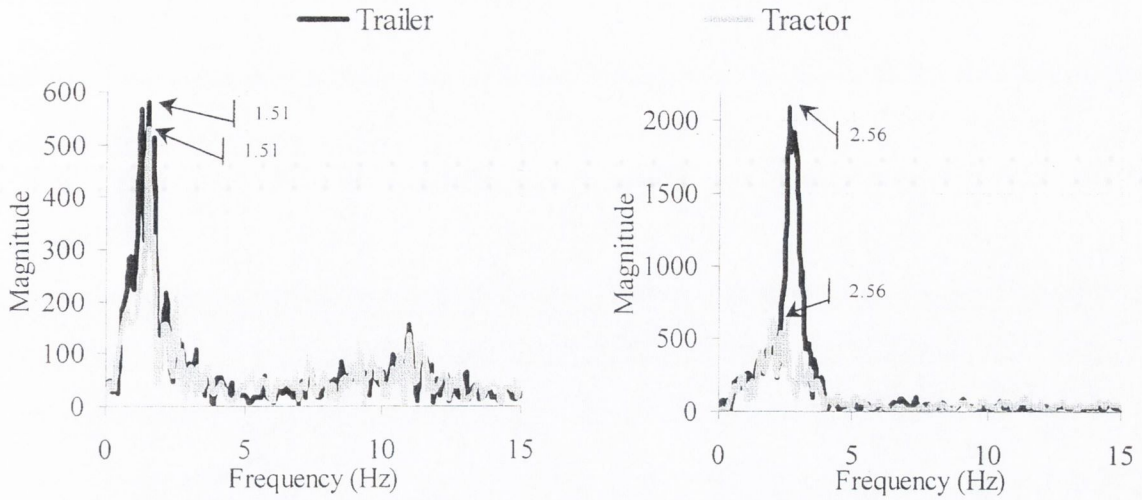

(a) Air suspension (b) Steel suspension

Figure 5.21 – Spectra of sum of axle forces for fully laden vehicle (70 km/h)

The Discrete Fourier Transforms of the difference in axle forces for the tractor and trailer are presented in Figure 5.22. A tractor and trailer pitch of 2.56 Hz is displayed by the air suspension vehicle, while a tractor and trailer pitch of 3.03 and 3.14 Hz respectively the steel-sprung vehicle.

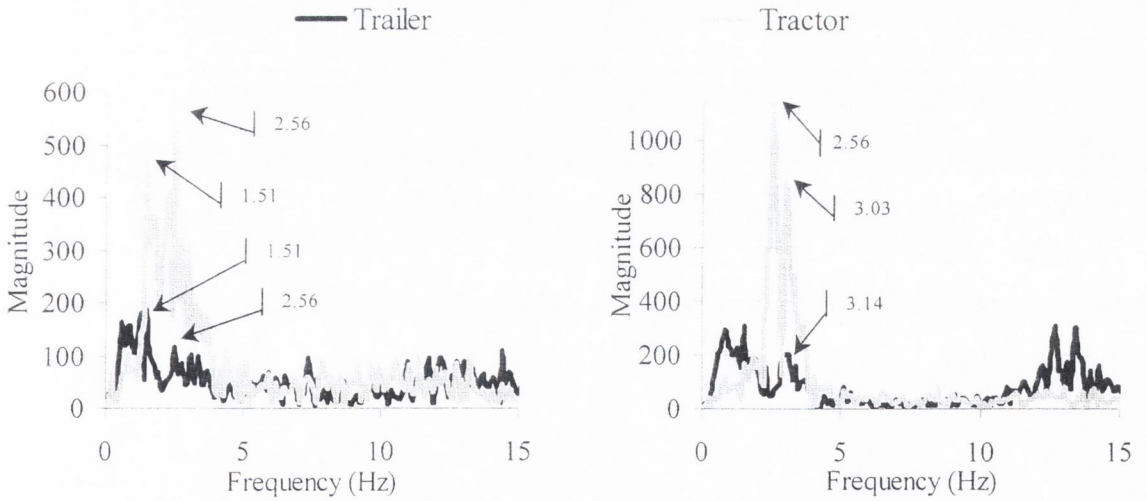

(a) Air suspension (b) Steel suspension

Figure 5.22 – Spectra of difference of axle forces for fully laden vehicle (70 km/h)

The strain response at the bridge midspan for a fully laden vehicle on a smooth profile is represented in Figure 5.23. As expected, steel suspension causes higher dynamic oscillations on strain than air-suspension vehicles.

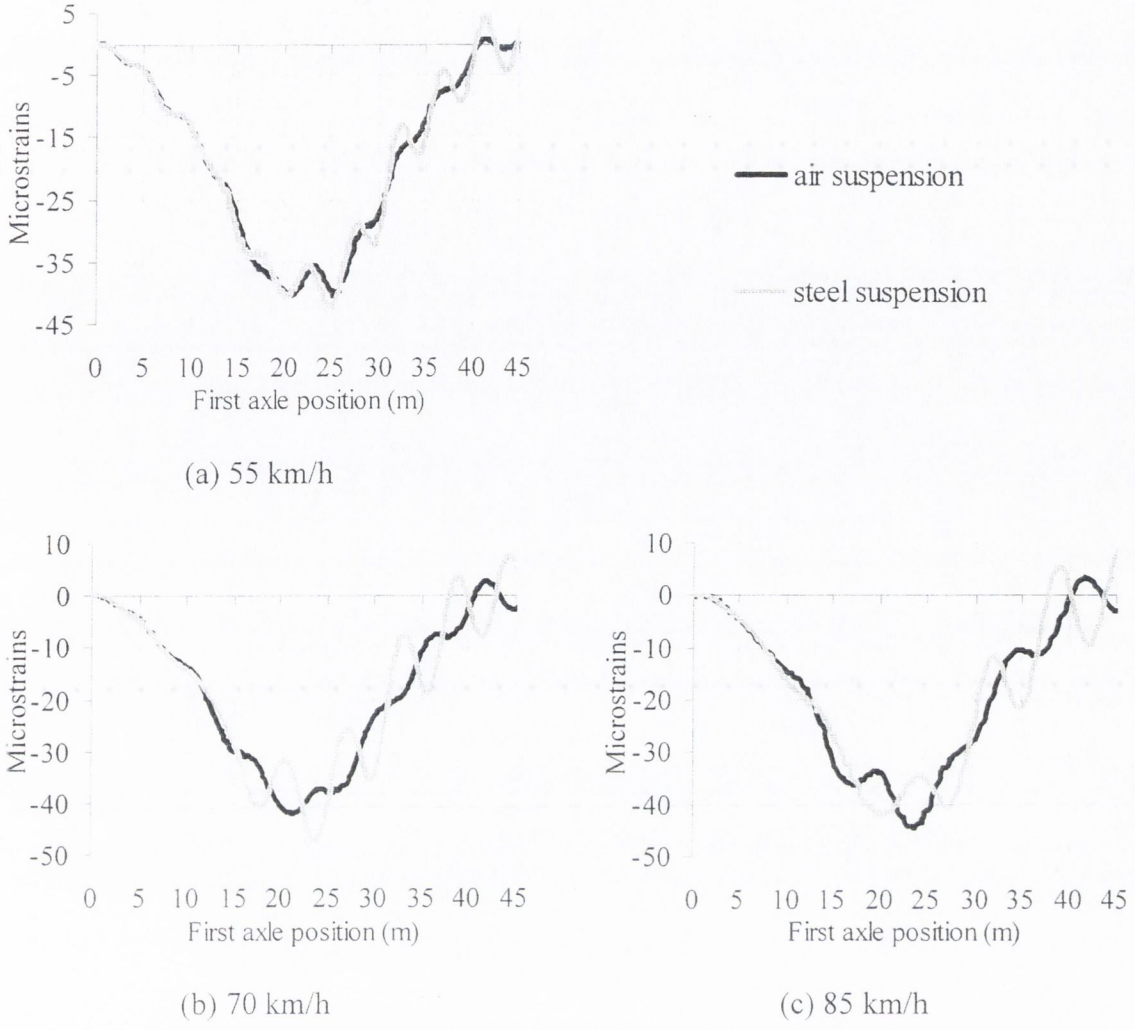

Figure 5.23 - Effect of speed on a smooth profile

Figure 5.24 shows the bridge response at midspan for the fully laden vehicle on a rough profile. The maximum dynamic response takes place at 70 km/h for the steel-sprung vehicle and 85 km/h for the air-sprung vehicle. It can be seen that the air-suspended vehicle causes significantly lower dynamic bridge response than the steel-spring suspended vehicle and it is less sensitive to a change in speed. In comparison to the smooth profile, the dynamic response due to the steel-sprung vehicle increases by over 100%. These high dynamics suggest the occurrence of frequency matching between the steel-sprung vehicle and the bridge. Consequently, Bridge WIM will tend to be less accurate in the cases of steel-spring suspensions, rough road profile, for this bridge, for vehicle speeds near 70 km/h.

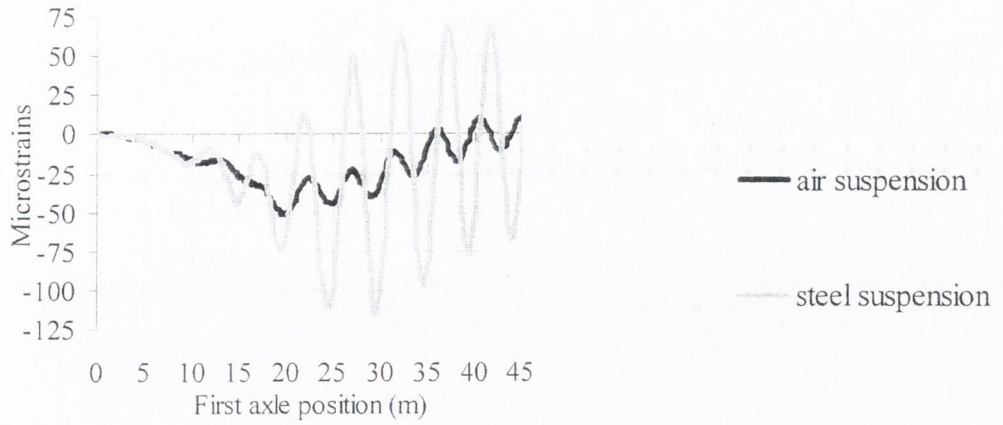

(a) 55 km/h

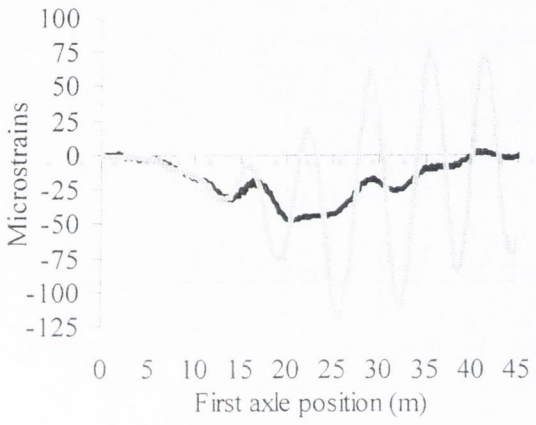

(b) 70 km/h

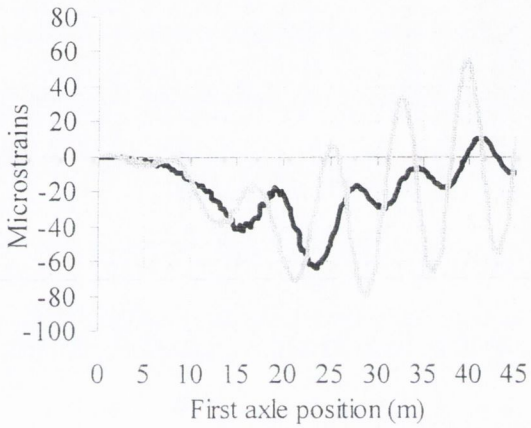

(c) 85 km/h

Figure 5.24 - Effect of speed on a rough profile

6

SIMULATIONS USING FINITE ELEMENT ANALYSIS

6.1 INTRODUCTION

Chapter 5 introduced the main features that govern the bridge behaviour when it is traversed by a truck. However, only a few degrees of freedom were considered and the influence of three-dimensional effects was neglected. In order to cover for more realistic models, this chapter describes the interaction of complex truck and bridge structures through a finite element technique. The structures are subdivided into a finite number of simple elements (such as plates, beams, bars, springs, masses, etc.), and the complex differential equations are then solved for the simple elements. Assemblage of the elements into a global matrix transforms the problem from a differential equations formulation over a continuum to a linear algebra problem.

Vehicles and bridges have been modelled with the general-purpose finite element analysis package MSC/NASTRAN for Windows[18] (1999), which provides the capability for performing statics, normal modes and transient dynamic response (Cifuentes 1989a). NASTRAN (**NA**SA **Str**uctural **An**alysis) initiated the implementation of the finite element method on computers under a project by the National Aeronautics and Space Administration (NASA) in the 1960's (Schaeffer 1977).

The author has developed a C++ program that derives the interaction forces for any arbitrary planar or spatial bridge and vehicle finite element models. This code incorporates the road surface profile and it is implemented using a set of auxiliary functions to enforce the compatibility conditions at the bridge/vehicle interface. The speed of the vehicles, their initial position, path on the bridge and road irregularities can be easily modified in the program input. Simultaneous traffic events running in the same or different lanes, in the same or opposite directions and singularities such as a bump at any location can also be specified. Different bridge/truck models and results of simulations are introduced at the end of this chapter. This data will be used for testing B-WIM algorithms in Chapter 9.

6.2 TECHNIQUE FOR DETERMINATION OF BRIDGE-VEHICLE DYNAMIC INTERACTION

The load imposed by a truck crossing a bridge is an enforced motion transient problem. MSC/NASTRAN has the ability to perform enforced motion analysis by placing extremely large masses or inertias to obtain the desired motion at selected locations (MSC/NASTRAN 1997d). Extremely large forces are applied to the large masses to cause the desired motion histories. However, this method has traditionally been prone to numerical error if the large masses are too large or too small (Flanigan 1994) and it is inadequate for the bridge-vehicle interaction problem. Accordingly, the author uses an alterrative approach based on a Lagrange technique that eliminates the need for large masses (Cifuentes 1989b, Baumgärtner 1999). The Lagrange Multiplier formulation allows for the representation of the compatibility condition at the bridge/vehicle interface through a set of auxiliary functions. Accordingly, software has been developed to generate an entry into the assembled stiffness matrix of the vehicle-bridge system. This entry allows for the definition of the forces acting on the bridge due to the moving wheels. A compatibility condition between the vertical displacement of the wheel and the bridge at the contact point is also established.

6.2.1 Equations of Motion and Compatibility

Cifuentes (1989b) gives an introduction to the problem of solving for the motion of a single circular mass moving at constant speed on a one-dimensional bridge model. This section extends the solution to allow for the presence of multiple masses travelling in given paths at different speeds. If the bridge structure along a mass path is divided into (N-1) finite elements, coordinates $x_1, x_2, \ldots x_N$ are adopted for the N nodes. The variables defining the behaviour of the bridge are:

$z(x,t)$: vertical deflection of the bridge in position x at time t,

$z_i = z_i(t)$: deflection of node i at time t,

$\theta_i = \theta_i(t)$: rotation of node i at time t,

$\ddot{z}_i = \ddot{z}_i(t)$: acceleration of vertical displacement in node i at time t,

$\ddot{\theta}_i = \ddot{\theta}_i(t)$: acceleration of rotation in node i at time t.

The one-dimensional problem for a single mass is represented in Figure 6.1.

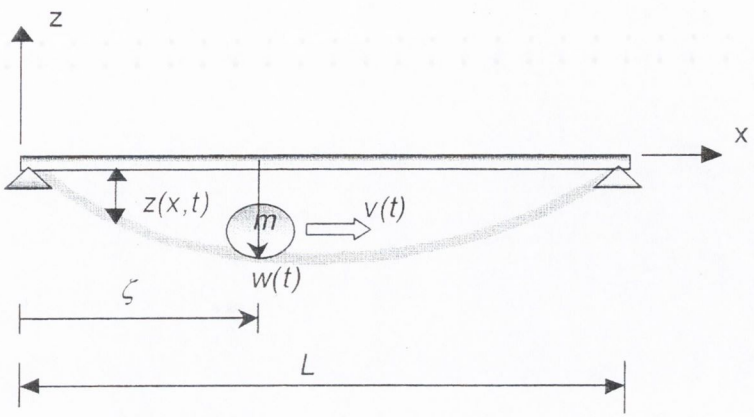

Figure 6.1 – Structure traversed by a mass m with velocity $v(t)$

The variables defining the behaviour of a series of moving masses j (one per wheel or one per axle in a 3D or 2D problem respectively) are:

$v_j = v_j(t)$: time-dependent velocity of the vehicle (defined by the user). If there are different vehicles, v_j might be different for each vehicle.

m_j : mass of wheel j (defined by the user),

$w_j = w_j(t) = z(\zeta_j, t)$: vertical displacement of wheel j measured with respect to the horizontal axis (the bridge geometry is assumed to be in a horizontal plane before deformation),

$R_j = R_j(t)$: Interaction force at contact point of wheel j,

$\zeta_j = \zeta_j(t)$: Distance x travelled on the bridge by moving wheel j at time t.

The variable ζ_j denoting position of mass j on the bridge at time t can be defined as a function of the velocity input $v_j(t)$ as:

$$\zeta_j = \int_{t_j} v_j(t)dt = \sum_{t=t_j}^{t} v_j(t)\Delta t \qquad 0 \le \zeta_j \le L \tag{6.1}$$

where time t_j is the instant at which mass j enters the bridge and L is the bridge length.

The equation of motion of the bridge finite element model can be written as:

$$\begin{bmatrix} m_{11} & m_{12} & . & . & . \\ m_{21} & m_{22} & . & . & . \\ . & . & . & . & . \\ . & . & . & m_{2N-1,2N-1} & m_{2N-1,2N} \\ . & . & . & m_{2N,2N-1} & m_{2N,2N} \end{bmatrix} \begin{Bmatrix} \ddot{z}_1 \\ \ddot{\theta}_1 \\ . \\ \ddot{z}_N \\ \ddot{\theta}_N \end{Bmatrix} + \begin{bmatrix} k_{11} & k_{12} & . & . & . \\ k_{21} & k_{22} & . & . & . \\ . & . & . & . & . \\ . & . & . & k_{2N-1,2N-1} & k_{2N-1,2N} \\ . & . & . & k_{2N,2N-1} & k_{2N,2N} \end{bmatrix} \begin{Bmatrix} z_1 \\ \theta_1 \\ . \\ z_N \\ \theta_N \end{Bmatrix} = \begin{Bmatrix} f_1 \\ M_1 \\ . \\ f_N \\ M_N \end{Bmatrix} \tag{6.2}$$

where *[m]* is the mass matrix of the finite element model and *[k]* is the stiffness matrix, representing the dynamic characteristics of the bridge model. *{z}* is a vector containing the displacements of the nodes and $\{\ddot{z}\}$ their acceleration at time *t*. Vector *{f}* represents the force $f_i(t)$ and moment $M_i(t)$ acting on node *i* at a certain time due to the moving loads.

A compatibility condition between the vertical displacement $w_j(t)$ of each mass *j* and the bridge at the contact point must be established at any time *t*. For this purpose a set of auxiliary functions $A_{ij}(t)$ and $B_{ij}(t)$ are defined for every mass *j*, and the compatibility condition at the contact point of mass *j* is formulated as (Cifuentes 1989b):

$$w_j(t) = z(\zeta_j, t) = \sum_{i=1}^{N} A_{ij}(t) z_i(t) + \sum_{i=1}^{N} B_{ij}(t) \theta_i(t) \qquad ; \quad j=1,2, \ldots p \tag{6.3}$$

where $z_i(t)$ and $\theta_i(t)$ are the displacement and rotation at each node *i*, *N* the total number of bridge nodes, *p* total number of moving loads, and $A_{ij}(t)$ and $B_{ij}(t)$ auxiliary functions for load *j*. $A_{ij}(t)$ and $B_{ij}(t)$ can adopt different values in each node *i* at each instant *t*. Equations 6.4 and 6.5 define these functions:

$$A_{ij}(t) = \begin{cases} 1 - 3\left[\dfrac{(t - t_{1,j} - t_{i,j})}{(t_{i+1,j} - t_{i,j})}\right]^2 + 2\left[\dfrac{(t - t_{1,j} - t_{i,j})}{(t_{i+1,j} - t_{i,j})}\right]^3 & \text{for } t_{i,j} \le t \le t_{i+1,j} \\ 1 - 3\left[\dfrac{(t_{i,j} - (t - t_{1,j}))}{(t_{i,j} - t_{i-1,j})}\right]^2 + 2\left[\dfrac{(t_{i,j} - (t - t_{1,j}))}{(t_{i,j} - t_{i-1,j})}\right]^3 & \text{for } t_{i-1,j} \le t \le t_{i,j} \\ 0 & \text{otherwise} \end{cases}$$

$$i=1,2,\ldots N; \quad j=1,2\ldots p \tag{6.4}$$

$$B_{i,j}(t)=\begin{cases}\left[-\dfrac{((t-t_{1,j})-t_{i,j})}{2(t_{i+1,j}-t_{i,j})}+\dfrac{((t-t_{1,j})-t_{i,j})^2}{2(t_{i+1,j}-t_{i,j})^2}\right][x_{i+1}-x_i] & \text{for } t_{i,j}\le t\le t_{i+1,j}\\ \left[-\dfrac{(t_{i,j}-(t-t_{1,j}))}{2(t_{i,j}-t_{i-1,j})}+\dfrac{(t_{i,j}-(t-t_{1,j}))^2}{2(t_{i,j}-t_{i-1,j})^2}\right][x_i-x_{i-1}] & \text{for } t_{i-1,j}\le t\le t_{i,j}\\ 0 & \text{otherwise}\end{cases}$$

$$i=1,2,\ldots N;\quad j=1,2\ldots p \qquad (6.5)$$

where t_{ij} is the time that moving mass j takes between the origin and the bridge node i. t_{1j} is the travelling time of mass j from the original position to the first node at the bridge.

The shape of these auxiliary functions is shown in Figure 6.2. They have zero value out of the interval between adjacent nodes.

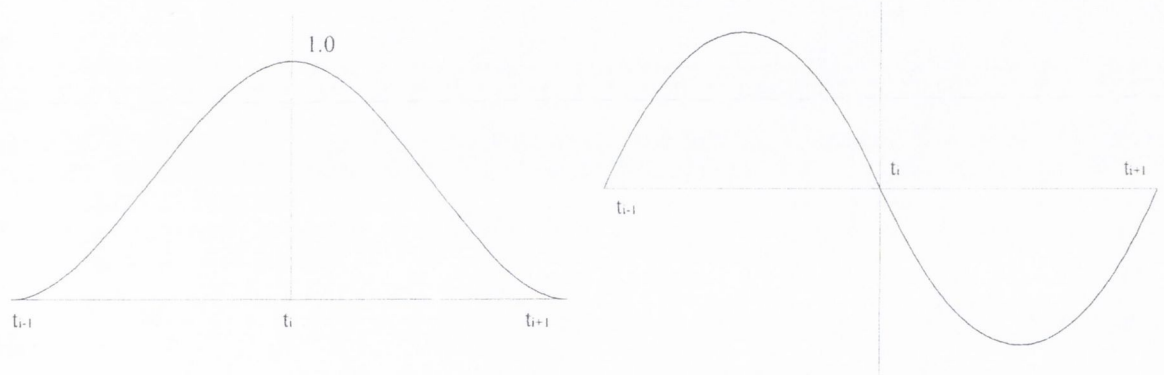

(a) $A_i(t)$ (b) $B_i(t)$

Figure 6.2 – Auxiliary Functions

The temporal variable t_{ij} can be determined numerically from the knowledge of velocity $v_j(t)$ and the geometry of the finite element model such that:

$$\sum_{t=0}^{t_{ij}} v_j(t)\Delta t = x_i + x_j + x_0 \qquad (6.6)$$

where $v_j(t)$ is the velocity function (same function for all masses j in a vehicle), x_i the coordinate of the node number i related to the bridge start, x_j the longitudinal spacing between the contact point corresponding to the first mass and the contact point of the j^{th} mass and x_0 is the length of the bridge approach. So, $A_{ij}(t)$ and $B_{ij}(t)$ are completely defined

once $v_j(t)$, approach length, axle spacings and the coordinates of the bridge nodes are known. Each axle takes a different time to reach the same node and each wheel of the same axle follows a different path on the bridge. Thus, auxiliary functions change at each mass j and time t.

According to Cifuentes (1989b), the interaction force $R_j(t)$ between a moving circular mass m_j and the bridge structure contains the following terms:

- Inertial force, due to vertical motion of the mass = $-m_j\left[\frac{\partial^2 z(x,t)}{\partial t^2}\right]_{(\xi_j,t)}$,
- Coriolis force, due to relative motion between the bridge and the load = $-2m_j v_j\left[\frac{\partial^2 z(x,t)}{\partial x \partial t}\right]_{(\xi_j,t)}$,
- Centripetal force, due to circular motion following the deformed shape of the bridge, acting towards the centre of the mass = $-m_j v_j^2\left[\frac{\partial^2 z(x,t)}{\partial x^2}\right]_{(\xi_j,t)}$,
- Weight, due to gravity force = $-m_j g$.

Hence the interaction force can be defined as:

$$R_j = -m_j\{\ddot{z} + 2v_j\dot{z}' + v_j^2 z'' + g\}\delta(x-\xi_j) \tag{6.7}$$

where $\ddot{z} = \left[\frac{\partial^2 z(x,t)}{\partial t^2}\right]_{(\xi_j,t)}$, $\dot{z}' = \left[\frac{\partial^2 z(x,t)}{\partial x \partial t}\right]_{(\xi_j,t)}$, $z'' = \left[\frac{\partial^2 z(x,t)}{\partial x^2}\right]_{(\xi_j,t)}$ and δ is the Dirac function. If $x \neq \zeta_j, R_j = 0$, where ζ_j is the distance travelled by the mass j as defined in Equation 6.1.

By combination of Equations 6.3 and 6.7, this interaction force R_j between the bridge and the j^{th} mass can also be expressed as:

$$R_j = -m_j\ddot{w}_j - m_j g - m_j[2v_j\dot{z}' + v_j^2 z''] \tag{6.8}$$

Aid using the Lagrange multiplier functions:

$$R_j = -m_j \ddot{w}_j - m_j g - m_j \sum_i A_i [2 v_{ij} \dot{z}_i' + v_{ij}^2 z_i'']$$ (6.9)

where $v_{ij} = v_j(t_i)$, that is, velocity of mass m_j when it reaches node i.

By re-ordering terms:

$$m_j \ddot{w}_j + R_j = -m_j g - m_j \sum_i A_i [2 v_{ij} \dot{z}_i' + v_{ij}^2 z_i'']$$ (6.10)

The roughness of the pavement surface $r(x)$ can be imported into Equation (6.10) by taking into account that vertical displacement of the mass m_j will be equal to the vertical deformation of the beam minus the depth of the irregularities at the same location. This gives:

$$m_j \ddot{w} + R_j = -m_j g - m_j \sum_i A_i [2 v_{ij} \dot{z}_i' + v_{ij}^2 z_i'' + v_{ij}^2 r_i'']$$ (6.11)

An initial deflected shape can be introduced in the same way. Therefore, the force $f_{ij}(t)$ and the moment $M_{ij}(t)$ due to a mass j, acting on bridge node i at time t can be expressed using the auxiliary functions as (Cifuentes 1989b):

$$f_{ij}(t) = A_{ij}(t) R_j$$ (6.12)

and

$$M_{ij}(t) = B_{ij}(t) R_j$$ (6.13)

Equation 6.14 defines the total force $f_i(t)$ and moment $M_i(t)$ acting on a bridge node i at time t due to p different masses:

$$\begin{Bmatrix} f_1 \\ M_1 \\ f_2 \\ M_2 \\ . \\ . \\ f_N \\ M_N \end{Bmatrix} = \begin{Bmatrix} A_{11} \\ B_{11} \\ A_{21} \\ B_{21} \\ . \\ . \\ A_{N1} \\ B_{N1} \end{Bmatrix} R_1 + \ldots + \begin{Bmatrix} A_{1p} \\ B_{1p} \\ A_{2p} \\ B_{2p} \\ . \\ . \\ A_{Np} \\ B_{Np} \end{Bmatrix} R_p \tag{6.14}$$

Finally, the equations of motion of the complete moving load plus finite element model are given by:

$$\begin{bmatrix} m_{11}\frac{\partial^2}{\partial t}+k_{11} & m_{12}\frac{\partial^2}{\partial t}+k_{12} & \ldots & \ldots & 0 & 0 & 0 & \ldots & 0 & 0 \\ m_{21}\frac{\partial^2}{\partial t}+k_{21} & m_{22}\frac{\partial^2}{\partial t}+k_{22} & \ldots & \ldots & 0 & 0 & 0 & \ldots & 0 & 0 \\ \ldots & \ldots & \ldots & \ldots & \ldots & \ldots & \ldots & \ldots & \ldots & \ldots \\ \ldots & \ldots & \ldots & m_{2N-1,2N-1}\frac{\partial^2}{\partial t}+k_{2N-1,2N-1} & m_{2N-1,2N}\frac{\partial^2}{\partial t}+k_{2N-1,2N} & 0 & 0 & \ldots & 0 & 0 \\ \ldots & \ldots & \ldots & m_{2N,2N-1}\frac{\partial^2}{\partial t}+k_{2N,2N-1} & m_{2N,2N}\frac{\partial^2}{\partial t}+k_{2N,2N} & 0 & 0 & \ldots & 0 & 0 \\ 0 & 0 & \ldots & 0 & 0 & m_1\frac{\partial^2}{\partial t} & 1 & \ldots & 0 & 0 \\ 0 & 0 & \ldots & 0 & 0 & 1 & 0 & \ldots & 0 & 0 \\ \ldots & \ldots & \ldots & \ldots & \ldots & \ldots & \ldots & \ldots & \ldots & \ldots \\ 0 & 0 & \ldots & 0 & 0 & 0 & 0 & \ldots & m_p\frac{\partial^2}{\partial t} & 1 \\ 0 & 0 & \ldots & 0 & 0 & 0 & 0 & \ldots & 1 & 0 \end{bmatrix} \begin{Bmatrix} z_1 \\ \theta_1 \\ \ldots \\ z_N \\ \theta_N \\ w_1 \\ R_1 \\ \ldots \\ w_p \\ R_p \end{Bmatrix} = \begin{Bmatrix} \sum_{j=1}^{r} A_{1j}R_j \\ \sum_{j=1}^{r} B_{1j}R_j \\ \ldots \\ \sum_{j=1}^{r} A_{Nj}R_j \\ \sum_{j=1}^{r} B_{Nj}R_j \\ -m_1 g + c_1 \\ \sum_{i=1}^{N}[A_{i1}z_i + B_{i1}\theta_i] \\ \ldots \\ -m_p g + c_p \\ \sum_{i=1}^{N}[A_{ip}z_i + B_{ip}\theta_i] \end{Bmatrix} \tag{6.15}$$

where the last $(2p)$ rows represent the equations of motion of each moving mass and the compatibility condition between deflections of the moving masses and the bridge. In these rows of the global load vector, the parameter c_j is given by:

$$c_j = -\sum_{i=1}^{N}\frac{2v_{ij}m_j}{x_i - x_{i-1}}\dot{z}_{ij}A_{ij} + \sum_{i=1}^{N}\frac{2v_{ij}m_j}{x_i - x_{i-1}}\dot{z}_{i-1j}A_{ij} + \sum_{i=1}^{N}\frac{v_{ij}{}^2 m_j}{x_i - x_{i-1}}\theta_{ij}A_{ij} + \sum_{i=1}^{N}\frac{v_{ij}{}^2 m_j}{x_i - x_{i-1}}\theta_{i-1j}A_{ij} \qquad j=1,\ldots,p \tag{6.16}$$

The following finite differences approximations might be necessary to calculate c_j:

$$\dot{z}_i' = \frac{\dot{z}_i - \dot{z}_{i-1}}{x_i - x_{i-1}} \tag{6.17}$$

$$z_i'' = \frac{-\theta_i + \theta_{i-1}}{x_i - x_{i-1}} \tag{6.18}$$

where $z_i' = -\theta_i$.

When the simulation of a truck travelling over a bridge is implemented in the following section, this term c is ignored. Centripetal and Coriolis forces are not taken into acount as most of the vehicle mass (except wheel mass) is not under circular motion and the vehicle speeds are relatively small.

6.2.2 Derivation of NASTRAN Input Code

The program generates an entry into the assembled stiffness matrix of the vehicle-bridge system as shown in Equation 6.15. The interaction forces F_j at the contact point of each wheel j on the bridge are defined as in Equation 6.14. The global stiffness matrix and the forcing vector is adapted to NASTRAN code in this section. In order to obtain the desired results, two sections must be manipulated in NASTRAN: The Case Control and the Bulk Data Sections.

1) The Case Control Section has several basic functions:

- Selects loads and constraints.
- Requests printing, plotting and/or typing of input and output data.
- Defines the subcase structure for the analysis.

2) The Bulk Data section contains entries that specify model geometry, element connectivity, element and material properties, constraints (boundary conditions) and loads. Some entries, such as loads and constraints, are selected by an appropriate Case Control command. Entries are prepared in either fixed or free field format.

A description of the code implementation is given in the following paragraphs. An example of these entries can be found in Appendix F. The whole process involved in the simulation of a truck over a bridge when using NASTRAN will be explained in Section 6.3.

Bulk Data Section

NASTRAN capability to define scalar degrees of freedom is used to define 2 scalar points, one to represent the displacement of the moving mass, w, and another to represent the interaction force F between the bridge and the mass. These scalar points are defined with the instruction SPOINT. The *bulk.dat* file to include in the NASTRAN analysis has a format of 10 fields of 8 characters each (small field format). Details about the format can be found in MSC/NASTRAN V70.5 Quick Reference Guide (1998).

In the case of two moving masses, the data format is illustrated in Figure 6.3.

SPOINT	400000								
SPOINT	401000								
SPOINT	500000								
SPOINT	501000								

Figure 6.3 – Data format for two moving masses

where the scalar points 500000 and 501000 represent the displacements w_1 and w_2, and 400000 and 401000 are the interaction forces, F_1 and F_2, for each moving load.

NASTRAN capability to input entries to the assembled stiffness matrix of the system is used to add 2 rows and columns per mass corresponding to *(w,F)* and *(F,w)*. These lines are added with the instruction DMIG. DMIG defines direct input matrices related to grid points. The matrix is defined by a single header entry and one or more column entries. Only one header entry is required. A column entry is required for each column with nonzero elements. The header and columns of this instruction have the format illustrated in Figure 6.4. The parameters are identified in Table 6.1.

DMIG	Name	"0"	IFO	TIN	TOUT	Polar		NCOL	
DMIG	Name	GJ	CJ		G1	C1	A1	B1	
	G2	C2	A1	B2	-etc.-				

Figure 6.4 – Header and columns for DMIG entry

Table 6.1 – Parameters used for DMIG entry (see Figure 6.4)

Field	Contents
Name	Name of the matrix
IFO	Form of the matrix input. IFO = 6 (symmetric) must be specified for matrices selected by the K2GG Case Control command.
TIN	Type of matrix being input (Integer): 1 = Real, single precision (One field is used per element), 2 = Real, double precision (One field is used per element), ...
TOUT	Type of matrix that will be created (Integer): 0 = Set by precision system cell (Default), 1 = Real, single precision, 2 = Real, double precision, ...
Polar	Input format of Ai, Bi. (Integer = blank or 0 indicates real, imaginary format; Integer >0 indicates amplitude, phase format.)
NCOL	Number of columns in a rectangular matrix. Used only for IFO=9. (Integer > 0)
GJ	Grid point identification number for column index. (Integer > 0)
CJ	Component number for grid point GJ (0<Integer<=6).
Gi	Grid point identification number for row index. (Integer > 0)
Ci	Component number for Gi for a grid point. (0<CJ<=6)
Ai, Bi	Real and Imaginary parts of a matrix element. If the matrix is real (TIN = 1 or 2), then Bi must be blank. (Real)

Matrices defined with this entry may be used in dynamics by selection in the Case Control with *K2GG = name*. This matrix is added to the structural matrix before constraints are applied. Each non-null column is started with a GJ, CJ pair. The entries for each row of that column follows. Only nonzero terms need be entered.

A matrix called *STIF* is defined in the line illustrated in Figure 6.5.

DMIG	STIF	0	6	1	1				

Figure 6.5 – Definition of STIF

In the case of two moving masses, the additional values are illustrated in Figure 6.6:

DMIG	STIF	400000			400000		0		
DMIG	STIF	401000			401000		0		
DMIG	STIF	500000			500000		1		
DMIG	STIF	501000			501000		1		

(a) Main diagonal values

DMIG	STIF	300000	3		400000		1		
DMIG	STIF	301000	3		401000		1		

(b) Off-diagonal values

Figure 6.6 – Adding of elements to the stiffness matrix

Another 2 sets of scalar points per moving load are used to define the auxiliary functions. The first moving load will consist of scalar points *100001, 100002, 100000+N* to represent auxiliary functions $A_{i1}(t)$, and a set *200001, 200002, .., 200000+N* to represent auxiliary functions $B_{i1}(t)$. In the case of a second moving load, *101001, 101002, 101000+N* represent $A_{i2}(t)$ and *200001, 200002, .., 200000+N* represent auxiliary functions $B_{i2}(t)$. Thus, if there are 4 nodes in each load path ($N=4$), the entry will be as illustrated in Figure 6.7(a). Unit stiffness is associated to each of these points (see Figure 6.7(b)).

SPOINT	100001	THRU	100004						
SPOINT	101001	THRU	101004						
SPOINT	200001	THRU	200004						
SPOINT	201001	THRU	201004						

(a) Specification of scalar points representing auxiliary functions

DMIG	STIF	100001			100001		1		
=	=	*1	=	=	*1	=	=		
2									
DMIG	STIF	101001			101001		1		
=	=	*1	=	=	*1	=	=		
2									
DMIG	STIF	200001			200001		1		
=	=	*1	=	=	*1	=	=		
2									
DMIG	STIF	201001			201001		1		
=	=	*1	=	=	*1	=	=		
2									

(b) Unit stiffness for each point

Figure 6.7 – Entry for four nodes in each load path

Then, auxiliary functions $A_{i1}(t)$ are applied to scalar points $100000+i$ ($i=1,2,...N$) and auxiliary functions $B_{i1}(t)$ to scalar points $200000+i$ ($i=1,2,...N$). $A_{i1}(t)$ and $B_{i1}(t)$ are

completely defined from the knowledge of $v_j(t)$ and the coordinates of the bridge nodes. The same applies to the scalar points and auxiliary functions corresponding to other moving masses.

The auxiliary functions and the excitation forces to be applied to the structure are established with the instructions DAREA and TLOAD2. The format of these 2 instructions is defined in Figure 6.8.

DAREA	SID	P1	C1	A1	P2	C2	A2		

Figure 6.8 - Columns for DAREA entry

Table 6.2 – Parameters used for DAREA entry (see Figure 6.8)

Field	**Contents**
SID	Identification number (Integer > 0)
Pi	Grid point identification number. (Integer > 0)
Ci	Component number (Integer 1 through 6 for grid point; 0 or blank for scalar point)
Ai	Scale factor. (Real)

DAREA define scale factors for dynamic loads and used in conjunction with TLOAD entries (see Figure 6.9).

TLOAD2	SID	DAREA	DELAY	TYPE	T1	T2	F	P	
	C	B							

Figure 6.9 - Columns for TLOAD2 entry

TLOAD2 represents a transient dynamic load $P(t)$ such that:

$$\{P(t)\} = \begin{cases} 0 & \text{for } t < (T1+\tau) \text{ or } t > (T2+\tau) \\ A\tilde{t}^{B} e^{Ct} \cos(2\pi F\tilde{t} + P) & \text{for } (T1+\tau) \square t \square (T2+\tau) \end{cases} \qquad (6.19)$$

where $\tilde{t} = t - T1 - \tau$.

Table 6.3 - Parameters used for TLOAD2 entry (see Figure 6.9)

Field	Contents
SID	Set identification number. (Integer >0)
DAREA	Identification number of DAREA entry set that defines A. (Integer > 0)
DELAY	Identification number of DELAY entry set that defines τ (Integer >=0 or blank)
TYPE	Defines the nature of the dynamic excitation. (Integer 0 (Force or Moment), 1, 2, 3)
T1	Time constant. (Real >=0.0)
T2	Time constant. (Real; T2>T1)
F	Frequency in cycles per unit time. (Real>=0.0; Default=0.0)
P	Phase angle in degrees. (Real; Default=0.0)
C	Exponential coefficient. (Real; Default=0.0)
B	Growth coefficient. (Real; Default=0.0)

The implementation of auxiliary functions $A_i(t)$ is shown in the following example. If each node is spaced 0.5 m from the following one, and the speed of the moving mass is constant and equal to 20 m/s, times t_i to reach each node *i* will be given as shown in Table 6.4.

Table 6.4 – Times t_i to reach each node

Node ID (identification number)	10	11	12	13	14
Coordinate (x_i)	0.0	0.5	1.0	1.5	2.0
Time (t_i)	0.0	0.025	0.05	0.075	0.1

The three constants "1", "$-3/(t_{i+1}-t_i)^2$" and "$2/(t_{i+1}-t_i)^3$" in the expression of $A_i(t)$ (Equation 6.4) can be represented with scalar factors. In the example above, as all nodes are equally spaced, $t_i-t_{i-1} = t_{i+1}-t_i = 0.025$, and $-3/(t_{i+1}-t_i)^2 = -4800$, $2/(t_{i+1}-t_i)^3 = 128000$. In the case of the first node of the path, only the part of Equation 6.4 corresponding to the interval $t_i \le t \le t_{i+1}$ is necessary, while for the last node, the part corresponding to the interval $t_{i-1} \le t \le t_i$ is the one to be used. For any node *i* different from these initial and final nodes, there will exist 2 definitions of the auxiliary function: One for the time that the load is preceding the node ($t < t_i$), and another for the time the load has passed the node ($t > t_i$) as given in Equation 6.4 (Scalar factors will have the same absolute values in both intervals, but the signs change for some terms to guarantee TLOAD2 is correctly related to *t*).

Once scalar factors have been defined and associated to a scalar point, it is necessary to define their relation with *t*. The output shown in Figure 6.10 corresponds to the path of the first moving load for an approach length of 10 m (at 20 m/s, earliest interaction force will act at 0.5 s). The same procedure applies to other moving loads and paths.

DAREA	100001	100001		1					
TLOAD2	100001	100001		0	0.5	0.525	0	0	
	0	0							
DAREA	110001	100001		-4800					
TLOAD2	110001	110001		0	0.5	0.525	0	0	
	0	2							
DAREA	120001	100001		128000					
TLOAD2	120001	120001		0	0.5	0.525	0	0	
	0	3							
DAREA	100002	100002		1					
TLOAD2	100002	100002		0	0.525	0.55	0	0	
	0	0							
DAREA	110002	100002		-4799.98					
TLOAD2	110002	110002		0	0.525	0.55	0	0	
	0	2							
DAREA	120002	100002		127999					
TLOAD2	120002	120002		0	0.525	0.55	0	0	
	0	3							
DAREA	130002	100002		4800.01					
TLOAD2	130002	130002		0	0.5	0.525	0	0	
	0	2							
DAREA	140002	100002		-128000					
TLOAD2	140002	140002		0	0.5	0.525	0	0	
	0	3							
DAREA	100003	100003		1					
TLOAD2	100003	100003		0	0.55	0.575	0	0	
	0	0							
DAREA	110003	100003		-4800					
TLOAD2	110003	110003		0	0.55	0.575	0	0	
	0	2							
DAREA	120003	100003		128000					
TLOAD2	120003	120003		0	0.55	0.575	0	0	
	0	3							
DAREA	130003	100003		4799.99					
TLOAD2	130003	130003		0	0.525	0.55	0	0	
	0	2							
DAREA	140003	100003		-127999					
TLOAD2	140003	140003		0	0.525	0.55	0	0	
	0	3							
DAREA	130004	100004		4800.01					
TLOAD2	130004	130004		0	0.55	0.575	0	0	
	0	2							
DAREA	140004	100004		-128000					
TLOAD2	140004	140004		0	0.55	0.575	0	0	
	0	3							

Figure 6.10 – Values of auxiliary function $A_i(t)$ for first moving load

The auxiliary functions $B_i(t)$ given in Equation 6.5 are expressed in a similar way. The elements "$-1/[2(t_i-t_{i-1})][x_i-x_{i-1}]$" and "$1/[2(t_i-t_{i-1})^2][x_i-x_{i-1}]$" in the expression of $B_i(t)$ can be represented with scalar factors. In the example above, as all nodes are equally spaced and velocity is constant, $t_i-t_{i-1} = 0.025$ and $(x_i-x_{i-1}) = 0.5$ for every node, $-1/[2(t_i-t_{i-1})][x_i-x_{i-1}] = -10.0$ and $1/[2(t_i-t_{i-1})^2][x_i-x_{i-1}] = 400.0$. As before, once the scalar factors have been defined and associated to a scalar point, it is necessary to define their relation with t through TLOAD2. The output for the first two nodes of the wheel path and the first moving load are shown in Figure 6.11.

DAREA	200001	200001		-10					
TLOAD2	200001	200001		0	0.5	0.525	0	0	
	0	1							
DAREA	210001	200001		400.001					
TLOAD2	210001	210001		0	0.5	0.525	0	0	
	0	2							
DAREA	200002	200002		-9.99998					
TLOAD2	200002	200002		0	0.525	0.55	0	0	
	0	1							
DAREA	210002	200002		399.999					
TLOAD2	210002	210002		0	0.525	0.55	0	0	
	0	2							
DAREA	220002	200002		10					
TLOAD2	220002	220002		0	0.5	0.525	0	0	
	0	1							
DAREA	230002	200002		-400					
TLOAD2	230002	230002		0	0.5	0.525	0	0	
	0	2							

Figure 6.11 – Values of auxiliary function $B_i(t)$ for first moving load

NASTRAN allows the definition of non-linear transient forcing functions through the instruction NONLIN2. This instruction defines the force to be applied to the node F_i as a function of a scalar S multiplied by the displacement of scalar p and velocity of a node q as $F_i = SX_pX_q$. The instruction has the format shown in Figure 6.12 and Table 6.5.

NOLIN2	SID	GI	CI	S	GJ	CJ	GK	CK	

Figure 6.12 – Columns for NOLIN2 entry

Table 6.5 – Parameters used for NOLIN2 entry

Field	Contents
SID	Non-linear load set identification number (Integer > 0)
GI	Grid or scalar point identification number at which non-linear load is to be applied (Integer > 0)
CI	Component number for GI. (Integer 1 through 6 for grid point; 0 or blank for scalar point)
S	Scale factor. (Real)
GJ, GK	Grid or scalar point identification number (Integer >0)
CJ, CK	Component number for GJ, GK (1 □Integer□ 6 for grid, and Blank or zero for scalar point if displacements) (11 □Integer□ 16 for grid, and 10 for scalar point if velocity)

These non-linear loads must be selected with the Case Control command, NONLINEAR=SID.

The forces A_iF and B_iF acting on the bridge nodes (Equation 6.14) are implemented as shown in Equation 6.20.

$$\begin{Bmatrix} A_1F \\ B_1F \\ A_2F \\ B_2F \\ \cdot \\ A_NF \\ B_NF \\ \cdot \end{Bmatrix} = \begin{Bmatrix} X_{100001}X_F \\ X_{200001}X_F \\ X_{100002}X_F \\ X_{200002}X_F \\ \cdot \\ X_{100000+N}X_F \\ X_{200000+N}X_F \\ \cdot \end{Bmatrix} \tag{6.20}$$

where $X_{100000+i}$ is displacement associated with scalar point $(100000+i)$ $(A_i(t))$, $X_{200000+i}$ is displacement associated with scalar point $(200000+i)$ $(B_i(t))$, and X_F is displacement associated with scalar point F (Interaction force defined by 400000). For example, if two masses and four nodes (ID node numbers 10,11,12 and 13 for the path of one mass and 20, 21, 22 and 23 for the other mass), these forces are expressed in NASTRAN code as illustrated in Figure 6.13.

NOLIN2	2	400000		1	100002		11	3	
NOLIN2	2	400000		1	100003		12	3	
NOLIN2	2	401000		1	101002		21	3	
NOLIN2	2	401000		1	101003		22	3	
NOLIN2	2	400000		1	200001		10	5	
NOLIN2	2	400000		1	200002		11	5	
NOLIN2	2	400000		1	200003		12	5	
NOLIN2	2	400000		1	200004		13	5	
NOLIN2	2	401000		1	201001		20	5	
NOLIN2	2	401000		1	201002		21	5	
NOLIN2	2	401000		1	201003		22	5	
NOLIN2	2	401000		1	201004		23	5	

NOLIN2	2	11	3	-1	100002		400000		
NOLIN2	2	12	3	-1	100003		400000		
NOLIN2	2	21	3	-1	101002		401000		
NOLIN2	2	22	3	-1	101003		401000		
NOLIN2	2	10	5	-1	200001		400000		
NOLIN2	2	11	5	-1	200002		400000		
NOLIN2	2	12	5	-1	200003		400000		
NOLIN2	2	13	5	-1	200004		400000		
NOLIN2	2	20	5	-1	201001		401000		
NOLIN2	2	21	5	-1	201002		401000		
NOLIN2	2	22	5	-1	201003		401000		
NOLIN2	2	23	5	-1	201004		401000		

Figure 6.13 – Definition of forces acting on the bridge nodes

The instruction *NONLINEAR = 2* should be added at the beginning of file *caseco.dat* to be included in NASTRAN analysis with the output queries. The term "$\sum_i A_i(t)z_i(t)+\sum_i B_i(t)\theta_i(t)$" corresponding to the compatibility forcing term in the stiffness matrix can also be implemented with the instruction NOLIN2 as illustrated in Figure 6.14.

NOLIN2	2	500000		1	100002		11	3	
NOLIN2	2	500000		1	100003		12	3	
NOLIN2	2	501000		1	101002		21	3	
NOLIN2	2	501000		1	101003		22	3	
NOLIN2	2	500000		1	200001		10	5	
NOLIN2	2	500000		1	200002		11	5	
NOLIN2	2	500000		1	200003		12	5	
NOLIN2	2	500000		1	200004		13	5	
NOLIN2	2	501000		1	201001		20	5	
NOLIN2	2	501000		1	201002		21	5	
NOLIN2	2	501000		1	201003		22	5	
NOLIN2	2	501000		1	201004		23	5	

Figure 6.14 – Definition of compatibility condition

The term *-mg*, though constant with *t*, can be regarded as a time-dependent term and modelled using DAREA and TLOAD2. If the moving load is located on a node *i*, the load will be *-mg*. If the moving load is between node *i* and node (*i*+1), the load will be distributed between adjacent nodes as follows:

For $x_i \le \xi \le x_{i+1}$ Load at node $i = -mg\ (x_{i+1}-\xi)/(x_{i+1}-x_i)$

Load at node $(i+1) = -mg(\xi-x_i)/(x_{i+1}-x_i)$ (6.21)

If speed is assumed to be constant along an element,

For $t_i \le t \le t_{i+1}$ Load at node $i = -mg\ (t_{i+1}-t)/(t_{i+1}-t_i)$

Load at node $i+1 = -mg(t-t_i)/(t_{i+1}-t_i)$ (6.22)

This can also be expressed as:

For $t_i \le t \le t_{i+1}$ Load at node $i = -mg\ [1-(t-t_i)/(t_{i+1}-t_i)]$

Load at node $i+1 = -mg(t-t_i)/(t_{i+1}-t_i)$ (6.23)

This is implemented by defining scalar factors $-mg/(t_{i+1}-t_i)$. In the example implemented in this section, $(t_{i+1}-t_i) = 0.025$ is the same for any node *i*, and if $m = 101.98$ *kg*, then, $g = 9.806$, "*-mg=1000*" and "$-mg/(t_{i+1}-t_i) = -40000.0$". The *bulk.dat* representation of gravity forces due to the first moving mass moving along the bridge path from ID node 10 to 14 is represented in Figure 6.15.

DAREA	10	10	3	1000					
TLOAD2	10	10		0	0.5	0.525	0	0	
	0	0							
DAREA	10010	10	3	-40000					
TLOAD2	10010	10010		0	0.5	0.525	0	0	
	0	1							
DAREA	11	11	3	40000					
TLOAD2	11	11		0	0.5	0.55	0	0	
	0	1							
DAREA	10011	11	3	-79999.8					
TLOAD2	10011	10011		0	0.525	0.55	0	0	
	0	1							
DAREA	12	12	3	40000					
TLOAD2	12	12		0	0.525	0.575	0	0	
	0	1							
DAREA	10012	12	3	-80000					
TLOAD2	10012	10012		0	0.55	0.575	0	0	
	0	1							
DAREA	13	13	3	40000					
TLOAD2	13	13		0	0.55	0.575	0	0	
	0	1							

Figure 6.15 – Definition of gravity forces

The forces due to the road profile are imposed on scalar points defining the interaction force F (this is, 400000, 401000, etc.). If the power spectral density function defining the road profile is divided into 100 frequency intervals, it will be necessary to define 100 values for each moving load. If there are 4 moving loads and 100 frequency intervals, there will be 400 DAREA and TLOAD2 instructions. These forces will be present all along the time the analysis takes place. The height of the road irregularities is given by (see Section 5.4):

$$x(t) = \sum_{n=1}^{N} \sqrt{4S(\omega_n)}\Delta\omega \cos(\omega_n t - \theta_n) \tag{6.24}$$

The correspondence with the parameters defining TLOAD2 is:

- τ = blank.; $T1 = 0$,
- $T2$ = approach_time + time_crossing_bridge + free_vibration_time,
- $A = \sqrt{4S(\omega_n)}\Delta\omega$ (defined by DAREA),
- $P = -\theta_n$ where θ_n in degrees is generated randomly,
- $F = \omega$ is temporal frequency in Hz.

Figure 6.16 shows a few frequency components of a road profile.

DAREA	310000	400000		0.0016					
TLOAD2	310000	310000		0	0	7.075	1	99.2744	
	0	0							
DAREA	310001	400000		0.00135					
TLOAD2	310001	310001		0	0	7.075	1.19	264.129	
	0	0							
DAREA	310002	400000		0.00116					
TLOAD2	310002	310002		0	0	7.075	1.38	53.8938	
	0	0							
DAREA	310003	400000		0.00102					
TLOAD2	310003	310003		0	0	7.075	1.57	32.8363	
	0	0							
DAREA	310004	400000		0.00091					
TLOAD2	310004	310004		0	0	7.075	1.76	0.30802	
	0	0							

Figure 6.16 – Definition of road profile

In the same way, a bump can be defined at a certain location by its wavelength and height. In the example illustrated in Figure 6.17, a 10 cm amplitude and 1 m length sinus wave is modelled 10 m prior to the bridge.

DAREA	350000	400000		0.1					
TLOAD2	350000	350000		0	0	0.05	10	0	
	0	0							
DAREA	351000	401000		0.1					
TLOAD2	351000	351000		0	0	0.05	10	0	
	0	0							

Figure 6.17 – Definition of a bump

A particular shape (i.e. a measured road profile) can be approximated by a combination of different sine functions. Finally, the instruction DLOAD defines the dynamic loading condition for the transient response problem as a linear combination of the sets defined via TLOAD2 entries. This is illustrated in Figure 6.18 and Table 6.6

DLOAD	SID	S	S1	L1	S2	L2	S3	L3	
	S4	L4	-etc.-						

(a) Format of DLOAD entry

Figure 6.18 (continued on following page)

DLOAD	999	1	1	100001	1	110001	1	120001	
	1	100002	1	110002	1	120002	1	130002	
	1	140002	1	100003	1	110003	1	120003	
	1	130003	1	140003	1	130004	1	140004	
	1	101001	1	111001	1	121001	1	101002	
	1	111002	1	121002	1	131002	1	141002	
	1	101003	1	111003	1	121003	1	131003	
	1	141003	1	131004	1	141004	1	200001	
	1	210001	1	200002	1	210002	1	220002	
	1	230002	1	200003	1	210003	1	220003	

(b) Implementation

Figure 6.18 – Definition of interaction forces

Table 6.6 – Parameters used for DLOAD entry (see Figure 6.18(a))

Field	Contents
SID	Load set identification number (Integer >0)
S	Scale factor (Real)
Si	Scale factor (Real)
Li	Load set identification numbers of TLOAD2 entries (Integer >0)

Dynamic load sets must be selected in the Case Control Section with *DLOAD=SID*. This will be explained in Section 6.3. Appendix F contains listings of *bulk.dat* files for different vehicle and bridge input parameters.

Caseco Control Section

An example of *caseco.dat* file used for dynamic analysis is presented in Table 6.7 where displacement, velocity and acceleration at nodes 10,11,12,13, displacements at nodes 300000,301000, and strain at elements 1,2,3,4 are required. *K2GG* selects a direct input stiffness matrix. *STIF* is the name of a matrix that is input on the Bulk Data Entry. Another line to include in *caseco.dat* is *PARAM, COUPMASS, 1* that requests the generation of coupled rather than lumped mass matrices for elements with coupled mass capabilities. *SORT1* presents the output as a tabular listing of elements for each time. Other output forms can be found in MSc/NASTRAN Quick Reference Guide (1998).

Table 6.7 – Example of Caseco.dat file

$ Input Specification

DLOAD=1

NONLINEAR=2

K2GG=STIF

PARAM,COUPMASS,1

$ SET- Definition of points and elements where output is required

SET 1 = 10,11,12,13

SET 2 = 1,2,3,4

SET 3 = 300000, 301000

$ Output Specification

DISPLACEMENT(SORT1) = 1,3

VELOCITY(SORT1,RALL) = 1

ACCELERATION(SORT1) = 1

STRAIN(SORT1,RALL) = 2

6.3 IMPLEMENTATION IN NASTRAN

This section explains the overall procedure to carry out a simulation in a NASTRAN environment. It can be summarised in the following steps:

[1] Creation of bridge model (*bridge.mod* file) and analysis of the model (*bridge.dat* file).

[2] Creation of truck model (*truck.mod* file).

[3] Static analysis of the truck model to obtain the reactions due to self-weight.

[4] Import analysis of the bridge model (*bridge.dat* file) into truck model (*truck.mod* file), saving combined system as a new file (*system.mod*).

[5] Edit input dynamic interaction file (*nasbti1.txt*) and specify:

- Static axle weights
- Speed
- Axle spacings
- Wheel path on the bridge
- Road profile

[6] Generate *bulk.dat* file by running *nastbti.exe*. The information required by *nasbti.exe* to perform calculations is taken from *input.txt*. The input code contained in *bulk.dat* was explained in Section 6.2.2 and more examples are given in Appendix F.

[7] Edit *caseco.dat* file to specify which output results are required.

[8] Open *system.mod* file, create dynamic load, time transient

[9] Export model analysis to a file (i.e. *test.dat*), Advanced Analysis, include *caseco.dat* and *bulk.dat*. Exit and Save.

[10] Open *test.dat*, change $D = 1$ to $D = 999$ and precede line *Loadset = 1* by *$*.

[11] Run *nastranw.exe* on *test.dat* to generate *test.f04* and *test.f06* files. *Test.f06* is the file containing the output results required in *caseco.dat*.

[12] Run *Convnas.exe* to convert sequential output *test.f06* into an output in columns that can be easily opened in Excel or other worksheet software. The information to be extracted from *test.f06* must be specified in *convnas.txt*

These steps are explained in further detail in the following sections.

Bridge finite element model

The creation of a bridge model (*bridge.mod* file) and analysis of the model (*bridg000.dat* file) are discussed in this section. This analysis can be static or dynamic. The objective is the generation of a **.dat* file that contains all the information relating to bridge material, properties, nodes, elements and constraints (MSc/NASTRAN 1997a, 1997b). When building this model (Figure 6.19(a)), a list of nodes should be defined along the wheel path on the structure. There are two aspects to this model that require further consideration:

- The identification of the number and spacing of the nodes corresponding to each wheel path.
- The identification of the numbers of the elements/nodes for which response (strains, displacements, forces, etc.) are to be generated.

Specific bridge models will be introduced in Section 6.5.

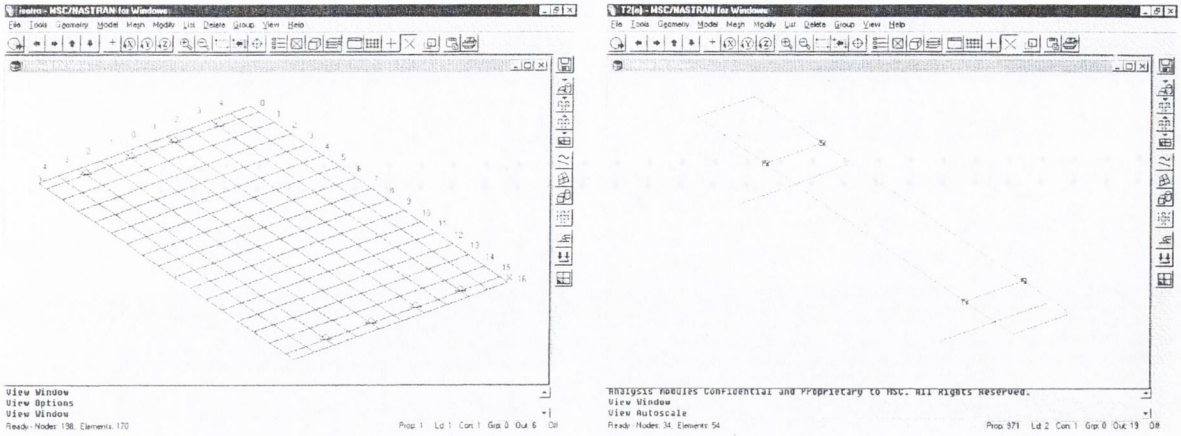

(a) Bridge model (b) Truck Model

Figure 6.19 – Finite Element models

Truck model

The truck is designed and saved in another file (*truck.mod*) independent from the bridge model. When the truck model is created (Figure 6.19(b)), its materials, properties, nodes and elements should have a different identification number from those used in the bridge model defined previously. Otherwise, error messages will be reported when combining both models.

In order to apply forces to the contact points of the truck with the ground, these nodes must have a predetermined numbering identified by the interaction program (Section 6.2.2). Hence, the contact points located on the inner side of the bridge are even numbers of thousands starting at 300000 for the first axle, 302000 for the 2nd axle and so on, while the contact points in the outer side are odd numbers of thousands starting at 301000, 303000, etc. If there were a second vehicle, the contact points of this vehicle would have identification numbers starting at 600000 at the steering wheel side and 601000 at the other side. Some details on the elements composing a truck model were given in Chapter 5. Section 6.4 will describe the truck models used for NASTRAN theoretical simulations.

Determination of static axle weights

A static analysis of the truck model must be carried out to obtain the reactions due to the self-weight. It is necessary to check that the wheel-ground points of contact are restrained in the x, y and z directions, so we can get the vertical reactions due to gravity. NASTRAN has an option for imposing body loading of this type (MSc/NASTRAN 1997a, 1997b).

Bridge-truck combined model

The file containing the truck model is opened (*truck.mod*). The information on the bridge data (*bridg000.dat*) is imported into the truck model (Figure 6.20(a)). Then, the combined system shown in Figure 6.20(b) is saved as a new file (i.e. *system.mod*). At the wheel-ground contact points the truck should be restrained in the x and y direction (only vertical deformation in z direction is allowed).

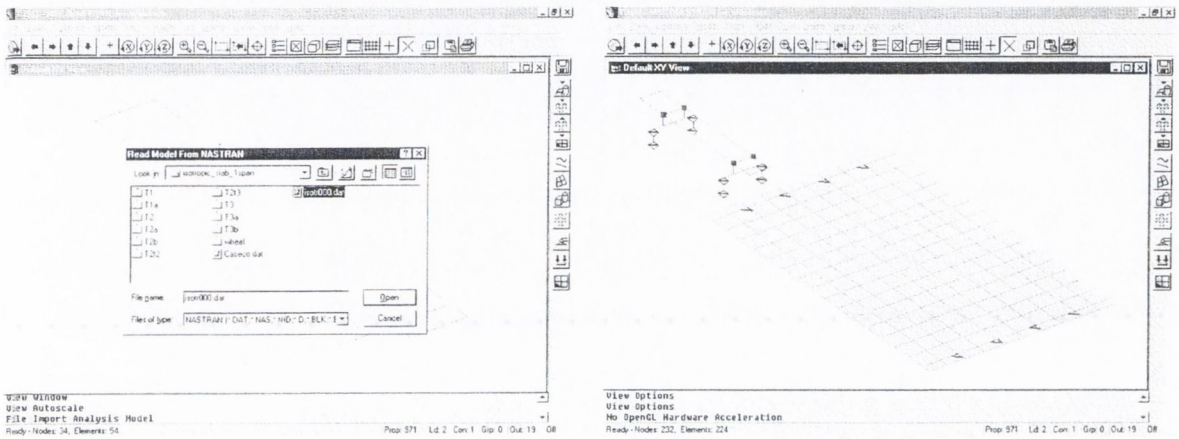

(a) Import of bridge data (b) Combined system

Figure 6.20 – Creation of combined finite element model

Edit input file

The input text file (*nasbti1.txt*) contains the number of vehicle events and, for each vehicle:

- Static axle weights,
- Speed as a function of time,
- Axle spacings,
- Wheel path on the bridge,
- Road profile.

An executable file (*input.exe*) allows the generation of *nasbti1.txt* through the computer screen (i.e. this program will fill up node numbers and spacings of the wheel path into *nastbti1.txt* automatically if they follow a consecutive order or pattern). The header of the file contains information on truck characteristics (Figure 6.21(a)). The definition of the wheel path is illustrated in Figure 6.21(b). This path is defined by the identification number for different nodes on the bridge followed by the total distance travelled by the wheel up to that node. Finally information on road profile is given (Figure 6.21(c)). The characteristics

of a second vehicle would follow the ones of a first vehicle in the same way. *Nasbti1.txt* has a special format to be read by *nasbti.exe*, an executable file that produces *bulk.dat*. Though *nasbti1.txt* is a text file that can be filled in directly (Each line contains information on a different input parameter), *input.exe* guarantees the correct format of *nasbti1.txt*.

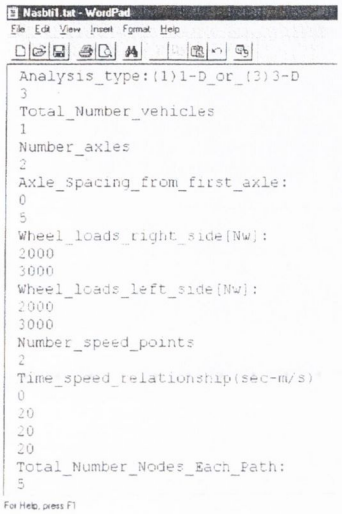

(a) Information on truck characteristics

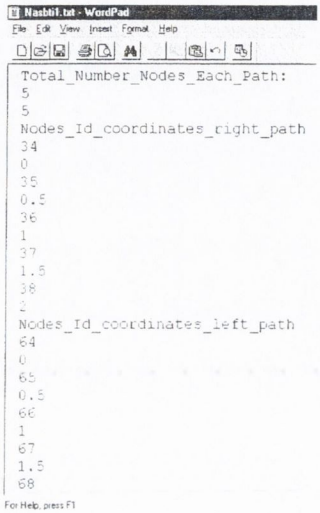

(b) Information on bridge path

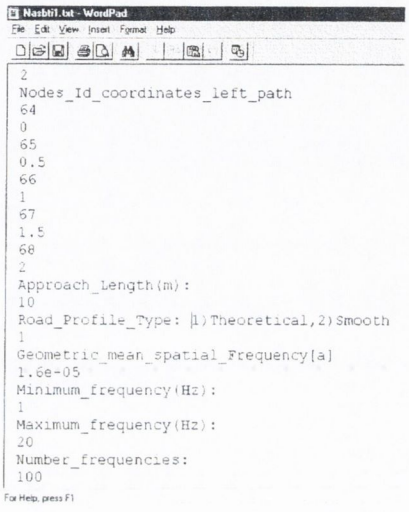

(c) Information on road profile

Figure 6.21 - Input file, *nasbti1.txt*, for generation of *bulk.dat*

Generation of Bulk file

Run *nasbti.exe* to generate *bulk.dat* file (Section 6.2.2). *Nasbti.exe* takes as reference the input data in *nasbti1.txt*. *Bulk.dat* contains the interaction forces applied to the structure at each instant in time. These applied forces are based on the theoretical background described in 6.2.1. Depending on how *nasbti.exe* has been compiled, static response can be obtained, special support conditions (such as fixed) can be specified, bumps can be prescribed at the desired positions and/or road profile can be output to a text file.

Output request

Edit *caseco.dat* file to choose those elements and the type of bridge response that is required. The lines starting with a $ sign are ignored by NASTRAN. The first three lines are caseco control commands for dynamic analysis (MSC/NASTRAN 1997c), and the following lines specify the output request (MSC/NASTRAN 1998). Figure 6.22 shows an example of *caseco.dat* file.

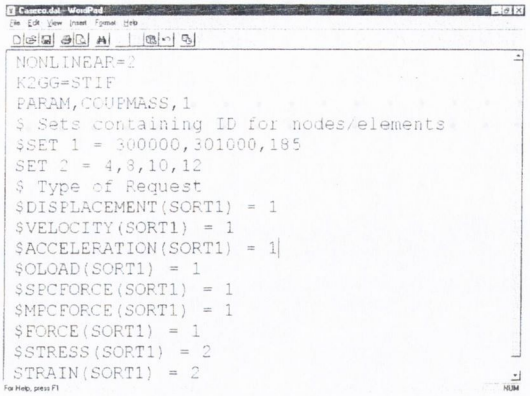

Figure 6. 22 – Output Request

Dynamic Transient Analysis

Open *system.mod* file and create a time transient dynamic load (Figure 6.23(a)) as specified by MSc/NASTRAN (1997a, 1997b). A direct numerical method is chosen for the transient response analysis. This method performs a numerical integration on the complete coupled equations of motion (unlike the modal method). The structural response is solved at discrete times, typically with a fixed integration time step. A central finite difference representation for the velocity and acceleration is used at discrete times, and the applied force is averaged over three adjacent time steps. The following features are defined on the Load Set Options for Dynamic Analysis Dialog Box (Figure 6.23(b)):

- Total number of steps, time per step and output interval.

  The time per step depends on the characteristics of the problem (generally 0.001).

  The total number of steps depends on the length to be recorded and vehicle speed. If speed is constant, *Total_number_steps=Total_length/(speed*time_per_step)*

  Some extra steps might be taken into account to study the free vibration of the bridge.

  The output time interval depends on the frequency desired for the output results. For example, if the solution is performed every 0.001 seconds, the results can be output every fifth step or every 0.005 seconds.

- Damping

  Damping represents the dissipation energy characteristics of the structure and it can be implemented in different ways (MSC/NASTRAN 1997c). Structural damping has been commonly used.

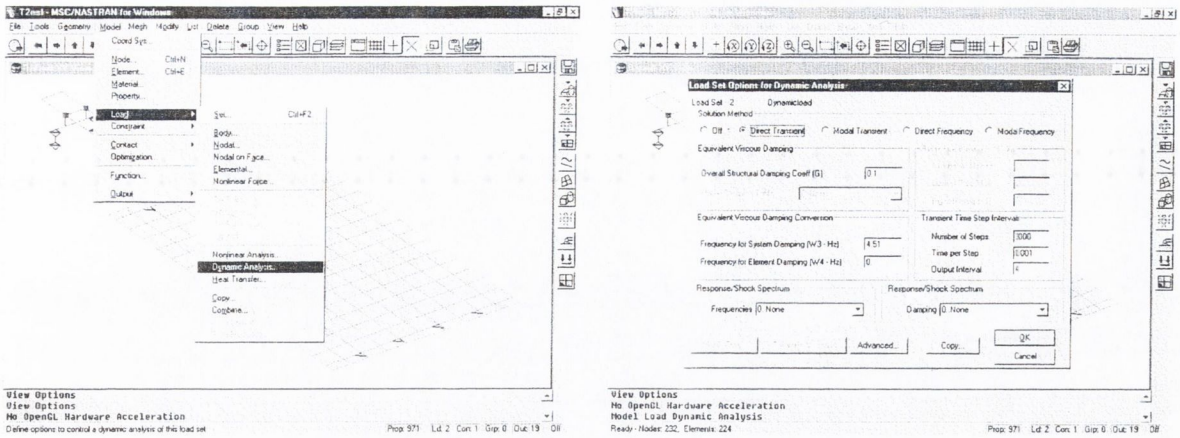

Figure 6.23 – Creation of dynamic transient load

Export model data

The File Export Analysis Model command allows for the writing of an interaction model into a file (i.e. *test.dat*) that can be read by NASTRAN solver (*nastranw.exe*). This file contains four different sections: Executive Control, Case Control, Bulk Data and all the information relating to the materials, properties, nodes and elements of the interaction model. *System.mod* is opened and the File Export command is selected. Different dialog boxes are displayed then. The options to be chosen are described in Appendix F.

Modify input data

Open *test.dat*, modify instruction line *D*=1 to *D*=999, and precede line *Loadset*=1 with *$* as shown in Figure 6.24(a).

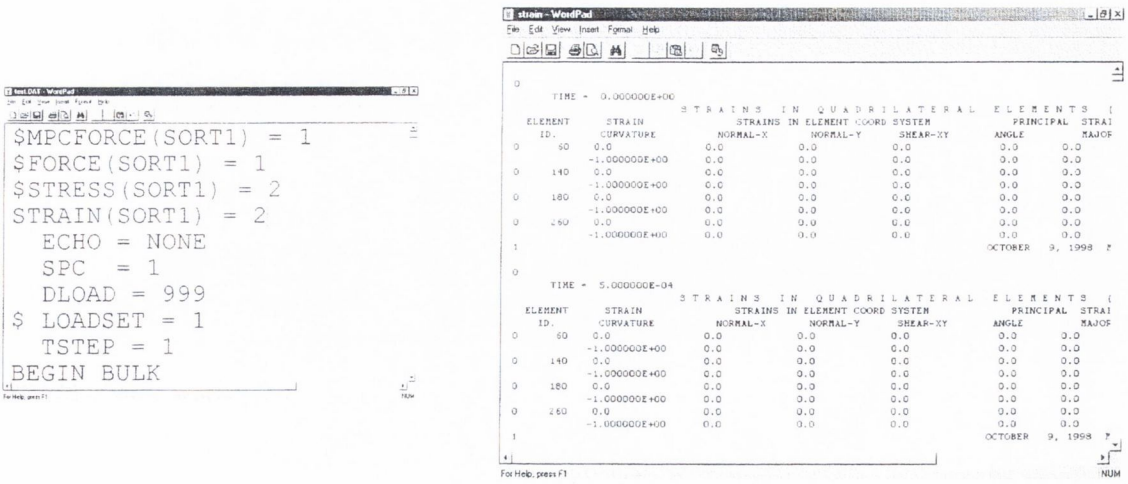

```
$MPCFORCE(SORT1) = 1
$FORCE(SORT1) = 1
$STRESS(SORT1) = 2
STRAIN(SORT1) = 2
  ECHO = NONE
  SPC  = 1
  DLOAD = 999
$ LOADSET = 1
  TSTEP = 1
BEGIN BULK
```

(a) Input file for *nastranw.exe* (*.dat)

```
                                    S T R A I N S   I N   Q U A D R I L A T E R A L   E L E M E N T S
  ELEMENT        STRAIN                    STRAINS IN ELEMENT COORD SYSTEM                PRINCIPAL  STRAI
    ID.        CURVATURE          NORMAL-X        NORMAL-Y        SHEAR-XY          ANGLE        MAJOR
0       50      0.0                0.0             0.0             0.0               0.0          0.0
                -1.000000E+00      0.0             0.0             0.0               0.0          0.0
0      140      0.0                0.0             0.0             0.0               0.0          0.0
                -1.000000E+00      0.0             0.0             0.0               0.0          0.0
0      180      0.0                0.0             0.0             0.0               0.0          0.0
                -1.000000E+00      0.0             0.0             0.0               0.0          0.0
0      260      0.0                0.0             0.0             0.0               0.0          0.0
                -1.000000E+00      0.0             0.0             0.0               0.0          0.0
1                                                                                    OCTOBER   9, 1998  P
```

(b) Output file from nastranw.exe (*.f06)

Figure 6.24 – Final Input and output simulation files

Run solver

Run *nastranw.exe* on *test.dat* which will generate *test.f04* and *test.f06* files (Figure 6.24(b)). *Test.f06* contains all information requested on *caseco.dat*. It also reports on any errors which have taken place during the execution of the simulation.

Output in columns

The results provided by NASTRAN in *test.f06* (Figure 6.24(b)) are difficult to manipulate. A program was written to display the information of *test.f06* in a column output (*column.txt*). This program, *convnas.exe*, reads from *convnas.txt* the identities of the elements to be extracted in *test.f06* and the type of request (i.e., longitudinal and transverse bending strain can be obtained by specifying 01100000. These numbers correspond to eight different types of strain output that NASTRAN gives. Only those positions marked with a 1 are extracted in columns). Figure 6.25 shows examples of *convnas.txt* and *column.txt* files respectively.

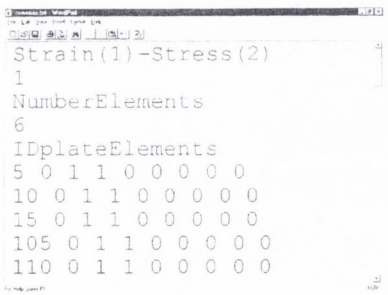

```
Strain(1)-Stress(2)
1
NumberElements
6
IDplateElements
5 0 1 1 0 0 0 0 0
10 0 1 1 0 0 0 0 0
15 0 1 1 0 0 0 0 0
105 0 1 1 0 0 0 0 0
110 0 1 1 0 0 0 0 0
```

(a) *convnas.txt*

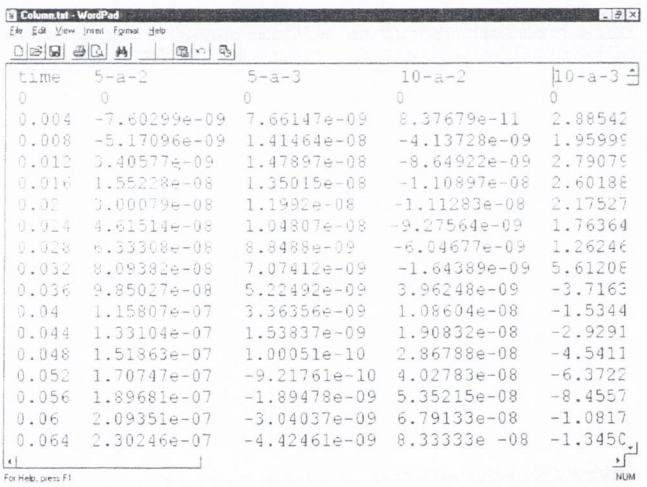

Column.txt - WordPad

File Edit View Insert Format Help

time	5-a-2	5-a-3	10-a-2	10-a-3
0	0	0	0	0
0.004	-7.60299e-09	7.66147e-09	8.37679e-11	2.88542
0.008	-5.17096e-09	1.41464e-08	-4.13728e-09	1.95999
0.012	3.40577e-09	1.47897e-08	-8.64922e-09	2.79079
0.016	1.55228e-08	1.35015e-08	-1.10897e-08	2.60188
0.02	3.00079e-08	1.1992e-08	-1.11283e-08	2.17527
0.024	4.61514e-08	1.04807e-08	-9.27564e-09	1.76364
0.028	6.33308e-08	8.8488e-09	-6.04677e-09	1.26246
0.032	8.09382e-08	7.07412e-09	-1.64389e-09	5.61208
0.036	9.85027e-08	5.22492e-09	3.96248e-09	-3.7163
0.04	1.15807e-07	3.36356e-09	1.08604e-08	-1.5344
0.044	1.33104e-07	1.53837e-09	1.90832e-08	-2.9291
0.048	1.51863e-07	1.00051e-10	2.86788e-08	-4.5411
0.052	1.70747e-07	-9.21761e-10	4.02783e-08	-6.3722
0.056	1.89681e-07	-1.89478e-09	5.35215e-08	-8.4557
0.06	2.09351e-07	-3.04037e-09	6.79133e-08	-1.0817
0.064	2.30246e-07	-4.42461e-09	8.33333e -08	-1.3450

For Help, press F1 NUM

(b) *column.txt*

Figure 6.25 – Input and output file for a final tabular display

Summarising, once the bridge and truck finite element models have been created, the files involved in the rest of the simulation process are as shown in Table 6.8.

Table 6.8 –Dynamic Interaction Files

Executable file	*Input File*	*Output file*
Generation of bridge data	*Bridge.mod*	*Bridge000.dat*
Creation of interaction model	*Truck.mod* *Bridge000.dat*	*System.mod*
Input.exe	screen	*Nastbi.txt*
Nasbti.exe	*Nasbti.txt*	*Bulk.dat*
Export input file for simulation	*System.mod* *Caseco.dat* *Bulk.dat*	*test.dat*
Nastranw.exe	*Test.dat*	*Test.f04* *Test.f06*
Convnas.exe	*Convnas.txt* *Test.f06*	*column.txt*

6.4 TRUCK MODELS

Only rigid frame structures have been modelled spatially, i.e., types T2 and T3 illustrated in Figures 6.26 and 6.27 respectively.

(a) Two-axle trailer (T2 type) (b) Finite Element Model

Figure 6.26 – Two-axle truck

(a) Three-axle trailer (T3 type) (b) Finite Element Model

Figure 6.27 – Three-axle truck

The elements of a two-axle truck are represented in Figure 6.28. Friction elements are not part of this modelling, though their influence in dynamic wheel forces could be significant.

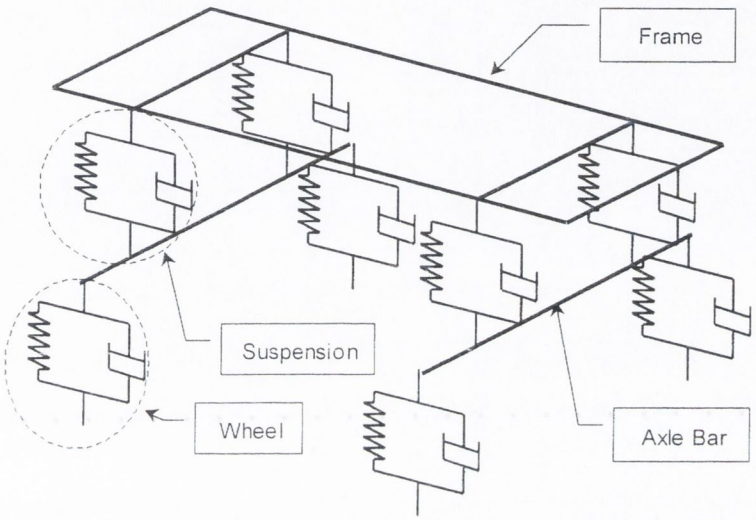

Figure 6.28 – Finite Element Two-Axle Truck Model

Table 6.9 gives the mechanical characteristics used in the design of both trucks. The data for the two-axle truck has been taken from manufacturers (Kirkegaard et al. 1997). The parameters of the three-axle truck have been obtained from experimental studies carried out in Munich (Baumgärtner 1998, Lutzenberger & Baumgärtner 1999) on a Finnish instrumented truck (Huhtala 1999). Details on this truck will be given in Chapter 8. Values are similar for both trucks, except for damping (The Danish model used friction elements in addition to dampers, but these elements have not been included).

Table 6.9 – Suspension and tyre properties

Truck Type	Spring (10^6 N*m)				Damping (10^3 Ns/m)			Axle mass (kg)		Mass moment of Inertia (kgm^2)	
	Tire		Suspension		Suspension	Tire					
	Front Axle	Rear axles	Front Axle	Rear axles		Front Axle	Rear axles	Front Axle	Rear axle	Front Axle	Rear axles
2-axle	1.0	2.0	1.8	0.3	5.0	3.0	3.0	700	1300	600	1000
3-axle	1.0	2.1	0.21	0.8	55.	40.	80.	343	1343	972.5	972.5

The axle spacing for the two-axle truck is 5 m. The three-axle truck has a rear tandem and the axle spacings are 4.2 m between the first and second axle and 1.2 m for the last two axles. Three different loading conditions and three speeds (55, 70 and 85 km/h) have been used for each truck configuration. Static weights of the two test vehicles are given in Table 6.10.

Table 6.10 – Static weights (kN)

Vehicle Type	1st Axle	2nd Axle	3rd Axle	GVW
T2(Lightly loaded)	55.703	71.195	-	126.897
T2(Half-Loaded)	69.660	87.899	-	157.559
T2(Heavily loaded)	83.904	104.945	-	188.849
T3(Lightly loaded)	59.279	92.818	63.647	215.744
T3(Half-Loaded)	75.226	115.785	77.973	268.985
T3(Heavily Loaded)	91.174	138.752	92.298	322.224

The main modes of vibration of the two-axle truck are represented in Figure 6.29.

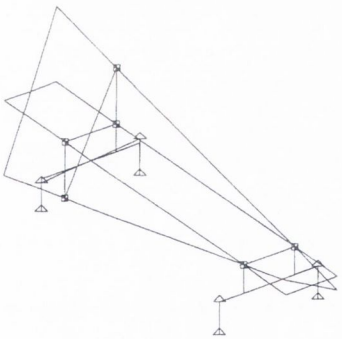

(a) Frame twist

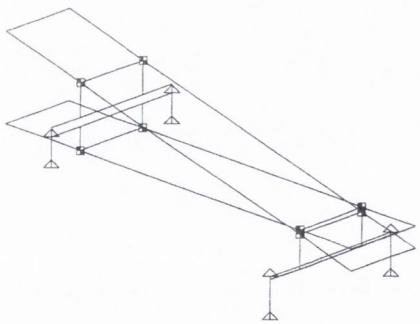

(b) Body pitch

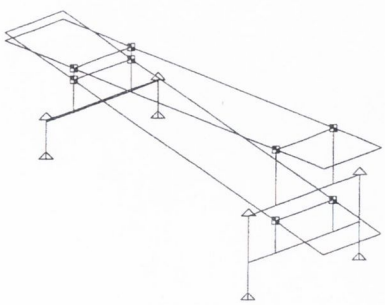

(c) Body bounce

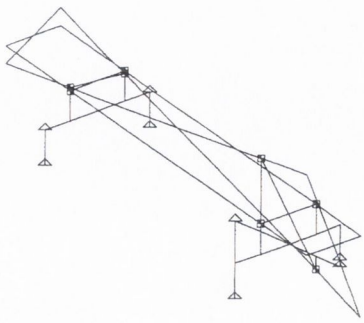

(d) Body roll

Figure 6.29 (continued on following page)

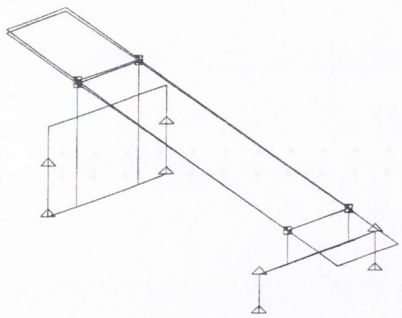

(e) Rear axle hop

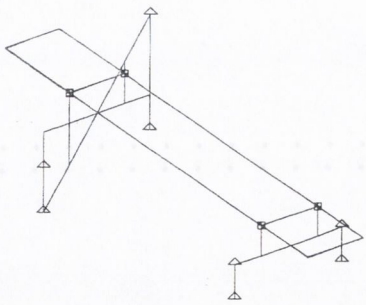

(f) Rear axle roll

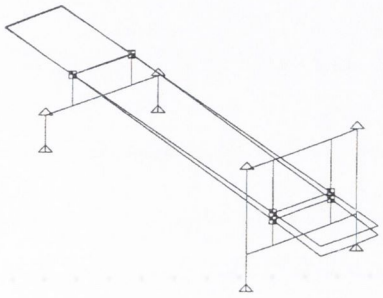

(g) Front axle hop

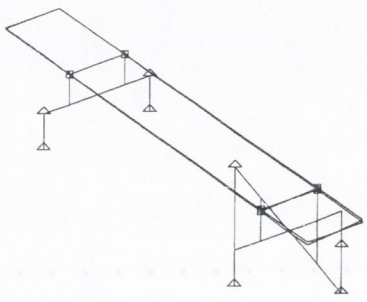

(h) Front axle roll

Figure 6.29 – Modes of vibration of a Two-Axle Truck

These modes of vibration are associated with a frequency given in Table 6.11. These frequencies change depending on the truck weight (Table 6.10) and they allow the assessment of the dynamic interaction with the supporting bridge. As the natural frequencies of the bridge and vehicle get closer, the dynamic response increases.

Table 6.11 – Main frequencies of vibration of the two-axle truck (Hz)

Truck load	Frame Twist	Body			Axle Hop		Axle Roll	
		Pitch	Bounce	Roll	Rear	Front	Rear	Front
Light	1.05	1.40	2.35	2.54	9.48	13.49	14.59	15.65
Half	0.99	1.23	2.08	2.37	9.47	13.49	14.51	15.63
Heavy	0.94	1.11	1.89	2.23	9.47	13.49	14.46	15.62

In the same way, Figure 6.30 shows modes of vibration corresponding to the three-axle truck.

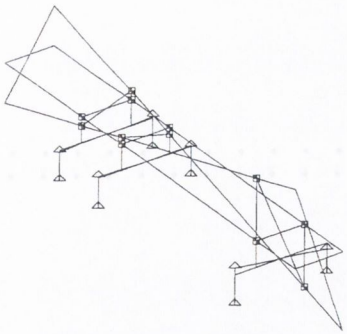

(a) Frame Twist

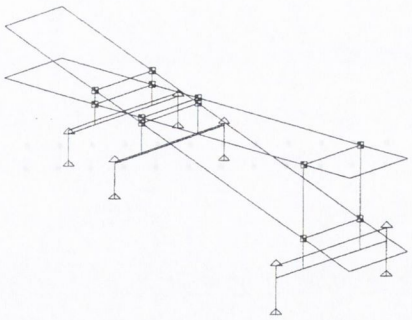

(b) Body Pitch

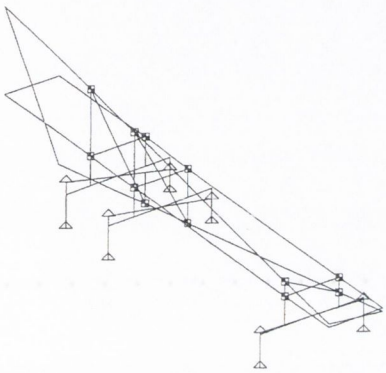

(c) Body roll

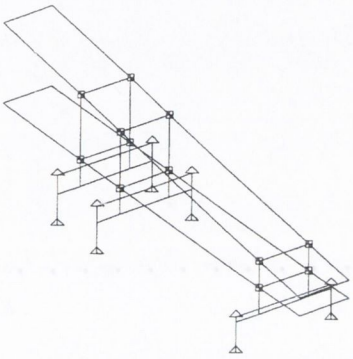

(d) Body bounce

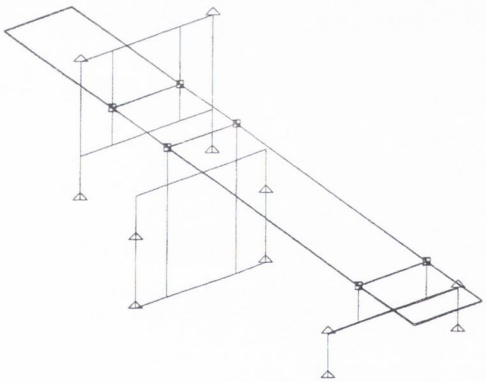

(e) 2nd and 3rd axle hop (out of phase)

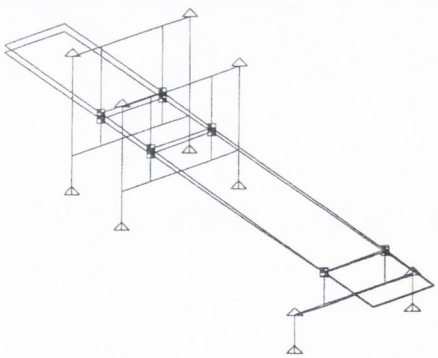

(f) 2nd and 3rd axle hop (in phase)

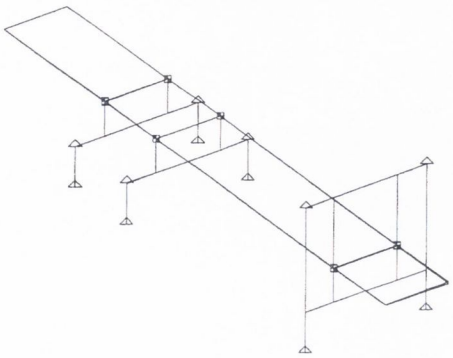

(g) First axle hop

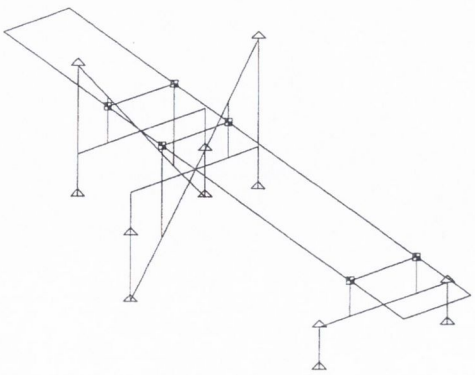

(h) 2nd and 3rd axle roll (out of phase)

Figure 6.30 (continued on following page)

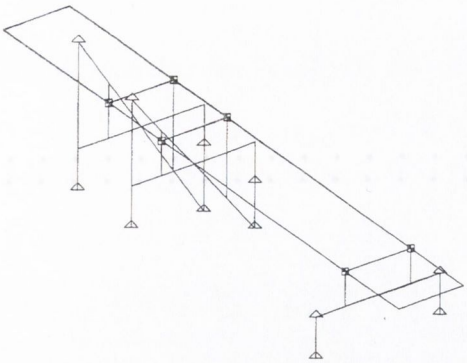

(i) 2nd and 3rd axle roll (in phase)

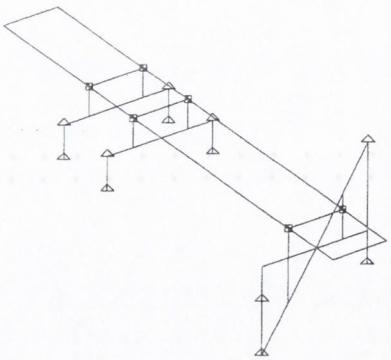

(j) First axle roll

Figure 6.30 – Modes of vibration of a Three-Axle Truck

Table 6.12 shows the frequencies of vibration for different weights (Table 6.10) of the three-axle truck.

Table 6.12 – Main Modes of Vibration of the Three-Axle Truck (Hz)

Truck load	Frame Twist	Body			Tandem Hop		Tandem Roll		Front axle	
		Pitch	Roll	Bounce	Out of phase	In phase	Out of phase	In Phase	Hop	Roll
Light	0.82	1.02	1.58	2.01	9.90	9.97	13.25	13.26	11.08	15.51
Half	0.76	0.90	1.48	1.77	9.90	9.96	13.25	13.26	11.08	15.51
Heavy	0.71	0.81	1.39	1.60	9.90	9.94	13.25	13.26	11.08	15.51

6.5 BRIDGE MODELS

In some cases, bridge decks can be idealised as plate elements with thickness and density properties that match the mass per unit length and inertia of the real bridge in the longitudinal and transverse direction. However, if distribution of mass is not uniform in both directions and very accurate results are required, a 3-D bridge model will be necessary. Simulations of single and simultaneous traffic events (Figures 6.31(a) and 6.31(b)) have been performed on a range of bridge forms to determine their suitability for B-WIM purposes. The results obtained are typically strains in elements, which are easily measurable in the field (Section 4.2). A single span isotropic slab, two-span isotropic slab, slab with edge cantilever, voided slab, beam and slab, skew and cellular bridges are tested. These models follow the guidelines proposed in the examples by O'Brien and Keogh (1999). Typical properties of reinforced/prestressed concrete have been chosen for the

bridge material. Bridge damping is considered to be 5% and the road condition is considered to be 'good' (Wong 1993) in all cases.

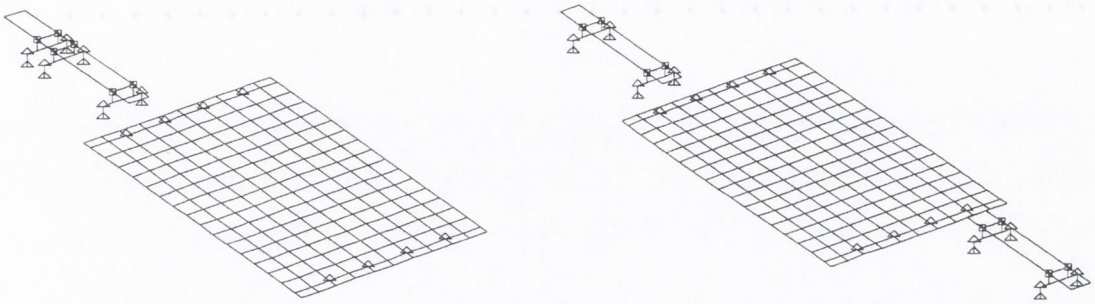

(a) Single Traffic Event (b) Simultaneous Traffic Events

Figure 6.31 – Finite Element Simulations

Static, eigenvalue and transient response analysis are necessary for a better understanding of the models and to ensure an accurate dynamic response. A static analysis is useful to determine influence lines at different locations. As seen in Section 3.5.1, accurate influence lines are very important in B-WIM systems. Though experimental influence lines can be obtained, they are limited to a reduced number of runs/trucks/sensors and a theoretical model can supply additional information on the accuracy in other situations. The natural frequencies and mode shapes are an indication of how the bridge will respond to a dynamic excitation. The bridge will then naturally vibrate at these frequencies.

6.5.1 Single Span Isotropic Slab

A slab deck behaves like a flat plate that is structurally continuous for the transfer of moments and torsions in all directions within the plane of the plate. Figure 6.32(a) shows a layout of the slab example (dimensions in m). Traffic direction is parallel to the x-axis. The deck is supported on four bearings at each end. The deck has a uniform rectangular cross-section of 0.6 m depth. It is built of prestressed concrete, 2500 kg/m^3 unit weight, 35x10^6 kN/m^2 modulus of elasticity and 0.15 Poisson's ratio. These general characteristics will be used in other models unless otherwise specified.

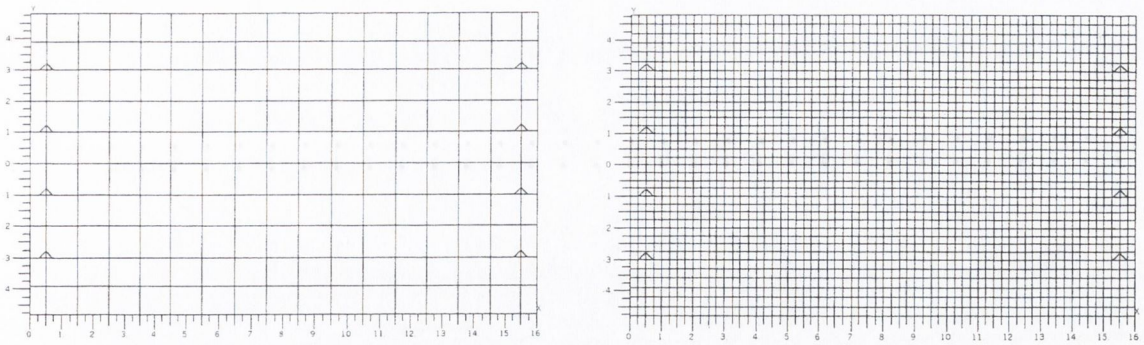

(a) Original Mesh (b) Finer Mesh

Figure 6.32 – Plan view of slab finite element model

Influence lines due to a unit axle load travelling along the slow lane are represented in Figure 6.33. Two different types of mesh are compared: one based on plate elements 1 m long (Figure 6.32(a)) and another based on plate elements 0.5 m long. The difference in strain response is not significant.

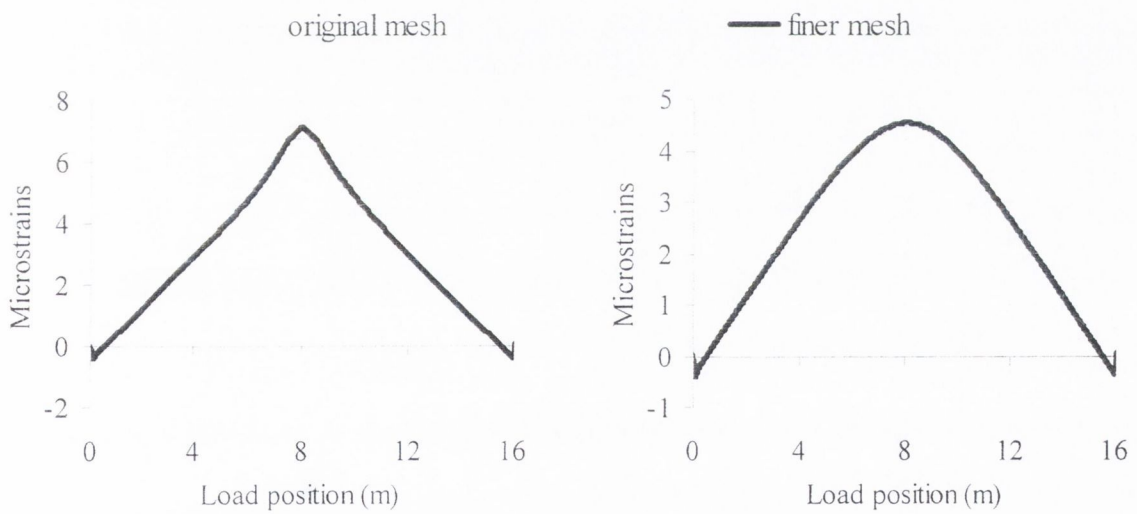

(a) Longitudinal strain, slow lane (b) Longitudinal strain, fast lane

Figure 6.33 (continued on following page)

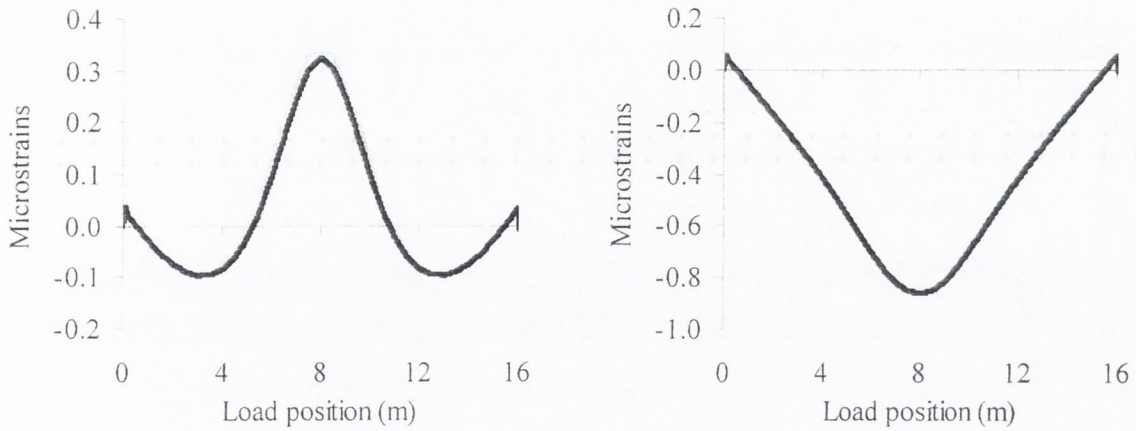

(a) Transverse strain, slow lane (b) Transverse strain, fast lane

Figure 6.33 - Influence line of strain at midspan (longitudinal distance of the sensor from start of the bridge: 8 m; transverse offset from bridge centreline: 2.5 m)

The main modes of vibration of the bridge are represented in Figure 6.34.

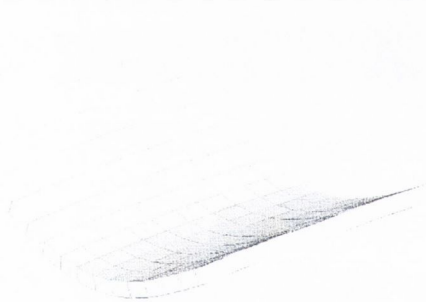

(a) 1st Mode (4.51 Hz)

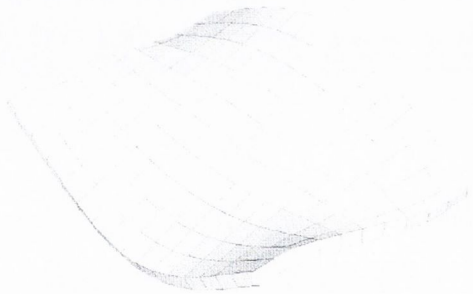

(b) 2nd Mode (10.4 Hz)

(c) 3rd Mode (17.84 Hz)

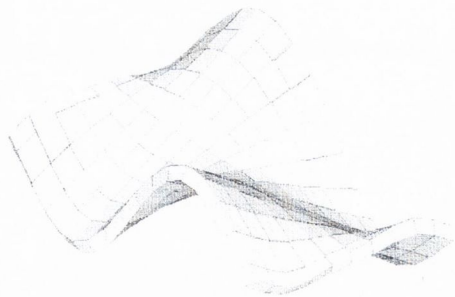

(d) 4th Mode (25.03 Hz)

Figure 6.34 (continued on following page)

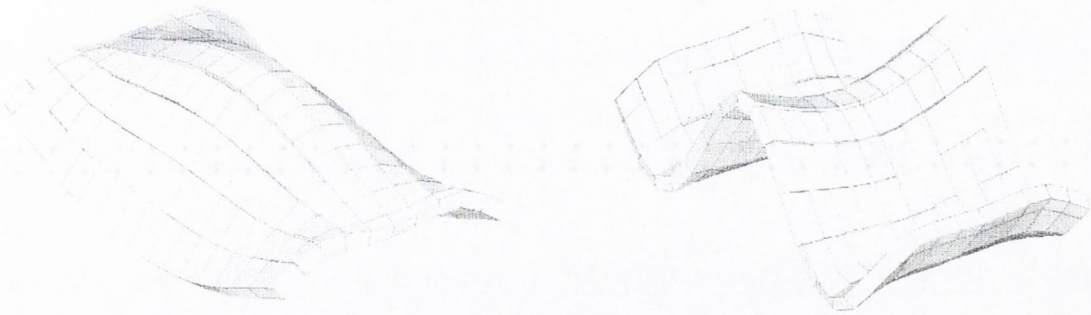

(e) 5th Mode (29.94 Hz) (f) 6th Mode (39.46 Hz)

Figure 6.34 – Modes of vibration of the slab

A finer model with elements 0.25 m long (Figure 6.32(b)) was also built to compare differences in results. The natural frequencies with the finer model are: 4.51, 10.55, 17.85, 25.50, 30.87 and 39.49 Hz. They are very close to the original model. The biggest difference in natural frequencies are for the 4th and 5th torsional mode shapes, which are represented in Figure 6.35 (compare to Figure 6.34(d) and (e)).

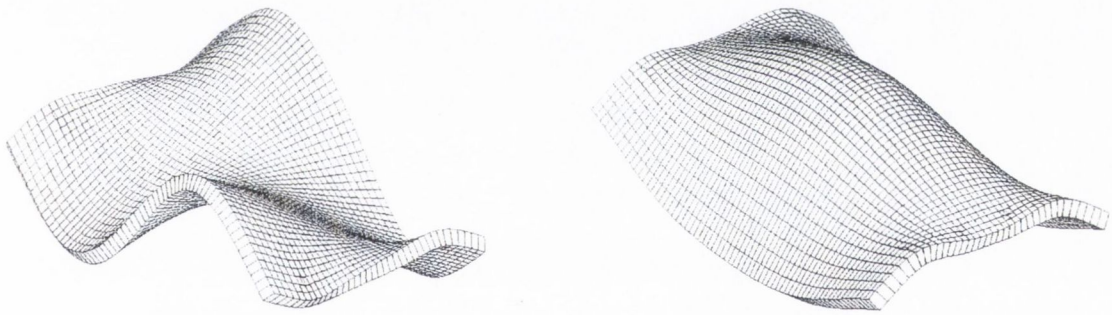

(a) 4th Mode Shape (25.50 Hz) (b) 5th Mode Shape (30.87 Hz)

Figure 6.35 – Modes of vibration with a finer mesh

A simulation of a three-axle truck (22 t) travelling along the slow lane is also carried out in both meshes. The output is very similar regardless of the mesh as shown in Figure 6.36. Accordingly, it is decided that elements 1 m long achieve enough accuracy for the purpose of simulations, saving memory space and running time.

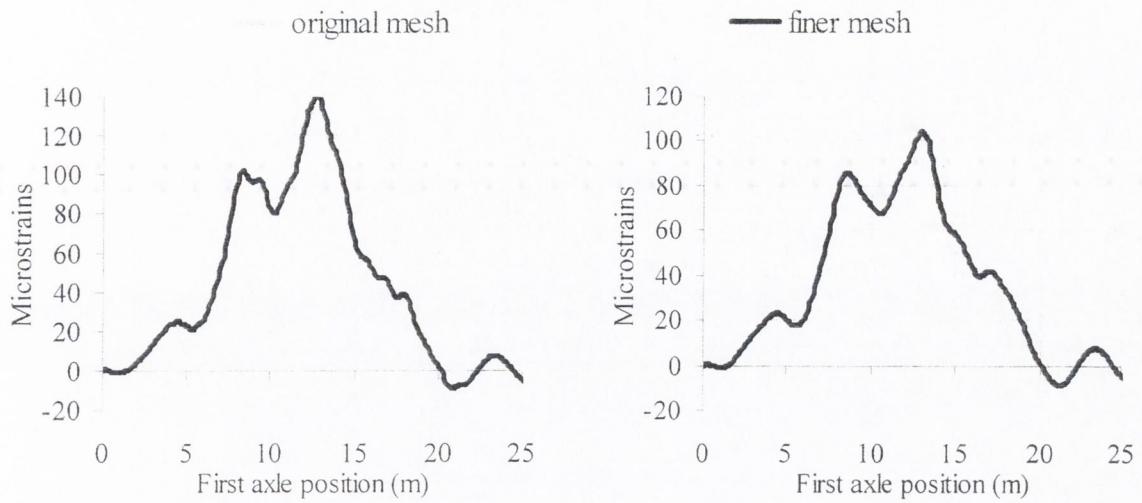

(a) Longitudinal strain, slow lane

(b) Longitudinal strain, fast lane

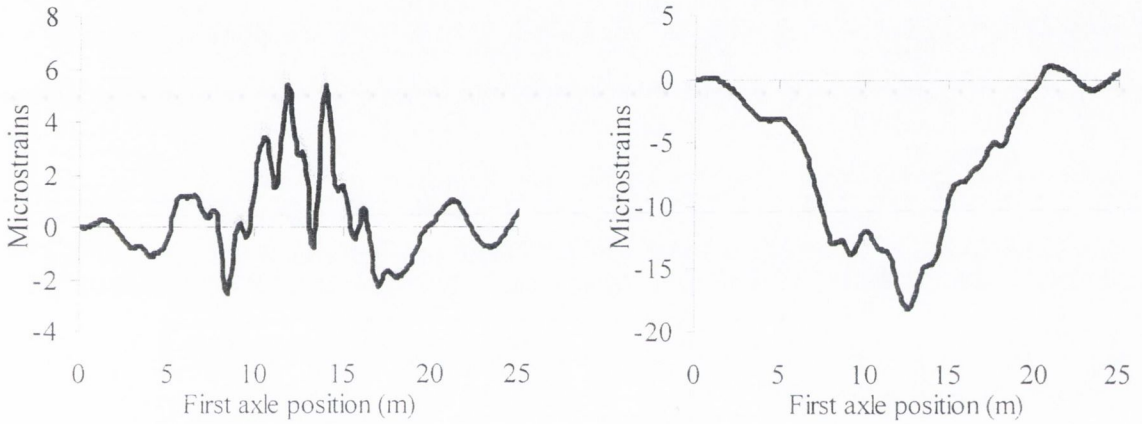

(c) Transverse strain, slow lane

(d) Transverse strain, fast lane

Figure 6.36 - Total strain caused by a 3-axle vehicle travelling at 70 km/h (longitudinal distance of the sensor from start of the bridge: 8 m; transverse location from bridge centreline: 2.5 m)

The results of strains at midspan for different transverse locations when the heaviest two-axle truck travels over the bridge at 85 km/h are illustrated in Figure 6.37. The truck wheels are located at 1 and 3 m from the centreline and the maximum longitudinal strain takes place at 3.5 m from it (Figure 6.37(a)). Longitudinal strain decreases as measurements take place towards the fast lane. Maximum transverse strain occurs in the fast lane, at the location furthest from the truck position and it decreases as measurements move towards the slow lane (Figure 6.37(d)).

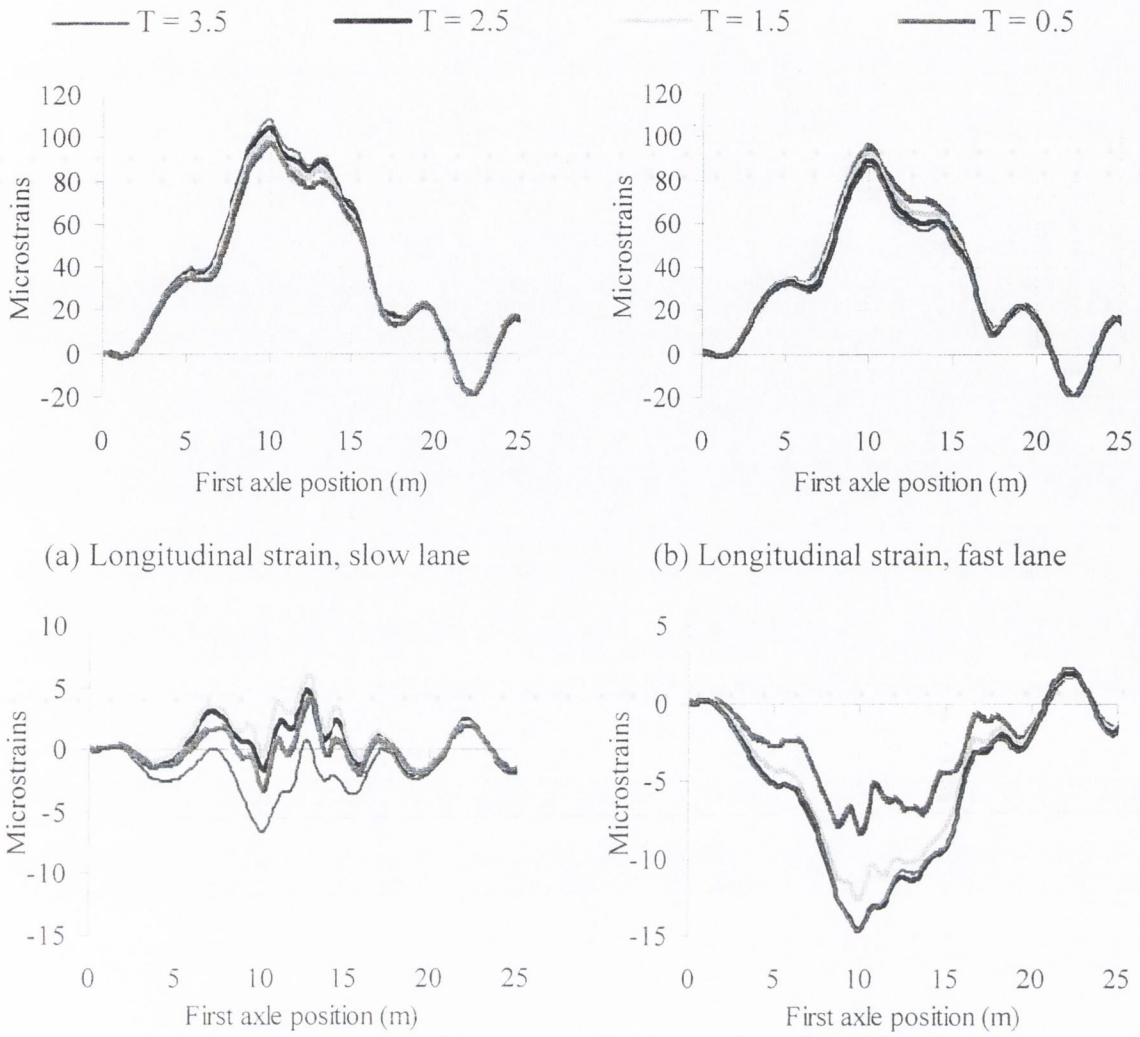

Figure 6.37 – Total strain at midspan (longitudinal distance of the sensor from start of the bridge: 8 m; *T*: Transverse location from bridge centreline)

The bridge response at 8 m from the bridge start and 2.5 m from the centreline (approximately centre of slow lane) when a two-axle truck travels over the slow lane at different speeds and weights is represented in Figure 6.38. Figures 6.38(b), (d) and (f) illustrate the importance of the dynamic component in the total transverse strain, especially at the highest speed. The dynamic component of longitudinal strain (Figures 6.38(a), (c) and (e)) is more significant at 70 and 85 km/h than at 55 km/h. The two heaviest vehicles (Figures 6.38(c) and (e)) follow a very similar strain pattern, though different in magnitude.

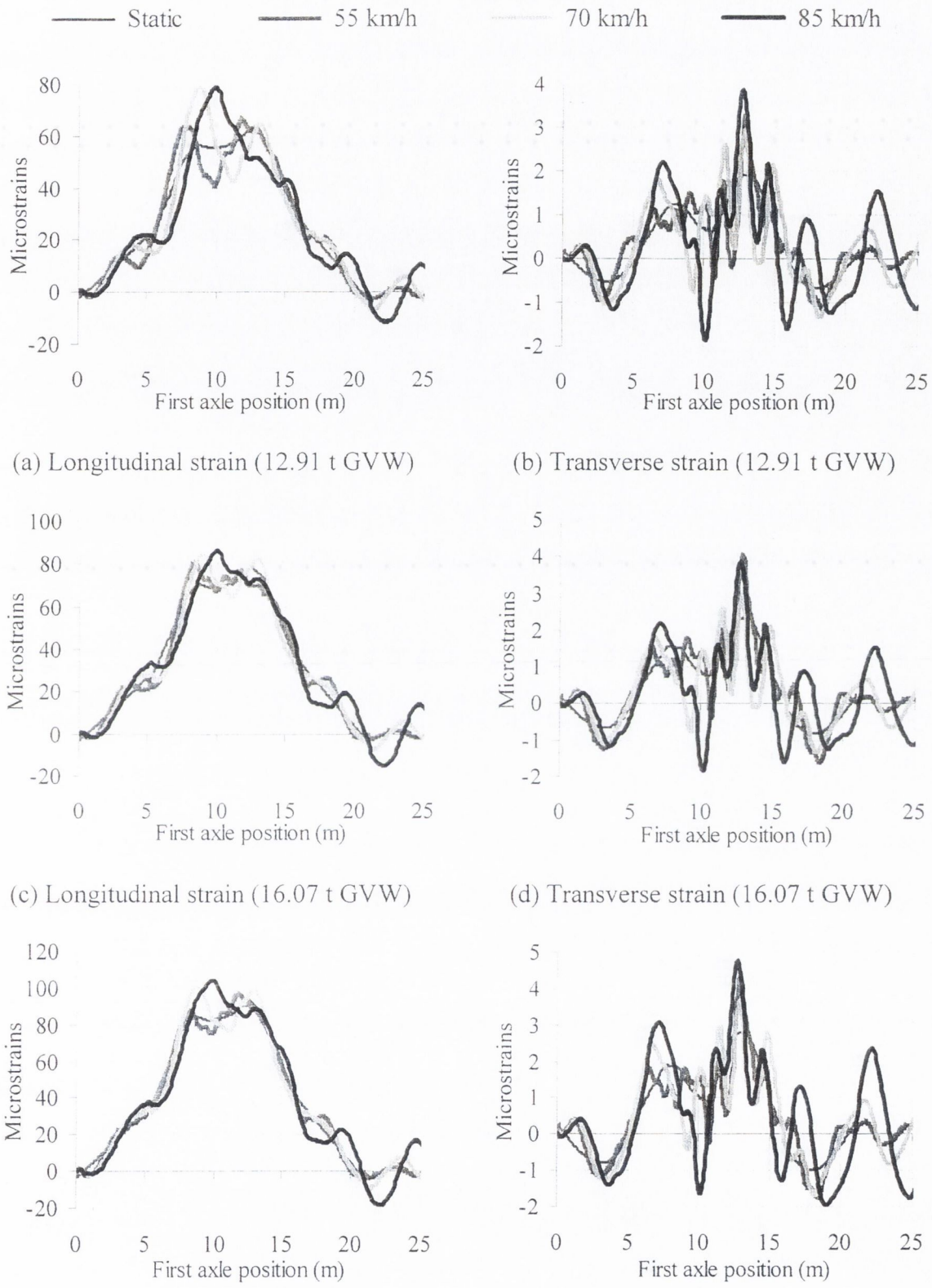

(a) Longitudinal strain (12.91 t GVW)

(b) Transverse strain (12.91 t GVW)

(c) Longitudinal strain (16.07 t GVW)

(d) Transverse strain (16.07 t GVW)

(e) Longitudinal strain (19.26 t GVW)

(f) Transverse strain (19.26 t GVW)

Figure 6.38 – Strain at midspan for different speeds and weights (sensor approx. in centre of slow lane) (GVW = gross vehicle weight)

The longitudinal and transverse strain caused by the lightest two-axle truck (12.91 t) travelling at 70 km/h is represented in the frequency domain in Figure 6.39. The spectrum of the total response reveal the presence of this dynamic component below 5 Hz. The spectrum of the static response have a significant component at frequencies close to 4.5 Hz (first natural frequency of the bridge), which is likely to cause interference with the dynamic response of the bridge.

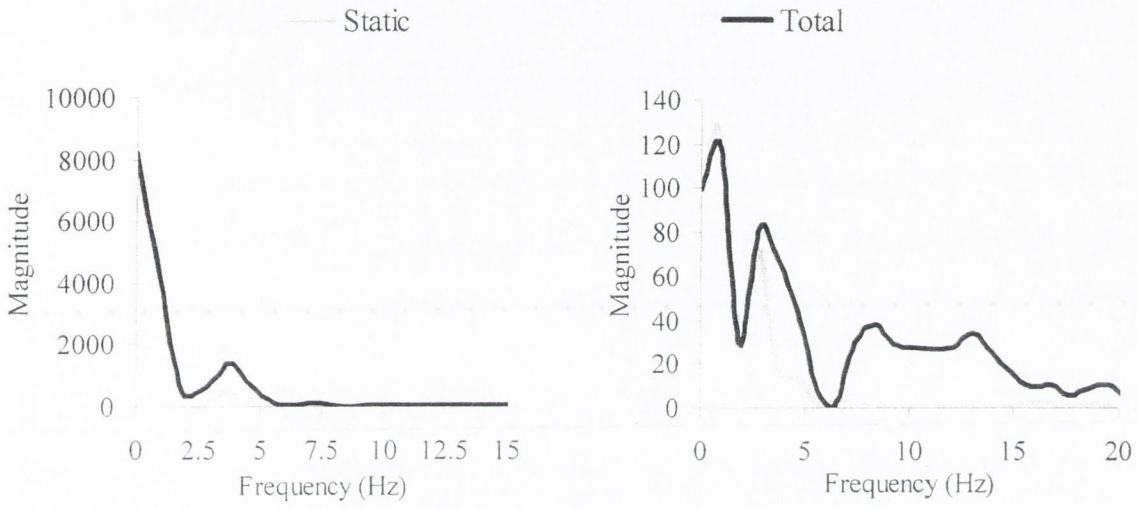

(a) Longitudinal strain (b) Transverse strain

Figure 6.39 – Spectra of strain at midspan (sensor approx. in centre of slow lane)

For vehicles travelling at speed lower than 70 km/h, the spectra of the static response will be defined for lower frequency components (as more time will be necessary to cross the bridge), and the dynamic interference will decrease.

Different Truck Transverse Locations

B-WIM systems normally add all strains transversely at each longitudinal location to compensate for the deviations introduced by different truck transverse positions. However, the bridge bends more at some particular transverse locations and the added strain is also bigger. This effect is shown in Figure 6.40. The inner wheels of the two-axle truck (16.07 t) are driven at 0, 1 and 2 m from the centreline. Four different measurements equally spaced along the bridge section are added together in Figure 6.40. It can be observed that the magnitudes differ for the same speed when the truck moves just 1 m laterally, and B-WIM systems might require further consideration of the truck transverse location.

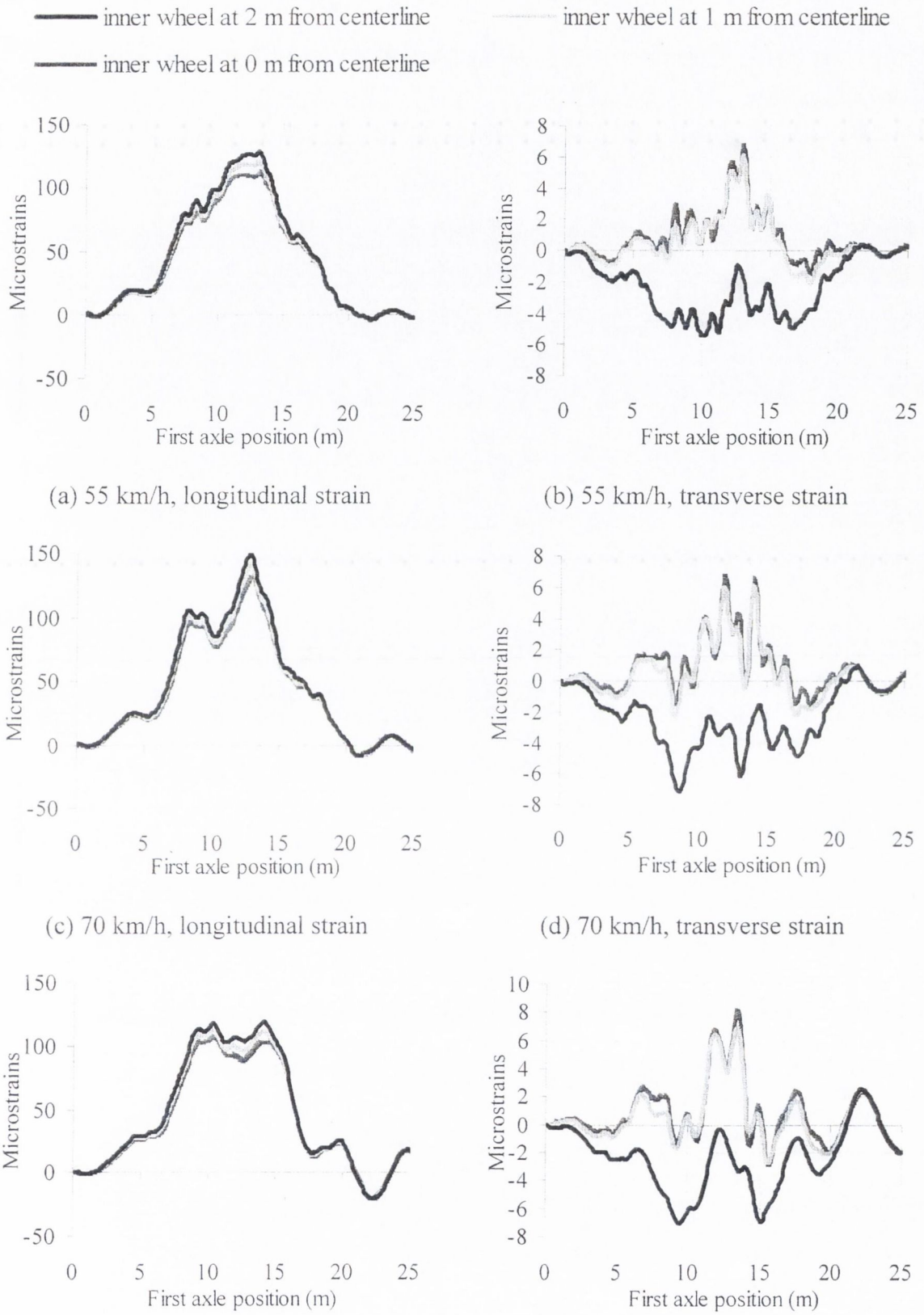

(a) 55 km/h, longitudinal strain

(b) 55 km/h, transverse strain

(c) 70 km/h, longitudinal strain

(d) 70 km/h, transverse strain

(e) 85 km/h, longitudinal strain

(e) 85 km/h, transverse strain

Figure 6.40 – Strain at midspan due to a two-axle (16.07 t) truck at different truck distances from centreline

Simultaneous Traffic Events

Figure 6.41 show the bridge response for different combinations of two-axle (16.07 t) and three-axle (22 t) trucks running in opposite directions (Figure 6.31(b)).

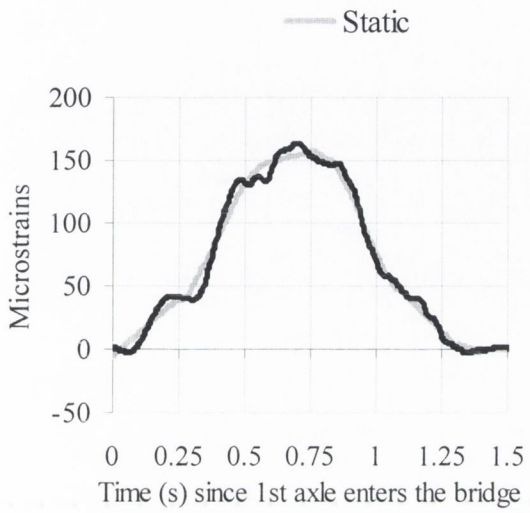

(a) 3-axle at 55 km/h and 2-axle at 70 km/h, longitudinal strain

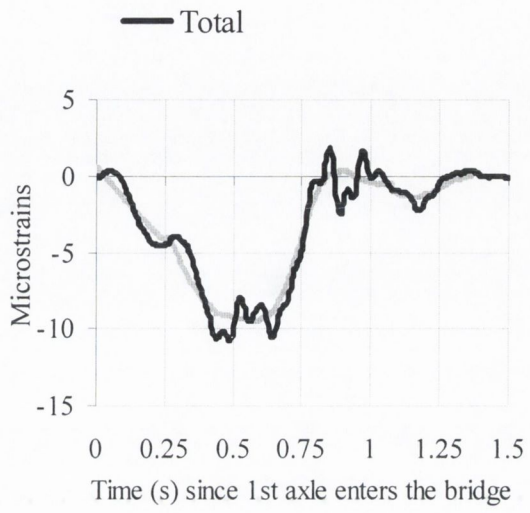

(b) 3-axle at 55 km/h and 2-axle at 70 km/h, transverse strain

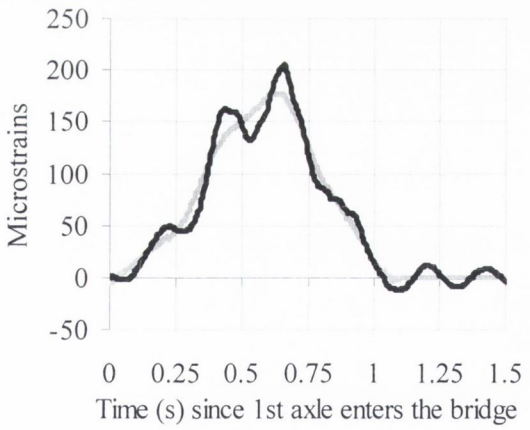

(c) 3-axle and 2-axle at 70 km/h, longitudinal strain

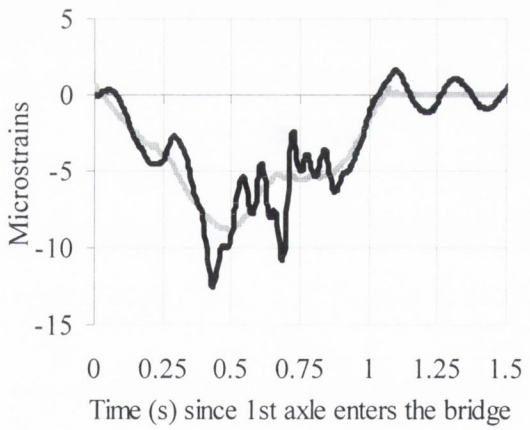

(c) 3-axle and 2-axle at 70 km/h, transverse strain

Figure 6.41 (continued on following page)

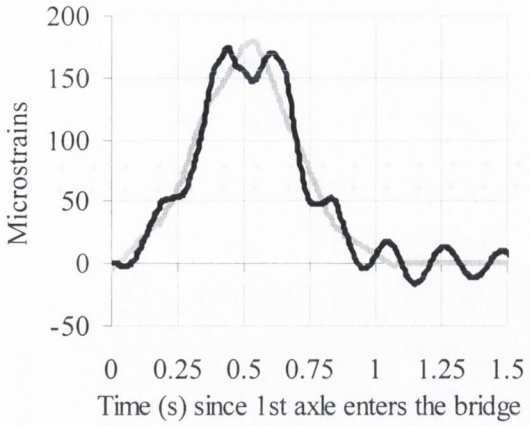

(e) 3-axle at 85 km/h and 2-axle at 70 km/h, longitudinal strain

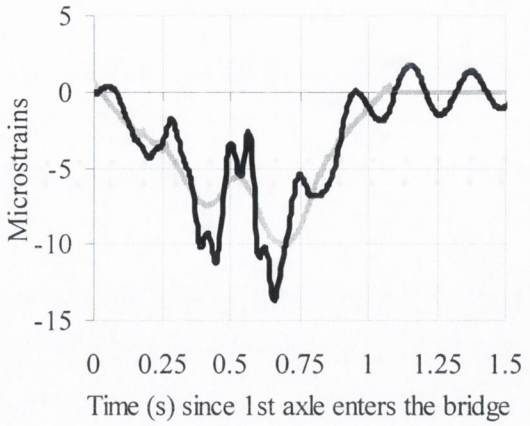

(f) 3-axle at 85 km/h and 2-axle at 70 km/h, transverse strain

Figure 6.41 – Longitudinal strain at midspan (sensor approx. in centre of slow lane)

B-WIM measurements are generally restricted to only one truck being on the bridge (Section 3.2). In the cases of Figure 6.41, the total response vibrates around the static response and it is more favourable at lower speeds from the point of view of B-WIM measurements (less amplitude and more oscillations).

6.5.2 Two-Span Isotropic Slab

A two-span isotropic bridge model is illustrated in Figure 6.42. The bridge has a uniform rectangular cross-section of 0.8 m depth. The deck is supported on four bearings at either end and on two bearings at the centre. Supports are spaced longitudinally at 18 m and horizontal translation is prevented at one end. The length of the elements along the span was chosen as 1.2 m and their width 1 m, except for the rows of elements at each edge which are 0.9 m wide and the elements at each end which are 0.5 m long.

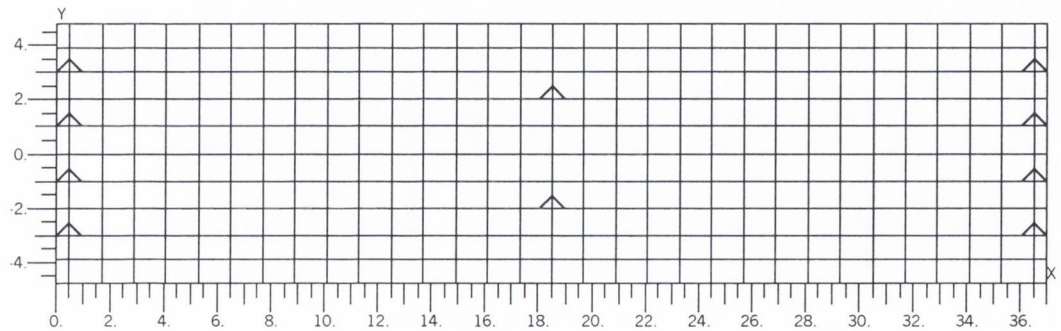

Figure 6.42 – Two-Span Slab Finite Element Model

Influence lines of longitudinal and transverse bending due to a unit axle load travelling on the slow lane are represented in Figure 6.43.

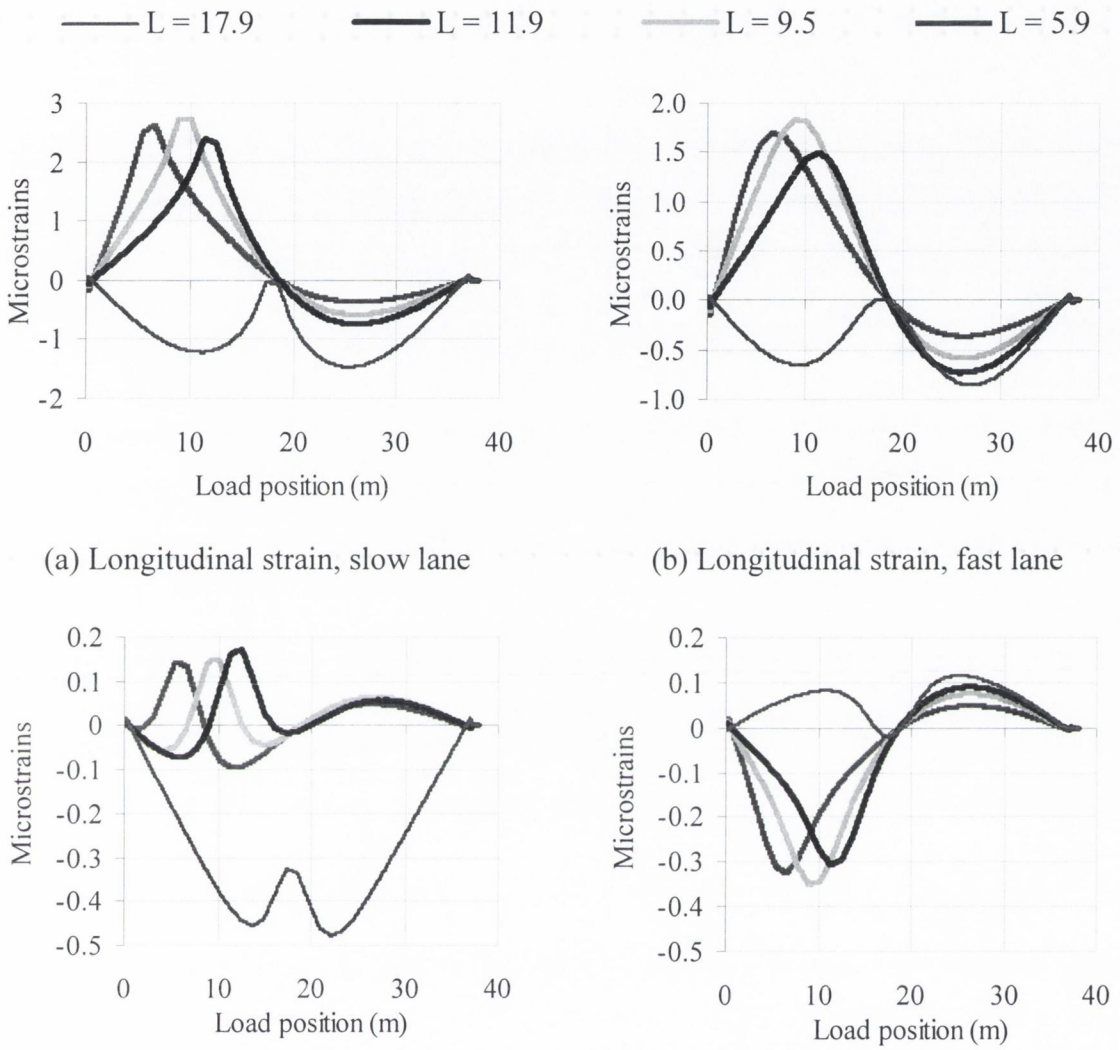

Figure 6.43 – Influence line of strain at different locations in first span (*L*: longitudinal distance of the sensor from start of the bridge; Transverse location from bridge centreline: 2.5 m)

Figure 6.44 shows the main six modes of vibration of this structure.

(a) 1st Mode (4.18 Hz)

(b) 2nd Mode (6.48 Hz)

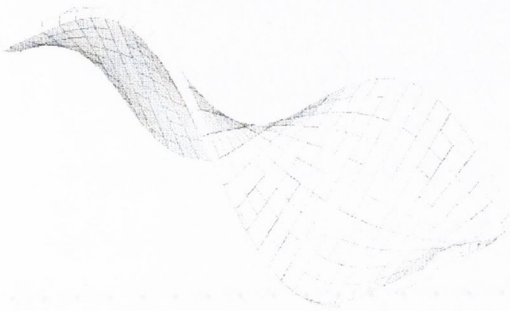

(c) 3rd Mode (11.43 Hz)

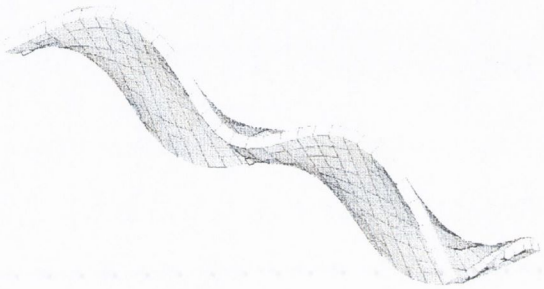

(d) 4th Mode (11.74 Hz)

(e) 5th Mode (16.62 Hz)

(f) 6th Mode (20.15 Hz)

Figure 6.44 - Modes of vibration of the Two-Span Slab

Results of simulations performed for a three-axle truck (22 t GVW) are illustrated in Figure 6.45.

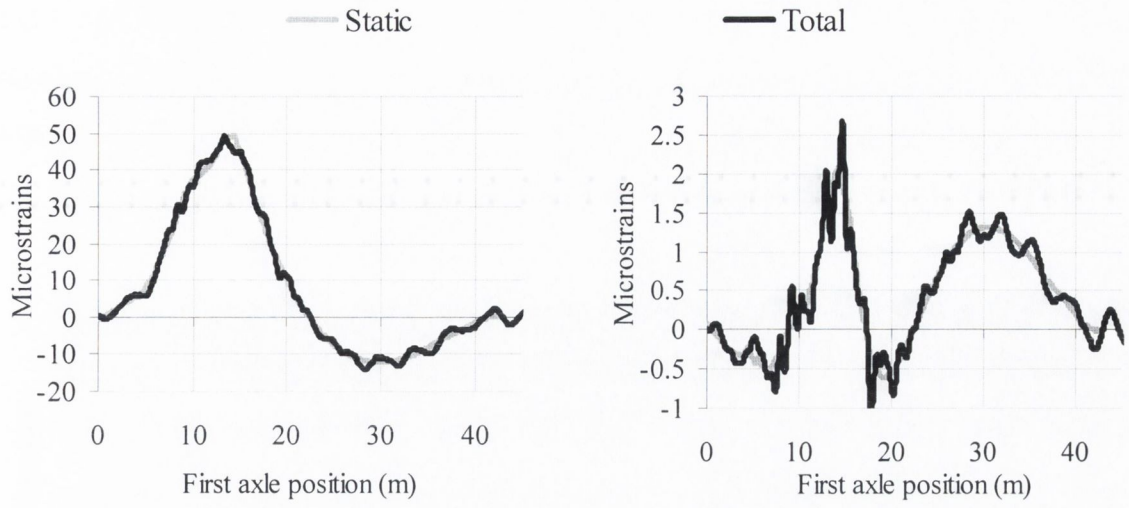

(a) 55 km/h, longitudinal strain

(b) 55 km/h, transverse strain

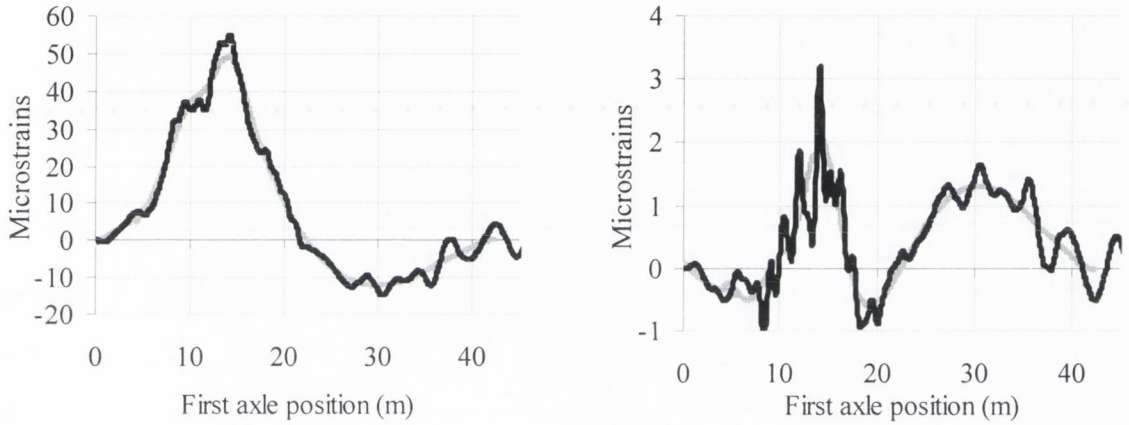

(c) 70 km/h, longitudinal strain

(d) 70 km/h, transverse strain

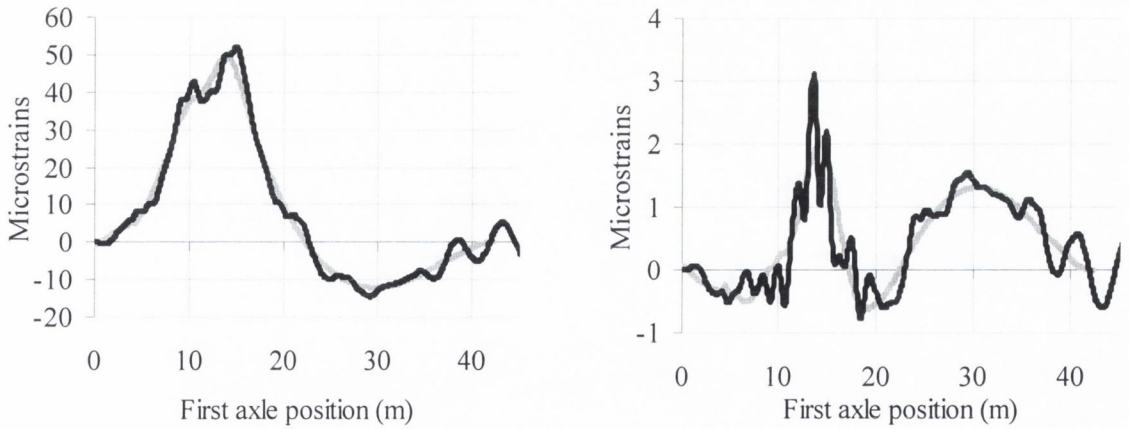

(c) 85 km/h, longitudinal strain

(c) 85 km/h, transverse strain

Figure 6.45 – Strain at midspan of first span (sensor approx. in centre of slow lane)

The results at 70 km/h are represented in the frequency domain in Figure 6.46. Though there are also significant dynamic components below 5 Hz, unlike the response of the

single span bridge, the highest component of the spectrum takes place over the zero frequency component for the longitudinal strain and it is maximum for the zero frequency component in the case of transverse bending.

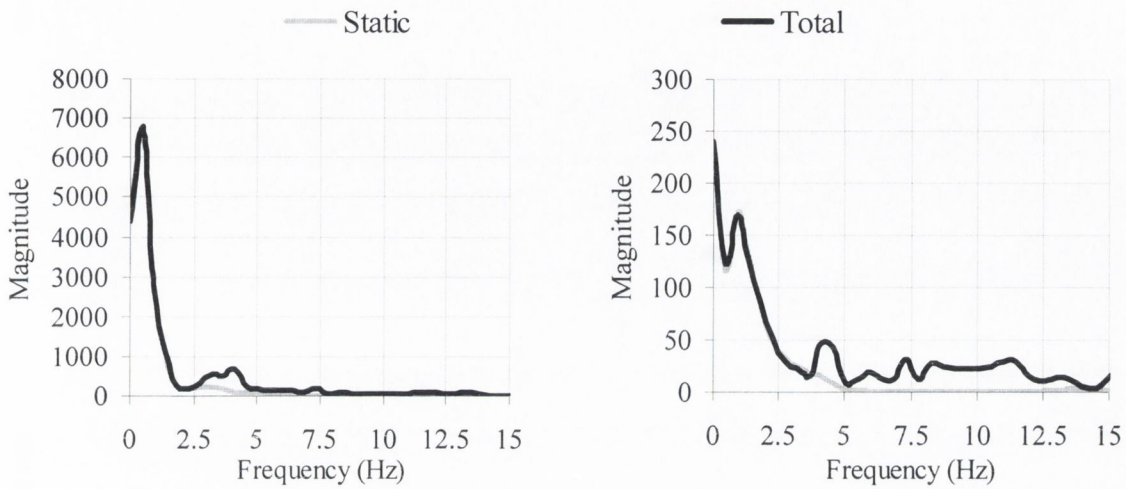

(a) Longitudinal strain (b) Transverse strain

Figure 6.46 – Spectra of strain at midspan (sensor approx. in centre of slow lane)

Sensors are less sensitive to low frequency dynamics in certain locations, i.e., near the central support. The response at this location under the slow lane is given in Figure 6.47. Figure 6.48 shows the spectra of this response for a speed of 70 km/h. Compared to the spectra in Figure 6.46, it can be seen the difference between static and total response below 5 Hz is greatly reduced.

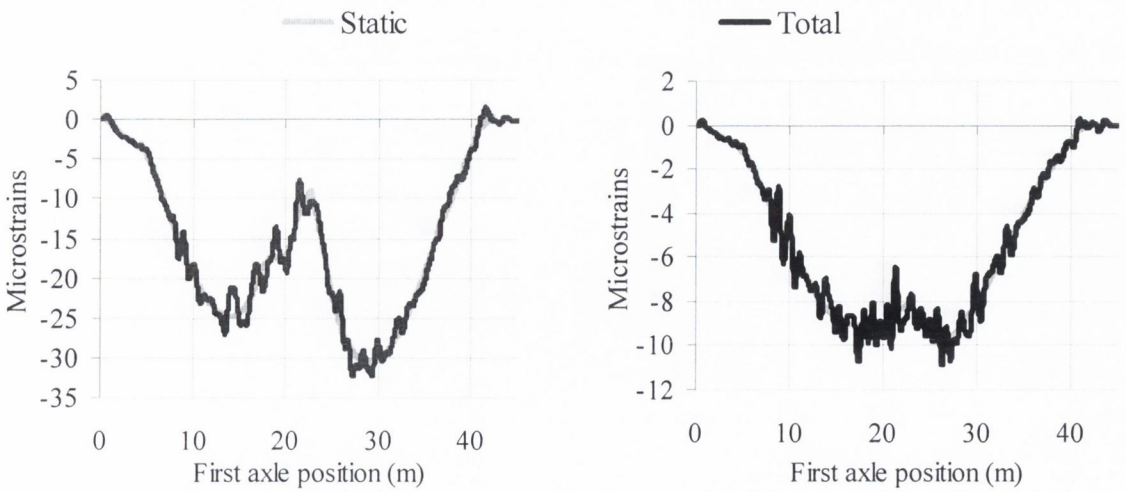

(a) 55 km/h, longitudinal strain (b) 55 km/h, transverse strain

Figure 6.47 (continued on following page)

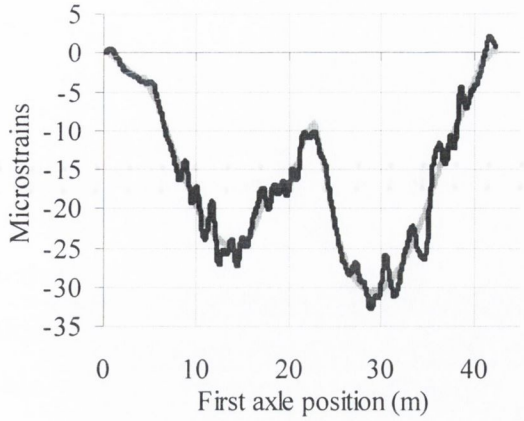

(c) 70 km/h, longitudinal strain

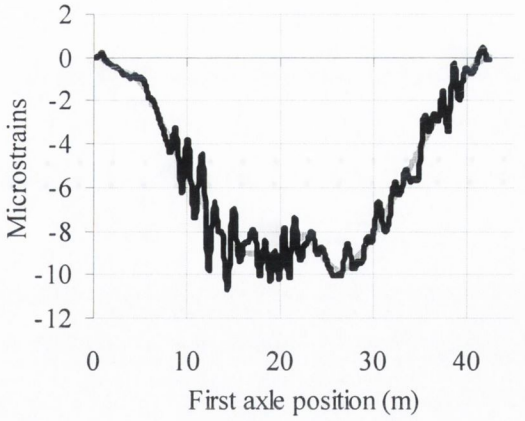

(d) 70 km/h, transverse strain

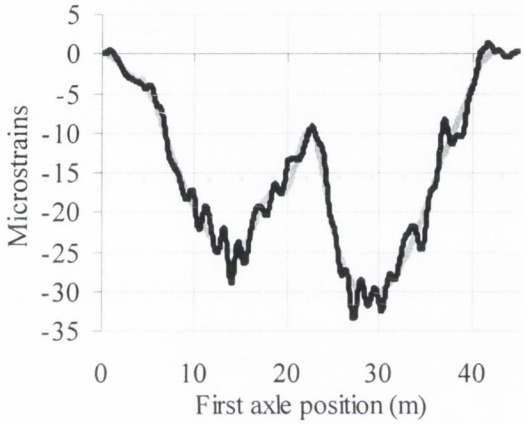

(e) 85 km/h, longitudinal strain

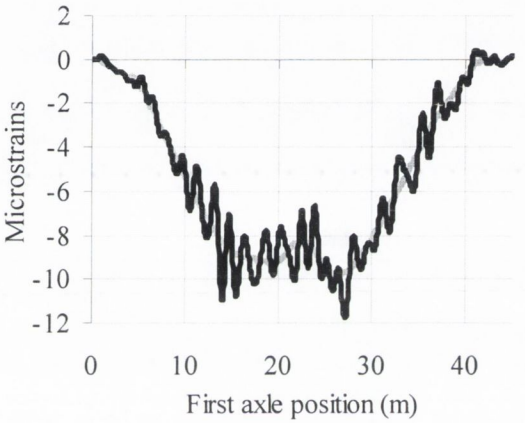

(e) 85 km/h, transverse strain

Figure 6.47 – Strain at central support (sensor approx. in centre of slow lane)

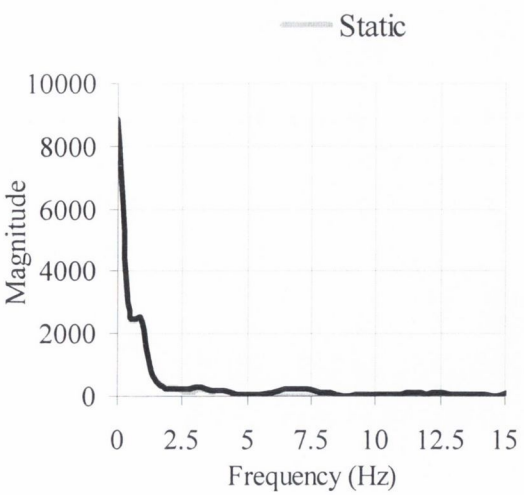

(a) Longitudinal strain

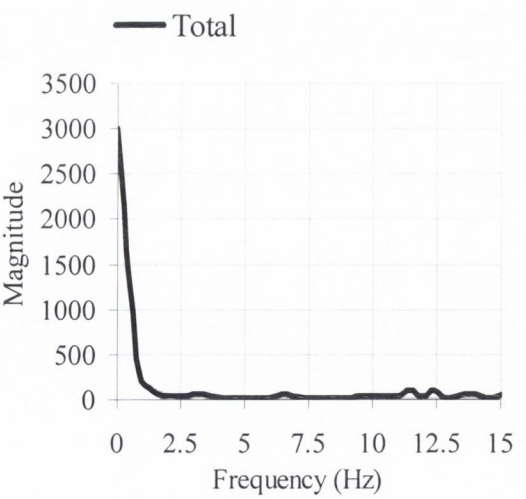

(b) Transverse strain

Figure 6.48 – Spectra of strain at central support (sensor approx. in centre of slow lane)

6.5.3 Slab with Edge Cantilever

A planar model as shown in Figure 6.37, is used to represent a bridge with edge cantilever, simply supported on three bearings at each end. The cross-section is divided into four different types of element. Three rows of plate elements are used to model each edge cantilever (element type numbers 2, 3 and 4 in Figure 6.49). The depth of these elements is calculated according to the real second moment of area and their density is also adjusted to achieve equal mass per unit length in the longitudinal direction. All elements are 1 m long. Two different elastic moduli are specified for each element type to allow for the variation of second moment of area in the two directions.

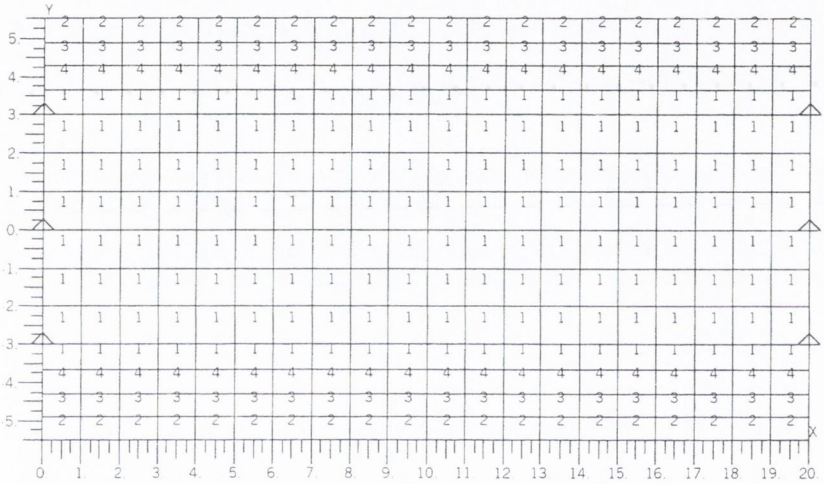

Figure 6.49 – Finite element model of slab with edge cantilever

Figure 6.50 illustrates the static response, at different bridge locations, to the passing of a unit axle load along the slow lane. Figure 6.51 shows the modes of vibration of this structure.

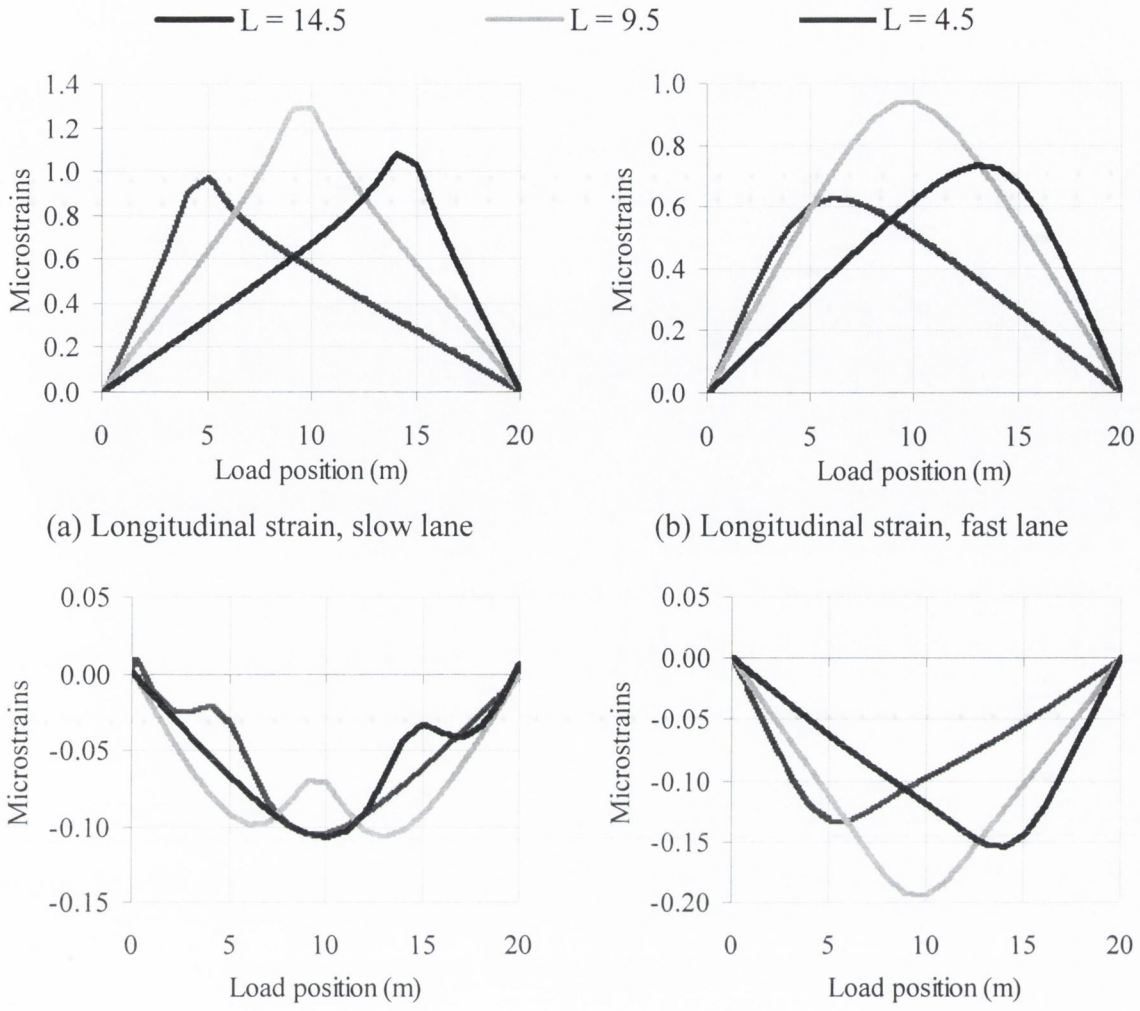

Figure 6.50 – Influence line of strain (*L*: longitudinal distance of the sensor from start of the bridge; transverse location from bridge centreline: 2.5 m)

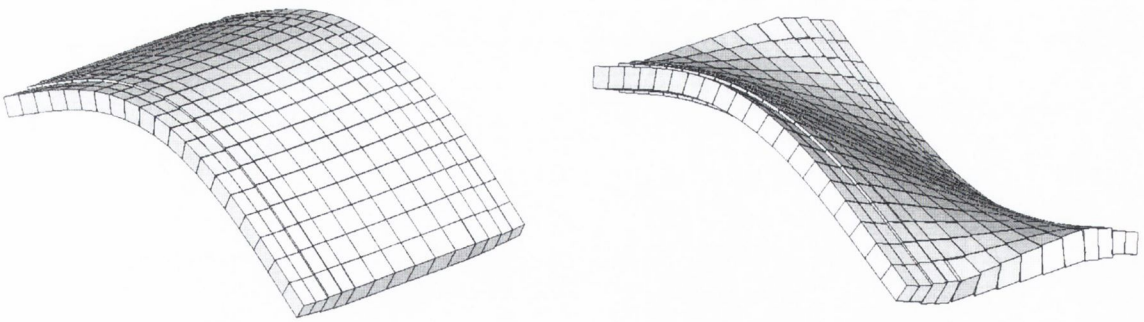

(a) 1st Mode (4.80 Hz) (b) 2nd Mode (13.03 Hz)

Figure 6.51 (continued on following page)

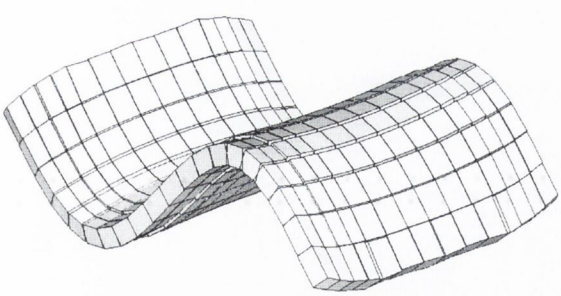

(c) 3rd Mode (18.84 Hz)

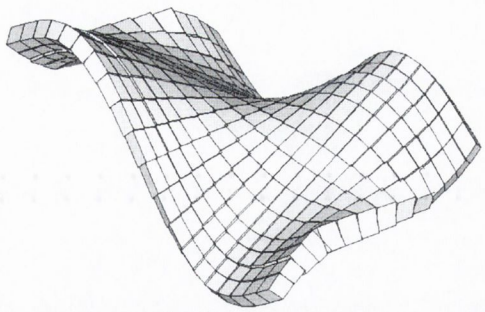

(d) 4th Mode (29.7 Hz)

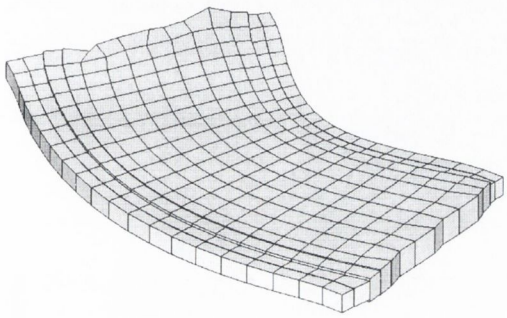

(e) 5th Mode (34.69 Hz)

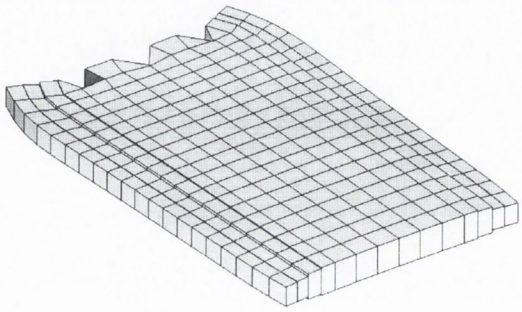

(f) 6th Mode (39.01 Hz)

Figure 6.51 - Modes of vibration of a Slab with Edge Cantilever

Results of simulations performed for the lightest three-axle truck (22 t) are illustrated in Figure 6.52. The spectra of the response at 70 km/h are represented in Figure 6.53. Differences between total and static are noticeable below 5 Hz due to the influence of the first natural frequency of the bridge (4.8 Hz).

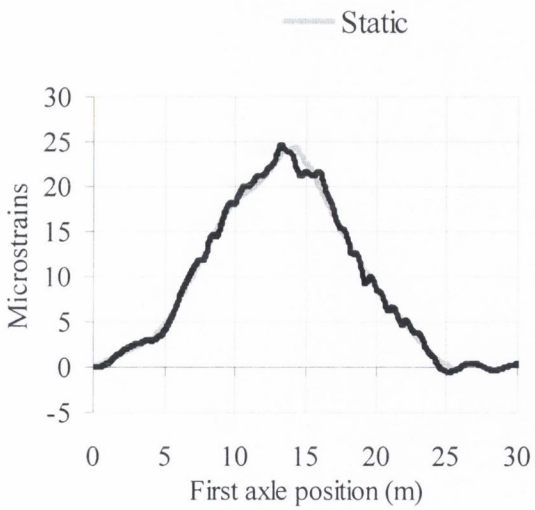

(a) 55 km/h, longitudinal strain

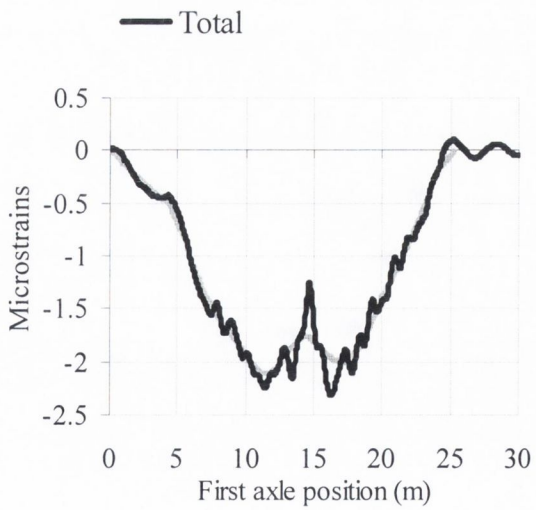

(b) 55 km/h, transverse strain

Figure 6.52 (continued on following page)

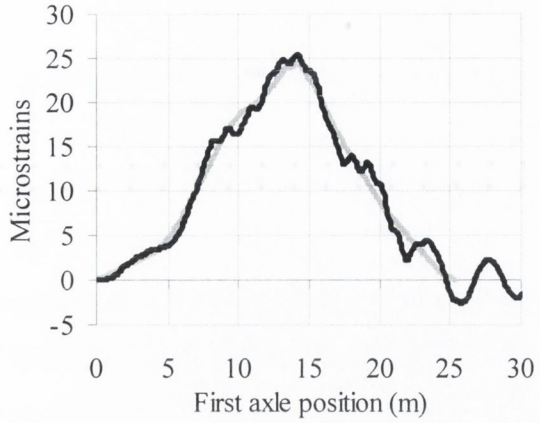

(b) 70 km/h, longitudinal strain

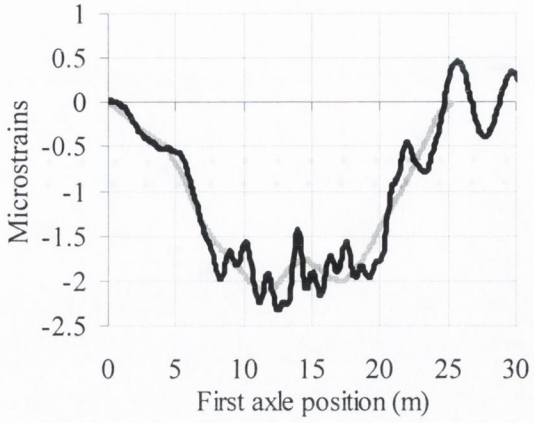

(c) 70 km/h, transverse strain

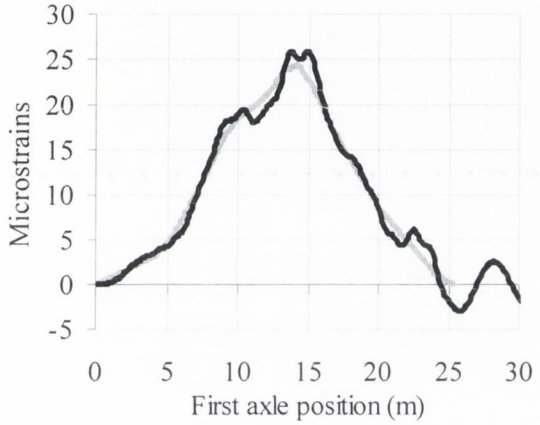

(c) 85 km/h, longitudinal strain

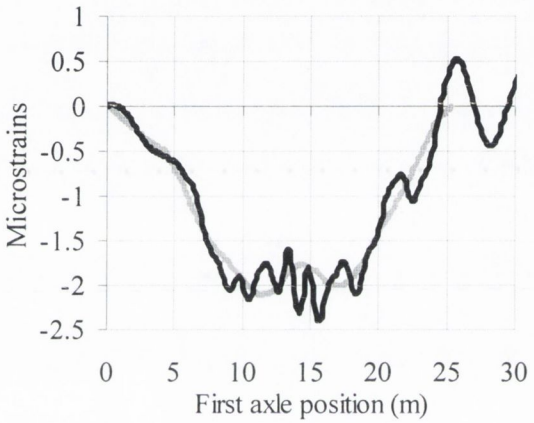

(c) 85 km/h, transverse strain

Figure 6.52 – Strain at midspan (sensor approx. in centre of slow lane)

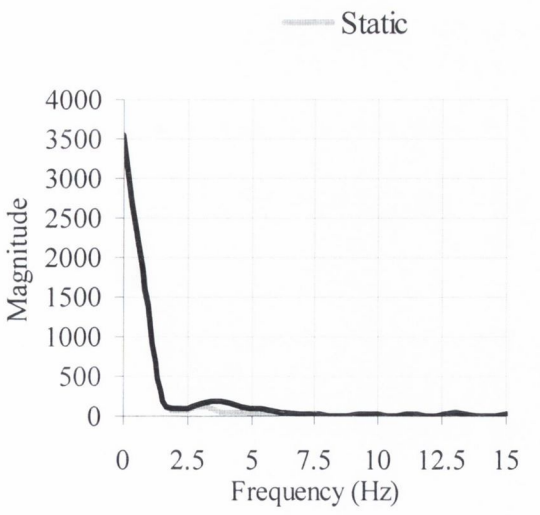

(a) Longitudinal strain

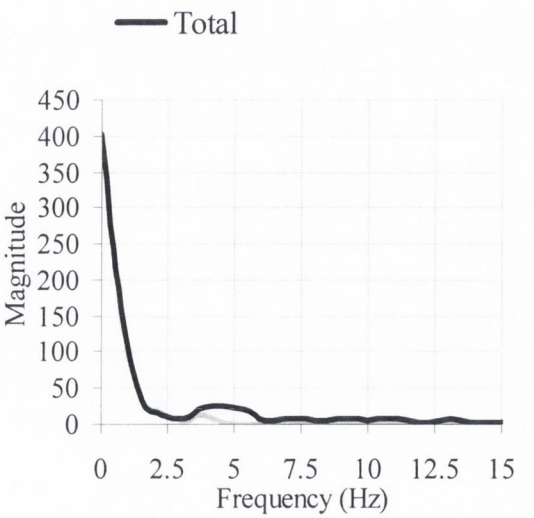

(b) Transverse strain

Figure 6.53 – Spectra of strain at midspan (sensor approx. in centre of slow lane)

6.5.4 Voided Slab Bridge

A 25 m voided slab deck, supported on four bearings at either end, is illustrated in Figure 6.54. The void stops short at each end forming solid diaphragm beams 1 m wide over the supports. The orthotropic geometry of the voided slab (different second moment of area in x and y directions) is modelled by selecting a different modulus of elasticity in the longitudinal and transverse directions (element type 1 in Figure 6.54) as recommended by O'Brien & Keogh (1999). The diaphragm beams are solid, and thus, they have the same modulus of elasticity in both directions (element type 2 in Figure 6.54).

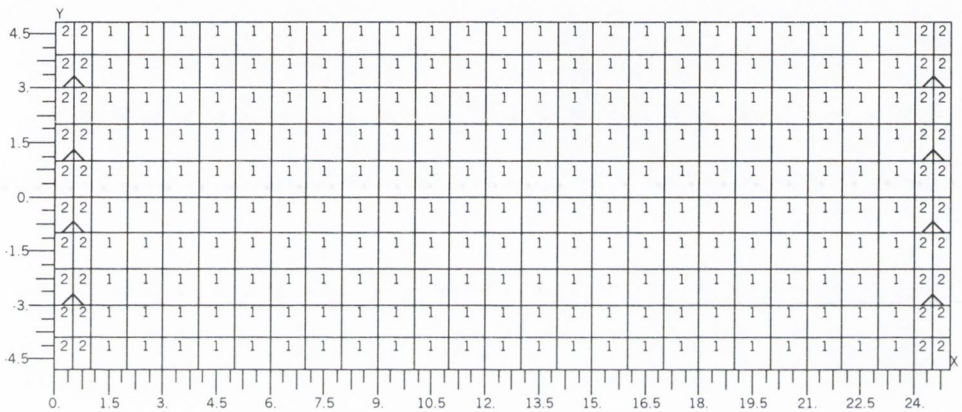

Figure 6.54 – Voided Slab Finite Element Model

Influence lines are shown in Figure 6.55.

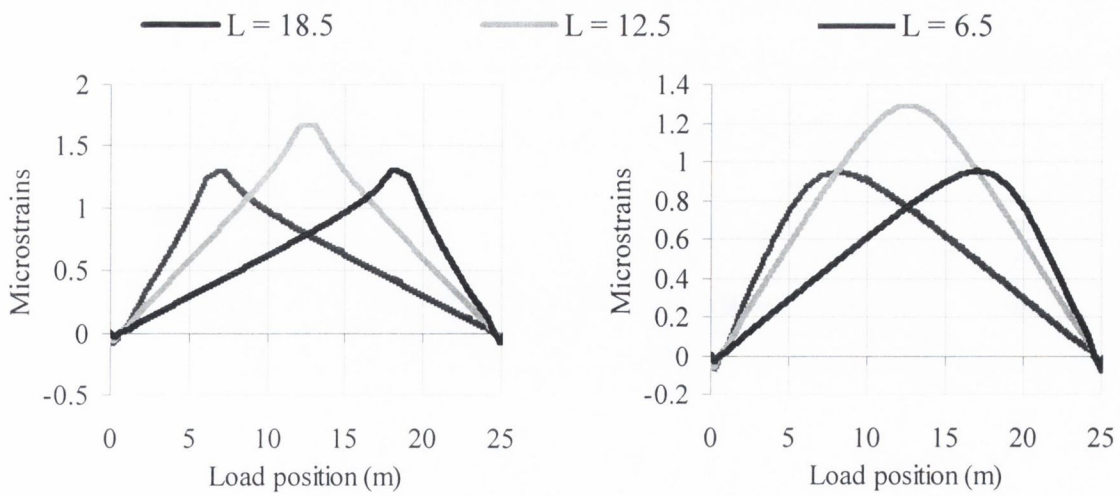

(a) Longitudinal strain, slow lane (b) Longitudinal strain, fast lane

Figure 6.55 (continued on following page)

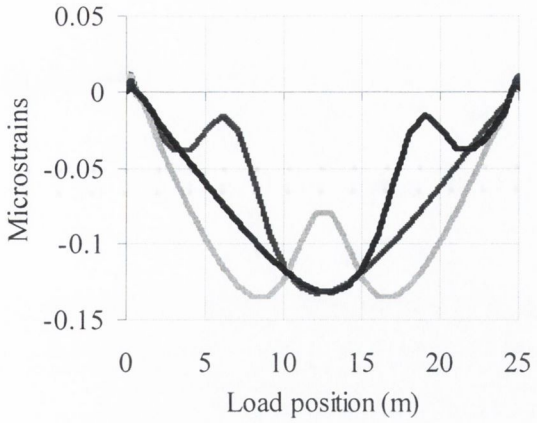

(c) Transverse strain, slow lane

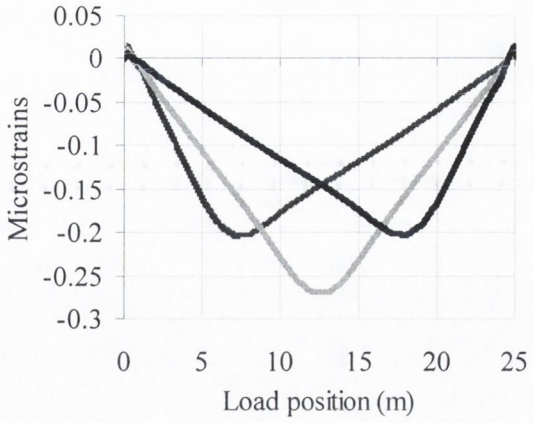

(d) Transverse strain, fast lane

Figure 6.55 – Influence line of strain (*L*: longitudinal distance of the sensor from start of the bridge; transverse location from bridge centreline: 2.5 m)

The main modes of vibration are represented in Figure 6.56.

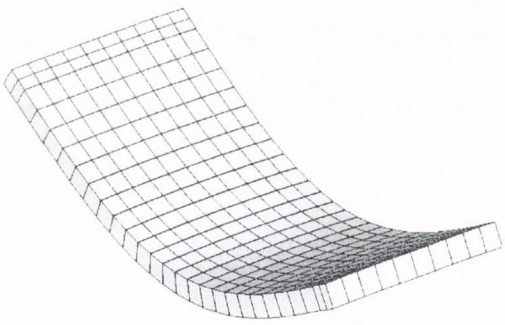

(a) 1st Mode (3.80 Hz)

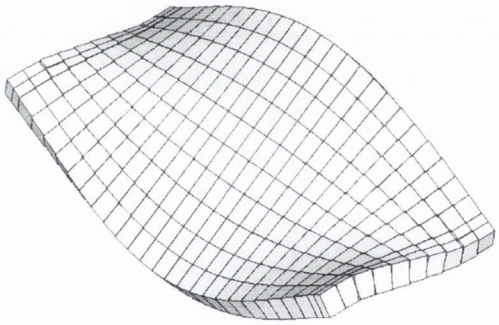

(b) 2nd Mode (12.73 Hz)

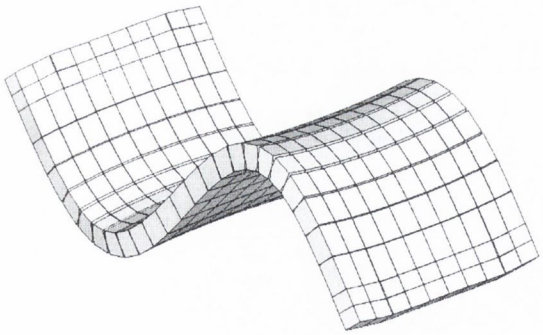

(c) 3rd Mode (15.08 Hz)

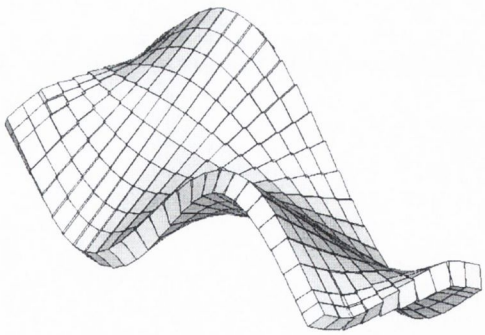

(d) 4th Mode (27.96 Hz)

Figure 6.56 (continued on following page)

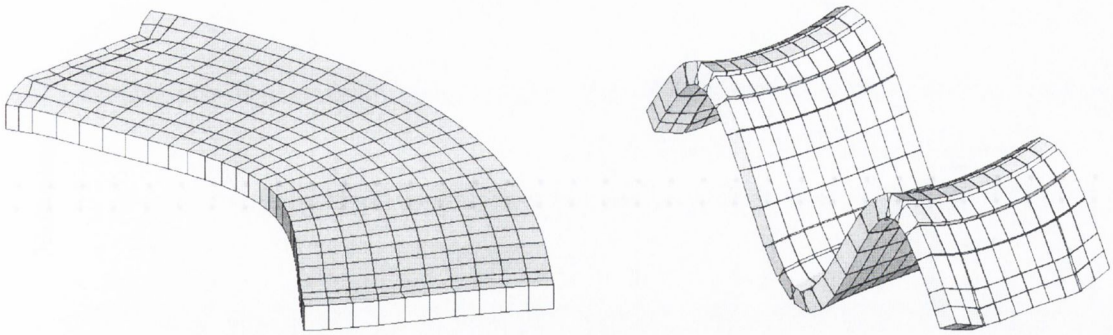

(d) 5th Mode (30.36 Hz) (e) 6th Mode (33.38 Hz)

Figure 6.56 - Modes of vibration of a Voided Slab

A three-axle truck (22 t) causes the response illustrated in Figure 6.57.

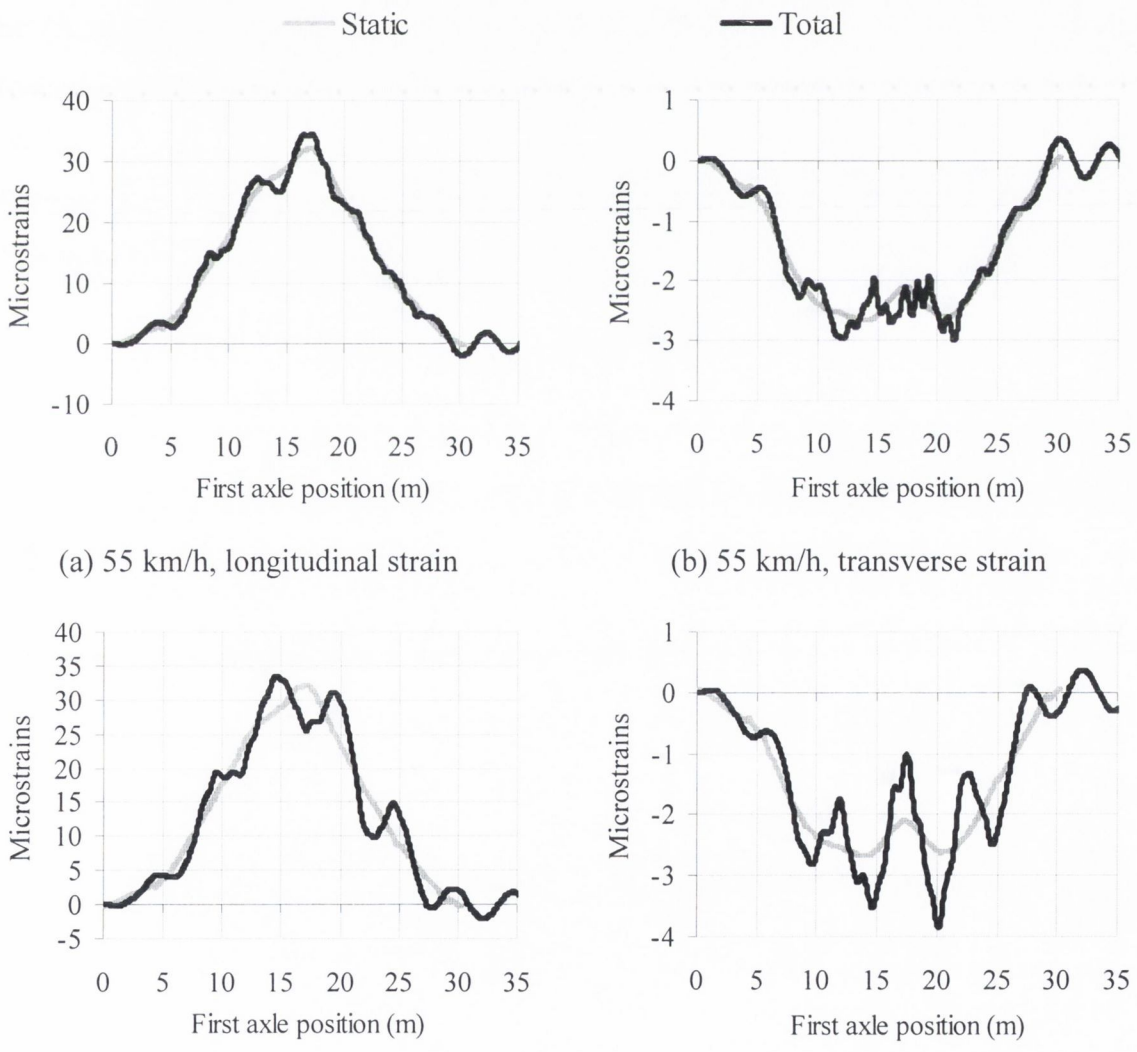

(a) 55 km/h, longitudinal strain (b) 55 km/h, transverse strain

(c) 70 km/h, longitudinal strain (d) 70 km/h, transverse strain

Figure 6.57 (continued on following page)

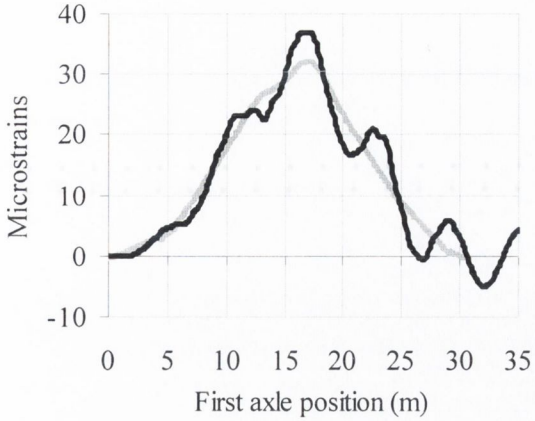

(e) 85 km/h, longitudinal strain

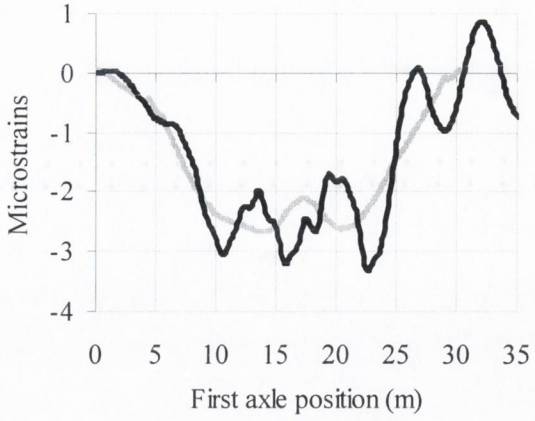

(f) 85 km/h, transverse strain

Figure 6.57 – Strain at midspan (sensor approx. in centre of slow lane)

The frequency domain representation of the response at 70 km/h shows a significant dynamic component below 5 Hz again (Figure 6.58). However, the dynamic component does not interfere as much as in previous cases (i.e. single span slab bridge). The bridge is longer, the vehicle takes more time in crossing and the static response is defined with lower frequency components than in shorter bridges.

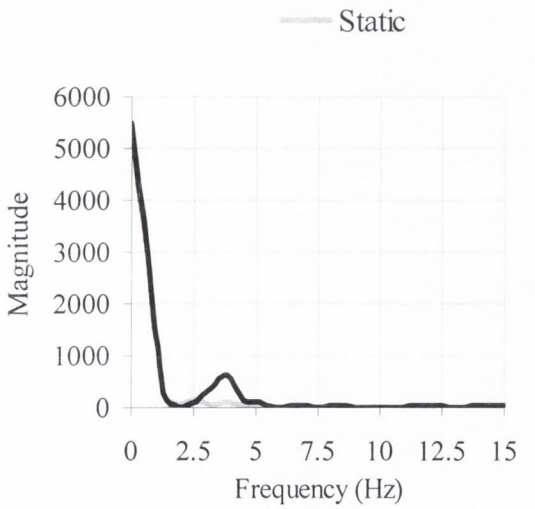

(a) Longitudinal strain

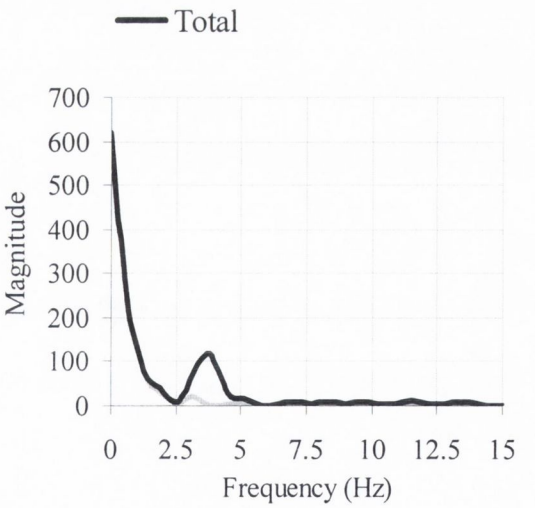

(b) Transverse strain

Figure 6.58 – Spectra of strain at midspan (sensor approx. in centre of slow lane)

6.5.5 Beam and Slab

A beam and slab deck consists of a number of longitudinal beams connected across their tops by a thin continuous structural slab. In transfer of the load longitudinally to the supports, the slab acts in concert with the beams as their top flanges. In addition it acts to ensure sharing of load between beams. Figure 6.59 shows a plan-view of the model used for the simulations. The model consists of 8 precast concrete beams supported on bearings at each end. Solid diaphragm beams are extended 1 m over the supports. The elastic modulus of the precast beams is 34 kN/mm^2 and the in-situ slab is 31 kN/mm^2. The plate elements are assigned a thickness of 0.16 m which is equal to the depth of the slab. In Figure 6.59, element type 1 represents the beam elements, element type 2 the diaphragm and element type 3 the slab elements.

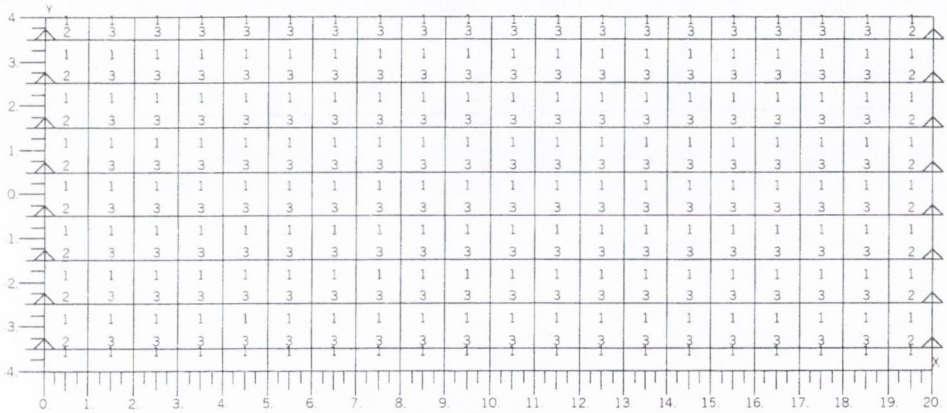

Figure 6.59 – Beam and Slab Bridge Finite Element Model

Figures 6.60 and 6.61 give influence lines for strain in plate elements and stress in beam elements respectively.

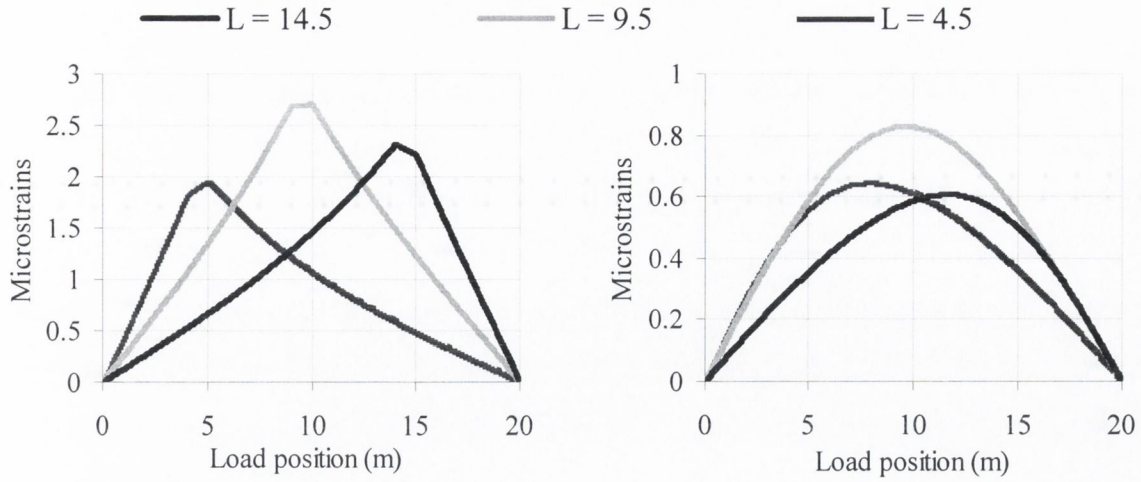

(a) Longitudinal strain, slow lane

(b) Longitudinal strain, fast lane

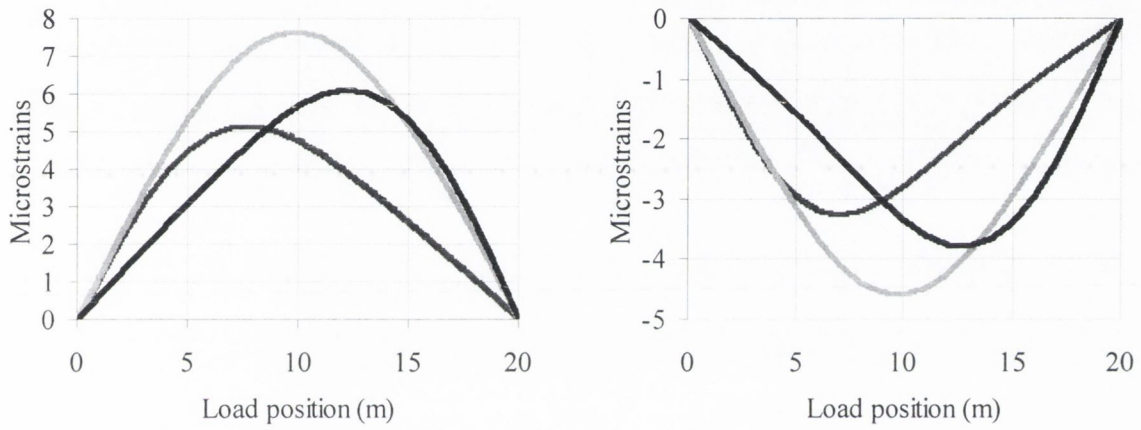

(c) Transverse strain, slow lane

(d) Transverse strain, fast lane

Figure 6.60 – Influence line of strain in plate elements (*L*: longitudinal distance of the sensor from start of the bridge; transverse location from bridge centreline: 2.0 m)

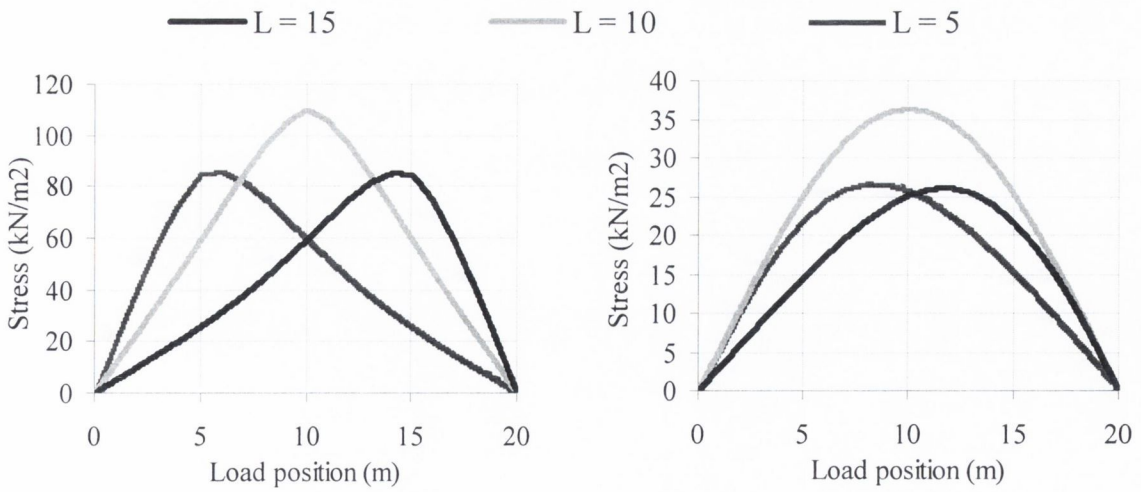

(a) Slow lane

(b) Fast lane

Figure 6.61 – Influence line of stress in beam elements (*L*: longitudinal distance of the sensor from start of the bridge; transverse location from bridge centreline: 1.5 m)

The modes of vibration of this beam and slab model are given in Figure 6.62.

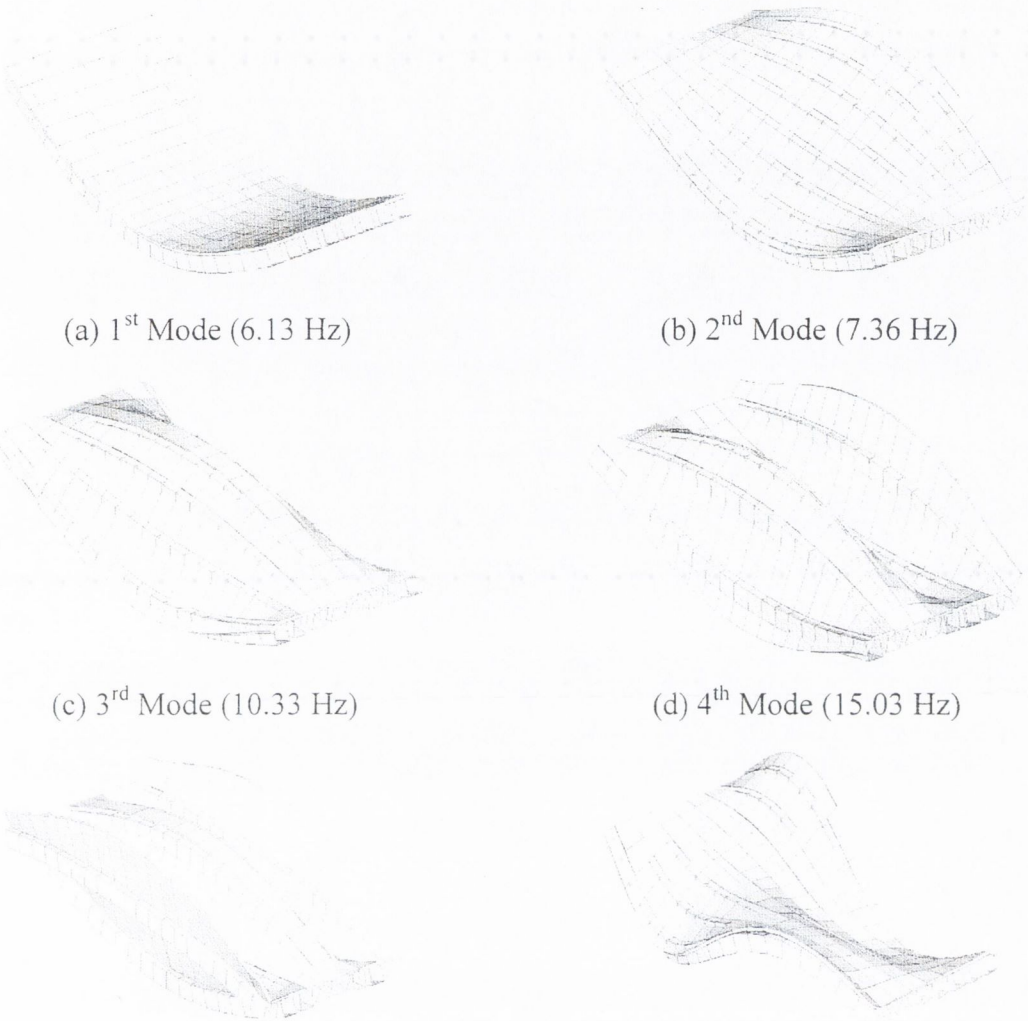

(a) 1st Mode (6.13 Hz)

(b) 2nd Mode (7.36 Hz)

(c) 3rd Mode (10.33 Hz)

(d) 4th Mode (15.03 Hz)

(e) 5th Mode (22.11 Hz)

(f) 6th Mode (22.85 Hz)

Figure 6.62 - Modes of vibration of a Beam and Slab Bridge

Figure 6.63 illustrates the results of the simulation for the lightest three-axle truck. In this model, transverse bending is more significant than longitudinal bending.

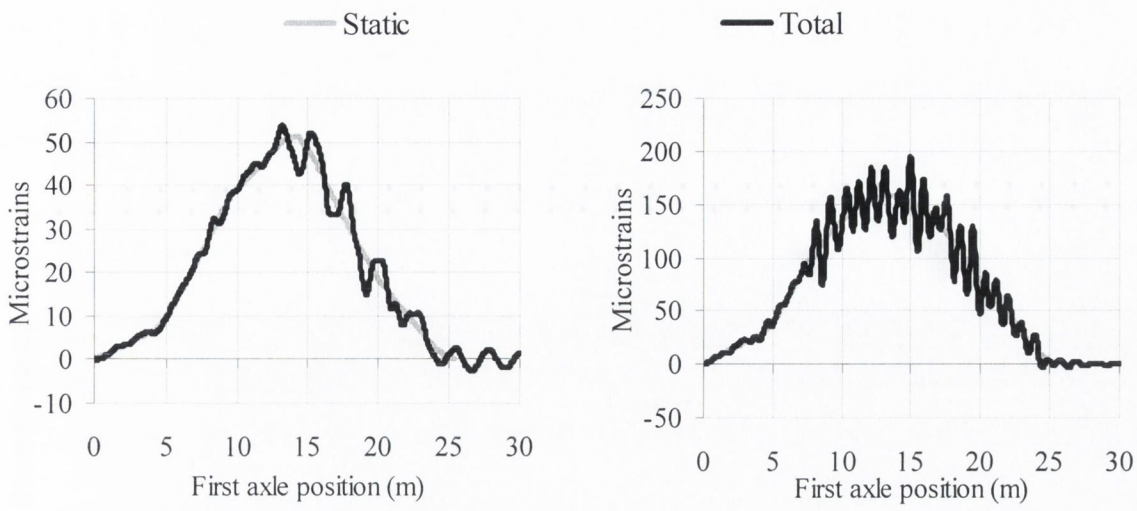

(a) 55 km/h, longitudinal strain

(b) 55 km/h, transverse strain

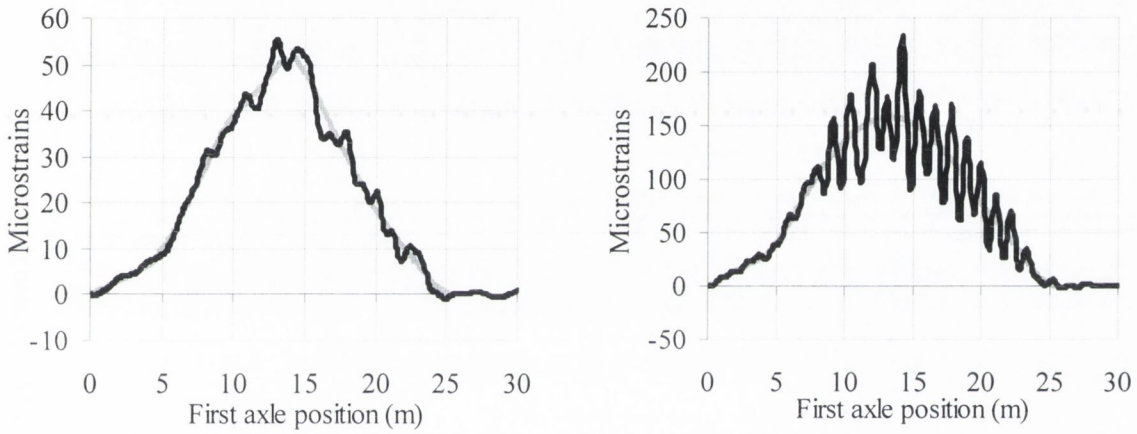

(c) 70 km/h, longitudinal strain

(d) 70 km/h, transverse strain

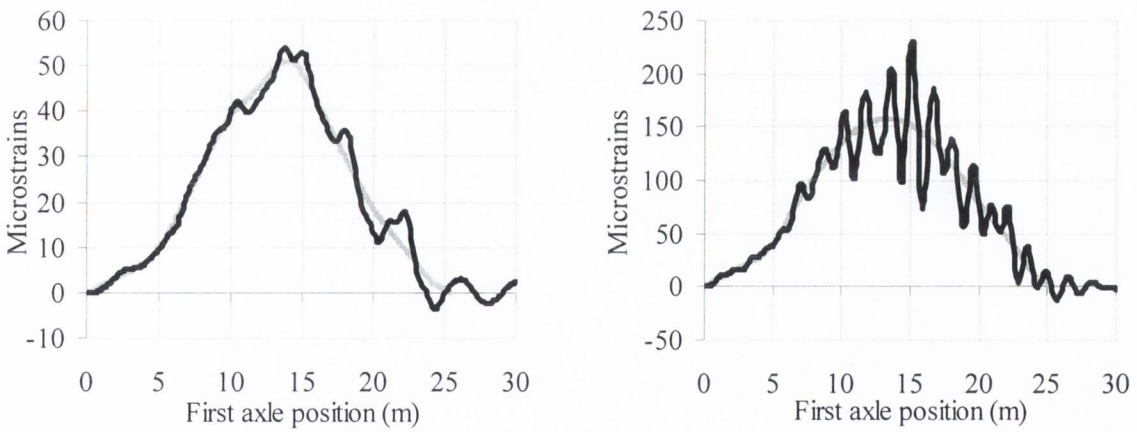

(e) 85 km/h, longitudinal strain

(f) 85 km/h, transverse strain

Figure 6.63 – Strain at midspan (sensor approx. in centre of slow lane)

Figure 6.64 represents the stress in a beam in a sensor located at 0.5 m from the plate element whose strain is shown in Figure 6.63. As expected, the longitudinal strain of Figure 6.63 and the stress in Figure 6.64 follow very similar patterns.

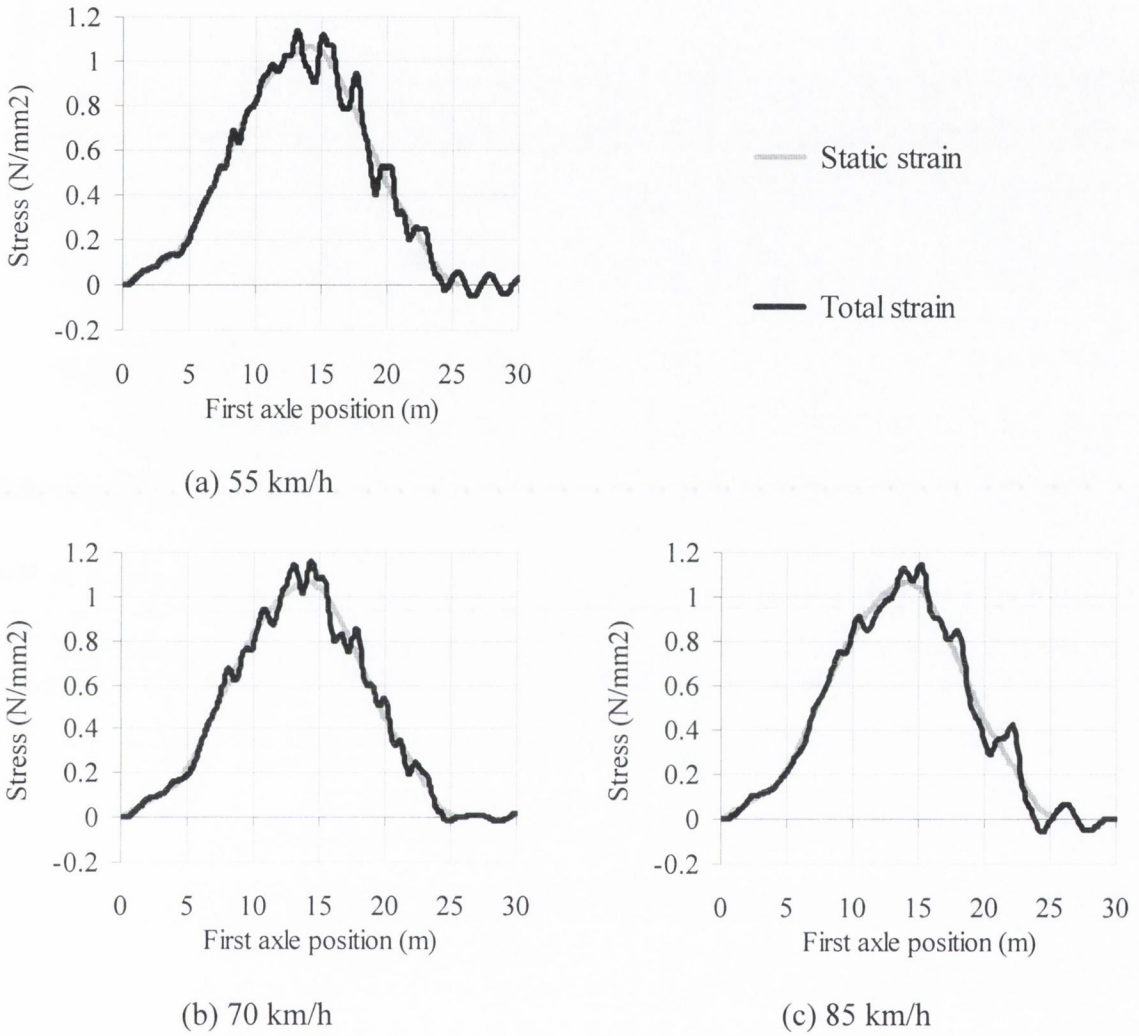

(a) 55 km/h

(b) 70 km/h

(c) 85 km/h

Figure 6.64 – Stress in beam at midspan (sensor in 2nd beam from section centre)

Figure 6.65 shows the spectra of Figure 6.63 for the case of 70 km/h speed. The differences between total and static are less in the case of transverse bending for frequencies below 5 Hz. The frequency components of the static response are more scattered in the case of longitudinal bending due to the 'sharper' shape of the influence line.

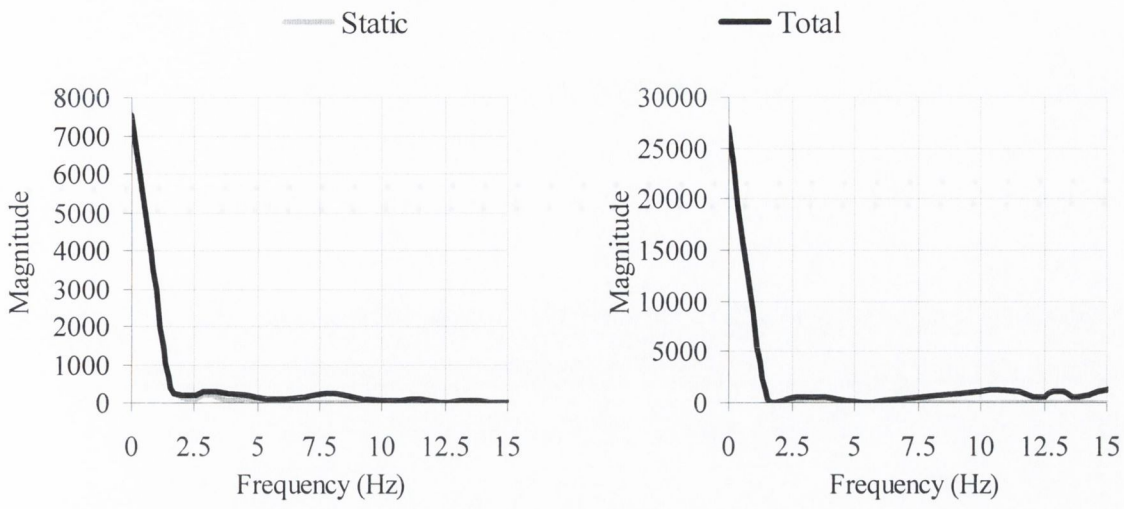

(a) Longitudinal strain (b) Transverse strain

Figure 6.65 - Spectra of strain at midspan (sensor approx. in centre of slow lane)

6.5.6 Skew

Most of bridge decks built recently are likely to have some form of skew. These bridges are subjected to considerable torsion and the direction of maximum strain changes across the width from near parallel to span at the edge to near perpendicular to the abutment in central regions. A 45° skew model as shown in Figure 6.54 was analysed. The slab deck is 0.6 m in depth.

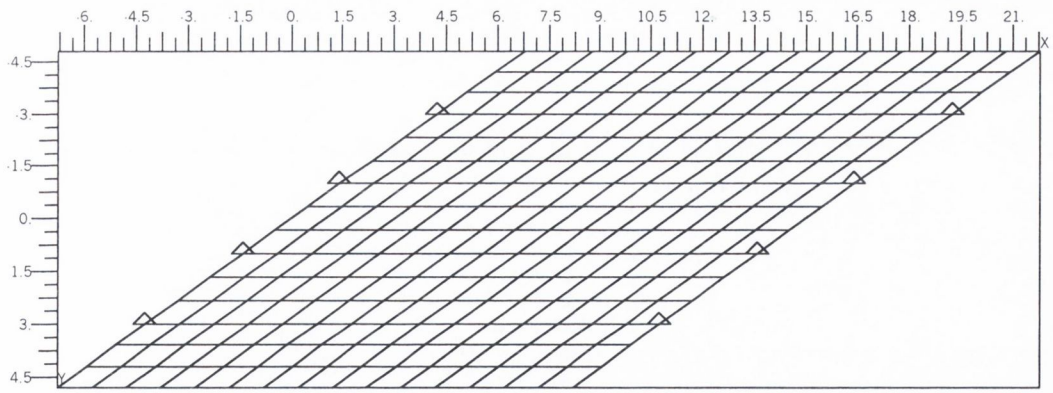

Figure 6.66 – Skew Bridge

The influence lines due to a unit axle on the slow lane are represented in Figure 6.67.

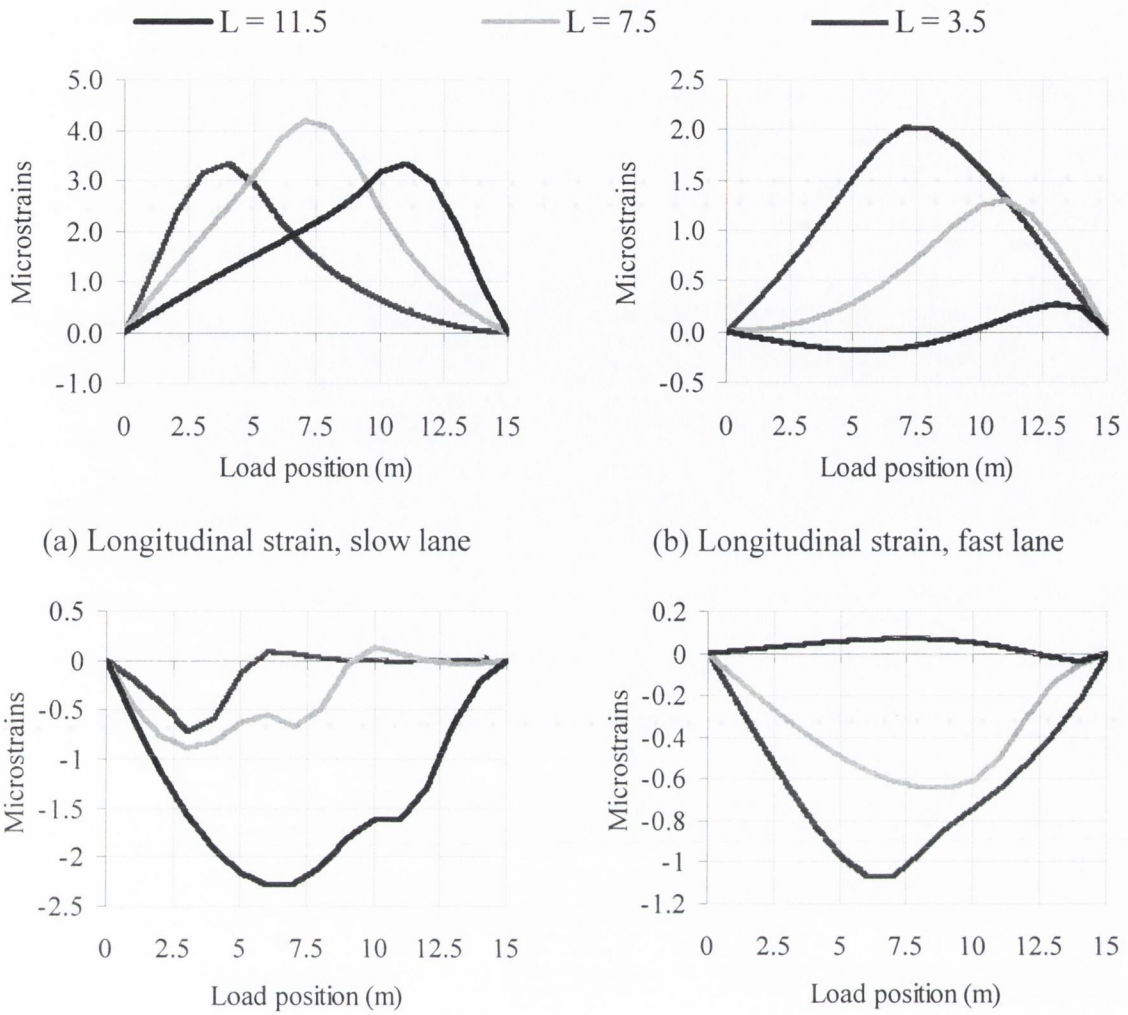

(a) Longitudinal strain, slow lane

(b) Longitudinal strain, fast lane

(c) Transverse strain, slow lane

(d) Transverse strain, fast lane

Figure 6.67 – Influence line of strain (*L*: longitudinal distance of the sensor from start of the bridge; transverse location from bridge centreline: 2.0 m)

The main modes of vibration are represented in Figure 6.68. The model was tested with a mesh based on triangular elements which gave the same modes of vibration.

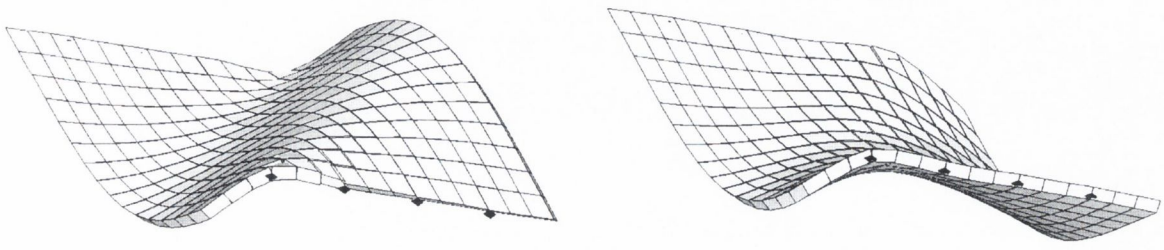

(a) 1st Mode (7.41 Hz)

(b) 2nd Mode (7.96 Hz)

Figure 6.68 (continued on following page)

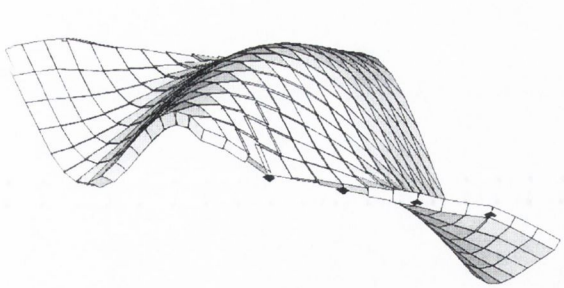

(c) 3rd Mode (19 Hz)

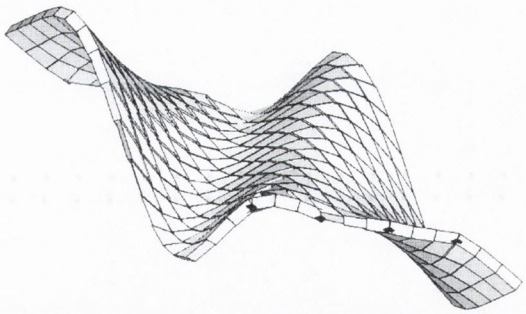

(d) 4th Mode (23.27 Hz)

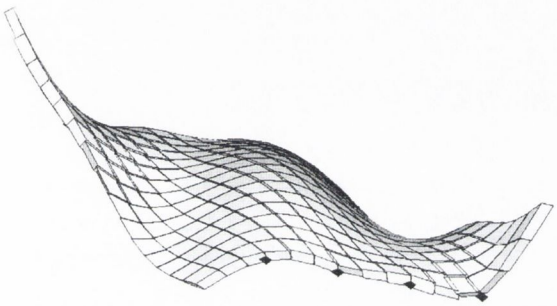

(c) 5th Mode (33.33 Hz)

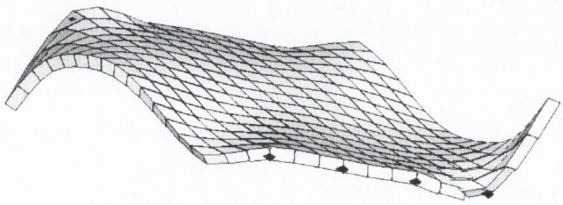

(d) 6th Mode (35.34 Hz)

Figure 6.68 – Modes of Vibration of a Skew Bridge

Results of simulations performed for a three-axle truck (22 t GVW) crossing the slow lane are illustrated in Figure 6.69.

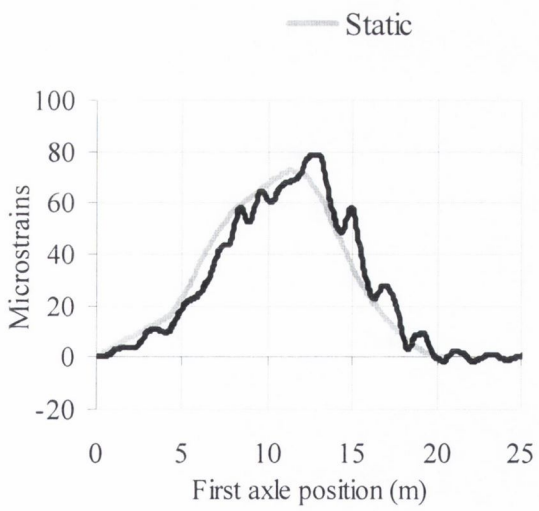

(a) 55 km/h, longitudinal strain

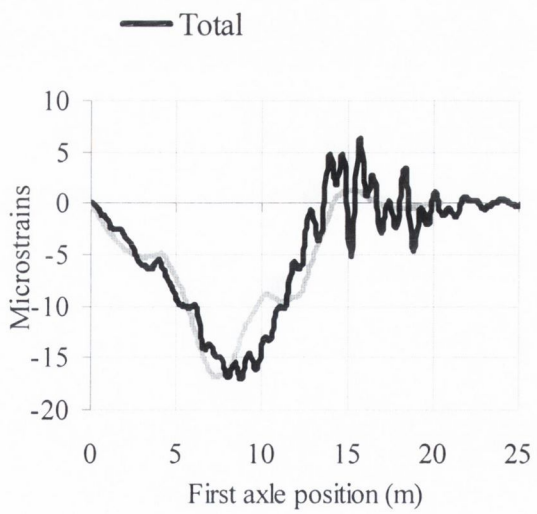

(b) 55 km/h, transverse strain

Figure 6.69 (continued on following page)

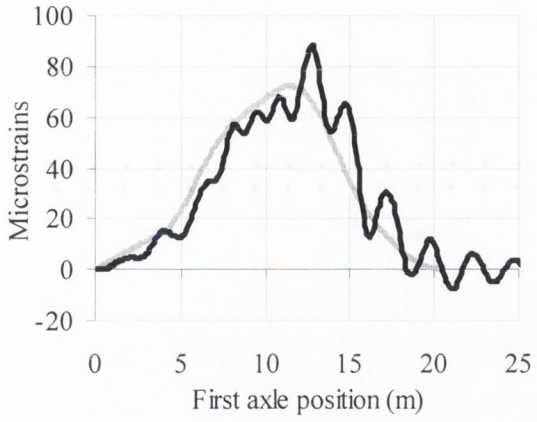

(c) 70 km/h, longitudinal strain

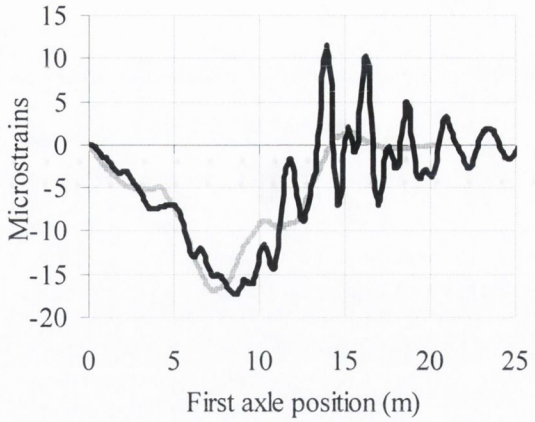

(d) 70 km/h, transverse strain

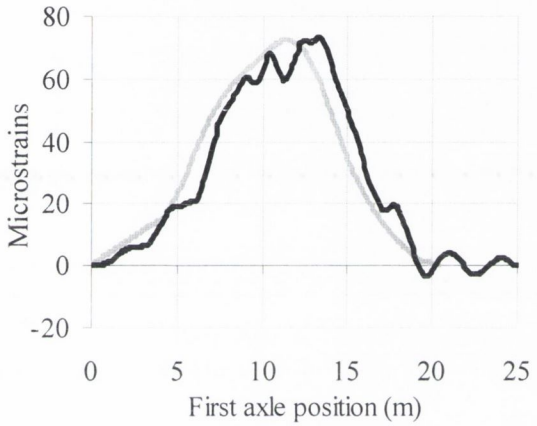

(e) 85 km/h, longitudinal strain

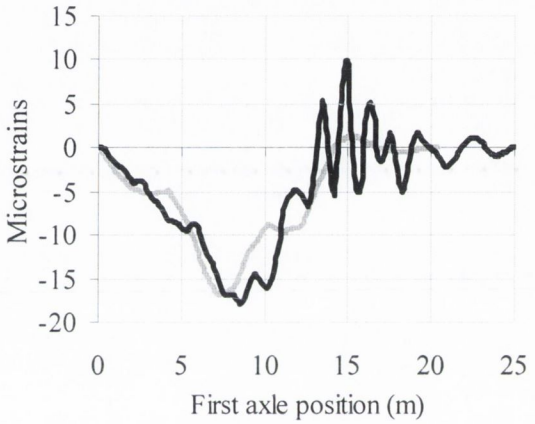

(f) 85 km/h, transverse strain

Figure 6.69 – Strain at midspan (sensor approx. in centre of slow lane)

The spectra of the previous figure are represented in Figure 6.70 for the 70-km/h run. The static response concentrates around a few harmonics of low frequency which interfere with dynamics below 5 Hz.

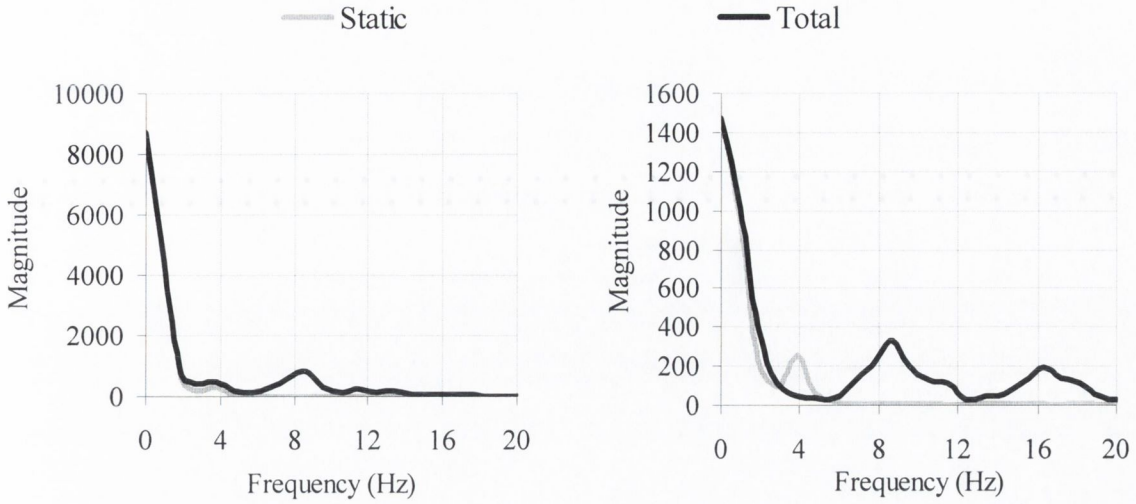

(a) Longitudinal strain (b) Transverse strain

Figure 6.70 – Spectra of strain at midspan (sensor approx. in centre of slow lane)

6.5.7 Cellular

The cross-section of a cellular or box deck is made up of a number of thin slabs and thin or thick webs which totally enclose a number of cells. These complicated structural forms are commonly used in preference to beam and slab decks for spans in excess of about 30 m because, in addition to the low material content, low weight and high longitudinal bending stiffness, they have high torsional stiffnesses which gives them better stability and load distribution characteristics (Hambly 1991). A spatial model is used to represent a two-span, three-cell bridge deck with edge cantilevers. The cross-section is represented in Figure 6.71(a) and a general overview is given in Figure 6.71(b). Solid diaphragms 2 m thick are located at the end and central supports.

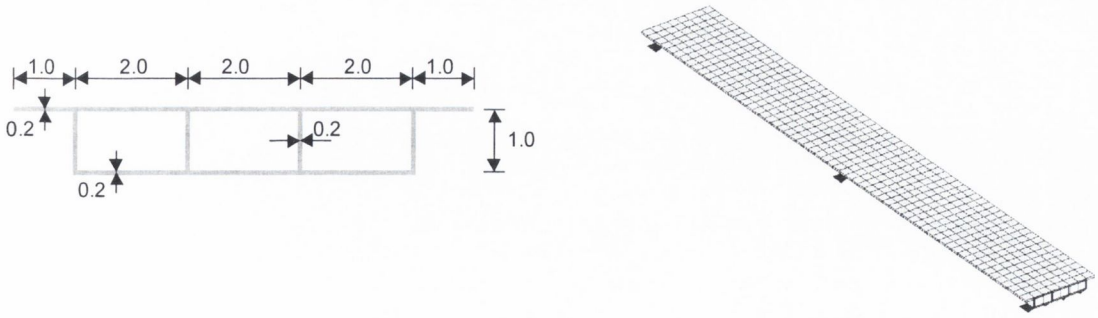

(a) Cross-Section (b) General overview

Figure 6.71 – Box Girder

The deck is supported transversely on a support under each. Dimensions and element composition are given in Figures 6.72(a) and (b).

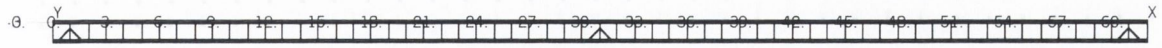

(a) Side view

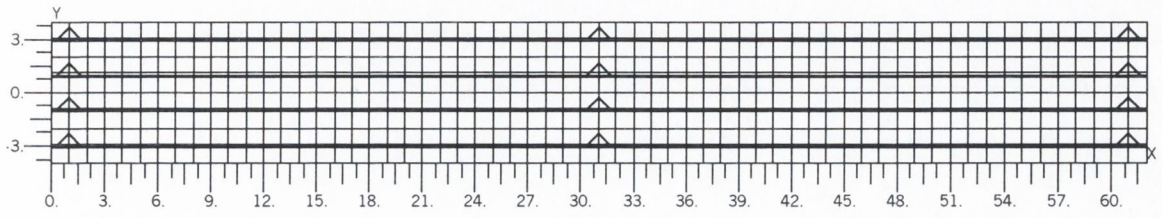

(b) Plan view

Figure 6.72 – Finite element model of cellular bridge finite element

Influence lines are given in Figure 6.73 and dynamic characteristics in Figure 6.74.

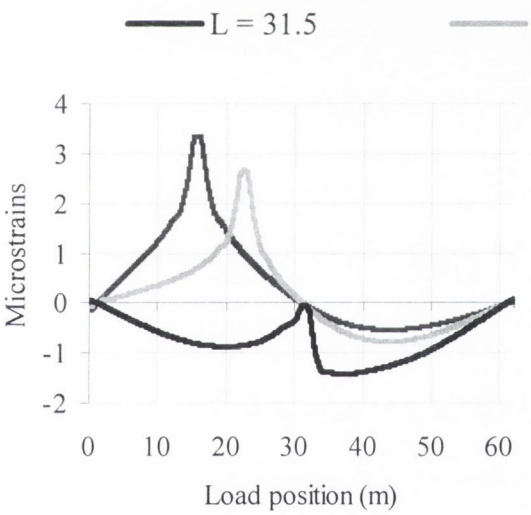

(a) Longitudinal strain, slow lane

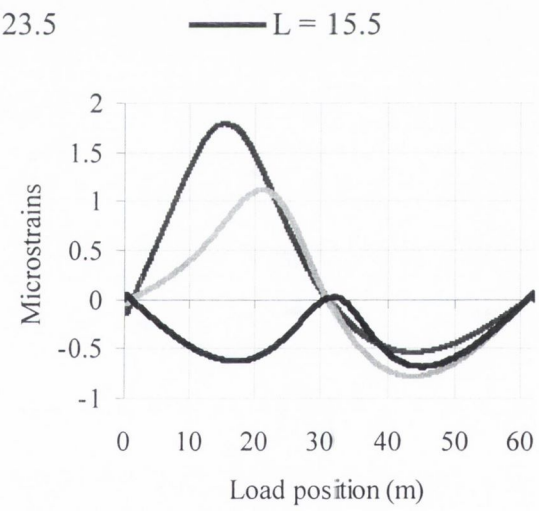

(b) Longitudinal strain, fast lane

Figure 6.73 (continued on following page)

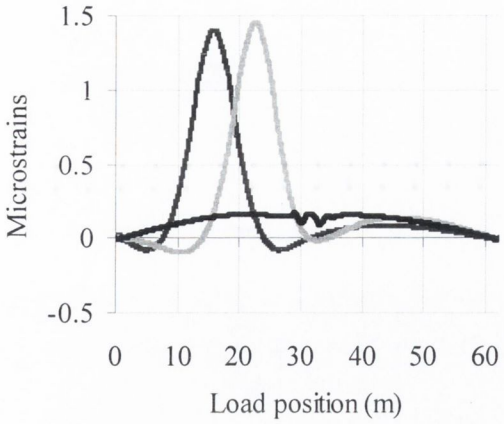

(c) Transverse strain, slow lane

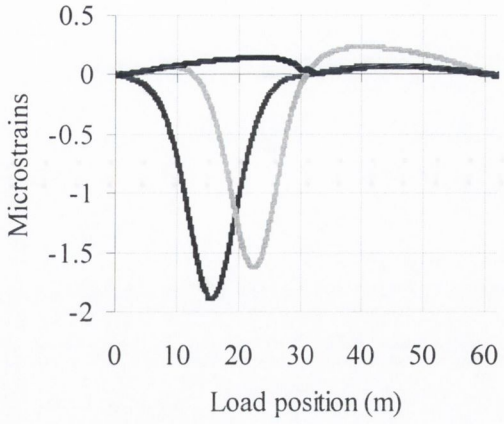

(d) Transverse strain, fast lane

Figure 6.73 – Influence line of strain at the bottom plate (*L*: longitudinal distance of the sensor from start of the bridge; transverse location from bridge centreline: 2.5 m)

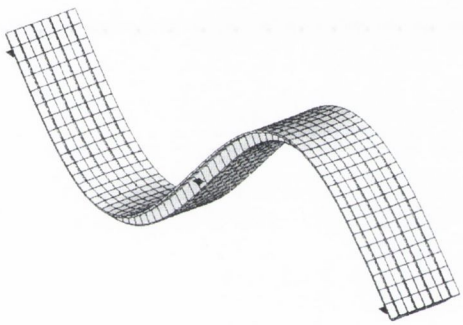

(a) 1st Mode (2.95 Hz)

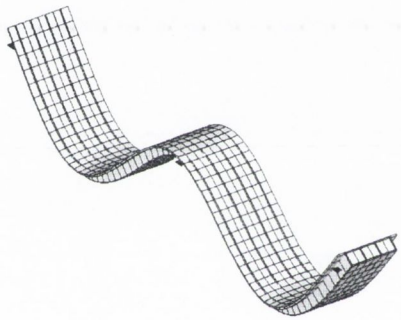

(b) 2nd Mode (4.60 Hz)

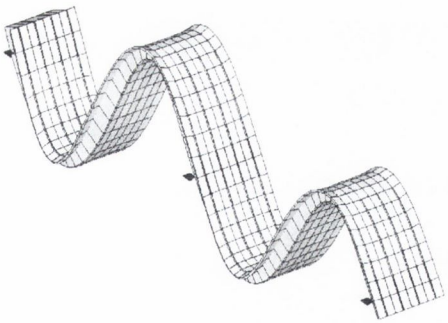

(c) 3rd Mode (10.98 Hz)

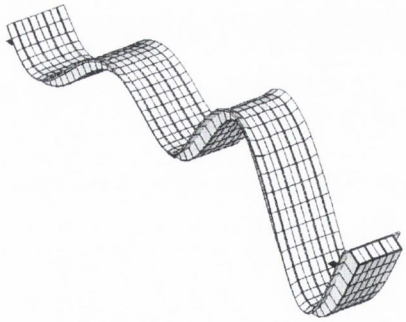

(d) 4th Model (13.14 Hz)

Figure 6.74 (continued on following page)

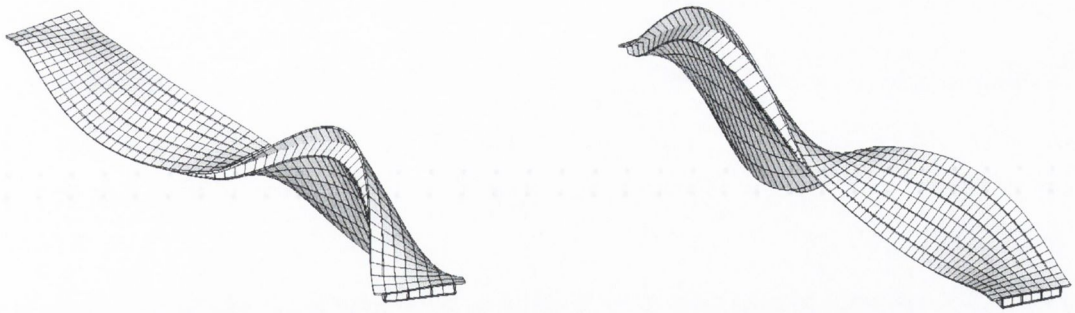

(c) 5th Mode (13.66 Hz) (d) 6th Model (14.11 Hz)

Figure 6.74 - Modes of vibration of Cellular Bridge

The dominant modes of vibration are in the longitudinal direction as shown in Figure 6.62. The longitudinal and transverse strain responses of the bridge under the crossing of a three-axle truck (22 t) over the slow lane are shown in Figure 6.75.

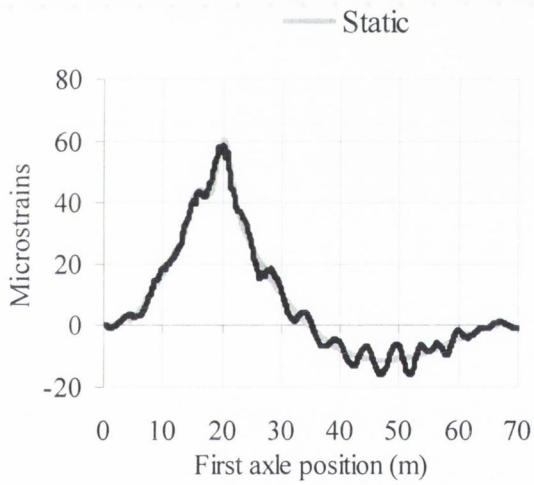

(a) 55 km/h, longitudinal strain

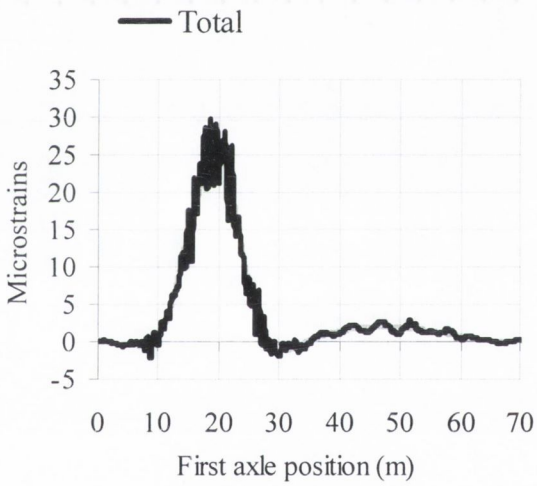

(a) 55 km/h, transverse strain

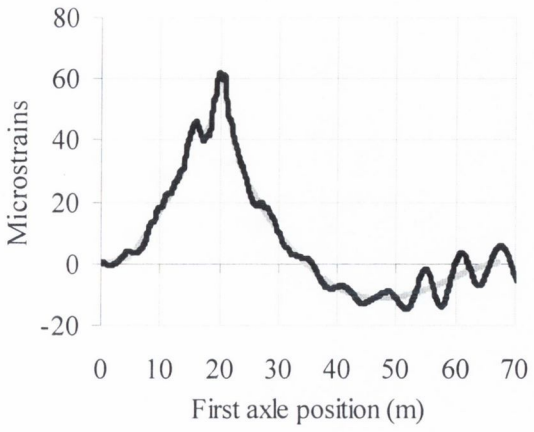

(b) 70 km/h, longitudinal strain

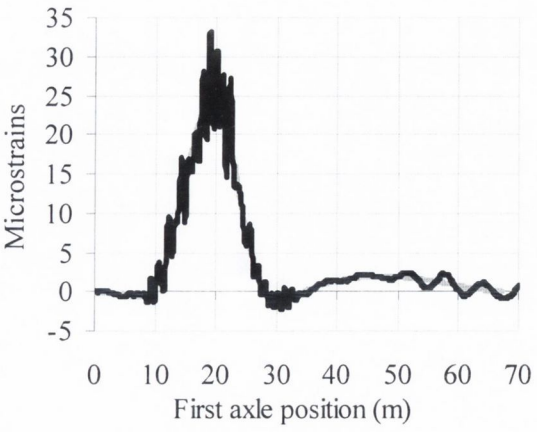

(b) 70 km/h, transverse strain

Figure 6.75 (continued on following page)

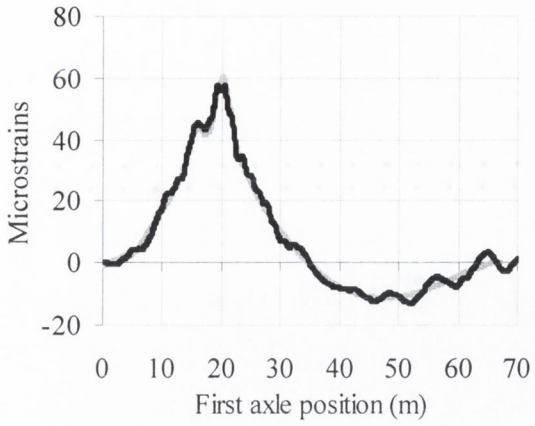

(c) 85 km/h, longitudinal strain

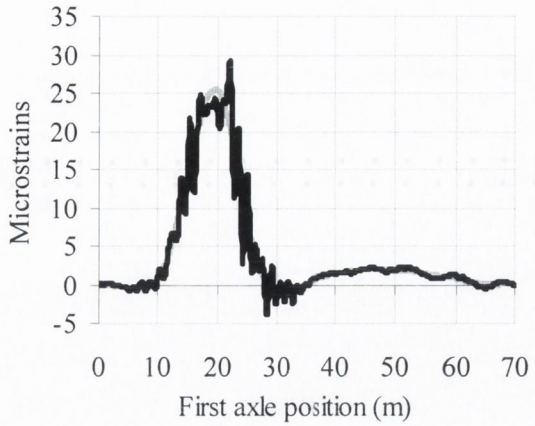

(c) 85 km/h, transverse strain

Figure 6.75 – Strain at midspan of first span (sensor approx. in centre of slow lane)

The spectra in Figure 6.76 correspond to the 70 km/h run of the previous figure. There are different dynamic frequency components interfering with the static response below 5 Hz (the first two modes of vibration of the bridge are below this frequency).

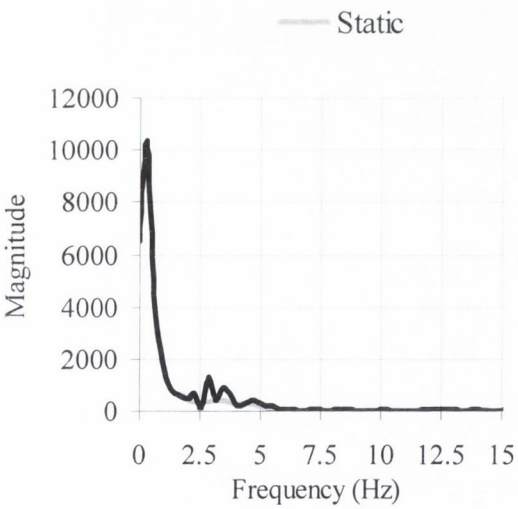

(a) Longitudinal strain

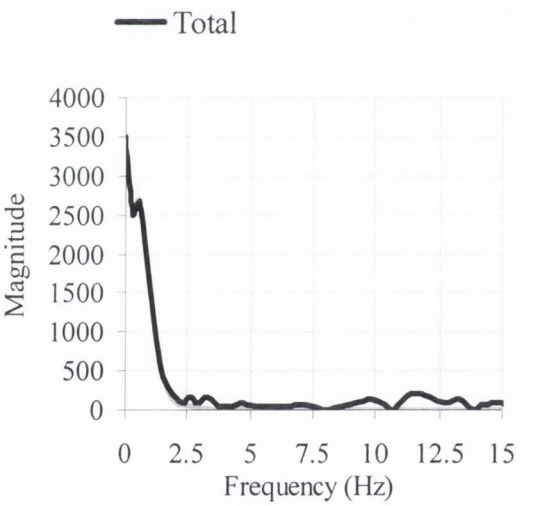

(b) Transverse strain

Figure 6.76 – Spectra of strain at midspan of first span (sensor approx. in centre of slow lane)

Simultaneous Traffic Events

Figure 6.77 shows the bridge response for different speed combinations of a pair of three-axle trucks (27.43 t) running in the same direction but in different lanes.

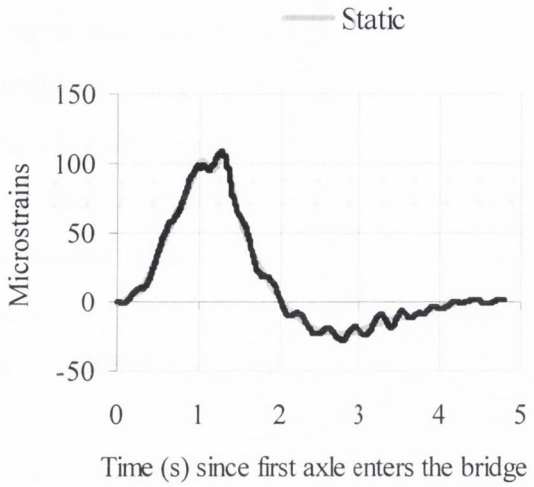

(a) 55 (slow lane) and 70 km/h (fast lane), longitudinal strain

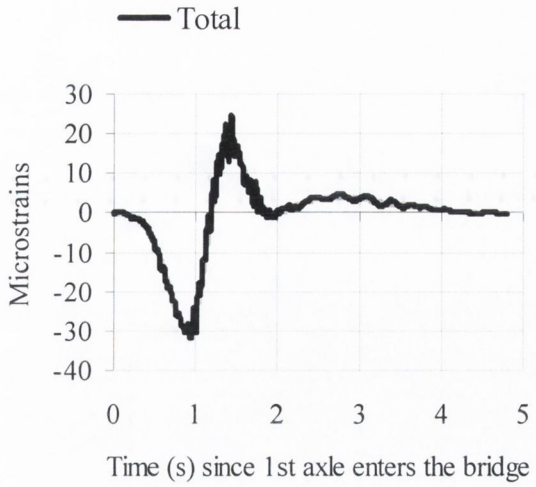

(b) 55 (slow lane) and 70 km/h (fast lane), transverse strain

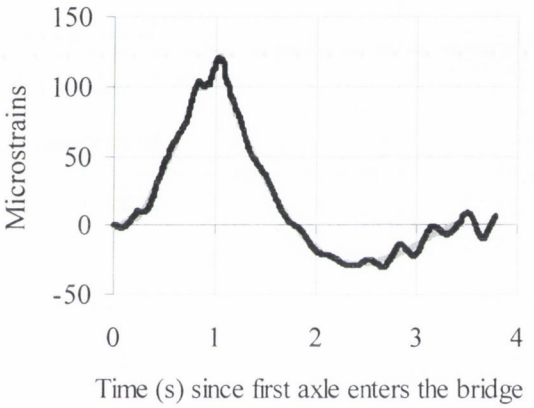

(c) Both at 70 km/h, longitudinal strain

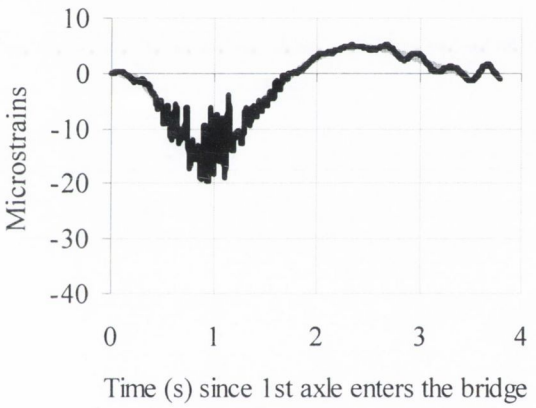

(d) Both at 70 km/h, transverse strain

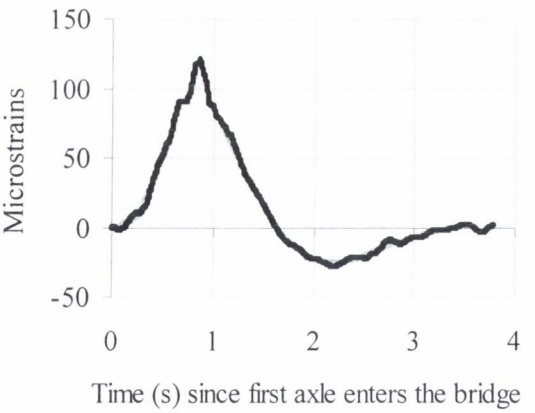

(e) 85 (slow lane) and 70 km/h (fast lane), longitudinal strain

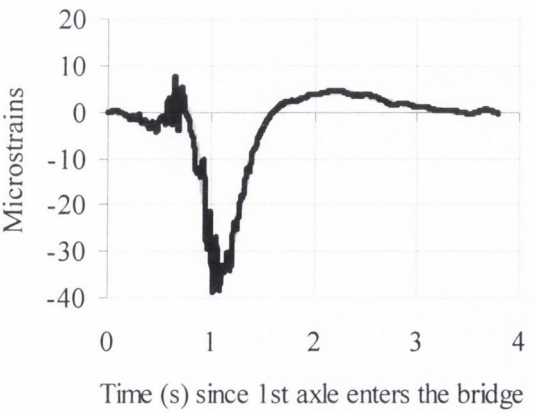

(f) 85 (slow lane) and 70 km/h (fast lane), transverse strain

Figure 6.77 – Strain at midspan of first span (sensor approx. in centre of slow lane)

Long bridges are likely to have two or more heavy vehicles crossing at the same time and BWIM accuracy might decrease considerably. In the case of Figure 6.77, the longitudinal strain is quite close to the static, though the magnitude of the dynamic oscillation increases with time. Higher frequency components can be detected in the transverse direction due to the smaller stiffness.

6.6 CONCLUSIONS

There is a need to determine the influence of bridge and vehicle dynamics on B-WIM accuracy. Test trials can only measure a small number of parameters in the field and cover a small sample of bridges and vehicles. Accurate modelling of the bridge-truck dynamic interaction is required for further testing. In this chapter, a Lagrange multiplier technique has been used for the simulation of a vehicle passing over a bridge using finite element models. The formulation used by the author for the implementation of this technique has been described. An example has also been given of how to carry out the simulation in the MSc/NASTRAN environment.

Different bridge and truck finite element models have been built that will be used to test a number of B-WIM algorithms in Chapter 9. Road profile has been generated stochastically from a power spectral density function for 'good' conditions. Trucks are modelled as rigid frame bodies. Frame twist, body pitch, bounce and roll, axle hop and roll are taken into account. Two types of truck configuration (two- and three-axle) with three different loading conditions and three different speeds are used in simulations (limited reproducibility conditions – Appendix B).

Longitudinal and transverse strain has been calculated at different locations in seven bridges:

- Single span isotropic slab (16 m): Transverse bending is not significant. Longitudinal bending is sharper and higher in the lane crossed by the vehicle and more suitable for B-WIM purposes. The first natural frequency is 4.51 Hz (longitudinal) and dynamic oscillations around the static response are important, especially at higher speeds. The strain response at different transverse locations of the same section differs slightly. Strain has also been calculated for different transverse locations of the truck path (0, 1

and 2 m from bridge centreline). Strain results are higher at 70 km/h and at 2 m from the bridge centreline. When running two trucks simultaneously on the bridge, total strain does not exhibit high deviations from the static response.

- Two-span isotropic slab (37 m): Transverse strain is much smaller than longitudinal strain. Unlike the influence line for longitudinal bending of a location near midspan, the influence line at the central support has the same sign regardless of the truck location. Therefore, dynamics, only noticeable when the truck is in the second span, are less significant in the central support location than in other locations.
- Slab with edge cantilever (20 m): The shape of the influence lines is very similar to the isotropic single slab, except for transverse bending in the driving lane. However, vibrations are less significant than in the isotropic slab due to the greater bridge mass.
- Voided slab deck (25 m): Static response is similar to the preceding slab with edge cantilever, but the mass per unit length is much smaller. The first natural frequency is 3.80 Hz and the total strain oscillates around the static component with significant amplitude.
- Beam and slab (20 m): The same level of dynamics appears for beam and longitudinal bending of the slab. A new possibility arises for this type of structural system: the measurement of transverse bending of the slab, of higher magnitude than the corresponding longitudinal bending. Dynamics of transverse strain have high amplitudes, but they oscillate with a higher frequency than longitudinal strain.
- Skew (15 m): In this 45° skew bridge, though the first natural frequency is relatively high (7.41 Hz), total strain shows a significant deviation from the expected static response.
- Cellular (62 m): This two-span continuous bridge is the longest and has the smallest first natural frequency (2.95 Hz) of all models being analysed. The influence line for longitudinal strain is less pronounced than for transverse bending. The first two mode shapes are longitudinal (unlike for the single span bridges under study, while the second mode of vibration is torsional), but these low frequency dynamic components have little importance in the total longitudinal strain until the vehicle reaches the second span. When calculating strain due to two trucks crossing the bridge simultaneously, the dynamic component is negligible compared to the static component.